**CARDIFF UNIVERSITY**

**PRIFYSGOL CAERDYD**

# Modelling intestinal cancer development and progression in the mouse

**Emma Jane Davies**

Cardiff University

Ph.D.

2007-2011

**MRC** Medical Research Council

UMI Number: U585525

UMI U585525

ProQuest LLC
789 East Eisenhower Parkway
P.O. Box 1346
Ann Arbor, MI  48106-1346

# Acknowledgments

I dedicate this thesis to my husband Rhodri and to my parents, Linda and Philip.

I would first like to thank my parents for their continual support both emotionally and financially through my school education and higher education, and for their constant encouragement to fulfill my goals and academic achievements. I would also like to thank my husband Rhodri, who has always been supportive in my career decisions and followed me willingly. He has also been my rock in getting me through my PhD, putting up with my long hours and weekends in the lab and making sure there was always food on the table for me when I arrived home. I would also like to thank to my sister Victoria, my grandmother Jane and Ann, Ian and Melissa, who have always encouraged me to do what I wanted to do. Finally, I would like to thank my parents-in-law, Kay and Steve, for supporting Rhodri and I in our decisions, and letting us move in with them for the last few months of my PhD.

I would like to thank everyone in the ARC group, past and present for helpful guidance and acceptance into the group. First and foremost I would like to thank my supervisor Alan for providing me with an extremely interesting project, and providing guidance whilst also giving me room to make my own decisions on the directions of the project. Secondly, I would like to thank Victoria Durban, for setting up the project and being my source of answers to various questions! I would also like to thank Mark Bishop and Lucie Pietzka for undertaking genotyping, weaning and ear marking of all my mice, and Derek Scarborough and Marc Isaac for undertaking tissue sample processing and tissue sectioning. I would also like to thank Valerie Meniel, who helped me greatly by taking care of my mouse colonies whilst I was writing up this thesis. Aliaksei for his continual correction of my errors, and for listening to my many moans and gripes! Alison and Owen, for many hours of interesting conversation. Meera Raja, for helping with my mouse colonies when I have been away, providing company in the basement and for her appreciation of after work drinks! Finally, I would like to thank everyone on the 4th and 5th floor for providing me with advice, humour and support.

# Contents

# List of Figures

# List of Tables

# Abbreviations and Definitions

## Symbols

°C = Degrees Celsius

µg = Micrograms

µl = Microlitres

µm = Micrometre

µM = Micromolar

## A

ABC = Avidin Biotin Complex

AhCreER$^T$ = Aryl Hydrocarbon Cre recombinase Estrogen Receptor transgene

Ascl2 = Achaete Scutelike 2

APC = Adenomatous Polyposis Coli

AXIN = Axis Inhibitor

## B

BCA = Bicinchoninic Acid

Bmi1 = polycomb ring finger oncogene

BMP = Bone Morphogenic Protein

BMPRII = Bone Morphogenic Receptor type II

bp = Base Pair

BrdU = 5-Bromo-2-deoxyuridine

BSA = Bovine Serum Albumin

## C

Cdh1 = Cadherin1

Col1A2CreER$^T$ = Collagen Type 1, Alpha 2 Cre recombinase Estrogen Receptor transgene

CRC = Colorectal Cancer

CBC cells = Crypt-Base-Columnar cells

cm = Centimetre

CSL = CBF1/RBP-Jκ/Suppressor of Hairless/LAG-1

CreER$^T$ = Cre recombinase-Estrogen receptor fusion transgene

C$_T$ = Cycle Time

## D

DAB = 3,3'-diaminobenzidine

dATP = Deoxyadenosine Triphosphate

DCAMKL-1 = Doublecortin and Calcium/Calmodulin-dependent protein Kinase-Like-1

DCC = Deleted in Colorectal Cancer

dCTP = Deoxycytidine Triphosphate

ddH$_2$O = double distilled water

dGTP = Deoxyguanosine Triphosphate

Dhh = Desert Hedgehog

dH$_2$O = deionised water

DNA = Deoxyribonucleic Acid

DNase = Deoxyribonuclease

dNTP = Deoxynucleotide Triphosphate

DSH = Dishevelled

DTT = Dithiothreitol

dTTP = Deoxythymidine Triphosphate

## E

E-cadherin = Epithelial Cadherin

ECL = Electrochemiluminescence

EDTA = Ethylenediamine Tetra-acetic Acid

EGFP = Enhanced Green Fluorescent Protein

EpCAM = Epithelial Cell Adhesion Molecule

EM = Electron Microscopy

EMT = Epithelial-to-Mesenchymal Transition

ER = Estrogen Receptor

Erk = Extracellular regulated MAP kinase

ES cells = Embryonic Stem cells

**F**

FAK = Focal Adhesion Kinase

FAP = Familial Adenomatous Polyposis

FKHR = Forkhead in Rhabdom/Forkhead Transcription Factors

FLP = flippase

FRT = FLP Recognition Target

**G**

gDNA = genomic DNA

GEF = Guanine Nucleotide Exchange Factor

GSK-3 = Glycogen Synthase Kinase-3

GTP = Guanosine Triphosphate

GTPase = Guanosine Triphosphatase

**H**

H&E = Haematoxylin and Eosin

HBSS = Hanks Balanced Salt Solution

HNPCC = Hereditary Nonpolyposis Colorectal Cancer

hr = Hour

HRP = Horse Radish Peroxidase

**I**

IGF-1 = Insulin-Like Growth Factor-1

IHC = Immunohistochemistry

Ihh = Indian Hedgehog

i.p. = Intraperitoneal

**J**

JNK = c-Jun N-terminal Kinase

JPS = Juvenile Polyposis Syndrome

**K**

KDa = Kilodaltons

kg = Kilograms

KRAS = Kirsten Rat Sarcoma viral oncogene homolog

kV = Kilovolts

**L**

l = Litre

LOH = loss of heterozygosity

loxP = Locus of crossover of Bacteriophage P1

Lgr5 = Leucine-rich repeat-containing G-protein coupled receptor 5

**M**

MAPK = Mitogen Activated Protein Kinase

MEK1/2 or MEK = Mitogen Activated Erk Kinase1/2

MDM2 = Mouse Double Minute 2 homolog

mg = Milligrams

MIN = Multiple Intestinal Neoplasia

mins = minutes

MLH1 = MutL homolog 1

mm = Millimetre

MMR = Mismatch Repair

MSH2 = MutS E.Coli homolog of 2

mTERT = mouse telomerase reverse transcriptase

mTOR = mammalian target of rapamycin

M/W = Microwave

**N**

NCID = Notch Receptor Intracellular Domain

NGS = Normal Goat Serum

NRS = Normal Rabbit Serum

**O**

Olfm4 = Olfactomedin 4

O/N = Overnight

**P**

pAkt = phospho-Akt

PBS = Phosphate Buffered Saline

P/C = Pressure Cooker

PCR = Polymerase Chain Reaction

PDK = Phosphoinositide-dependent Protein Kinase 1

pErk = phospho-Erk

PKA = Protein Kinase A

PLL = Poly-L-Lysine

pMEK = phospho-MEK

pmTOR = phospho-mTOR

PTEN = Phosphatase and tensin homolog deleted on chromosome ten

PTHS = PTEN Hamartoma Syndromes

PI3K = Phosphatidylinositol-3-Kinase

$PIP_2$ = phosphatidylinositol 4,5-bisphosphate

$PIP_3$ = phosphatidylinositol (3,4,5)-trisphosphate

**Q**

qRT = Quantitative Real-Time

**R**

RNA = Ribonucleic Acid

RNase = Ribonuclease

RPM = Revolutions Per Minute

RT = Room Temperature

rtTA = reverse Tetracycline-controlled Transactivator

RTK = Receptor Tyrosine Kinase

**S**

SDS = Sodium Dodecyl Sulphate

SDS-PAGE = Sodium Dodecyl Sulphate-Polyacrylamide Gel Electrophoresis

secs = Seconds

SEM = Scanning Electron Microscopy

Shh = Sonic Hedgehog

**T**

TA = Transit-Amplifying

TACE = Tumour Necrosis Factor Converting Enzyme

Taq = DNA polymerase from *Thermus aquaticus*

TBE = Tris Borate EDTA

TBS/T = Tris Buffered Saline with Tween 20

Tcf/Lef = T-cell factor and Lymphoid enhancer factor

TEMED = N,N,N',N'-teramethylethylenediamine

tetO = Tet Operon

TGF-$\beta$ = Transforming Growth Factor-$\beta$

tTA = Tetracycline-controlled Transactivator

**U**

UICC = Union for International Cancer Control

UV = Ultra Violet

**V**

V = Volts

VillinCreER$^T$ = Villin Cre recombinase ER transgene

**W**

W/B = Waterbath

W/V = Weight per Volume

WT = Wild Type

Wnt = Wingless-type murine mammary tumour virus Integration site family

**X**

x g = times gravity

**123**

$^3$HTdR = Tritiated Thymidine

# Abstract

Colorectal cancer is the second most common cause of death from cancer in the UK. One of the reasons for this high mortality rate is the late presentation of patients to the clinic, i.e. when they have late stage invasive or metastatic tumours. The development of new therapeutic compounds for late stage disease is therefore paramount to tackling the disease. Better models of colorectal cancer are also needed to test new therapeutic compounds, and to try to improve understanding of the processes underlying tumour progression and metastasis. Currently, most mouse models of colorectal cancer only recapitulate the early stages of the disease and rarely progress to an invasive late-stage tumour. The tumour suppressor PTEN, the oncogene KRAS and the cell adhesion component E-cadherin have all been implicated in the progression, or poor prognosis of colorectal cancer. I have used the cre-loxP recombination system to alter the expression of these genes in the mouse intestine, and to further define their role in tumourigenesis.

I have shown that mutations in Pten and Kras synergise in the context of Wnt initiated intestinal tumours to promote progression from adenoma to invasive adenocarcinoma. It is also reported here that mutations in Pten and Kras alone, predispose to non-Wnt initiated tumours that progress to metastatic carcinoma in the intestine. In addition to the synergy of Pten and Kras mutations in tumourigenesis, I have shown that they synergise to disrupt normal intestinal homeostasis resulting in increased cell number and villus bifurcation. These phenotypes are potentially driven through hyperactivation of the phosphatidylinositol-3-kinase (PI3K) pathway.

Investigation of the role of E-cadherin in the small intestine revealed that E-cadherin is indispensable for the structural maintenance of the epithelial layer. However, heterozygous loss of E-cadherin is viable, and mice do not develop any tumourigenic phenotype. Further, despite loss of E-cadherin correlating with invasion in human tumours, heterozygous loss of E-cadherin in the context of intestinal tumourigenesis does not promote tumour progression in the mouse.

I also investigated the role of Pten in the small intestinal stroma. PTEN is a major tumour suppressor in humans. Constitutive heterozygous loss of Pten in the mouse gives rise to intestinal tumours, as does intestinal specific, conditional deletion of Pten in the epithelium and the underlying supporting stroma and smooth muscle. However, epithelial specific loss of Pten does not give rise to rapid tumourigenesis. I therefore, used the cre-loxP system to conditionally delete Pten from the stromal fibroblasts and smooth muscle of the intestine. These mice developed benign tumours along the length

of the intestine, in particular the caecum and colon. These findings demonstrate the role of Pten in stromal-epithelial interactions in the intestine.

Taken together, my data demonstrate that appropriate regulation of Pten and Kras together, contribute to the maintenance of homeostasis in the small intestinal epithelium, and alteration of the expression of these genes concomitantly in intestinal epithelial cells leads to the formation of intestinal metastatic carcinoma. My findings also indicate that the tumour suppressor function of Pten is not confined to epithelial cells, as deficiency of Pten exclusively in the supporting stroma and smooth muscle of the intestine results in tumourigenesis.

# Chapter 1:    General Introduction

## 1.1    *Colorectal Cancer*

### 1.1.1    Colorectal cancer statistics and causes

After breast and lung cancer, bowel cancer or colorectal cancer (CRC) is the third most commonly diagnosed cancer in the UK (excluding non-melanoma skin cancer) (CancerResearchUK, 2011). After lung cancer it is the second most common cause of death from cancer in the UK (CancerResearchUK, 2010). Its high incidence is likely to be attributed to two factors, the high proliferative rate of the epithelium and poor diet. The epithelium of the intestinal tract renews itself frequently, this high rate of replication increases the likelihood of replication errors coupled with the direct contact of these cells with potential carcinogens in foodstuffs increases the chance of accumulation of mutations. The high incidence of CRC is linked to obesity and a diet rich in red and processed meats, lacking in fibre, and to a lesser extent fruit and vegetables (Moghaddam et al., 2007, Renehan et al., 2008, Park et al., 2005, Norat et al., 2005). Lack of exercise is also thought to be a contributory factor, increasing the risk of CRC by up to 24% (Wolin et al., 2009). Wolin et al suggest a number of possible reasons why exercise decreases your risk of CRC, these include: quicker transit of food through the gut, anti-inflammatory action and reduced insulin resistance (Wolin et al., 2009). The high mortality rates associated with CRC are in part due to the relatively late detection of the disease i.e. usually when it has metastasised. In this regard, it has been shown that one round of fecal occult blood screening reduces the risk of death by 25% (Hewitson et al., 2007), confirming that early detection of the disease increases the patients chance of survival.

### 1.1.2    Dukes staging of CRC

When a patient presents with CRC the course of treatment used will depend on the severity of the cancer. Cuthbert Dukes first proposed a system of classification of the differing stages of CRCs in 1932. This system classified colorectal tumours into four categories A-D, A - a tumour confined to the intestine, B – a tumour that has invaded through the muscle wall of the intestine, C – a tumour that has infiltrated regional lymph nodes and D – a tumour with distant metastases (Dukes, 1980). This system has since been modified by the Union for International Cancer Control (UICC), the system takes into account the size of the primary tumour (T), the invasiveness of the primary tumour i.e. whether it has invaded through the muscle wall and underlying serosa of

the intestine, if there are the presence of tumour cells in the lymph nodes (N) and if it has spread to other organs (local or distant) (M) (Table 1.1) (Sobin and Wittekind, 1997, CancerResearchUK, 2009).

| UICC/TNM | | Modified Dukes' |
|---|---|---|
| Stage 0 | Carcinoma in situ | |
| Stage I | No nodal involvement, no distant metastasis | A |
| | Tumour invades submucosa (T1, N0, M0) | |
| | Tumour invades muscularis propria (T2, N0, M0) | |
| Stage II | No nodal involvement, no distant metastasis | B |
| | Tumour invades into subserosa (T3, N0, M0) | |
| | Tumour invades into other organs (T4, N0, M0) | |
| Stage III | Nodal involvement, no distant metastasis | C |
| | 1 to 3 regional lymph nodes involved (any T, N1, M0) | |
| | 4 or more regional lymph nodes involved (Any T, N2, M0) | |
| Stage IV | Distant metastasis (any T, any N, M1) | D |

**Table 1.1 Colorectal cancer staging (taken from Cancer Research UK, Cancer Stats) (CancerResearchUK, 2009)**

### 1.1.3 Current therapeutic strategies for CRC patients

The high mortality rate of CRC patients is largely due presentation of patients with late-stage disease, owing to the relatively mild symptoms that occur with early-stage disease e.g. diarrhea and frequent bowel movements. Once the stage of the cancer is established there are a number of clinical options. These predominantly involve resection of the tumour and metastases if possible and the patient is well enough, in conjunction with the use of a number of chemotherapeutics in differing combinations depending on the severity of the tumour stage (NICE, 2011). Cytotoxics such as 5-Fluorouracil, irinotecan and oxaliplatin are used, as well as frequently the EGFR inhibitor cetuximab. These are used singularly or in combination to treat CRC patients. Cetuximab is used in combination with chemotherapy, or in patients in which irinotecan and oxaliplatin have failed. Despite these treatments CRC mortality rates

remain high, and it is clear that better understanding of how CRC develops and progresses, and better drugs are needed for treating late stage metastatic disease.

## 1.2 Basic anatomy and function of the intestines

The intestines form part of the digestive system, its function is to digest and absorb nutrients and water from ingested food, and form part of the body's defense against ingested pathogens. The intestinal structure consists of an open-ended tube extending from the stomach to the anus, made up of the small intestine and large intestine. The small intestine is made up of three parts, the duodenum (responsible for much of the chemical digestion of food), the jejunum and the ileum (distal small intestine) (Williams et al., 1989). The luminal surface of the small intestine is covered in a single cell layer of polarised epithelial cells that form invaginations called the crypts of Lieberkühn (commonly referred to as crypts) and projections called villi (Williams et al., 1989), these increase the surface area of the tissue to maximise nutrient absorption (Figure 1.1). The single-cell epithelial layer is supported by mesenchymal (stromal) fibroblasts that occupy the space around the crypts and extend up into each villus (the stromal component is referred to as the lamina propria). The stromal and epithelial component of the small intestine is encased in a layer of smooth muscle responsible for peristalsis. Stromal fibroblasts in the intravillus region also encase a blood supply to the cells for the transport of sugars and amino acids, and a lacteal (part of the lymphatic system), for the transport of lipids in the form of lipoproteins. The small intestine also contains nodules of lymphoid tissue called peyer's patches, these help recognise and defend against pathogens that enter the body through ingestion (Williams et al., 1989).

The large intestine is made up of the caecum (proximal), colon and rectum (distal). The caecum is found at the distal end of the small intestine, at the region where the small intestine joins the large intestine, the caecum is also the region of the large intestine where the appendix is located. The large intestine is the site in which most of the water is absorbed from ingested foodstuffs. At the distal end of the large intestine is the rectum, where faeces is stored before egestion. The rectum then opens out into the anal canal (Williams et al., 1989). The large intestine, similarly to the small intestine has a single cell layer of columnar epithelium, but unlike the small intestine, the large intestine epithelium is entirely made up of elongated crypts and does not possess any villus projections, and cells instead form a flat surface epithelium (Figure 1.1).

3

## Small Intestinal Structure



Stromal fibroblasts

Simple columnar epithelium

Villus

Lamina propria

Lacteal

Mucosa

Submucosa

Muscularis

Crypt

Smooth muscle fibroblasts

## Large Intestinal Structure

Surface epithelium



Mucosa

Crypt

Submucosa

Muscularis
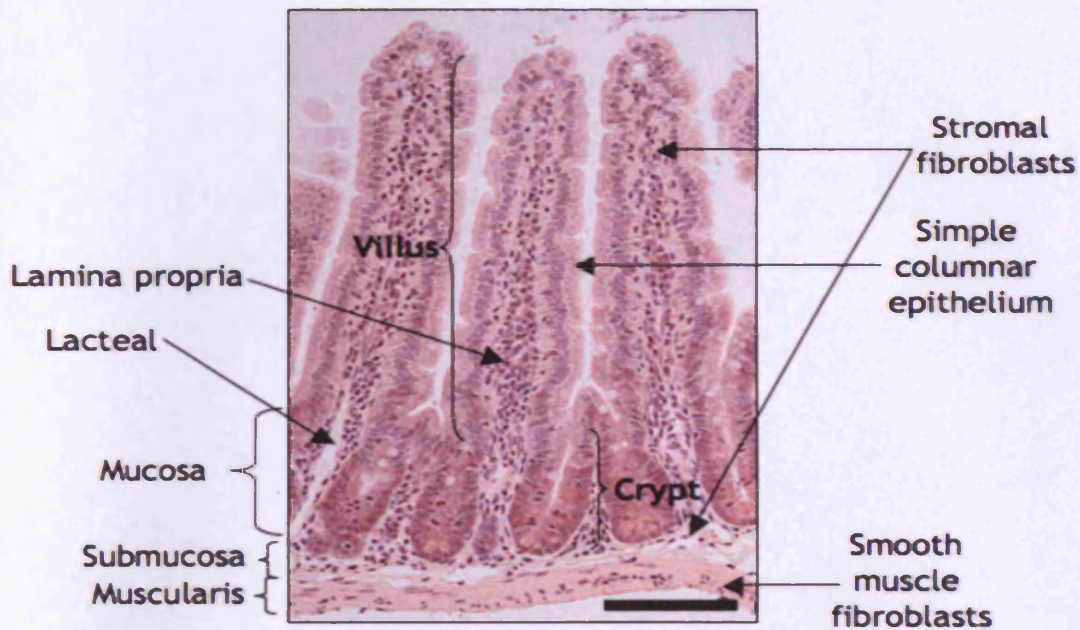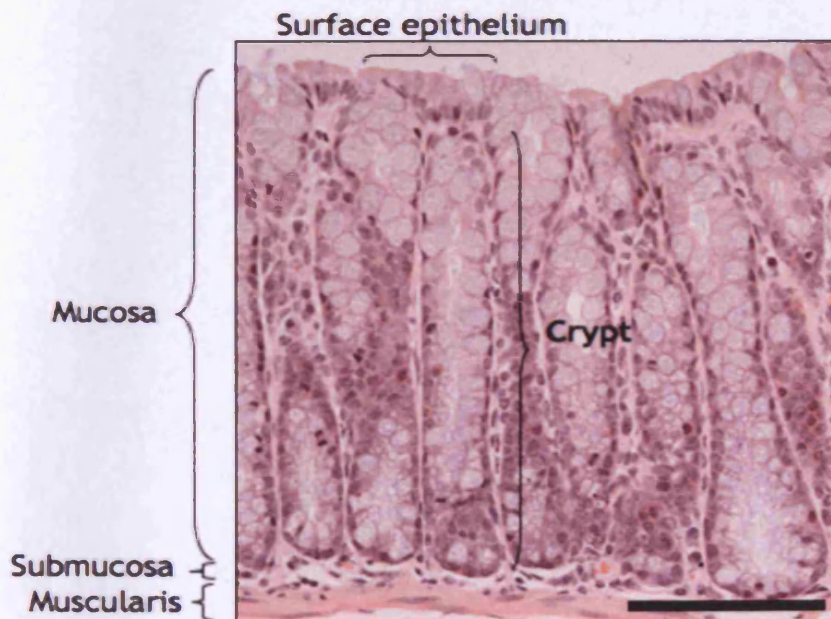
**Figure 1.1 Photomicrographs of the mouse small and large intestine**

The small intestine is made up of finger-like projections called villi and invaginations called crypts. Single cell layers of epithelium supported by stromal fibroblasts make up these structures. They face into the lumen and are surrounded on the outside by a layer of smooth muscle. The large intestine is comprised of a single cell layer of enterocytes and goblet cells but these only form crypts. Scale bars represent 100μm.

## 1.3 Small intestinal histology

The small intestine has a rapidly renewing epithelium that turns over every 2-3 days in the mouse and 5-6 days in humans (Wright and Alison, 1984, Creamer, 1967), this renewal is driven by the proliferative cell compartment found in the crypts. Crypts are much more numerous than villi, approximately 9 crypts feed each villus with cells (Cosentino et al., 1996). Stem cells are found in the base of the crypts that give rise to progenitor cells, which are found in the transit-amplifying (TA) zone of the crypt. These cells rapidly divide and migrate up the crypt into the villus region. As they migrate from the crypt to the villus they become terminally differentiated, with the exception of paneth cells that migrate to the base of the crypt. The other major cell types found in the villus includes: enterocytes, goblet cells and enteroendocrine cells (Figure 1.2). Terminally differentiated cell types continue to migrate up the villus axis where they undergo apoptosis and are sloughed from the villus tip (Hall et al., 1994, Grossmann et al., 2002). Due to sustained cell proliferation, migration and shedding of cells required for continual epithelial renewal, mechanisms controlling proliferation, differentiation and apoptosis are tightly controlled in order to maintain intestinal homeostasis.

### 1.3.1 The intestinal stem cell

Stem cells are long-lived pluripotent cells that divide asymmetrically, producing daughter cells that give rise to all mature cell types of a particular tissue and are required for tissue maintenance. Due to their longevity in intestinal crypts and presumed repeated divisions, they are considered to be susceptible to the accumulation of mutations and may be the initiating cells that give rise to cancers. Evidence in support of this is derived from *in vivo* experiments in the intestine, here the tumour suppressor Adenomatous polyposis coli (Apc) was selectively deleted from either the stem cell compartment or the TA progenitor cell region of the crypt. Mice that possessed Apc deficient stem cells had macroscopic tumours present in the small intestine after 3-5 weeks, whereas mice with Apc deficient cells in the TA region possessed few macroscopic intestinal tumours, even after 30 weeks post deletion of Apc (Barker et al., 2009). Intestinal stem cells possess a number of intrinsic mechanisms in an effort to prevent these cells from becoming neoplastic. Stem cells are thought to be slow cycling (or quiescent), undergo conservative strand replication of DNA and a have high susceptibility to apoptosis after genetic insult to prevent accumulation of mutations (Potten et al., 1997, Potten et al., 1978). By unknown mechanisms stem cells are able to replicate their DNA by conserved strand replication.

**Legend:**
- Transit-amplifying (TA) cell
- Absorptive enterocyte
- Goblet cell
- Enteroendocrine cell
- Actively cycling stem cell
- Quiescent stem cell
- Paneth cell
- Stromal cell

Cell shedding

Villus

Migration
Differentiation

TA zone

Crypt

Stem cell compartment

Stem cell niche
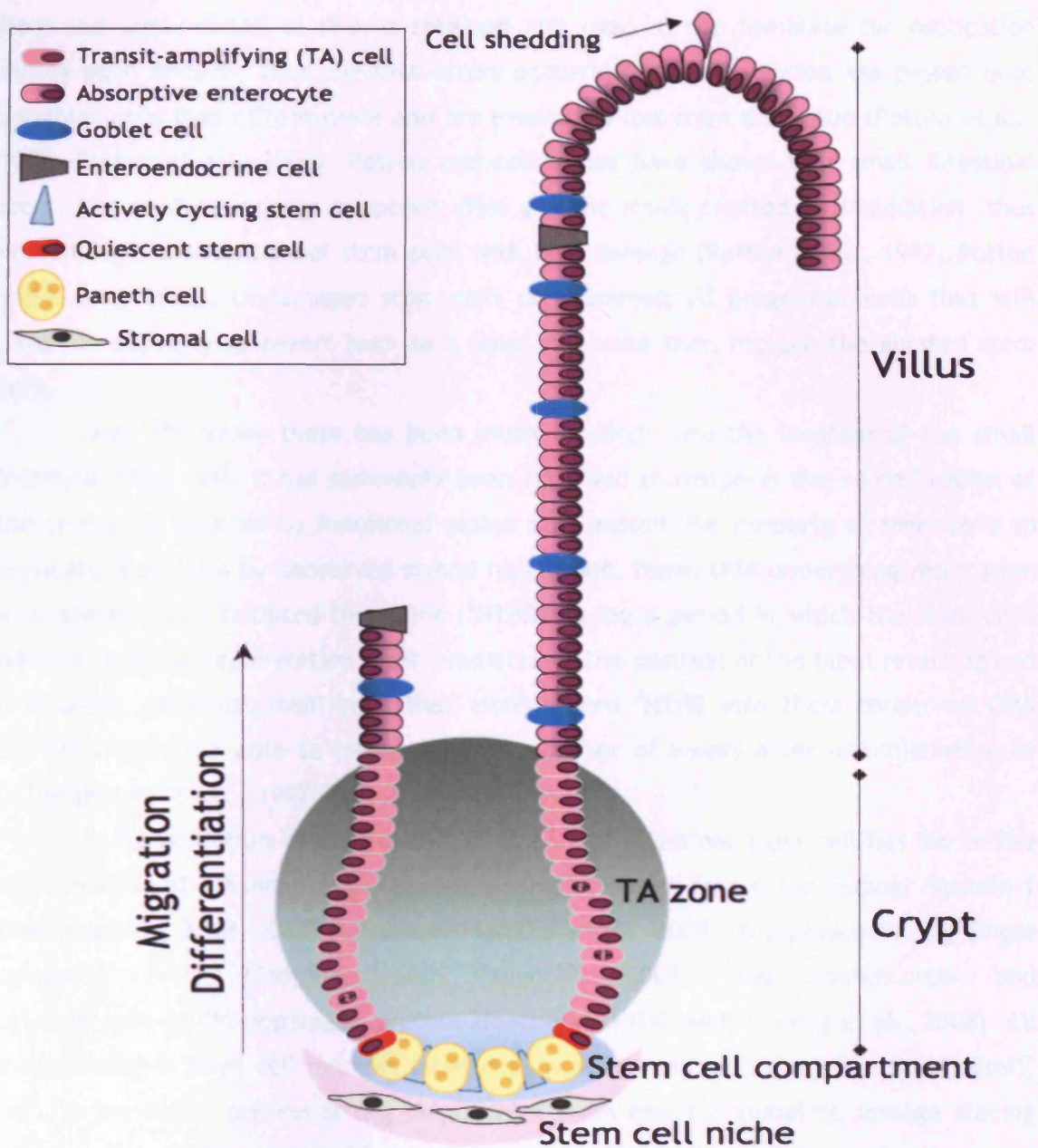
**Figure 1.2 Schematic diagram of the small intestinal cell types**

The intestinal epithelium is divided into two distinct cellular compartments: the crypt, which constitutes the proliferative transit-amplifying (TA) zone made up of immature progenitor cells, and the villus, which is made up of differentiated cells. The stem cell compartment is found at the base of the crypt, the stem cells are surrounded by paneth cells and stromal fibroblasts, which are thought to provide factors to maintain stem cell pluripotency and therefore constitute the stem cell niche. As the progenitor cells divide they migrate up the crypt-villus axis, as the cells migrate out of the crypt into the villus region they become terminally differentiated into enterocytes, goblet cells and enteroendocrine cells (paneth cells terminally differentiate and migrate to the base of the crypt). These mature cells continue to migrate up the villus (driven by repeated division of crypt progenitor cells) and are sloughed from the villus tip.

Here the same strand of DNA is retained and used as the template for replication during each division, thus any DNA errors occurring from replication are passed onto daughter cells that differentiate and are eventually lost from the tissue (Potten et al., 1978, Potten et al., 2002). Potten and colleagues have shown that small intestinal stem cells readily undergo apoptosis after genetic insult created by irradiation, thus preventing the retention of stem cells with DNA damage (Potten et al., 1997, Potten and Grant, 1998). Undamaged stem cells or uncommitted progenitor cells that still have the capacity to revert back to a stem cell state then replace the ablated stem cells.

Over the years there has been much research into the location of the small intestinal stem cell. It has commonly been regarded to reside in the +4 cell region of the crypts, elucidated by functional assays that exploit the property of stem cells to replicate their DNA by conserved strand replication. Here, DNA undergoing replication was labeled using tritiated thymidine ($^3$HTdR) during a period in which the stem cells were undergoing regeneration (post irradiation). The position of the label retaining cell (i.e. small intestinal stem cells that incorporated $^3$HTdR into their conserved DNA strand) were then able to be visualised a number of weeks after administration of $^3$HTdR (Potten et al., 1997, Potten et al., 1978).

The elucidation of the position of the small intestinal stem cell has led to the identification of a number of putative intestinal stem cell markers including, musashi-1 (Potten et al., 2003), CD133 (prominin-1) (Zhu et al., 2009), the polycomb ring finger oncogene Bmi1 (Sangiorgi and Capecchi, 2008) and doublecortin and calcium/calmodulin-dependent protein kinase-like-1 (DCAMKL-1) (May et al., 2008). All these putative stem cell markers label cells predominantly at the +4 position. Bmi1$^+$ cells in particular possess strong evidence of stem cell functionality, lineage tracing has shown that they are capable of giving rise to all intestinal cell types (Sangiorgi and Capecchi, 2008) and single Bmi1$^+$ cells are capable of forming intestinal organoids in culture (Ootani et al., 2009). However, recent work from Hans Clevers' group has amassed evidence to show that the previously identified crypt-base-columnar cells (CBC) (Cheng and Leblond, 1974), found at the crypt base interspersed between paneth cells, can function as small intestinal stem cells. These cells can be identified by their unique expression of the Wnt target gene Leucine-rich repeat-containing G-protein coupled receptor 5 (Lgr5) (Barker et al., 2007), they were found to be actively cycling in contrast to the traditional view of a largely quiescent stem cell. The CBC compartment can also be located by expression of the markers achaete scutelike 2 (Ascl2) and olfactomedin 4 (Olfm4) (van der Flier et al., 2009b, van der Flier et al.,

2009a). Clevers' group has also shown that when Lgr5^{+} cells are isolated they can be cultured *in vitro* to successfully form intestinal organoids, further validating that Lgr5^{+} cells are small intestinal stem cells (Sato et al., 2009). Barker et al also noted that Lgr5^{+} cells also constitute the stem cells in the colon (Barker et al., 2007). Clevers' group have shown that each small intestinal crypt contains approximately 16 Lgr5^{+} cells, and along with Douglas Winton's group, have shown that the monoclonality of cells in the crypt-villus axis is attributed to the neutral drift of one stem cell populating the stem cell compartment with its progeny (Lopez-Garcia et al., 2010, Snippert et al., 2010). The study by Snippert et al suggests that stem cells may actually divide symmetrically. They propose that progenitor cells may arise not from asymmetric division but as they divide some stem cells move out of the stem cell niche and lose their 'stemness' to become progenitor cells (Snippert et al., 2010).

## 1.3.2   Quiescent and active stem cells?

The studies described above establishes that Lgr5 clearly marks a CBC stem cell population, however as previously mentioned there is also evidence that Bmi1 may also mark a population of stem cells. This has led to the hypothesis that there may be two pools of small intestinal stem cells, one actively cycling Lgr5 expressing cell, and a quiescent Bmi1 expressing cell (Li and Clevers, 2010). Studies investigating Bmi1 and Lgr5 as putative stem cell markers have revealed some similarities between the properties and positions of Bmi1 and Lgr5 expressing cells. For example, both Bmi1^{+} and Lgr5^{+} cells are capable of populating the crypt-villus axis with their progeny as evidenced by lineage tracing experiments (Barker et al., 2007, Sangiorgi and Capecchi, 2008), and both are able to be cultured to give rise to intestinal organoids (Sato et al., 2009, Ootani et al., 2009). There were also rare incidences of CBC cells that express Bmi1 and +4 position cells that express Lgr5 (Barker et al., 2007, Sangiorgi and Capecchi, 2008). However, despite Bmi1 being predominantly expressed in cells found at position +4 (the position of the label retaining cell in the Potten experiments) it is not known whether these cells are actively cycling, so it cannot be concluded that Bmi1^{+} cells are indeed quiescent. It was suggested by Potten et al that stem cells can be replaced by another uncommitted cell during stem cell loss (Potten et al., 1997), and maybe the Bmi1 expressing pool of cells represent that subpopulation of cells. This would give some explanation as to why both Bmi1 and Lgr5 expressing cells can form intestinal organoid cultures. Further support of a quiescent stem cell population has come from a study by Montgomery et al. They show that cells expressing mouse

telomerase reverse transcriptase (mTERT) are long-lived, slowly cycling cells found at position +4. mTERT$^+$ cells were able to produce all intestinal cell types (established by lineage tracing experiments) and contribute to regenerative response after injury. Interestingly, mTERT$^+$ cells were also predominantly Bmi1$^+$, and mTERT$^+$ cells were also found to give rise to Lgr5$^+$ cells, which suggests that these cells can replace Lgr5$^+$ actively cycling cells when needed (Montgomery et al., 2011). However, it is not addressed in this study whether this is a unique property of mTERT$^+$ cells or any cell within the crypt could give rise to an Lgr5$^+$ cell.

It may also be possible that the +4 position of the crypt (which lies just above the CBC/paneth cell compartment), may act as a 'lay-by' or 'pit-stop' for actively cycling stem cells that have sustained DNA damage. Damaged CBC cells may migrate into the +4 position and enter a quiescent state and remain like this until either the damage is repaired and they re-enter the CBC compartment, or they undergo apoptosis. This hypothesis gives some explanation as to why Bmi1$^+$ cells can produce intestinal organoids in culture, and are capable of populating the crypt-villus axis with their progeny in lineage tracing experiments *in vivo*. It may also provide an explanation as to why Potten and colleagues frequently observed apoptosis at the +4 position after irradiation, and why these cells retain DNA labeling long term. Why the intestine would require such a system is unclear, one hypothesis may be to preserve an epigenetic signature present in CBC cells that allows them to maintain pluripotency. Much more research is needed to fully understand the role and reason for these two cell populations.

### 1.3.3   Regulation of intestinal stem cell function and the stem cell niche

Stem cell function must be tightly controlled in order to maintain intestinal homeostasis, and it is thought that all stem cells require a niche to provide factors to control its activity, such that if the stem cells were removed from this niche they would lose their stem cell functionality. The mesenchymal stromal fibroblasts in the lamina propria surrounding the crypts are thought not just to provide structural support but they are also thought to constitute the intestinal stem cell niche (Shaker and Rubin, 2010) (Figure 1.2). Recent work from Sato et al has shown that the mature paneth cells provide a niche for Lgr5$^+$ crypt base columnar stem cells (Sato et al., 2011). Stromal-epithelial interactions between the intestinal stem cell niche and the overlying epithelium have been demonstrated in the intestine *in vivo*, with deletion of genes that alter signalling pathways in the underlying stroma of mice being shown to

impact on normal intestinal homeostasis. Deletion of the bone morphogenic signalling pathway receptor type II (BMPRII) specifically in the underlying stroma of the colon in mice resulted in the formation of epithelial hamartomas (Beppu et al., 2008). Similarly, stromal specific deletion of the serine/threonine kinase LKB1, which regulates AMPK and insulin receptor signalling, causes the development of epithelial hamartomas throughout the intestine through downregulation of the TGFβ pathway (Katajisto et al., 2008). Knockout mice have also been generated in which genes are disrupted that are expressed specifically in stromal cells, such as epimorphin (a protein involved in targeting vesicles to the plasma membrane) and the transcription factor FoxL1 (also known as Forkhead homologue 6 – Fhk6). Ablation of epimorphin in the mouse induced proliferation of the intestinal epithelium, in turn resulting in the alteration of crypt-villus architecture, evidenced by the lengthening of crypts and villi and villus bifurcation. Epimorphin loss was accompanied by concurrent downregulation of BMP signalling and upregulation of Wnt signalling, providing a mechanism by which this phenotype arises (Wang et al., 2006). Similarly, deletion of FoxL1 caused disruption of intestinal homeostasis resulting in abnormal crypt and villus size, expansion of the proliferative zone in the crypt and increased numbers of goblet cells. Again these phenotypes were coupled with downregulation of bone morphogenic proteins (BMPs), implicating the pathway in intestinal homeostasis (Kaestner et al., 1997). The Hedgehog signalling pathway is strongly implicated in intestinal homeostasis through its regulation of the Wnt pathway. Ligands secreted from the crypt epithelial cells activate the Hedgehog signalling pathway in neighbouring intestinal stromal cells, which in turn regulate epithelial cell function through upregulation of BMP expression. These interactions are further discussed in section 1.4.2. The role of signalling pathways in intestinal homeostasis will also be discussed further in section 1.4.


### 1.3.4   The colorectal cancer stem cell

It is known that each tissue type contains a number of stem cells that have the ability to give rise to many tissue cell types and maintain tissue homeostasis, the cancer stem cell theory postulates that cancers also possess 'stem cell-like' cells that have the capacity to maintain the bulk of the tumour with cells. It is thought that cancer stem cells may also be refractory to chemotherapy, therefore after the bulk of the tumour cells are depleted the cancer stem cells divide and give rise to more tumour cells causing relapse (Wicha et al., 2006, Clarke et al., 2006). There has been much research to identify these pools of cancer stem cells in order to develop

therapeutics that could potentially target these cells, thus preventing tumour growth. A number of studies have identified various cell surface markers that potentially identify cells with increased proliferative capacity, either by the ability to form colonies in culture or by serial transplantation in xenograft mouse models. Some of the candidate intestinal cancer stem cell markers include CD133, Lgr5, the epithelial cell adhesion molecule (EpCAM) and CD166 (Dalerba et al., 2007, O'Brien et al., 2007, Ricci-Vitiani et al., 2007, Takahashi et al., Vermeulen et al., 2008). Some of these markers are currently implicated as markers of normal intestinal stem cells. One could postulate that as these proteins mark cells that have increased proliferative and self-renewal capacity in normal tissue, they could also mark intestinal cancer stem cells. The ability of cancer cells to efflux drugs has also been used to select for the cancer stem cell population (Hirschmann-Jax et al., 2004), however this has been found not to be a useful marker of cancer stem cells in CRC (Burkert et al., 2008)

CD133 has been the most prominent candidate as a colorectal cancer stem cell marker. CD133$^+$ cells have been shown to have the capacity to initiate tumours upon transplantation into non-obese diabetic/severe combined immune deficiency (NOD/SCID) mice, but at low frequencies (O'Brien et al., 2007, Ricci-Vitiani et al., 2007). Vermeulen et al suggested that the cells used in these studies were not monoclonal, and this resulted in low frequency of tumour formation. They showed, by single cell cloning experiments, that 1 in 16 CD133+ cells produced a colony, and 1 in 5 cells that expressed both CD133 and CD24 produced a colony. All colonies were able to form tumours when transplanted into mice, which resembled the primary CRC from which they were derived (Vermeulen et al., 2008). Other proposed markers to determine the colorectal cancer stem cell population include EpCAM expressing cells (EpCAM$^{high}$/CD44$^+$/CD166$^+$) (Dalerba et al., 2007), Lgr5 and Wnt activated cells (Takahashi et al., Vermeulen et al., 2010).

Despite many elegant experiments in which cells are purified by their cell surface marker expression, and then serially transplanted into mice to produce tumours consistent in morphology to the primary tumour, there are a number of caveats raised by Hill and Kelly et al. to be taken into consideration. 1. Dissociation and culture of tumour cells may alter the cell surface marker expression, therefore cells expressing the markers with increase proliferative capacity *in vitro* may be different to those found *in vivo* (Hill, 2006). 2. Transplantation of tumour cells into mice does not recapitulate the human situation entirely, as it is unlikely that cells can be transplanted into the same environment from which they came, which may affect tumour cell growth (Hill, 2006). 3. Mouse growth factors required for tumour

propagation may not be compatible with growth of human tumours, so occasions when cells failed to reproduce tumours *in vivo* may be attributed to lack of compatible growth factors rather than the cells capacity to proliferate (Kelly et al., 2007). Finally in addition to the points raised by Hill and Kelly et al, 4. The *in vivo* transplantation experiments are carried out in immunocompromised mice, and thus is an artificial environment lacking in immune response to tumour cells. This could impact upon the frequency at which cells reproduce tumours. Despite these caveats, the possibility of identifying a pool of tumour cells that are responsible for sustained tumour growth and progression has great therapeutic implications.

## 1.3.5 Terminally differentiated intestinal cell types

### 1.3.5.1 The main mature cell lineages of the small intestine

The four main mature cell types in the small intestinal epithelium are either of an absorptive or secretory lineage. Enterocytes make up the majority of the differentiated cell types found in the villus and are of the absorptive lineage, responsible for uptake of nutrients. Enterocytes are specialised cells that are tightly packed together via cell-to-cell adhesions, this close association of cells helps to maintain cell polarity and provides a barrier to prevent microbes from entering the blood stream. The apical surface of enterocytes is made up of microvilli, which are specially adapted to increase the surface area of the cell to maximise absorption (Wright and Alison, 1984). Enterocytes express the enzyme alkaline phosphatase on their apical surface, which is a useful indicator of maturity of the enterocytes and polarisation of the epithelium.

The other three main cell types found in the small intestine are goblet cells, enteroendocrine cells and paneth cells, which are all of the secretory lineage. Goblet cells are found throughout the villus and are often found in the crypt around the crypt-villus junction. The function of goblet cells is to secrete mucins required for lubrication and protection of the epithelium, as it is subject to a substantial amount of mechanical stress through movement of food through the intestine. They also secrete trefoil proteins, which facilitate repair to damaged tissue (Mashimo et al., 1996). Alcian blue staining can be used to stain intestinal tissue sections to visualise the location of goblet cells. The stain binds to mucins present in goblet cells and marks them blue in colour. Enteroendocrine cells are found throughout the crypt-villus axis and are the least abundant of the four major cell types. They are part of the endocrine system and secrete hormones responsible for controlling gut function (Wright and

Alison, 1984). Grimelius silver staining can be used to locate enteroendocrine cells in the intestinal epithelium, argyrophilic granules present in the cells reduce silver ions marking the cells with black deposits. Goblet and enteroendocrine cells along with enterocytes, differentiate towards the upper region of the crypt, migrate upwards, and are lost from the villus tip after 2-3 days. The final mature cell type, paneth cells, are located at the base of the crypt and their migration pattern and turnover does not follow the same pattern as the other three cell types. Paneth cells differentiate and migrate downwards where they are long-lived cells. There is debate as to their lifespan, but it is thought to be between 3-8 weeks (Bjerknes and Cheng, 1981b, Ireland et al., 2005). Paneth cells are found exclusively in the small intestine and are responsible for innate immunity against pathogens through the secretion of anti-microbials such as lysozyme (Peeters and Vantrappen, 1975) and crypt defensins (Ouellette and Selsted, 1996). Recent findings suggest that paneth cells also form part of the stem cell niche for the CBC actively cycling stem cell pool (Sato et al., 2011). Paneth cells can be visualised by immunohistochemistry (IHC) in the small intestine by their exclusive expression of lysozyme.

### 1.3.5.2 Other cell types

Amongst the main four terminally differentiated cell types are two other lesser cell types, termed tuft cells and M cells respectively. The functions of these cell types are not well established. Tuft cells (also known as brush cells) are infrequently found in the intestinal epithelium and are so named due to a protruding 'tuft' of microvilli on their apical surface. The function of these cells is currently not fully understood, they are found throughout the respiratory epithelia and other epithelia of the digestive system. However, it is thought that these cells may have a sensory function in the intestine and may act as chemoreceptors (Gebhard and Gebert, 1999). Tuft cells are found in crypts and villi of the small intestine, and recently the putative stem cell marker DCAMKL-1 was proven to mark tuft cells rather than the small intestinal stem cell (Gerbe et al., 2009). M cells represent another intestinal cell type that form part of the mucosal immune defense against pathogens. These cells are associated with the peyer's patch lymphoid tissue found in the small intestine (Owen and Jones, 1974), and they function as transporters of antigens from the lumen to the underlying immune cells (Kraehenbuhl and Neutra, 2000).

## 1.4 Maintenance of intestinal homeostasis

### 1.4.1 The Canonical Wnt pathway

The canonical Wnt signalling pathway (Clevers, 2006) was identified through analysis of mutations in the Wingless (Wg) gene discovered in Drosophila and the Int-1 (Int) gene in mice (a site of insertion for the mouse mammary tumour virus) (Rijsewijk et al., 1987), combination of the two gene names resulted in the term Wnt. The Wnt pathway is one of the key developmental pathways, and is strongly associated with cancer, and in particular CRC. The Wnt pathway is normally in its 'off state' (outlined in Figure 1.3), activation of the pathway results in transcription of an array of Wnt target genes conducive to tumourigenesis, for example genes involved in proliferation, migration and adhesion. The Wnt pathway involves many proteins that regulate the accumulation and cellular localisation of the transcription transactivator β-catenin. The Wnt pathway is controlled by frizzled receptors (7 pass transmembrane proteins) on the cell surface that bind Wnt ligands. In the 'off-state', when no Wnt ligands are present, a number of proteins form the β-catenin destruction complex that prevent β-catenin from accumulating in the cytoplasm and entering the nucleus where it can activate transcription of Wnt target genes. The β-catenin destruction complex involves the association of a number of proteins, three of the key proteins involved are: adenomatous polyposis coli (APC), glycogen synthase kinase-3 (GSK-3) and axis inhibitor (AXIN). These proteins bind to β-catenin present in the cytoplasm, allowing GSK-3 to phosphorylate β-catenin, marking it for degradation by the proteasome. When the Wnt pathway is in its 'on-state', Wnt ligands bind to the frizzled receptor, activating the dishevelled protein, which leads to the inhibition the β-catenin destruction complex. β-catenin then accumulates in the cytoplasm where it then enters the nucleus and allows the transcription of T-cell factor and Lymphoid enhancer factor (Tcf/Lef) Wnt target genes (Figure 1.3).

The canonical Wnt signalling pathway drives proliferation in the intestine and maintains homeostasis. Studies in which the Wnt signalling pathway was inhibited at various points in the pathway, have shown that loss of Wnt signalling perturbs normal intestinal structure and proliferation. Overexpression of the Wnt antagonist Dkk1 resulted in shortening of crypts and villi, a decrease in proliferation and depletion of secretory cells (Pinto et al., 2003). Similarly, deletion of β-catenin and the Wnt target gene c-Myc in adult mouse intestine results in ablation of the crypts, and in the case of β-catenin deficiency, loss of goblet cells (Ireland et al., 2004, Muncan et al., 2006). Mice deficient for the Wnt transcription factor Tcf-4, possess no intestinal proliferative

compartments, only differentiated cells (Korinek et al., 1998). These studies highlight the dependence of the proliferative capacity of intestinal stem and progenitor cells on activation of the Wnt signalling to maintain intestinal mucosal structure. Conversely, studies have also been carried out in which the Wnt pathway is aberrantly activated. Homozygous deletion of Apc causes rapid activation of the Wnt pathway throughout the epithelium, due to loss of the β-catenin destruction complex. This confers a 'crypt-progenitor' phenotype on all the epithelial cells, mislocalisation of paneth cells and increased proliferation and migration (Sansom et al., 2004). Andreu et al showed that it is activation of the Wnt pathway in crypt progenitor cells that drives the Apc loss phenotype, even though villus cells are also deficient for Apc they have lost the capacity to proliferate (Andreu et al., 2005). Sansom et al showed that the Wnt target gene c-Myc is required for the intestinal phenotype after Apc loss, as shown when concomitant deletion of Apc and c-Myc rescued the Apc phenotype (Sansom et al., 2007).

Appropriate control of the Wnt signalling pathway in the stem cell compartment via the stem cell niche is pivotal for normal intestinal development and homeostasis. In order to achieve this, specific spatial expression of many Wnt agonists and antagonists can be detected throughout the intestinal epithelium and underlying stroma (Gregorieff et al., 2005). The expression of these Wnt agonists and antagonists maintains a gradient of Wnt activity throughout the crypt-villus axis, with the cells found at the base of the crypt (i.e. intestinal stem cells) maintaining a high level of Wnt activation and progenitors and differentiated cells having no Wnt activation (Gregorieff et al., 2005). Tight regulation of when and where the Wnt pathway is activated is also necessary for correct migration and localisation of cell types, as well as control of proliferation and homeostasis. Deletion of the Wnt target genes EphB2 and EphB3 results in perturbed cell migration and positioning of paneth cells (Batlle et al., 2002). The Wnt pathway is the main driving force behind maintaining intestinal homeostasis, Wnt signalling is therefore the subject of much control by other signalling pathways (see below).


1.4.2   The Hedgehog pathway

The Hedgehog signalling pathway is similar to the canonical Wnt signalling pathway, in that both pathways involve tight control between degradation and activation of a protein involved in the transcription of target genes. The Hedgehog pathway is outlined in Figure 1.3. Hedgehog signalling is governed by two membrane-

spanning proteins called Patched and Smoothened. In the pathways 'off-state', Patched normally suppresses the activation of Smoothened via the pumping of inhibitory molecules that inhibit the action of Smoothened. When Smoothened is inactive, protein kinase A (PKA) is able to phosphorylate the cytoplasmic transcription factors Gli2/3, resulting in preferential targeting of the Gli2 part of the complex for degradation, leaving the truncated Gli3 protein. The truncated Gli3 protein then enters the nucleus, binds to the Hedgehog target genes and acts as a transcriptional repressor. There are three Hedgehog ligands found in vertebrates, Sonic Hedgehog (Shh), Indian Hedgehog (Ihh) and Desert Hedgehog (Dhh). When these bind to Patched they prevent the suppression of Smoothened, which when activated prevents the phosphorylation and subsequent partial degradation of Gli2/3. This active form of Gli2/3 is then able to enter the nucleus and bind to Hedgehog target genes and initiate transcription of the genes reviewed in (van den Brink, 2007). The FoxL1 and FoxF1 transcription factors have been shown by Madison et al to be Hedgehog target genes through the demonstration that they have Gli binding sites in the non-coding regions of the genes (Madison et al., 2009). This finding, along with the previous finding by Kaestner et al that FoxL1 deletion downregulates BMP signals and in turn activates Wnt signals (Kaestner et al., 1997), places Hedgehog signalling as an upstream regulator of canonical Wnt activation. Hedgehog signalling acts in a paracrine manner, Hedgehog ligands are expressed in the epithelium and secreted, in turn activating Hedgehog signalling in stromal cells (Yauch et al., 2008, Kolterud et al., 2009, Madison et al., 2005).

The Hedgehog signalling pathway appears to be near the top of a chain of signalling events that ultimately leads to the regulation of Wnt signalling and intestinal homeostasis. Recently two similar studies by van Dop et al and Kosinski et al showed that deletion of the Ihh gene specifically within the intestinal epithelium causes increased proliferation, crypt fission, expansion of the stem cell pool, an increase in secretory cells, a block of enterocyte differentiation and loss of cellular components of the underlying muscularis mucosae (Kosinski et al., 2010, van Dop et al., 2010). Both studies showed that these effects were controlled by downregulation of BMPs and concomitant upregulation of Wnt signalling. Kosinski et al also demonstrated that Ihh signals in a paracrine manner to the underlying stromal and smooth muscle fibroblasts, by deleting the Hedgehog activator Smoothened from the intestinal epithelium with no phenotypic effects. However, they used an epithelial deletion strategy that resulted in post-natal lethality so could not investigate the long term effects of Ihh loss (Kosinski et al., 2010). Van Dop et al showed that prolonged deletion of Ihh within adult
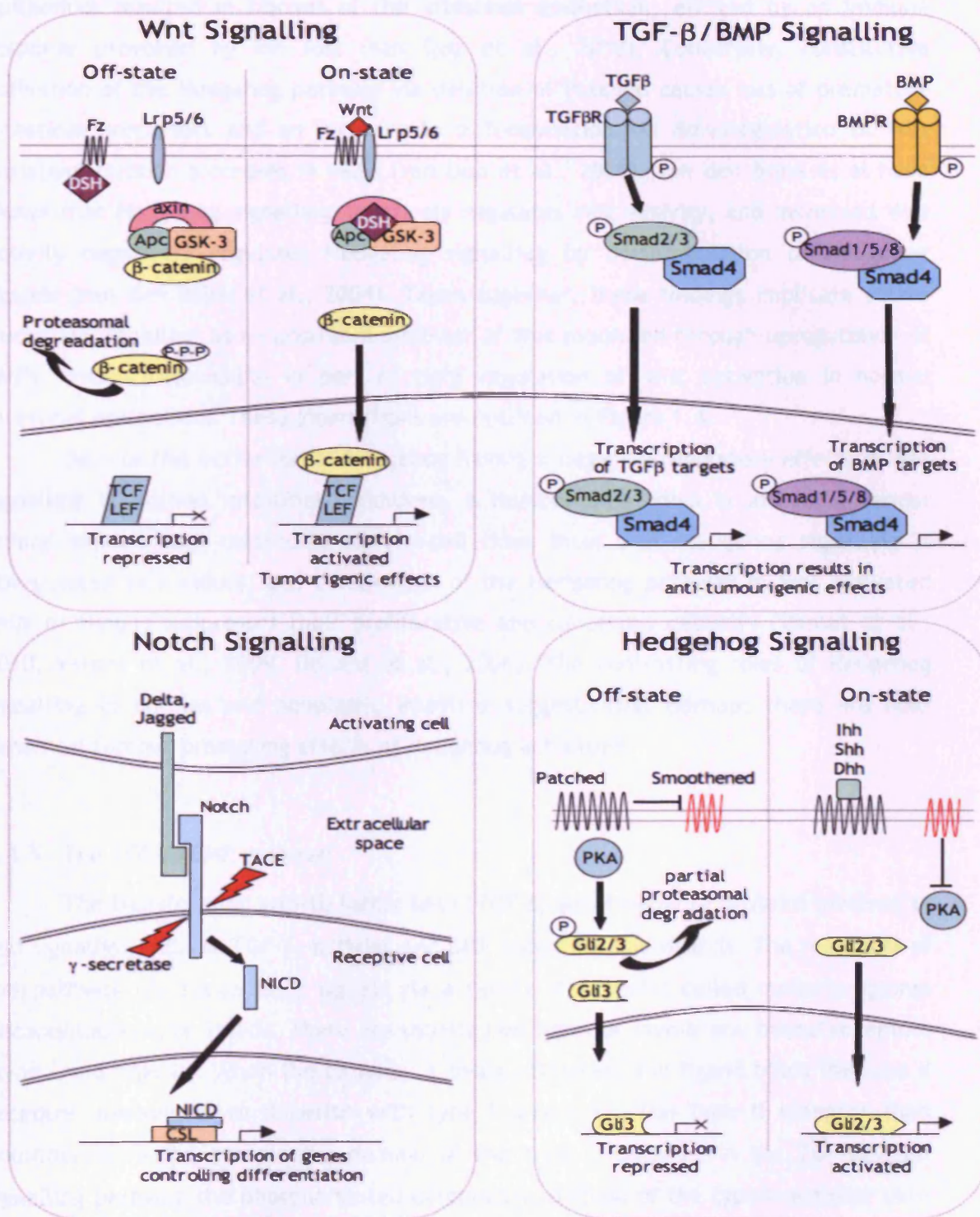
**Figure 1.3 Four main pathways that govern intestinal homeostasis**

Schematic outlines of the four main signalling pathways involved in maintaining intestinal homeostasis. The canonical-Wnt pathway primarily controls proliferation, and Hedgehog and BMP signalling form part of a feedback mechanism that controls activation of the canonical-Wnt pathway. Notch signalling primarily governs differentiation, high Notch activity maintains crypt cells in an immature state. The Wnt, TGF-β/BMP and Hedgehog signalling pathways can be activated by autocrine and paracrine signalling. The Notch pathway is activated by juxtacrine signalling.

epithelium resulted in fibrosis of the intestinal epithelium, elicited by an immune response provoked by Ihh loss (van Dop et al., 2010). Conversely, constitutive activation of the Hedgehog pathway via deletion of Patched causes loss of premature intestinal precursors and an increase in differentiation via downregulation of Wnt signalling through increases in BMPs (van Dop et al., 2009). van den Brink et al have shown that Hedgehog signalling negatively regulates Wnt activity, and increased Wnt activity negatively regulates Hedgehog signalling by downregulation of Hedgehog ligands (van den Brink et al., 2004). Taken together, these findings implicate active Hedgehog signalling as an upstream inhibitor of Wnt mediated through upregulation of BMPs, and is responsible in part of tight regulation of Wnt activation in normal intestinal epithelium. These interactions are outlined in Figure 1.4.

Despite the activation of Hedgehog having a negative regulatory effect on Wnt signalling in normal intestinal conditions, a number of studies in intestinal cancer animal models and colorectal cancer cell lines show that Hedgehog signalling is upregulated in tumours, and inactivation of the Hedgehog pathway in Wnt activated cells or tissues suppresses their proliferative and cancerous capacity (Varnat et al., 2010, Varnat et al., 2009, Douard et al., 2006). The contrasting roles of Hedgehog signalling in normal and neoplastic intestine suggests that perhaps there are non-canonical tumour promoting effects of Hedgehog activation.

### 1.4.3 The TGF-β/BMP pathway

The transforming growth factor beta (TGF-β) superfamily of proteins involved in cell signalling include TGF-β, activins and BMP receptors and ligands. The receptors of the pathway transduce their signals via a family of proteins called mothers against decapentaplegic or Smads. There are usually two types of membrane bound receptors (type I and type II). When the pathway is being activated, the ligand binds the type II receptor allowing it to dimerise with type I receptors. The type II receptor then phosphorylates the cytoplasmic domain of the type I receptor. In the TGF-β/Smad signalling pathway the phosphorylated cytoplasmic domain of the type I receptor then recruits and phosphorylates either the Smad2 or Smad3 cytosolic proteins. In the case of BMP signalling the type I receptor recruits and phosphorylates either Smad1, Smad5 or Smad8. The Smads that are recruited to the receptors and phosphorylated are collectively known as the receptor regulated Smads (or R-Smads). The R-Smads then dissociate from the receptor and form a complex with Smad4 (or also known as the
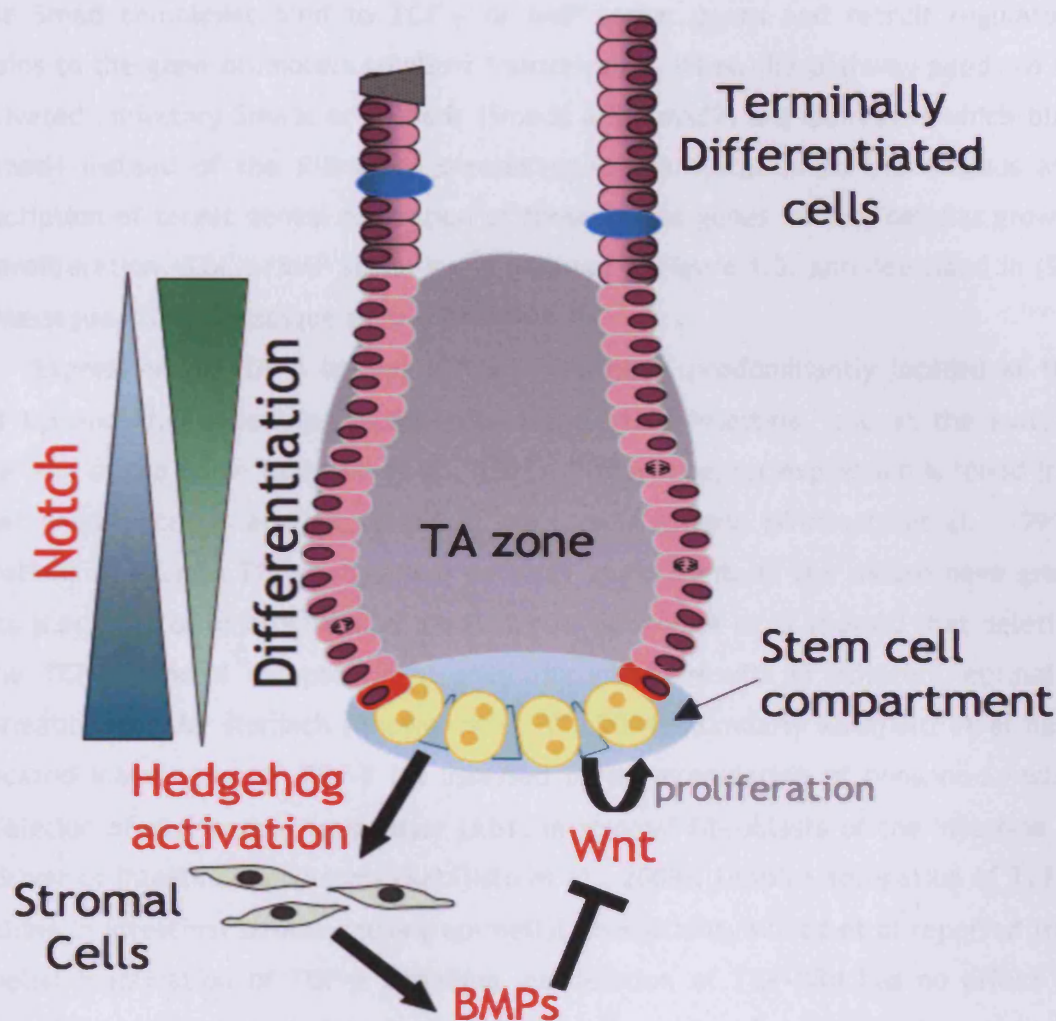
**Figure 1.4 Signalling pathway interactions that maintain intestinal homeostasis**

Appropriate control of the various signalling pathways controlling proliferation, differentiation and apoptosis is paramount to maintain intestinal homeostasis. The canonical-Wnt pathway drives proliferation of stem and progenitor cells to replace the rapid loss of cells from the villus tip. Thus, Wnt pathway activation is tightly controlled by secretion of Hedgehog ligands by epithelial cells, that activate Hedgehog signalling in the underlying stromal cells of the stem cell niche governing transcription of TGF-β and BMP agonists, which control activation of the Wnt pathway in adjacent epithelial cells. Juxtacrine activation of the Notch signalling pathway maintains epithelial progenitor and stem cells in an undifferentiated state. Notch activation is present in a decreasing gradient up the crypt axis, which inversely correlates with differentiation state of the epithelial cells along the axis.

co-Smad), which then allows the translocation of the complex into the nucleus. These active Smad complexes bind to TGF-β or BMP target genes and recruit regulatory proteins to the gene promoters to allow transcription. When the pathway needs to be inactivated inhibitory Smads or I-Smads (Smad6 and Smad7) are expressed which bind to Smad4 instead of the R-Smads, preventing its translocation to the nucleus and transcription of target genes. Activation of these target genes inhibits cellular growth and proliferation, TGF-β/BMP signalling is outlined in Figure 1.3, and described in (Shi and Massague, 2003, Massague et al., 2000).

Expression of TGF-β ligands in the intestine is predominantly located at the villus tip and the underlying muscularis of the small intestine, and at the surface epithelium of the colon (Barnard et al., 1993). TGF-β receptor expression is found in a similar pattern but is also expressed in the lamina propria (Winesett et al., 1996). Alterations of various TGF-β signalling pathway components in the mouse have given rise to a number of gastrointestinal phenotypes. Bhowmick et al showed that deletion of the TGF-β type II receptor in stromal fibroblasts results in adjacent epithelial abnormalities in the stomach (Bhowmick et al., 2004). Similarly Katajisto et al have implicated inactivation of TGF-β (as assessed by downregulation of phospho-Smad2), via deletion of the tumour suppressor Lkb1, in stromal fibroblasts of the intestine as the driver of intestinal neoplasms (Katajisto et al., 2008). Despite abrogation of TGF-β signalling in intestinal stroma causing epithelial aberrations, Muñoz et al reported that epithelial inactivation of TGF-β signalling via deletion of TGF-βRII has no effect on intestinal homeostasis and does not predispose to tumour formation (Munoz et al., 2006). Mouse models heterozygous for constitutive mutations of Smad4 (the mediator of both TGF-β and BMP signalling pathways) are predisposed to the formation of intestinal tumours (Takaku et al., 1999, Hohenstein et al., 2003). However, intestinal epithelial specific deletion of Smad4 does not give rise to intestinal tumours (Kim et al., 2006). TGF-β inactivation in the immune system (particularly T cells) has been shown to induce colitis and irritable bowel disease in mice, therefore indicating a role for TGF-β in suppression of autoimmune response on the intestine (Coombes and Maloy, 2007). Loss of Smad4 specifically within T cells predisposes the mouse to intestinal tumours (Kim et al., 2006). It can be concluded from these studies that TGF-β potentially acts through stromal-epithelial interactions through both the intestinal supporting stroma and immune cells to maintain intestinal homeostasis, and inactivation of the pathway results in epithelial aberrations.

The role of BMP signalling in maintaining intestinal homeostasis is well characterised. As previously mentioned, Hedgehog signalling appears to control Wnt

signalling by controlling the expression of BMPs that in turn inhibit Wnt signalling (see section 1.4.2). Ectopic expression of the BMP inhibitor Noggin in the mouse intestine resulted in the *de novo* formation of crypts and hyperplastic epithelium (Haramis et al., 2004). The hyperplastic epithelium observed in these mice resembled the intestinal epithelium of Juvenile Polyposis Syndrome (JPS) patients, a hereditary gastrointestinal tumour predisposition disease, in which Smad4 and BMPR deletions have been implicated (Howe et al., 2001, Howe et al., 1998). Consistent with the Haramis et al study, intestinal inactivation of BMP signalling through deletion of the BMP receptor 1a leads to the formation of hyperplastic polyps (He et al., 2004). He et al also noted an expansion of the proliferative compartment of the intestine (He et al., 2004). Another study in which BMPR1a was deleted from the intestinal epithelium resulted in increased proliferation and elongated villi but did not result in *de novo* crypt or polyp formation (Auclair et al., 2007). The differences between the Auclair et al study and the He et al study may be attributable to differing BMPR1a ablation strategies. He et al used a conditional transgenesis technique that acts not only in the intestinal epithelium but also in the underlying stroma, thereby implicating a role for stromal inactivation of BMP signalling in intestinal tumourigenesis. The role of the BMP pathway in stromal-epithelial interactions has previously been mentioned (see section 1.3.3). Stromal specific deletion of BMP receptor type II results in the formation of epithelial polyps (Beppu et al., 2008). The observation that stromal inactivation of BMP signalling is sufficient to initiate tumourigenesis, but that epithelial loss of BMP signalling also promotes proliferation, suggests that BMP signalling acts in both a paracrine and autocrine manner. The observation that the ligand BMP2 is expressed by colonic epithelial cell lines and acts in an autocrine manner (Hardwick et al., 2004) further supports this.


## 1.4.4   The Notch pathway

The Notch signalling pathway (Mumm and Kopan, 2000) involves juxtacrine transduction of signals between cells outlined in Figure 1.3. The Notch receptor is a single pass transmembrane protein expressed on the surface of responding cells, named after the disruption of the gene in Drosophila that causes notches in the fly wing (Hunt Morgan, 1919). Mammalian Notch receptors include Notch 1-4. Notch ligands (mammalian Notch ligands are Delta like 1,3 and 4 and Jagged 1 and 2)) are expressed on the cell surface of adjacent cells and are able to bind Notch receptors of neighbouring cells when in close contact. The binding of Notch ligands to the Notch

receptor causes two irreversible proteolytic cleavages of the extracellular domain by the membrane-bound enzyme, tumour necrosis factor converting enzyme (TACE), and an intramembrane cleavage by γ-secretase which in turn releases a the Notch receptor intracellular domain (NICD) into the cytoplasm. Once the released cytoplasmic fragment of the Notch receptor is in the cytoplasm it translocates to the nucleus where it binds to the transcription factor CBF1/RBP-Jκ/Suppressor of Hairless/LAG-1 (CSL) to activate Notch target genes. The Notch receptor, once activated, undergoes irreversible cleavage, so therefore the extracellular domain must undergo recycling and the receptors and ligands must be replaced. This is in contrast to other types of signalling where the receptors can switch between on and off states by ligand binding (e.g. Wnt, PI3K, TGF-β signalling).

Notch signalling plays a role in controlling the differentiation of intestinal epithelial cells, Notch is predominantly active in the intestinal crypts and is thought to maintain the crypt progenitors in an undifferentiated state via upregulation of transcriptional repressor Hes1, which in turn represses Math1 (van Es et al., 2005). Loss of Math1 results in loss of secretory goblet and enteroendocrine cells (Yang et al., 2001, van Es et al., 2010). Whereas inhibition of Notch signalling, either via deletion of the Notch transcription factor CSL, the administration of γ-secretase inhibitors (therefore preventing the cleavage of the NICD) or ectopic expression of Math1 in the adult intestine, causes the conversion of immature progenitors into terminally differentiated secretory cells (van Es et al., 2005, VanDussen and Samuelson, 2010). VanDussen and Samuelson also showed that epithelial ectopic expression of Math1 also induces expansion of stromal cells, which suggests that the intestinal stem cell niche may have expanded to try and maintain the undifferentiated status of the epithelial stem cells (VanDussen and Samuelson, 2010). A recent study by Pellegrinet et al further implicates inactivation of Notch, via deletion of Notch ligands Delta1 and Delta4, with regulation of intestinal cell differentiation. Consistent with previous studies, inactivation of Notch signalling in the adult mouse intestine resulted in conversion of immature progenitors into secretory cell types. Interestingly these mice died rapidly after loss of Delta1 and 4 due to crypt loss. Quantification of intestinal stem cells in this model indicated that loss of Delta1 and 4 ablates the stem cell population (Pellegrinet et al., 2011). The observation made in Pellegrinet et al that intestinal epithelial specific deletion of Notch ligands Dll1 and 4 phenocopies intestinal epithelial deletion of CSL and Notch receptor suggests that paracrine Notch signalling must be activated by neighbouring epithelial cells, unlike Hedgehog signalling which relies on stromal-epithelial interactions (see section 1.4.2). However, as manipulation

of Notch components in the stroma has not been investigated the contribution of activation of Notch from neighbouring stromal cells cannot be ruled out.

From the conditional manipulation of Notch signalling in the adult intestine it is established that Notch signalling is essential for maintaining the progenitor status of intestinal crypt cells and in maintaining stemness. Notch works in concert with Wnt activation to prevent differentiation of crypt cells whilst Wnt controls homeostasis by regulating proliferation.

### 1.4.5 The JNK pathway

The c-Jun N-terminal Kinase (JNK) signalling pathway is one of the Mitogen Activated Protein Kinase (MAPK) cascades. It phosphorylates the N-terminal of the oncoprotein c-Jun (a canonical-Wnt target gene) and activates it, amongst other proteins such p53 and Smad4, which then go on to allow the transcription of their target genes. JNK can be activated in many ways through the non-canonical Wnt signalling pathway (Boutros et al., 1998), receptor tyrosine kinases (RTKs), cytokine receptors (Minden et al., 1994, Sluss et al., 1994), G protein-coupled receptors (Coso et al., 1995) and through stress conditions (Adler et al., 1995). Most of the pathways converge on activation of Mitogen activated protein kinase kinase kinases (MAPKKK), which in turn activates MAP kinase kinase4/7 (MKK4/7) that activates JNK, others activate Rac which is upstream of MAPKKK.

There has been little research into the role of JNK in the intestine, however one study by Sancho et al showed that intestinal specific activation of JNK disrupts intestinal homeostasis (Sancho et al., 2009). JNK activation in mice caused an in increase in villus length, the proliferative zone and an increase in proliferation of CBC cells. They found an upregulation of c-Jun target genes such as cyclin D1 and CD44, interestingly they also found upregulation of genes associated only with the canonical-Wnt pathway, which were also Tcf4 target genes. They showed that certain Tcf4 target genes also have binding sites for c-Jun. This overlap in gene expression between the JNK and canonical-Wnt pathways is likely to be driving the JNK activated phenotype, as deletion of c-Jun results in a contrary phenotype of shorter villi and decreased proliferation. They also noted that activated JNK accelerates colitis-induced tumourigenesis, but has no effect on tumourigenesis in the Apc^{Min} mouse intestinal tumour model (Sancho et al., 2009). Sancho et al postulated that this differential effect of JNK activation on the two models of intestinal tumourigenesis is due to activation of c-Jun. c-Jun is present at low levels in colitis induced intestinal tumours,

so therefore JNK activation would accelerate tumourigenesis in this model by activation of c-Jun. However, tumours present in the Apc$^{Min}$ mouse model already have high levels of c-Jun present so activation of JNK would have no effect on tumourigenesis (Sancho et al., 2009).

## 1.5 The Fearon-Vogelstein model of colorectal cancer progression

Modulation of the aforementioned signalling pathways involved in intestinal homeostasis, through mutations in key tumour suppressors and oncogenes gives rise to CRC. The development of CRC is a multistep process in which the accumulation of a number of genetic mutations leads to the progression of a tumour from dysplastic epithelium, to benign adenoma through to metastatic carcinoma. In their seminal paper Fearon and Vogelstein proposed a model of the genetic pathway of CRC progression, by the comprehensive review of available histopathological and genetic data (Fearon and Vogelstein, 1990). This model has become the classical view of CRC progression. It describes mutations in the APC gene as the initiating mutation in the formation of a benign lesion, then subsequent mutations in kirsten rat sarcoma viral oncogene homolog (KRAS), allelic loss of 18q locus and mutation in p53, all contributing to the progression of a benign tumour to malignant disease (Figure 1.5). However, it would be naïve to assume that all CRCs followed this pathway of progression exactly, Fearon and Vogelstein observed an increase in the number of these specific genetic alterations in more advanced tumours but each advanced tumour did not possess all alterations. They also suggested that it is not necessarily the order that these alterations occur for the formation of carcinoma but simply the accumulation of alterations that leads to advanced disease (Fearon and Vogelstein, 1990). A further study by Smith et al into the common genetic alterations outlined by Fearon and Vogelstein, found that in a large cohort of CRCs only 6.6% of the tumours analysed carried concomitant mutations in APC, KRAS and p53, suggesting that alternative pathways to the Fearon-Vogelstein progression pathway must also be involved in progression to carcinoma in the intestine (Smith et al., 2002).

### 1.5.1 APC and the canonical-Wnt pathway

APC is the first mutation implicated in the formation of CRC, loss of APC results in early adenoma formation (Powell et al., 1992). APC encodes a protein that plays a central role in the canonical-Wnt signalling pathway. As previously described, the canonical-Wnt signalling pathway is the main driving force behind sustained proliferation in the crypt and intestinal homeostasis (see section 1.4.1). Mutations that

activate the canonical-Wnt pathway are thought to be the primary mutation in intestinal tissue that leads to tumour initiation. This is easy to understand, as acute Wnt pathway activation in the mouse driven by homozygous Apc deletion leads to rapid expansion of crypt progenitor-like cells and mouse morbidity (Sansom et al., 2004). There are other mutations in CRC, as well as loss of APC function, that result in Wnt pathway activation i.e. mutations that stabilise β-catenin (Morin et al., 1997) and deletion of the scaffold protein AXIN (Liu et al., 2000). Germline mutations in the gene APC give rise to the inherited condition familial adenomatous polyposis (FAP), where the patient is predisposed to the formation of many intestinal polyps that frequently progress to CRC (Kinzler et al., 1991). Deletion of APC or stabilisation of β-catenin renders the destruction complex of the canonical-Wnt pathway useless. APC associates with β-catenin allowing it to be marked for degradation via phosphorylation by GSK-3 (the canonical Wnt pathway is outlined in Figure 1.3). Loss of Apc, Axin or mutation of β-catenin preventing its phosphorylation results in constitutively active Wnt signalling.
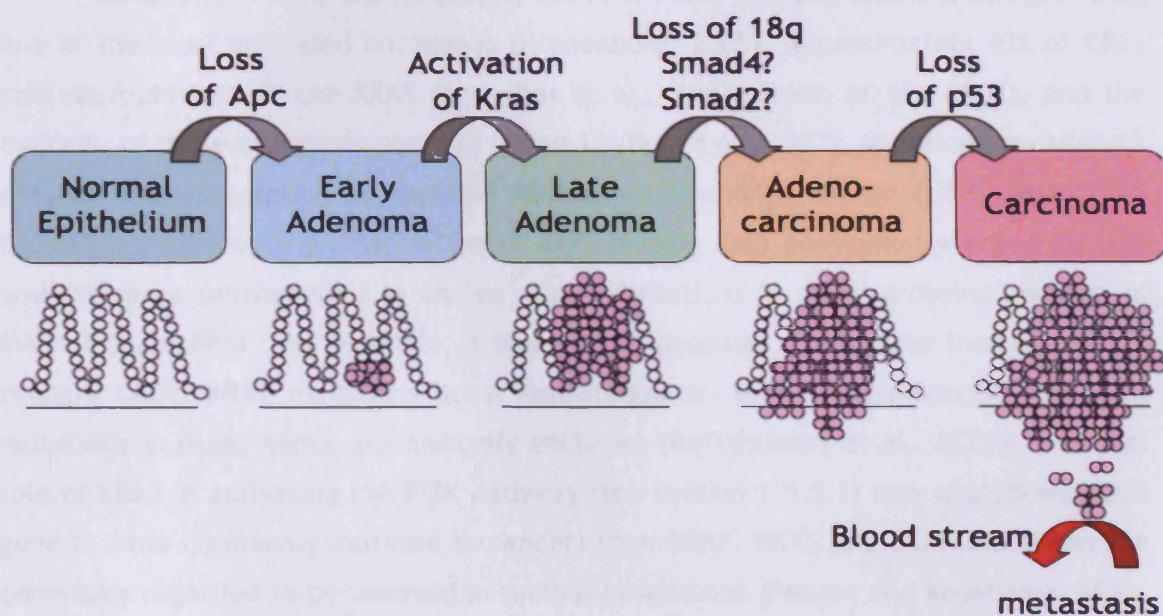


**Figure 1.5 The Fearon-Vogelstein step wise progression of CRC**

The schematic diagram outlines the proposed pathway of progression in the formation of metastatic colorectal cancer from normal epithelium. Below each stage is a schematic view of the intestinal epithelium, the pink circles represent neoplastic cells, the straight line represents the smooth muscle wall. Loss of APC is regarded as the initiating mutation and the first step towards tumour formation, additional activation of oncogenes such as KRAS and loss of the 18q chromosome arm culminate in the formation of invasive adenocarcinomas. Finally, loss of the tumour suppressor p53 promotes metastasis of the tumour.

## 1.5.2 Kras and the MAPK/Erk pathway

Mutations in the oncogene KRAS are the next step in progression from early adenoma to intermediate adenoma. KRAS is the downstream mediator of the Mitogen activated protein kinase/Extracellular regulated MAP kinase (MAPK/Erk) pathway. The MAPK/Erk pathway is an elaborate kinase cascade signalling pathway, one of the family of MAPK cascades, which is primarily implicated in development, growth and cancer. The MAPK/Erk pathway is stimulated by RTKs, integrins and influx of calcium ions. In the case of RTKs and integrin mediated stimulation, activation of the receptors lead to the activation of Growth factor receptor-binding protein 2 (Grb2), which activates Sons of Sevenless homolog (SOS) that in turn activates the small GTPase KRAS. SOS facilitates the dissociation of GDP and subsequent binding of GTP to Kras, which causes the protein to become active. Kras activates both CRAF and BRAF, which phosphorylates the mitogen activated kinase1/2 (MEK1/2), and which in turn phosphorylates Erk that then goes on to act on its cytoplasmic and nuclear targets, the majority of which are transcription factors.

Mutations in KRAS are frequently found in many cancers, and it is thought to be one of the most activated oncogenes (Kranenburg, 2005). Approximately 40% of CRCs contain mutations in the KRAS gene (Bos et al., 1987, Smith et al., 2002), and the majority of these mutations occur at codon 12 (Bos et al., 1987). Mutations in codon 12 prevent the association of guanine nucleotide exchange factor (GEF) with KRAS therefore inhibiting the dissociation of ATP, leaving Kras permanently bound to GTP and therefore permanently in an 'on state'. Mutations in other proteins involved in MAPK include BRAF. For example, a study by Rajagopalan et al found that in a set of primary CRCs, BRAF mutations occur less frequently than KRAS mutations and that mutations in these genes are mutually exclusive (Rajagopalan et al., 2002). The dual role of KRAS in activating the PI3K pathway (see section 1.5.5.1) may explain why this gene is more commonly mutated in cancers than BRAF. KRAS and BRAF mutations are commonly regarded to be involved in tumour progression (Fearon and Vogelstein, 1990, Rajagopalan et al., 2002). However, there is also evidence to suggest that these oncogenes may also be involved in the initiation of intestinal tumours (Jass et al., 1999) and they form the basis of an alternative pathway of CRC formation called the Serrated Adenocarcinoma pathway (Makinen, 2007).

### 1.5.3 Allelic loss of 18q and TGF-β/BMP pathway

Fearon and Vogelstein describe allelic loss of the 18q chromosomal region as a common genetic aberration found in 70% of carcinomas and 50% of late adenomas. They suggest that the candidate tumour suppressor deleted in colorectal cancer (DCC) found in this region of the chromosome may be responsible for tumour progression, as it is commonly lost in carcinomas but present in normal mucosa (Fearon and Vogelstein, 1990, Fearon et al., 1990). The DCC gene encodes a receptor for the ligand netrin that controls axonal growth in development (Keino-Masu et al., 1996). The role of DCC in the intestine is unclear despite its loss in carcinomas, deletion of gene in the mouse had no phenotypic effect on the intestine (Fazeli et al., 1997). DCC$^{-/-}$ mice died shortly after birth, however DCC$^{+/-}$ mice survived into adulthood but did not possess any predisposition for intestinal tumours. Heterozygous DCC loss did not promote tumour progression or multiplicity in Apc$^{Min}$ mice. Fazeli et al suggest that the loss of DCC in human CRC may only be a consequence of loss of part of chromosome 18 and other linked genes may be responsible for tumour phenotypes (Fazeli et al., 1997).

Another gene found at the 18q locus that may be linked to CRC is Smad4 (also known as DPC4) (Thiagalingam et al., 1996). As previously described in section 1.4.3, Smad4 is involved in the downstream signalling of the TGF-β/BMP pathway, known also as the co-Smad. When bound to its coactivators, Smad4 activates transcription of the pathways target genes. Smad4 is commonly found to be mutated in the germline of JPS patients (Howe et al., 1998). As previously mentioned, Smad4$^{+/-}$ mice are predisposed to intestinal tumours, through loss of heterozygosity (LOH) of the gene (Hohenstein et al., 2003, Takaku et al., 1999). In another study Takaku et al showed that Smad4 deletion *in cis* with Apc mutation (Apc is also on chromosome 18 in the mouse) enhances the malignancy of tumours arising in these mice through LOH, specifically loss of the remaining whole chromosome 18 (Takaku et al., 1998). Despite these studies confirming a role for Smad4 in intestinal tumourigenesis, epithelial specific loss of Smad4 does not promote tumour initiation, but T cell specific loss does (Kim et al., 2006). Takaku et al show evidence of enhanced stromal components in Apc$^{Min}$ Smad4$^{+/-}$ tumours (Takaku et al., 1998). Evidence in JPS patients also suggests a stromal role for the gene in promoting tumourigenesis (Kinzler and Vogelstein, 1998). Taken together these findings suggest that stromal loss of Smad4 plays a role in tumourigenesis. Another gene associated with CRC also located on chromosome 18q and implicated in TGF-β signalling is Smad2 (Eppert et al., 1996). There have been no reported mouse models of intestinal specific Smad2 knockout, and constitutive Smad2 knockout mice are embryonic lethal so no intestinal phenotype has been observed (Waldrip et al.,

1998). Taken together, allelic loss of 18q is closely associated with CRC progression, this association is likely to be linked to a number of tumour suppressors found at this locus most likely Smad4 and Smad2.


## 1.5.4 Mutation of p53 and malignancy

The final mutation in the Fearon-Vogelstein model of CRC progression occurs in the p53 gene, which is thought to be responsible for progression to malignant disease (Fearon and Vogelstein, 1990). The p53 gene was the first tumour suppressor gene to be discovered (Vogelstein et al., 2000), it responds to cellular stresses that cause DNA damage allowing the cell to either repair the damaged DNA, or undergo apoptosis. In normal cellular conditions p53 is present in cells at low levels and bound to the protein mouse double minute 2 homolog (MDM2), MDM2 ubiquitinates p53 causing it to be degraded. Modifications of the p53 protein (e.g. phosphorylation, acetylation and sumoylation) induced by cellular stress and DNA damage cause conformational changes in p53 preventing its association with MDM2, which allow it to enter the nucleus and promote transcription of cell cycle inhibitors or mediate apoptosis, p53 function is reviewed in (Vogelstein et al., 2000). Loss of p53 function therefore removes the 'braking-system' of the cell that allows it to repair DNA damage or undergo apoptosis before continuing to proliferate, thus predisposing the cell to mutations and neoplastic transformation. Germline mutations in the p53 gene underline the hereditary condition called Li-Fraumeni syndrome, in which the individual is predisposed to cancers at multiple sites (Malkin et al., 1990). The fundamental role of p53 as 'guardian of the genome' means that as observed in Li-Fraumeni patients, p53 mutations are found in an array of sporadic cancers (Nigro et al., 1989). In CRC, Iacopetta et al found that in a large cohort study p53 mutations are more frequent in late stage tumours and are associated with poor prognosis (Iacopetta et al., 2006). Despite the strong association of p53 mutations with CRC, mouse models of p53 loss in the context of intestinal tumourigenesis have failed to show progression to malignancy. Clarke et al demonstrated that mice predisposed to intestinal tumour formation and deficient for p53 ($Apc^{Min}$ $p53^{-/-}$) displayed no increase in intestinal tumourigenicity or tumour progression (Clarke et al., 1995). Similarly Reed et al showed that p53 loss has no effect on acute activation of the Wnt pathway in the intestine, and hence no role in early adenoma formation (Reed et al., 2008). One caveat with mouse models of p53 deficiency is that in humans, more frequently the p53 gene acquires point mutations that do not compromise the production of the full length p53 protein but render it

unable to transactivate gene transcription (Petitjean et al., 2007). In light of this Muller et al crossed mice bearing a mutated allele of p53 with mice heterozygous for Apc ($Apc^{fl/+}$) and compared them to mice that were had heterozygous deficiency of p53 and Apc. They found that the mice bearing the mutated p53 allele bore similar numbers of intestinal tumours to mice deficient for p53, but the tumours in the mutant p53 mouse were more advanced. They suggest that some mutations in p53 cause a gain-of-function in which the mutated p53 is able to promote invasion, so in intestinal mouse models of p53 deficiency the tumours do not become more malignant as they do not have the gain-of-function mutation (Muller et al., 2009).

## 1.5.5  Other signalling pathways implicated in CRC

### 1.5.5.1  The PI3K/mTOR pathway

Alterations in a number of genes in the PI3K/mTOR pathway are associated with CRC. Genes such as phosphatase and tensin homolog deleted on chromosome ten (PTEN), which is a negative regulator of the PI3K pathway and serine theronine kinase 11 (STK11 or LKB1), which is negative regulator of the mammalian target of rapamycin (mTOR) pathway (which is activated by PI3K) are both implicated in famlial intestinal tumour predisposition syndromes. The germline mutation of tumour suppressor PTEN is associated with PTEN Hamartoma Syndromes (PTHS) the most common of which being Cowden's syndrome (Blumenthal and Dennis, 2008), and germline mutation of LKB1 is associated with Peutz-Jeghers syndrome (Jenne et al., 1998).

The Phosphatidylinositol-3-Kinase (PI3K) signalling pathway (Katso et al., 2001) controls proliferation, apoptosis and cell growth by regulating the activation of thymoma viral oncogene homolog also known as Akt or Akt1, the downstream effector protein of the pathway. The PI3K protein is activated either by receptor ligand binding (receptors include, receptor tyrosine kinases, integrins, G protein coupled receptors and cytokine receptors) or by direct activation of its p110 catalytic subunit by activated KRAS. When activated PI3K phosphorylates the inositol ring of phosphatidylinositol 4,5-bisphosphate ($PI[4,5]P_2$ or $PIP_2$) converting it to phosphatidylinositol (3,4,5)-trisphosphate ($PI[3,4,5]P_3$ or $PIP_3$), $PIP_3$ allows the recruitment of Akt to the membrane where it is phosphorylated and therefore activated by phosphoinositide-dependent protein kinase 1 (PDK1). Akt is a kinase and when phosphorylated it is able to, in turn phosphorylate many proteins such as mTOR, GSK-3 and $p21^{Cip}$, phosphorylation of these proteins results in increased proliferation, protein synthesis, glucose metabolism and enhanced cell survival. Negative regulation of Akt activation is controlled by the phosphatase PTEN. PTEN dephosphorylates the

inositol ring of PIP$_3$ converting it back to PIP$_2$ thus preventing recruitment of Akt to the cell membrane and its subsequent phosphorylation. In sporadic CRCs Samuels et al showed that mutations in the PIK3CA gene that encodes the catalytic subunit of PI3K were found in 32% of CRCs that they analysed, and these mutations were more frequently found in more advanced cancers (Samuels et al., 2004). Findings by Parsons et al corroborate this, with 40% of CRCs bearing mutations in genes involved in the PI3K pathway (Parsons et al., 2005). The association of PI3K activation with more advanced carcinomas was demonstrated *in vivo* in a study by Marsh et al, in which invasive adenocarcinomas were observed in mice that were heterozygous for Apc and were also deficient for Pten (Marsh et al., 2008).

### 1.5.5.2 Mutations in DNA repair machinery

Other mutations that are commonly associated with CRC occur in genes associated with mismatch repair of DNA. Mismatch repair (MMR) involves proteins that proofread newly synthesized DNA and repair erroneous bases or microsatellite repeats that have been miscopied and have become elongated. Germline mutations of genes involved in MMR cause Hereditary Nonpolyposis Colorectal Cancer (HNPCC), commonly mutation of the genes MutS E.Coli homolog of 2 (MSH2) and MutL homolog 1 (MLH1) are associated with the condition (Fishel et al., 1993, Leach et al., 1993, Bronner et al., 1994). HNPCC is an autosomal dominant disease, patients have an increased risk of CRC but are not subject to multiple intestinal polyps. It is reported that an estimated 4-6% of all CRC cases are a result of HNPCC (Lynch et al., 1991). As well as mutation of mismatch repair genes, epigenetic silencing of MSH2 has also been observed as a mechanism of heritable CRC (Chan et al., 2006). As expected mice that are deficient for Mlh1 bear many intestinal tumours (Prolla et al., 1998). Msh2 deficient mice develop lymphomas at an early age and most mice die from these tumours, however the mice that do not succumb to lymphoma develop Apc deficient intestinal tumours (Reitmair et al., 1996).

### 1.6 Conditional transgenesis techniques

Development of the techniques by Capecchi, Evans and Smithies required to generate mice with targeted disruptions in a gene of interest (knockout mice) (Evans and Kaufman, 1981, Thomas and Capecchi, 1987, Doetschman et al., 1987), was a turning point in how we now investigate how genes work in a whole body system. Prior to this technology cancer research relied on the random disruption of genes induced by

a mutagenic compound, and once a tumour arose the arduous task of identifying the gene that was responsible had to be undertaken. Some, but not all, of the genes required for carcinogenesis are often also required for development (i.e. genes controlling cell proliferation, death and growth), so when these genes are inactivated in the mouse it often results in embryonic or perinatal lethality. Despite this, often a mouse can reach adulthood with only one intact copy of the gene. These mice can therefore be used to study the heterozygous effects of gene loss. The drawbacks with this kind of study are that homozygous loss or mutation of gene is often needed for tumourigenesis. Gene loss in the context of a particular tissue is also difficult to evaluate as knockout is achieved in every cell type, often resulting in tumours arising in a number of tissues. To circumvent the drawbacks with constitutive knockout mice, the techniques pioneered by Capecchi, Evans and Smithies have been used to incorporate systems into the mouse genome that allow the conditional alteration of gene expression in a specific tissue of interest at a particular point in mouse development or at adulthood.

## 1.6.1  Tet-on and Tet-off systems of conditional gene expression

The tet-on system of gene expression is a reversible system used to spatially and temporally control the expression (or knock in) of a particular transgene, for example the oncogenic form of a gene. The tet-on system utilises the protein-DNA interactions of the tetracycline repressor protein and its target 19-bp DNA operator sequences of the tetracycline operon from *E. coli*, and the transactivating domain of the herpes simplex virus protein VP16 to direct transcription of a specific gene inserted downstream of the tetracycline operon. Two transgenes are inserted into the mouse genome, one under the control of a tissue specific promoter encoding the tetracycline-controlled transactivator (tTA) - a fusion protein of the tetracycline repressor protein and the VP16 protein transactivation domain, and the other encoding the gene of interest downstream of Tet operon (tetO) sequences. The tTA is expressed in the tissue of interest and binds to the tetO sequences, present only in the transgene. The transactivating domain of the tTA protein then allows expression of the downstream target gene of interest. Tissue specific expression of the tTA occurs constitutively, so therefore expression of the transgenic gene of interest is also constitutively active. However, when doxycycline is present it binds to the tTA and prevents it from binding the tetO sequences and switches off expression of the transgenic gene of interest (Gossen and Bujard, 1992, Kistner et al., 1996). The tet-off system of transgene

expression utilises the reverse tetracycline-controlled transactivator (rtTA), which only binds tetO DNA sequences in the presence of doxycycline. The tet-on/off systems can be used to allow expression of an oncogenic form of a gene, or to allow tissue specific expression of a cre recombinase gene that in turn deletes a gene of interest (see section 1.6.2).

## 1.6.2  Site specific DNA recombination

Recombinase enzymes, found in bacteria and yeast, are able to recognise small specific sequences of DNA, cut and ligate DNA at these sequences, resulting in deletion or inversion of a region of DNA. The insertion of recombinase transgenes, along with their recognition sequences into the mouse genome has allowed site-specific recombination of DNA in the mouse that can be temporally and spatially controlled. These systems can be used to delete sections of DNA in a gene to cause knockout of the gene, delete sequences to alter the function of a gene and they can also be used to activate expression of a gene (knock-in genes). The two recombinase genes that have been inserted into the mouse genome are the cre recombinase gene from bacteria, and the flippase (FLP) gene from yeast, along with their 34-bp recognition sites, locus of crossover of bacteriophage P1 (loxP) and FLP recognition target (FRT) sites respectively, flanking the gene of interest. LoxP and FRT sites are not found endogenously in the mouse genome, hence genetic manipulation is restricted to the DNA sequence of interest. Recombination events can also occur between loxP or FRT sites inserted in different regions of a chromosome and in different chromosomes to give rise to chromosomal translocations and rearrangements.

The cre-loxP system was first shown to be useful for site-specific recombination in mammalian cells to manipulate the genome (Sauer and Henderson, 1988), and later shown to be useful *in vivo* (Schwenk et al., 1995, Orban et al., 1992). Manipulation of the mouse genome by the addition of a cre recombinase transgene and homologous recombination of a loxP flanked gene of interest (replacing the endogenous gene) is carried out in mouse embryonic stem (ES) cells and inserted into separate embryos, therefore producing mice with just the cre recombinase transgene and mice with the loxP targeted allele. An animal bearing a specific cre recombinase transgene can then be crossed with an animal bearing loxP sites to generate mice that have both. When cre recombinase is expressed in this mouse it will recombine the DNA at the loxP sites, removing the section of DNA between them. A tissue specific promoter upstream of the cre recombinase gene allows spatial control over where it is expressed in the mouse,

further temporal control of cre recombinase can be achieved by using the CreER$^T$ transgene. The CreER$^T$ transgene encodes for a cre recombinase-estrogen receptor fusion protein, cre recombinase is fused to a mutated ligand binding domain of the human estrogen receptor, which is activated by only tamoxifen binding but not by endogenous mouse estradiol (Figure 1.6). When tamoxifen binds it allows re-localisation of cre recombinase to the nucleus where it can act on the DNA (Feil et al., 1996). The insertion of an inducible promoter upstream of cre recombinase constitutes another mechanism of temporal control of cre recombinase action. Examples of this type of cre recombinase induction include *Ah*cre and *Mx1*cre. *Ah*cre recombinase is expressed from the cyp1a1 promoter, which is induced in response to introduction of a xenobiotic. Xenobiotics such as β-naphthoflavone can be administered via intraperitoneal (i.p.) injection. These then bind to Ah (aryl hydrocarbon) receptors that are translocated to the nucleus to induce expression of cyp1a1 target genes – allowing the expression of cre recombinase (Ireland et al., 2004). Similarly to *Ah*cre, *Mx1*cre expression is induced by the introduction of synthetic double stranded DNA or interferon (Kuhn et al., 1995). Inducible and tissue-specific expression of cre recombinase is outlined in Figure 1.6.

The FLP-FRT system works in the same manner as the cre-loxP system. A site specific recombinase from the yeast *saccharomyces cerevisiae* FLP is inserted as a transgene (with a tissue specific promoter) into the mouse genome, along with its recognition sequences (FRT sites) flanking the gene of interest (O'Gorman et al., 1991, Dymecki, 1996). Much like the cre recombinaseER transgene, a flippaseER transgene has been generated that allows temporal control of its action (Hunter et al., 2005).

The Cre-loxP and FLP-FRT systems as well as being used to excise a region of DNA they can also be used to change its orientation. This is achieved by inserting loxP or FRT sites so that they are in opposite orientation to each other. The cre recombinase or flippase then excises the region of DNA between them and inverts the section of DNA. The Brainbow© system exploits the excision and inversion properties of the recombinase systems to allow the expression of a number of different coloured fluorescent proteins. This system allows the labeling of cells with up to 90 different colours due to the inversion or excision of four different coloured fluorescent proteins in different combinations (Livet et al., 2007).

### 1.6.3 Modeling colorectal cancer in the mouse

One of the first mouse models to demonstrate intestinal tumourigenesis was the Min (Multiple Intestinal Neoplasia) mouse. The Min mouse was derived from a line of

mice which were treated with ethylnitrosurea and were predisposed to the formation of intestinal tumours (Moser et al., 1990). These mice developed multiple benign adenomas but they did not progress to adenocarcinoma. After establishment of the Min mouse line, the gene mutation responsible for the phenotype was mapped and discovered to be present in murine homologue of the APC gene. Therefore, the Min (Apc$^{Min}$) mouse was a model of the human hereditary CRC predisposition syndrome FAP (Su et al., 1992). This mouse model has been used extensively to study how environmental changes, genetic alterations and drugs impact on intestinal tumourigenesis, as frequently mentioned throughout this introduction. As homozygous Apc loss is embryonic lethal, a conditional Apc knockout mouse was generated, therefore allowing temporal and spatial control of Apc deletion as well as investigation of homozygous Apc loss, which is not possible in the Apc$^{Min}$ mouse (Shibata et al., 1997).

Conditional transgenesis allows the generation of mice that bear many loxP targeted tumour suppressors and oncogenes, that can be deleted or activated in a spatial and temporal manner, thus allowing more faithful recapitulation of human cancer, which has mutations in many genes. The availability of many loxP targeted genes and the development of tissue specific transgenic expression of cre recombinase, such as *Villin*Cre (intestinal specific) and *Ah*Cre (intestinal and other epithelial tissues) (El Marjou et al., 2004, Ireland et al., 2004), has allowed the development of mouse models that possess more invasive intestinal tumours than those observed in the Apc$^{Min}$ mouse. For example the Apc$^{fl/+}$ Pten$^{fl/fl}$ mouse that develops invasive adenocarcinoma of the small intestine (Marsh et al., 2008) and the Ink4a/Arf$^{fl/fl}$ Kras$^{G12D}$ mouse that develops metastatic intestinal carcinoma (Bennecke et al., 2010). Currently all drug testing is carried out on xenografted human tumours in immunocompromised mice which often fail when they reach clinical trials (Garber, 2006), so the development of mouse models of CRC that represent the array of human tumour types and the differing stages of malignancy observed in the clinic is advantageous for the future of translational research.
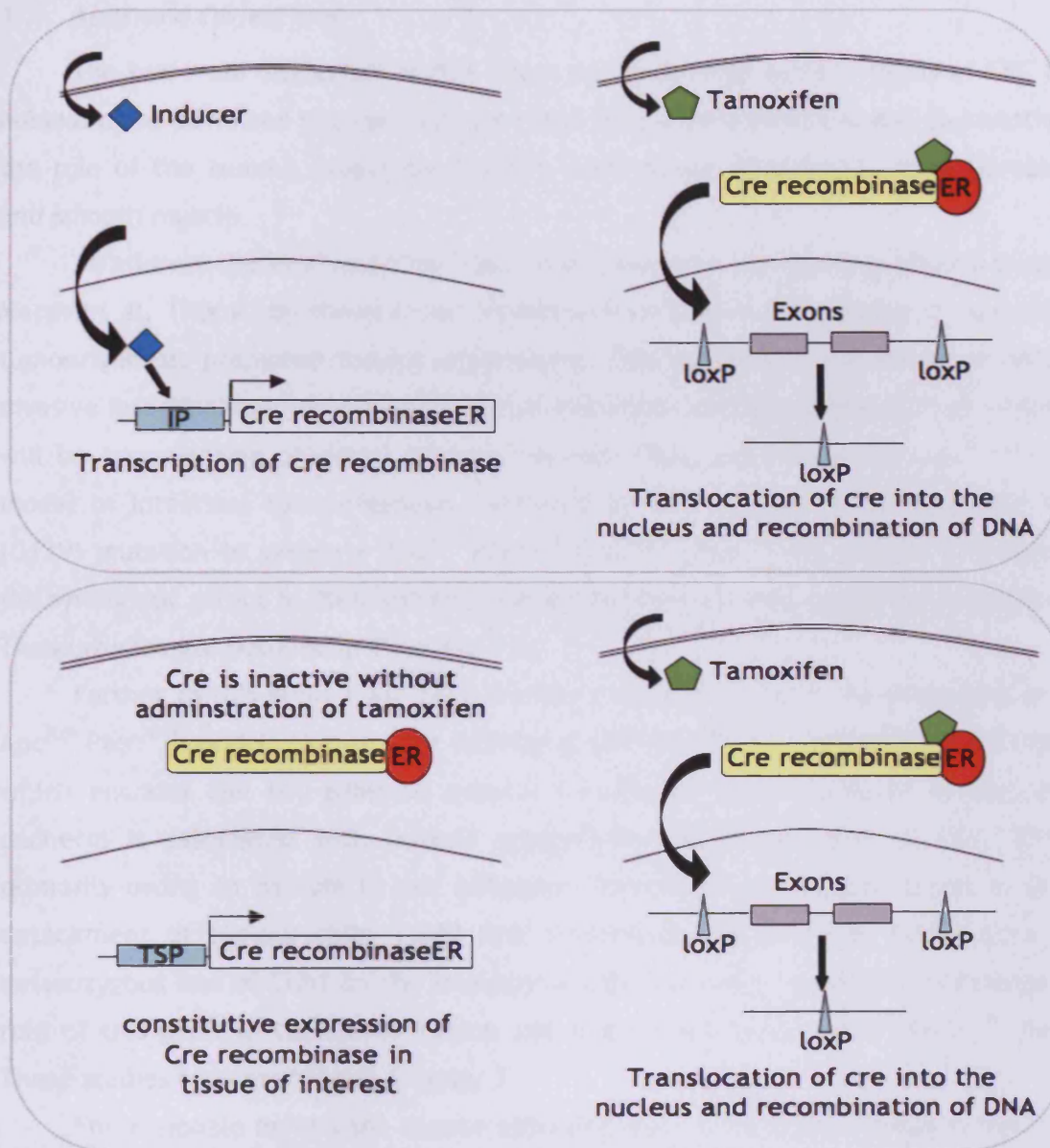
**Figure 1.6 Mechanisms of controlling the activity of Cre recombinase**

Key: IP – inducible promoter, TSP – tissue specific promoter

Top panel: Schematic diagram of inducible Cre recombinase. Mice are administered an inducing molecule such as interferon or β-naphthoflavone, which enters the cell and initiates transcription of the Cre recombinase gene. For further control of Cre recombinase activity it is sometimes fused to a mutated estrogen receptor that requires tamoxifen binding to translocate the protein to the nucleus. In this case tamoxifen is administered with the inducing molecule.

Bottom panel: Schematic diagram of tissue specific expression of Cre recombinase. Some mice possess a Cre recombinase transgene that is expressed from a tissue specific promoter so is only expresses in the tissue of interest. In order to gain temporal control an estrogen receptor-Cre recombinase fusion protein is expressed (as described above) so Cre recombinase even though is constitutively expressed only translocates to the nucleus after administration of tamoxifen.

## 1.7 Aims and Objectives

The two main objectives of this thesis are to develop better models of CRC that possess more advanced disease than the currently published models, and to investigate the role of the tumour suppressor Pten in adult mouse intestinal stromal fibroblasts and smooth muscle.

To address the first objective I will be drawing on a previously published study by Marsh et al. This study showed that intestinal Pten loss in the context of Apc driven tumourigenesis promoted tumour progression. This resulted in the mouse developing invasive intestinal adenocarcinoma but not metastatic carcinoma (Marsh et al., 2008). I will be investigating potential synergy between Pten and Kras in the Apc$^{fl/+}$ Pten$^{fl/fl}$ model of intestinal tumourigenesis, achieved by the addition of an oncogenic Kras (G12V) mutation to generate Apc$^{fl/+}$ Pten$^{fl/fl}$ Kras$^{LSL/+}$ mice. I will also be investigating the synergistic effect of Pten loss and Kras activation on normal intestinal homeostasis. These studies are outlined in Chapters 3-6.

Further to this study I will take another approach to achieving metastasis in the Apc$^{fl/+}$ Pten$^{fl/fl}$ model, through the additional deletion of the Cadherin1 (Cdh1) gene, which encodes the cell-adhesion protein E-cadherin. Downregulation or loss of E-cadherin is associated with tumour progression and invasiveness of CRC. This is primarily owing to its role in cell adhesion. Therefore, its loss may result in easier detachment of tumour cells. I will first investigate the effect of homozygous and heterozygous loss of Cdh1 on the intestinal epithelium, and I will then investigate the role of this gene in tumour formation and progression in the Apc$^{fl/+}$ Pten$^{fl/fl}$ model. These studies are described in Chapter 7.

The rationale behind the second objective also arises from findings in the Marsh et al study. Here, intestinal epithelial Pten loss does not result in predisposition to intestinal tumours (Marsh et al., 2008). However, a study by He et al found that Pten loss from both the intestinal epithelium and underlying stroma gives rise to rapid tumourigenesis (He et al., 2007). To address the stromal role of Pten in intestinal tumourigenesis, I will investigate the short term and long term effects of Pten loss in the intestinal stroma. This will be achieved by conditionally deleting Pten homozygously from intestinal stromal and smooth muscle fibroblasts, using a fibroblast specific Cre recombinase (Col1A2 cre). This study is described in Chapter 8.

# Chapter 2: Materials and Methods

## 2.1 Experimental Animals

The house mouse (*Mus musculus*) was used as an experimental model in this thesis. All mice used were of outbred background.

### 2.1.1 Genetic Mouse Models

A number of transgenic mouse models were obtained from various laboratories (outlined in Table 2.1) and crossed to investigate their compound effects on intestinal tumourigenesis. Two different cre recombinase transgenes were used, *Villin*CreER$^T$, which is expressed in the intestinal epithelium, and *Col1A2*CreER$^T$, which is expressed in fibroblasts. Both cre recombinase transgenes were fused to a mutated estrogen receptor, this allows the cre recombinase protein to only be translocated to the nucleus in the presence of tamoxifen. Mice bearing a cre recombinase transgene were crossed with mice bearing one or more loxP targeted alleles including Pten, Apc, Cdh1 and an oncogenic Kras allele controlled by a loxP flanked transcriptional stop cassette. A schematic representation of how gene knockout and Kras knock-in was controlled is outlined in Figure 2.1.

| Transgene | Tissue expression |
|---|---|
| Villin Cre ER$^T$ (El Marjou et al., 2004) | Intestinal epithelial cells, tamoxifen inducible |
| Col1a2 Cre ER$^T$ (Zheng et al., 2002) | Fibroblasts and smooth muscle, tamoxifen inducible |
| loxP targeted Pten allele (Suzuki et al., 2001) | Endogenous Pten allele bearing loxP sites flanking exons 4 and 5 |
| LoxP targeted Apc allele (Shibata et al., 1997) | Endogenous Apc allele bearing loxP sites flanking exon 14 |
| Kras knock-in (Guerra et al., 2003) | Mutated Kras allele (G12V) bearing a loxP flanked transcriptional stop cassette in the 5'UTR replacing the endogenous allele |
| loxP targeted Cdh1 (E-cadherin) allele (Derksen et al., 2006) | Endogenous Cdh1 allele bearing loxP sites flanking exons 3 and 15 |

**Table 2.1 Outline of the transgenic mice used in this thesis**
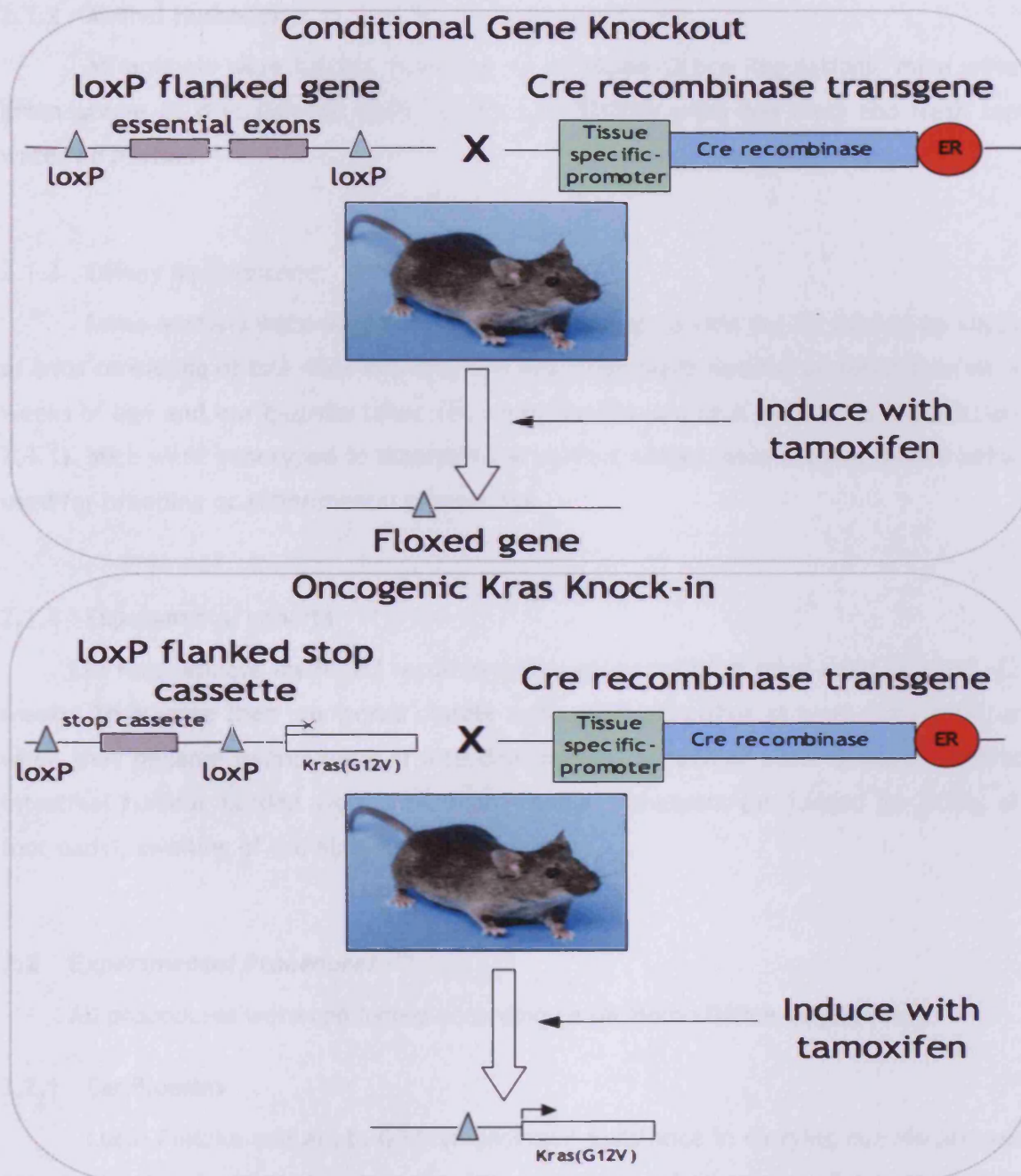
**Figure 2.1 Outline of conditional transgenesis models used**

Mice were generated that bore both loxP flanked genes and a cre recombinase transgene. Conditional knockout animals such as Apc, Pten and Cdh1 had the endogenous allele replaced by an allele containing loxP sites flanking essential exons of the gene. When cre recombinase is activated it recombines DNA at these loxP sites causing gene knockout. Conditional knock-in animals such as the oncogenic Kras knock-in mouse have one endogenous allele of Kras replaced with an oncogenic version of the gene (in this case G12V missense mutation), the expression of this oncogenic allele is controlled by the insertion of loxP flanked transcriptional stop cassette upstream of the gene. When cre recombinase is activated in this case, it removes the transcriptional stop cassette and allows expression of the oncogenic allele.

## 2.1.2 Animal Husbandry

All animals were housed according to UK Home Office Regulations, mice were given access to diet (Special Diets Service UK, RM3[E] expanded diet) and fresh tap water *ad libitum*.

## 2.1.3 Colony Maintenance

Some animals were used for breeding. This was carried out by setting up cages of trios consisting of one male and two females. Pups were weaned at approximately 4 weeks of age and ear biopsies taken for identification and DNA extraction (see section 2.3.1). Mice were genotyped to ascertain the correct alleles were present before being used for breeding or experimental procedures.

## 2.1.4 Experimental cohorts

Cre recombinase mediated recombination was induced in mice aged around 6-12 weeks. They were then monitored closely and sacrificed either at a set time point or when they became symptomatic of intestinal tumour burden or other disease. Signs of intestinal tumour burden were intestinal prolapse, anaemia (as judged by paling of foot pads), swelling of the abdomen and diarrhoea.

## *2.2 Experimental Procedures*

All procedures were conducted according to UK Home Office Regulations.

## 2.2.1 Ear Biopsies

Lucie Pietzka and Aneta Gerstyn provided assistance in carrying out routine ear biopsies on newly weaned mice. Ear biopsies were taken using a 2mm ear punch (Harvard Apparatus) from each mouse for identification, and the tissue removed was subsequently used to extract DNA for genotyping (see section 2.3.1).

## 2.2.2 Administration of Tamoxifen

Induction of cre recombinase activity in mice bearing the *Villin*CreER$^T$ and *Col1A2*CreER$^T$ transgenes was controlled by tamoxifen binding to a mutated estrogen receptor fused to the cre recombinase protein. Tamoxifen (Sigma) was dissolved at a concentration of 1mg/ml in corn oil (Sigma) in a waterbath at 80°C. An 80mg/kg dose

of tamoxifen was administered to each experimental mouse via intraperitoneal (i.p.) injection daily, for four consecutive days. For the administration of an 8mg/kg dose, 1mg/ml tamoxifen in corn oil stock was diluted 1 in 10 in corn oil, and was used to administer an 8mg/kg dose via i.p. injection for four consecutive days.

### 2.2.3  Administration of 5-Bromo-2-deoxyuridine

Some experimental animals were injected i.p. with an excessive dose of 0.2ml of 5-Bromo-2-deoxyuridine (BrdU, Amersham Biosciences) (a thymidine analogue) either 2, 24 or 48 hours before sacrifice in order to label cells currently undergoing or have passed through S-phase in the two hours in which the molecule is bioavailable.

## 2.3  Polymerase Chain Reaction (PCR) Genotyping

Mark Bishop and Lucie Pietzka provided assistance in routine PCR genotyping of animals.

### 2.3.1  DNA extraction from tissue samples

DNA was extracted from ear biopsies, taken from mice after weaning and/or intestinal mucosal scrapings (see section 2.4.5.1). The tissue sample was stored at -20°C prior to extraction. Tissue was digested in 250μl lysis buffer (Puregene) containing 0.4mg/ml Proteinase K (20mg/ml stock, Roche), overnight at 37°C with agitation. Protein was precipitated by addition of 100μl of protein precipitation solution (Puregene), the solution was mixed by inversion and protein and any insoluble debris was pelleted by centrifugation at 14000 x g for 10 mins. The supernatant was removed and added to a tube containing 250μl of isopropanol to precipitate the DNA. The tube was inverted to mix, and centrifuged at 14000 x g for 15 mins to pellet the DNA. The supernatant was removed and the pellet left to air dry for 1 hour, the DNA was then resuspended in 250μl of PCR grade water (Sigma).

DNA extracted from ear biopsies was used to carry out the polymerase chain reaction (PCR) to determine the genotypes of newly weaned animals, and on DNA from experimental animals that had been dissected to re-confirm the original PCR genotyping. DNA extracted from intestinal mucosal scrapings was used to determine the presence of the recombined loxP targeted alleles (described in section 2.10)

## 2.3.2 Generic protocol for PCR genotyping

PCR reactions were carried out to detect the presence of loxP sites in targeted alleles, and a cre-specific PCR was used to detect the presence of both *Villin*CreER$^T$ and *Col1A2*CreER$^T$ recombinase transgenes. The primers used in each PCR reaction (unless previously published primers were used) were designed using the web-based program Primer 3 (http://frodo.wi.mit.edu/primer3/), and then primers were verified for mis-priming using a web-based *in silico* PCR program, UCSC *In-Silico* PCR (http://genome.cse.ucsc.edu/cgi-bin/hgPcr?command=start). Reactions were carried out in either 96-well PCR plates (Grenier Bio-One), or thin-wall 12-well strip tubes (Grenier Bio-One). 2.5μl of gDNA extracted from ear biopsies (described in section 2.3.1) or control PCR grade water was pipetted into each well (singular reactions for each gene of interest were carried out on each sample, but were repeated when mouse was dissected to confirm genotype), and a PCR reaction mix containing PCR grade water (Sigma), magnesium chloride (Promega), dNTPs (25mM, dATP, dTTP, dCTP, dGTP, Bioline), DNA polymerase (either Dream Taq [Fermentas] or GO Taq [Promega]), PCR buffer (Promega) and gene specific primers (Sigma Genosys) were added to each well to make a final volume of 50μl (specific primer sequences for each reaction are outlined in Table 2.2. Reaction mixtures for each PCR are outlined in Table 2.3). 96-well plates were sealed with aluminium foil (Grenier Bio-One) and 12-well strip tubes sealed with caps (Grenier Bio-One), air bubbles were removed by tapping the sealed wells on a hard surface. The PCR reaction was then run in a GS4 thermocycler (G storm). Cycling conditions for each reaction are described in Table 2.3.

## 2.3.3 Visualisation of PCR products

After the PCR reactions were carried out, PCR products were visualised by gel electrophoresis. 2% agarose gels were made by dissolving agarose (Eurogentech) 2% [w/v] in 1X Tris-Borate-EDTA (TBE) buffer (Sigma) and heated in a microwave until boiling. Once boiled the gel was cooled quickly under cold running water and 14μl of Safe View (NBS Biologicals) was added per 400ml of gel (Safe View is a nucleic acid stain that binds to DNA and fluoresces under UV light allowing visualisation of DNA). Gel was then poured into moulds (Bio-Rad) and combs placed to create wells. After gels were set they were placed in a gel electrophoresis tank (in their moulds) and covered with 1X TBE (Sigma). Safe View (NBS Biologicals) was also added to the buffer.

PCR product samples were prepared by adding 5μl of loading dye (50% Glycerol [Sigma], 50% ultrapure dH₂O, 0.1% [w/v] bromophenol blue [Sigma]), ensuring adequate mixing by gentle pipetting. PCR samples (20μl) were added to the wells and a molecular weight marker e.g. 100bp ladder (Promega) was added to one well in order to assess PCR product size. The gel was then run at 120V for approximately 30 mins, and products visualised using a GelDoc UV transilluminator (Bio-Rad), and images of PCR products captured using GelDoc software (Bio-Rad).

| Gene | Forward Primer Sequence (5'-3') | Reverse Primer Sequence (5'-3') |
|---|---|---|
| Cre specific | TGACCGTACACCAAAATTTG | ATTGCCCCTGTTTCACTATC |
| Pten-loxP | CTCCTCTACTCCATTCTTCCC | ACTCCCACCAATGAACAAAC |
| Apc-loxP | GTTCTGTATCATGGAAAGATAGGTGGTC | CACTCAAAACGCTTTTGAGGGTTGATTC |
| Kras-lox-stop | AGGGTAGGTGTTGGGATAGC | CTGAGTCATTTTCAGCAGGC |
| Cdh1-loxP | TCAATCTCAGAGCCCCACCTA | CCTGCCATGATTGTCATGGAC |

Table 2.2 Primer sequences used for each gene specific PCR

| | Cre specific | Pten-loxP | Apc-loxP | Kras | Cdh1-loxP |
|---|---|---|---|---|---|
| **PCR reaction mix** | | | | | |
| gDNA | 2.5µl | 2.5µl | 2.5µl | 2.5µl | 2.5µl |
| PCR-grade water | 31.7µl | 31.7µl | 31.7µl | 31.7µl | 31.7µl |
| GO Taq PCR buffer (5X) | 10µl | 10µl | 10µl | 10µl | 10µl |
| $MgCl_2$ (25mM) | 5µl | 5µl | 5µl | 5µl | 5µl |
| dNTPs (25mM) | 0.4µl | 0.4µl | 0.4µl | 0.4µl | 0.4µl |
| Primer 1 (100mM) | 0.1µl | 0.1µl | 0.1µl | 0.1µl | 0.1µl |
| Primer 2 (100mM) | 0.1µl | 0.1µl | 0.1µl | 0.1µl | 0.1µl |
| Taq DNA polymerase | 0.2µl | 0.2µl | 0.2µl | 0.2µl | 0.2µl |
| Brand of Taq polymerase | GO Taq | Dream Taq | Dream Taq | Dream Taq | GO Taq |
| **PCR cycling conditions** | | | | | |
| Initial denaturation | 3 min, 94°C | 5 min, 94°C | 3 min, 95°C | 5 min, 94°C | 2.5 min, 94°C |
| Cycle number | 30 cycles of: | 35 cycles of: | 30 cycles of: | 30 cycles of: | 35 cycles of: |
| Step 1: denaturation | 30 sec, 95°C | 1 min, 94°C | 30 sec, 95°C | 1 min, 94°C | 30 sec, 94°C |
| Step 2: annealing | 30 sec, 55°C | 1 min, 58°C | 30 sec, 60°C | 1 min, 60°C | 30 sec, 60°C |
| Step 3: Extension | 1 min, 72°C | 1 min, 72°C | 1 min, 72°C | 1 min, 72°C | 1 min, 72°C |
| Final extension | 5 min, 72°C | 5 min, 72°C | 5 min, 72°C | 5 min, 72°C | 5 min, 72°C |
| | Hold at 15°C | Hold at 15°C | Hold at 15°C | Hold at 15°C | Hold at 15°C |
| PCR product sizes | Presence of transgene: 1000bp | WT: 228bp Targeted: 335bp | WT: 226bp Targeted: 315bp | WT: 403bp Targeted stop cassette: 621bp | WT: 200bp Targeted: 330bp |

Table 2.3 Outline of PCR reaction mixtures, cycling conditions and product sizes

## 2.4 Tissue Sample Preparation

Tissues were dissected immediately after animal sacrifice in order to prevent degradation of RNA, protein and phospho-proteins.

### 2.4.1 Tissue Dissection

#### 2.4.1.1 Dissection of Organs

Mice were culled by cervical dislocation, 70% ethanol was sprayed over the abdomen of the mouse and the abdominal cavity opened by cutting first through the skin then through the smooth muscle wall. The genitourinary tract (i.e. bladder, testes, seminal vesicles, prostate and preputial glands) was taken out and fixed together (fixation is described in section 2.4.2.1). The stomach and the intestines were then dissected out (see section 2.4.1.2), the stomach was opened up and the contents removed, the kidneys were dissected out and one cut transversely and the other longitudinally, spleen, pancreas and lungs were also removed and fixed together (fixation is described in section 2.4.2.1).

#### 2.4.1.2 Dissection of Intestines

The intestines were removed by first cutting the attachment of the stomach to the oesophagus, then gently removing the intestine, being careful to remove all attached mesentery, (mesentery was then fixed separately see section 2.4.2.1). Once the length of the small intestine was removed, it was cut at the ileal-caecal junction and the stomach removed and fixed separately (see section 2.4.1.1). The colon was then removed with the caecum and the caecum was cut from the colon, contents emptied and fixed separately (see section 2.4.2.1 and 2.4.2.2). In some cases the length of the small intestine was measured using a ruler. The contents of the intestines were removed by flushing with 1X Phosphate Buffered Saline (PBS) (Invitrogen) and fixed as described in section 2.4.2.

### 2.4.2 Fixation of Tissues

#### 2.4.2.1 Formalin Fixation

Most of the tissues taken were fixed in 10% neutral buffered formalin (Sigma), as formalin fixed tissues work well with the majority of commercially available antibodies for immunohistochemistry applications.

The liver, lungs, pancreas, spleen, kidneys, mesentery and genitourinary tract of each mouse was fixed immediately after dissection in ice cold 10% neutral buffered formalin (Sigma) for 24 hours prior to processing. The contents of the small intestine and colon were removed by flushing with 1X PBS and were fixed in 10% neutral buffered formalin in one of two ways. Either 1cm sections were fixed and sectioned transversely, or the gut was opened longitudinally and rolled into a 'swiss roll-like' structure (secured by a needle), and was then sectioned end-on, allowing sectioning of the whole length of the intestine.

### 2.4.2.2 Methacarn Fixation of Intestines

To assess the total macroscopic tumour number, methacarn fixation of the small intestine and colon was utilised. The contents of the small intestine and colon were removed by flushing with 1X PBS. Then, the intestines were placed on a piece of blotting paper and opened up longitudinally. The paper was then placed in a bath of methacarn (made up from Methanol, Chloroform, Glacial Acetic Acid in a 3:2:1 ratio) and fixed overnight. The intestines were then rolled into a 'swiss roll-like' structure and placed in 96% ethanol. The action of Methacarn fixation on the intestine allowed the number of macroscopic tumours to be visualised and accurately measured, so this method was of intestinal fixation was primarily used for quantifying overall macroscopic intestinal tumour number. Methacarn fixed intestines were also sectioned and stained with haematoxylin and eosin (H&E) for histological analysis.

### 2.4.2.3 Fixation of Small Intestine for Scanning Electron microscopy (SEM)

The small intestine was flushed with PBS and 1cm sections were opened longitudinall. The intestine was then pinned, mucosal side up, to a petri dish half filled with hardened paraffin wax. Pinning the tissue on the wax dish kept it flat and prevented the tissue from curling. The pinned intestinal sections were fixed in 2.5% Glutaraldehyde, EM grade (Agar Scientific) in Sörensen's phosphate buffer (pH 7.4, buffer was made by adding 95ml of a 0.015M $KH_2PO_4$ solution to 405ml of a 0.075M $Na_2HPO_4$ solution [Sigma]) for 1 hour. The tissue was then prepared for SEM (described in section 2.5)

### 2.4.3  Processing of Fixed Tissues

Derek Scarborough and Marc Isaac provided assistance in carrying out the processing of fixed tissues, sectioning of embedded tissue and H&E staining of tissue sections.

After fixation for 24 hours, all tissues were removed from fixative, placed in a cassette (Fisher) and processed using an automatic processor (Leica TP1050). The tissues were dehydrated through an increasing gradient of alcohols (70% ethanol for 1 hour, 95% ethanol for 1 hour, 2x 100% ethanol for 1 hour 30 mins, 100% ethanol for 2 hours) and then in xylene (2 x xylene for 2 hours). The tissue was then placed in liquid paraffin for 1 hour, then again twice for 2 hours. The tissue samples were then removed from the cassette and embedded in paraffin wax by hand and left to harden.

### 2.4.4  Sectioning of Fixed Tissues

Paraffin embedded tissues were then cut to 5μm sections using a microtome (Leica RM2135) and were then placed on Poly-L-Lysine (PLL) coated slides, and then baked at 58°C for 24 hours. The sections were then prepared either for Haematoxylin and Eosin (H&E) staining (described in section 2.6.2) or immunohistochemistry (IHC) (described in section 2.7).

### 2.4.5  Epithelial Cell Enrichment for DNA, RNA and Protein samples

In order to obtain intestinal samples for DNA, RNA or protein extraction that were enriched for epithelial cells two methods were used: crude epithelial cell enrichment and HBSS-EDTA epithelial cell extraction (see below).

#### 2.4.5.1  *Crude Epithelial Cell Enrichment for DNA and RNA*

The small intestine was flushed with 1X PBS and cut into small sections (1-5cm), and opened up longitudinally. A crude enrichment of epithelial cells was obtained by scraping the mucosal surface of the intestine with a scalpel. These samples were then used either for DNA extraction (described in section 2.3.1), or placed immediately into Trizol for RNA extraction (described in section 2.9.1). The samples were then stored at -20°C prior to extraction.

## 2.4.5.2 HBSS-EDTA Epithelial Cell Enrichment for RNA and Protein

The method used for isolation of intestinal epithelial cells was adapted from Bjerknes and Cheng (Bjerknes and Cheng, 1981a).

The small intestine was flushed with 1X PBS and a 5cm section was inverted by tying off one end of the intestine with non soluble suture (Mersilk, Ethicon), and then using a needle, the intestine was inverted by piercing the intestine below the tied off section and pulling the end of the intestine in on itself. The inverted intestine was then placed in a 50ml conical tube containing approximately 45ml of pre warmed (37°C) extraction buffer solution (1X Hanks Balanced Salt Solution [HBSS] [Gibco], containing no calcium or magnesium ions and 10mM EDTA pH 8.0 [Sigma]). The intestine was then agitated in the solution by attachment to a vortex mixer set to the lowest setting for 15 mins. After 15 mins the intestine was removed and placed in another 50ml conical tube containing extraction buffer and agitated for a further 15 mins, to obtain a second cell extract. The two extracts were obtained from each 5cm section of intestine and were temporarily stored on ice until needed. Tubes containing extracts were then centrifuged at 3000g at 4°C for 15 minutes to yield a pellet of epithelial cells. The remaining extraction buffer was then decanted off and the pellet was either prepared for RNA or protein extraction (see below).

## 2.4.5.3 Preparation of epithelial cell extract for RNA extraction

In preparation for RNA extraction, the pellet was resuspended in Trizol (Invitrogen), and stored at -20°C prior to RNA extraction (described in section 2.9).

## 2.4.5.4 Preparation of epithelial cell extract for protein extraction

In preparation for protein extraction the pellet was resuspended in 1ml 1X PBS, transferred to a 1.5ml microcentrifuge tube and re-pelleted by centrifugation at 3000 x g at 4°C for 15 mins. The 1X PBS was carefully removed using a pipette and the pellet was then snap frozen and stored at -80°C for subsequent protein extraction (as described in section 2.8.1).

## 2.5 Scanning Electron Microscopy

Dr Anthony Hann provided assistance in preparing small intestinal samples for scanning electron microscopy.

### 2.5.1 Preparation of samples and scanning EM

The tissue was fixed and prepared as described in section 2.4.2.3. The excess fixative was then washed off the tissue samples using Sörensen's phosphate buffer (recipe is described in section 2.4.2.3), the samples were washed 3 times for 5 mins with agitation, followed by 2 x 5 min washes in 0.15M glycine (Sigma) diluted in Sörensen's phosphate buffer. The samples were washed well in order to quench excess aldehyde groups from the glutaraldehyde to allow better uptake of osmium tetroxide. The tissue was then fixed in osmium tetroxide (Sigma) for 1-2 hours. The samples were then washed again for 2 x 5 mins in Sörensen's phosphate buffer, and for 10 mins in deionised water before being dehydrated through a gradient of ethanols (30%, 60%, 70%, 80%, 90%, 2 x 100%, Fisher Scientific) and finally in acetone (Sigma). The sample was flushed with liquid $CO_2$, then was critical point dried using critical point drying apparatus (Balzers) at 45°C and 1450Psi. The samples were then mounted on 12mm metal stubs and coated in gold, and viewed using a Philips XL20 scanning electron microscope operated at an accelerating voltage of 20-25 kV.

## 2.6 Histological Analysis

### 2.6.1 Preparation of Sections for IHC or Staining

Paraffin embedded tissue sections on PLL coated slides were first de-waxed by placing in a bath of xylene for 5 mins, and then transferred to another xylene bath for a further 5 mins. The sections were now devoid of all paraffin wax and could be rehydrated down a gradient of alcohols. The sections were washed in baths of descending gradients of ethanol (100%, 100%, 95%, 70%) for 2 mins each and finally placed in a bath of deionised water (dH$_2$O) in preparation for immunohistochemistry (IHC) or staining.

### 2.6.2 Haematoxylin and Eosin (H&E) Staining

In order to visualise tissue sections for phenotypic analysis, tissue sections were stained with haematoxylin to mark nuclei and eosin to stain the cytoplasm of cells. Tissue sections on PLL coated slides were de-waxed and rehydrated as previously

described in section 2.6.1, and were then stained by immersing the sections in a bath of Mayer's Haemalum (R. A. Lamb) for 45 secs, then washed in running tap water for 5 mins. Sections were then stained in an aqueous solution of 1% Eosin (R. A. Lamb) for 5 mins followed by two 15 second washes in tap water. Tissue sections were then dehydrated, cleared and mounted as described in section 2.7.1.9.

## 2.6.3   Cell Type Specific Stains

### 2.6.3.1   Alcian blue Staining for Goblet Cells

Alcian blue stains the mucins present in Goblet cells, the secretory cell lineage of the intestinal epithelium.

Tissue sections were de-waxed and dehydrated as previously described and immersed in a bath of Alcian blue staining solution pH 2.5 (1% [w/v] Alcian blue [Sigma] in 3% [v/v] Acetic acid [Fisher Scientific]) for 5 mins, then washed in running tap water for a further 5 mins. The tissue sections were then counter stained with 0.1% Nuclear fast red in 5% aluminium sulphate (Sigma) for 5 mins, and washed in running tap water for a further 5 mins. Tissue sections were then dehydrated, cleared and mounted as described in section 2.7.1.9.

### 2.6.3.2   Grimelius Staining for Enteroendocrine Cells

Grimelius staining marks argyrophilic granules, found in hormone secreting enteroendocrine cells of the intestinal epithelium. Argyrophillic granules bind silver ions, which are then precipitated in the presence of a reducing solution staining the cells turn black in colour.

Tissue sections were de-waxed and dehydrated, all glassware used was washed in ultrapure double distilled water (ddH$_2$O) to eliminate any reducing agents that may be present. All solutions were freshly prepared according to the recipes in Table 2.4. Sections were incubated in silver staining solution at 65°C for 3 hours, the sections were then immersed in preheated reducing solution at 45°C for 1-10 mins until tissue sections had a yellow background stain (no counter stain was required due to yellow background stain).

| Silver Staining Solution |
|---|
| 10ml Acetate Buffer pH 5.6 (see below) |
| 87ml ddH$_2$O |
| 3ml 1% w/v Silver nitrate |
| **Acetate Buffer** |
| 4.8ml 0.2M Acetic acid |
| 45.2ml 0.2M Sodium acetate |
| 50ml ddH$_2$O |
| **Reducing Solution** |
| 2.5g Sodium sulphite (hydrated) |
| 0.5g Hydroquinone |
| 50ml ddH$_2$O |

Table 2.4 Recipe for solutions required for Grimelius staining

### 2.6.3.3 Alkaline Phosphatase Staining for Enterocytes

Alkaline phosphastase is an enzyme expressed specifically on the brush border of the enterocytes, which make up the vast majority of the intestinal epithelial layer. Alkaline phosphastase staining allows visualisation of these cells by utilisation of the enzymatic activity of the alkaline phosphatase that is expressed. Alkaline phosphatase catalyses a chromogen to produce a red stain, which demarcates the epithelial brush border.

Tissue sections were de-waxed and dehydrated as described in section 2.6.1. The Liquid Permanent Red kit (DAKO) was used according to manufacturer's instructions. The alkaline phosphatase substrate was made up by the addition of 1 drop of Liquid Permanent Red chromagen (DAKO) to 3ml of Liquid Permanent Red substrate buffer (DAKO). Tissue sections were demarcated using a hydrophobic barrier pen (Vector labs) and 200μl of the prepared substrate solution was applied to slides and incubated at room temperature for 20 mins. Sections were then washed briefly in dH$_2$O and counterstained with Mayer's Haemalum for 45 secs, then washed for 5 mins with running tap water. The slides were then mounted using Vector Shield Aqueous Mounting Medium (Vector Labs), as alcohol and xylene have adverse effects on liquid permanent red staining.

## 2.6.4  Cell Scoring

Scoring the number and type of cells present along the crypt-villus axis can reveal alterations in intestinal homeostasis. 50 half crypt-villi from each section were scored for various indicators of disrupted intestinal homeostasis (outlined below), at least 3 biological replicates per cohort were scored.

### 2.6.4.1  Crypt Cell Scoring

To assess small intestinal crypt length, the number of cells per half crypt were scored from H&E stained sections. Cells were counted from the base of the crypt adjacent to the paneth cells, upwards to the top of the crypt at the crypt-villus junction.

### 2.6.4.2  Villus Cell Scoring

To assess villus length, the number of cells were scored per half villus from the crypt villus junction to the tip of the villus from H&E stained sections.

### 2.6.4.3  Apoptosis and Mitosis Scoring

The presence of mitotic figures and apoptotic bodies per half crypt were scored from H&E stained sections.

### 2.6.4.4  Caspase 3 Scoring

Caspase 3 IHC was carried out on tissue sections as described in section 2.7.1 (specific antibody conditions outlined in Table 2.7), and positive cells were scored per half crypt and half villus.

### 2.6.4.5  Ki67 Scoring

Ki67 is an antigen that is expressed in cells that are undergoing all stages of the cell cycle. IHC against Ki67 antigen was carried out on tissue sections, and the number of positive cells per half crypt were scored.

### 2.6.4.6  BrdU Scoring

Some animals were given a pulse of BrdU via i.p. injection at either 2 hours or 48 hours prior to sacrifice. The incorporation of BrdU was then visualised via IHC and then the number of positive cells and their position along the crypt villus axis was scored.

## 2.6.4.7 Cell type scoring

Goblet cells and enteroendocrine cells were scored per half crypt-villus from tissue sections alcian blue and grimelius stained sections (as described previously 2.6.3.1 and 2.6.3.2) respectively. Goblet cell and enteroendocrine cell scores were normalised to take into account alterations in the number of cells present along the crypt-villus axis. This was achieved by dividing the total number of goblet or enteroendocrine cells per half crypt-villus with the total number of cells per half crypt-villus. The number of paneth cells per whole crypt were scored from small intestinal sections immunostained for lysozyme (see section 2.7).

### 2.6.5 Tumour severity grading

Tumour grading was carried out on intestinal tumours found in $Apc^{fl/+}$ $Pten^{fl/fl}$ $Kras^{LSL/+}$ mice and control cohorts. H&E stained sections of 'swiss-rolled' whole intestine were examined under the microscope, and the number and severity of tumour invasiveness was scored. Each tumour was scored and graded according to the following criteria outlined in Table 2.5 and in Figure 2.2. Intestines from a minimum of n=3 mice for each cohort were examined and graded.

| Tumour grade | Tumour description |
|---|---|
| 1 | microadenoma |
| 2 | adenomas with no evidence of invasion |
| 3 | adenocarcinoma with evidence of invasion into the intestinal submucosa |
| 4 | adenocarcinoma with evidence of invasion through the smooth muscle wall and underlying serosa |

Table 2.5 Tumour invasiveness scoring system

52
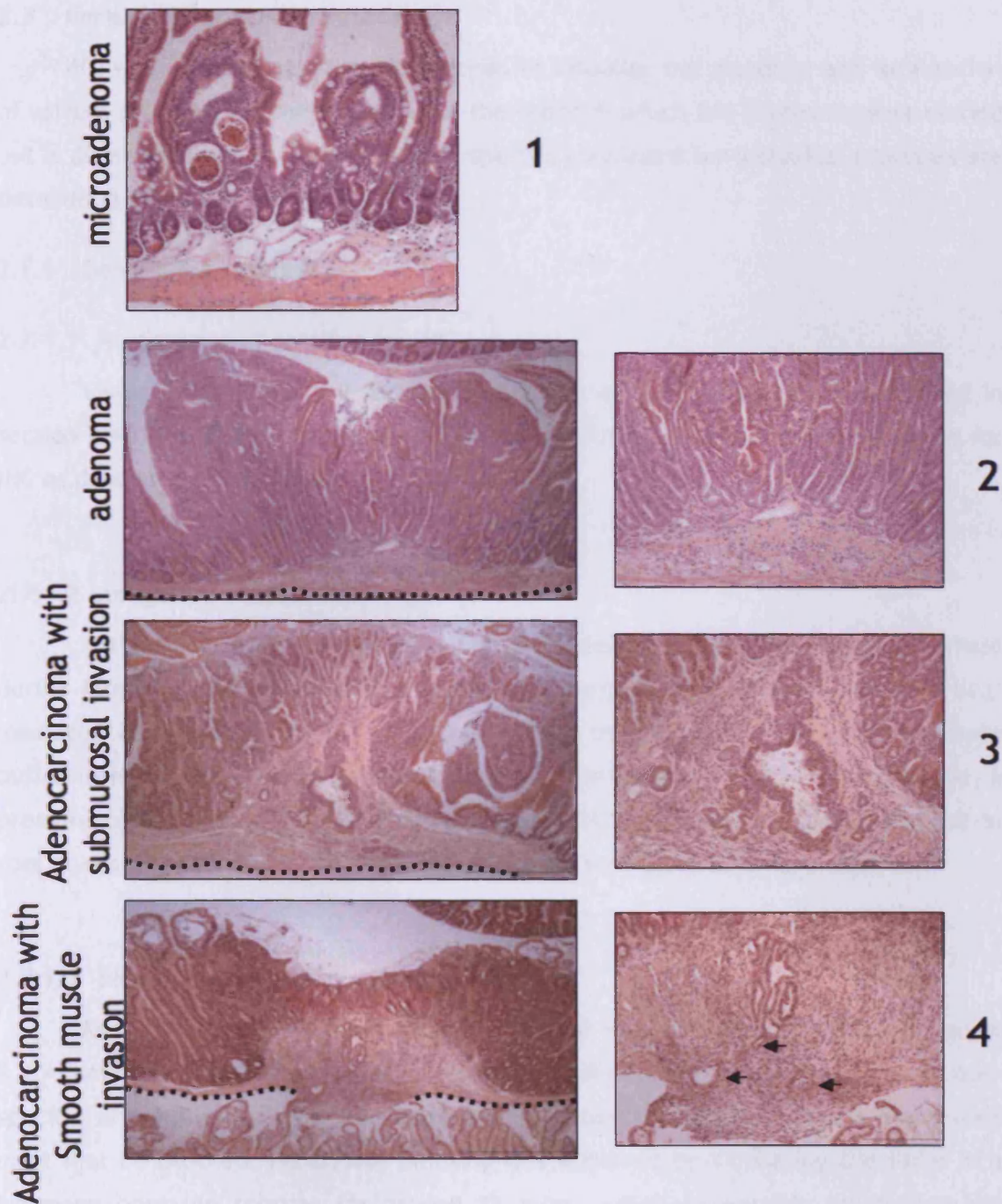
**Figure 2.2 Stages of intestinal tumour progression**

H&E stained sections of the whole small intestine were examined, and the level of progression of each tumour observed within the intestine was graded (staged). Grade 1 – microadenomas, small lesions often observed within villi, Grade 2 – adenomas, tumours that vary in size but do not invade into the underlying submucosa, Grade 3 – adenocarcinoma with submucosal invasion, a tumour that has progressed further than an adenoma and has evidence of invasion into the underlying submucosa but does not break through the smooth muscle cover of the intestine, Grade 4 – adenocarcinoma with smooth muscle invasion, a tumour that has progressed further and invaded through the smooth muscle and has invaded locally into the peritoneum.

## 2.7 Immunohistochemistry (IHC)

IHC was carried out on tissue sections to visualise the presence and localisation of various proteins. A generic outline of the order in which IHC protocols were carried out is detailed in this section. However, specific conditions for individual protocols are detailed in Table 2.6 and Table 2.7.

### 2.7.1 Generic IHC protocol

#### 2.7.1.1 Preparation of sections for IHC

Tissues were fixed and sectioned onto PLL coated glass slides as described in section 2.4. The tissue sections were then dewaxed and dehydrated in preparation for IHC as described in section 2.6.1.

#### 2.7.1.2 Antigen retrieval

Antigen retrieval was carried out in order to break cross-linking bonds formed during fixation, and therefore unmasking the antigens. This typically involved heat mediated retrieval carried out by either boiling the tissue section slides in citrate buffer (pH6, Thermo) or antigen unmasking solution (DAKO), in either a microwave, a pressure cooker or a 100°C water bath for around 30 mins, then the slides were left to cool at room temperature for 30 minutes and then washed in deionised water.

#### 2.7.1.3 Blocking of endogenous peroxidases

As the system of antibody visualisation used involves the enzymatic reaction of 3,3'-diaminobenzidine (DAB) catalysed by horse radish peroxidase (HRP), to avoid non-specific enzymatic action of the endogenous peroxidases present in the tissue they must first be blocked. Peroxidase blocking was achieved by incubating the slides in a hydrogen peroxide solution for around 15 mins, which irreversibly inactivates the endogenous peroxidases. After peroxidase blocking the slides were then washed in deionised water and then in wash buffer.

#### 2.7.1.4 Blocking of non-specific antibody binding

Non-specific binding of antibodies was blocked by incubating tissue sections with serum obtained from an animal that is different to the animal in which the primary antibody was raised, for example normal goat serum could be used to block

54

tissue sections that will be incubated with antibodies raised in rabbit. Tissue sections on PLL coated slides were first outlined using a hydrophobic barrier pen, Immedge pen (Vector labs) before incubation with serum. Serum was diluted in wash buffer to a concentration that adequately blocks non-specific binding and therefore decreases background DAB staining. Serum block was removed and then tissue sections were incubated with primary antibody without washing.

### 2.7.1.5 Primary antibody incubation

Tissue sections were then incubated with a primary antibody at an optimised concentration or one recommended by the manufacturer. Antibodies were diluted in the same serum at the same concentration used for the previous blocking stage (specific antibody concentrations can be found in Table 2.6 and Table 2.7). Antibodies were generally incubated over night in a humidified chamber at 4°C, or at room temperature for 1 hour. After incubation the slides were then washed three times in TBS/T to remove residual unbound primary antibody.

### 2.7.1.6 Secondary antibody incubation

Tissue sections were then incubated with the secondary antibody, diluted typically 1 in 200 in normal serum. Secondary antibodies are raised against antibodies from the animal in which the primary antibody was raised, so they bind to any primary antibodies that are bound to the antigen of interest. Tissue section slides were incubated with secondary antibody for 30 mins in a humidified chamber. The slides were then washed in wash buffer three times. Typically the secondary antibodies were biotinylated, so therefore an additional signal amplification step was required in which HRP binds to the secondary antibody. However, a few of the protocols required the use of the Envision plus kit (DAKO). In these cases the tissue sections were incubated with a prediluted secondary antibody conjugated to HRP so an amplification step was not needed, and antibody binding could be visualised after washing off the secondary antibody.

### 2.7.1.7 Signal amplification

When biotinylated secondary antibodies were used, a signal amplfication step was required. This involved the formation of a complex between the biotin bound to the secondary antibody and a protein called avidin, which was bound to HRP, the

Vectastain Avidin-Biotin Complex (ABC) kit (Vector labs) was used. The ABC reagent was prepared in wash buffer 30 mins before use and left at room temperature. Tissue sections were incubated with ABC reagent for 30 mins before being washed three times in wash buffer. HRP enzyme was now bound to secondary antibodies that remained bound to primary antibodies, so the antigen could be visualised.

## 2.7.1.8 Detection of signal

The presence of the antigen of interest was visualised by the production of a coloured stain, produced from a substrate catalysed by the HRP enzyme bound to the secondary-primary antibody complex. The substrate used was 3,3'-diaminobenzidine (DAB), which could be catalysed by HRP to produce a brown stain. The DAB reagents (DAKO) were prepared just prior to incubation, tissue sections were incubated with DAB reagents for 2-10 mins or until adequate staining was achieved visually by eye. Excess DAB reagent was removed and tissue sections washed in deionised water.

## 2.7.1.9 Counterstaining and slide mounting

The slides were incubated in Mayer's Haemalum (R.A. Lamb) for 45 secs to stain nuclei, and washed in tap water for 5 mins. Slides were then dehydrated through a gradient of alcohols (1 x 2 mins 70% ethanol, 1 x 2 mins 95% ethanol, 2 x 2 mins 100% ethanol) and then cleared in 2 x 5 mins xylene. Slides were then removed from xylene, mounted in DPX mounting medium (R.A. Lamb) then coverslipped and left to air dry in a fume hood.

| Primary Antibody | Manufacturer | Antigen retrieval | Non-specific signal block | Wash buffer | Primary antibody conditions | Secondary antibody | Signal amplification step |
|---|---|---|---|---|---|---|---|
| Anti-Pten | Cell Signaling Technology #9188 | 30mins, 100°C W/B, citrate buffer (Thermo) | Peroxidase:3% $H_2O_2$ 10mins<br>Serum: 5% NGS 30mins both RT | 3 washes in TBS/T, 5mins | 1:50 in 5% NGS 1hr @ RT | Biotinylated anti-rabbit 1:200 (Vector Labs), 30mins | ABC kit (Vector Labs) |
| Anti-phospho Akt (ser473) | Cell Signaling Technology #4060 | 30mins, 100°C W/B, citrate buffer (Thermo) | Peroxidase:3% $H_2O_2$ 10mins<br>Serum: 5% NGS 30mins both RT | 3 washes in TBS/T, 5mins | 1:50 in 5% NGS O/N @ 4°C | Biotinylated anti-rabbit 1:200 (Vector Labs), 30mins | ABC kit (Vector Labs) |
| Anti-phospho44/42 MAPK (phospho-ERK1/2) (Thr202/Tyr204) | Cell Signaling Technology #4376 | Boil 15mins in M/W, citrate buffer (Thermo) | Peroxidase:1.5% $H_2O_2$ 15mins<br>Serum: 10% NGS 30mins both RT | 3 washes in TBS/T, 5mins | 1:75 in 10% NGS O/N @ 4°C | Biotinylated anti-rabbit 1:200 (DAKO), 30mins RT | ABC kit (Vector Labs) |
| Anti-phospho MEK1/2 (ser221) | Cell Signaling Technology #2338 | Boil 15mins in M/W, citrate buffer (Thermo) | Peroxidase:1.5% $H_2O_2$ 15mins<br>Serum: 10% NGS 30mins both RT | 3 washes in TBS/T, 5mins | 1:100 in 10% NGS O/N @ 4°C | Biotinylated anti-rabbit 1:200 (DAKO), 30mins RT | ABC kit (Vector Labs) |
| Anti-phospho mTOR (ser2448) | Cell Signaling Technology #2971 | Boil 15mins in M/W, citrate buffer (Thermo) | Peroxidase:3% $H_2O_2$ 20mins<br>Serum: 10% NGS 45mins both RT | 3 washes in TBS/T, 5mins | 1:100 in 10% NGS O/N @ 4°C | Biotinylated anti-rabbit 1:200 (DAKO), 30mins RT | ABC kit (Vector Labs) |
| Anti-Ki67 | Vector Labs #VPK452 | 30mins, 100°C W/B, citrate buffer (Thermo) | Peroxidase:0.5% $H_2O_2$ 20mins<br>Serum: 20% NRS 30mins both RT | 3 washes in TBS/T, 5mins | 1:20 in 20% NRS O/N @ 4°C | Biotinylated anti-mouse 1:200 (DAKO), 30mins RT | ABC kit (Vector Labs) |

Table 2.6 Table 1 of IHC conditions

Key: W/B - water bath, M/W - microwave, NRS - normal rabbit serum, NGS - normal goat serum, BSA - bovine serum albumin, RT - room temperature, O/N - over night, TBS/T - tris buffered saline with tween, PBS - phosphate buffered saline

| Primary Antibody | Manufacturer | Antigen retrieval | Non-specific signal block | Wash buffer | Primary antibody conditions | Secondary antibody | Signal amplification step |
|---|---|---|---|---|---|---|---|
| Anti-BrdU | BD Biosciences #347580 (Thermo) | 20mins, 100°C W/B, citrate buffer (Thermo) | Peroxidase: envision+ block (DAKO) 20mins Serum: 1% BSA 1hr both @ RT | 3 washes in PBS, 5mins per wash | 1:150 in 1% BSA for 1hr @ RT | Envision+ HRP-conjugated anti-mouse (DAKO) 30mins @ RT | N/A |
| Anti-lysozyme | Neomarkers #RB-372-A (Thermo) | 20mins, 100°C W/B, citrate buffer (Thermo) | Peroxidase: 1.5% $H_2O_2$ 15mins Serum: 10% NGS 30mins both RT | 3 washes in TBS/T, 5mins per wash | 1:100 in 10% NGS for 1hr @ RT | Envision+ HRP-conjugated anti-rabbit (DAKO) 30mins | N/A |
| Anti-β-catenin | BD Transduction labs #610154 | Boil in citrate buffer (Thermo) in P/C 10mins @ pressure | Peroxidase: envision+ block (DAKO) 5mins Serum: 5% NRS 30mins both RT | 3 washes in TBS/T, 5mins per wash | 1:200 in 5% NRS O/N @ 4°C @ RT | Envision+ HRP-conjugated anti-mouse (DAKO) 30mins @ RT | N/A |
| Anti-E-cadherin | BD Transduction labs #610182 | Boil 15mins in M/W, 1:100 antigen unmasking solution (DAKO):dH₂O | Peroxidase: 0.5% $H_2O_2$ 20mins Serum: 20% NRS 20mins both RT | 3 washes in TBS/T, 5mins per wash | 1:100 in 20% NRS O/N @ 4°C | Biotinylated anti-mouse 1:200 (DAKO) 30mins @ RT | ABC kit (Vector Labs) |
| Anti-CD44 | BD Pharmingen #550538 (Thermo) | 20mins, 100°C W/B, citrate buffer (Thermo) | Peroxidase: 1.5% $H_2O_2$ 15mins Serum: 10% NRS 35mins both RT | 3 washes in TBS/T, 5mins per wash | 1:50 in 10% NRS for 1hr @ RT | Biotinylated anti-rat 1:200 (DAKO) 30mins @ RT | ABC kit (Vector Labs) |
| Anti-Cleaved Caspase 3 (Asp175) | Cell Signaling Technology #9661 | Boil in citrate buffer (Thermo) in P/C 15mins @ pressure | Peroxidase:3% $H_2O_2$ 10mins Serum: 5% NGS 1hr both RT | 3 washes in TBS/T, 5mins per wash | 1:200 in 5% NGS for 2 days @ 4°C | Biotinylated anti-rabbit 1:200 (Vector Labs) 30mins @ RT | ABC kit (Vector Labs) |

**Table 2.7 Table 2 of IHC conditions**

Key: W/B – water bath, M/W – microwave, P/C - Pressure Cooker, NRS – normal rabbit serum, NGS – normal goat serum, BSA – bovine serum albumin, RT – room temperature, O/N – over night, TBS/T – tris buffered saline with tween, PBS – phosphate buffered saline

## 2.8 Protein Extraction and Western Blot Analysis

### 2.8.1 Protein Extraction and quantification

Protein was extracted from epithelial cell pellets obtained from HBSS-EDTA epithelial cell extraction, the pellet was prepared as described in section 2.4.5.4, and stored at -80°C prior to protein extraction.

#### 2.8.1.1 Protein extraction

Pellets were removed from frozen storage and immediately placed on ice, 200μl of lysis buffer (20mM Tris-HCl pH 8.0, 2mM EDTA pH8.0, 0.5% [v/v] NP-40 [Sigma]) containing protease inhibitors (Complete mini protease inhibitor tablets, one tablet per 5ml lysis buffer [Roche]), and phosphatase inhibitors (25mM sodium beta-glycerophosphate [Calbiochem], 100mM sodium fluoride [Sigma], 20nM Calyculin A from *Discodermia calyx* [Sigma], 10mM sodium pyrophosphate [Sigma]), was added to each epithelial cell pellet (400μl was added for larger pellets). Whilst the pellet defrosted, the cells were lysed by shear action to extract proteins by passing through a 21 or 23 gauge needle. The samples were then left on ice for 10 mins before centrifugation at 9500 x g for 10 mins at 4°C. Centrifugation allowed formation of a pellet of insoluble material. The supernatant containing the extracted proteins was then removed, aliquoted and snap frozen in liquid nitrogen before being stored at -80°C.

#### 2.8.1.2 Protein quantification

After protein extraction and prior to snap freezing, an aliquot of each sample was taken and the protein content quantified. Proteins were quantified using the bicinchoninic acid (BCA) method. The BCA method utilises the biuret reaction in which $Cu^{2+}$ ions are reduced to $Cu^{1+}$ ions to produce a purple colour. The reaction is facilitated by the presence of the amino acids cysteine, tyrosine and tryptophan and the universal peptide backbone. The extent to which the copper ions are reduced can be quantified by the colourimetric detection as the BCA reagent strongly absorbs light at 562nm. A high absorbance reading therefore indicates a high protein concentration. Protein samples were measured in duplicate, 2μl was added to 198μl of PBS, mixed and serially diluted twice more to produce three concentrations of protein sample (1 in 100, 1 in 200 and 1 in 300), in a final volume of 100μl. As a standard bovine serum albumin (BSA) was diluted from stock in lysis buffer (recipe above), and then in PBS to

generate a concentration range of 5-25μg/ml. All samples were diluted in a colourless, flat bottom 96-well plate, BCA reagents were made up according to manufacturer's instructions and 100μl added to each sample. The plate was then incubated at 37°C for 1-2 hours. The absorbance of each sample was read on a plate reading spectrophotometer at the nearest wavelength to the optimum (562nm). Samples were read on an ELx800 plate reading spectrophotometer (BioTek) at 590nm. The concentration of each diluted sample was calculated using the standard curve.

## 2.8.2 Western Blot Analysis

### 2.8.2.1 Preparation of protein samples

Protein samples were removed from -80oC freezer and defrosted on ice prior to resolution of the proteins. 30μg of total protein samples were used and made up to 25μl using Laemmli buffer (0.125M Tris-HCl pH6.8, 4% w/v sodium dodecyl sulphate [SDS][Sigma], 40% [v/v] Glycerol [Sigma], 0.1% [w/v] bromophenol blue [Sigma], 6% [v/v] β-mercaptoethanol [Sigma] in double deionised water). Samples were then kept on ice prior to loading into gels. The samples were then heated to 95°C for 5-10 mins and quenched on ice before loading into wells.

### 2.8.2.2 Casting of polyacrylamide gels

The Mini-Protean III (Bio-Rad) gel casting apparatus was used to prepare polyacrylamide gels. Gel solutions were made up to produce a 5% stacking gel and 10% resolving gel (for gel mix solutions see Table 2.8), without the addition of TEMED. Combs were placed in the assembled gel apparatus, and the gel glass plates were then marked with a line approximately 0.5cm below the edge of the comb teeth as a guide for pouring the resolving gel. Combs were removed and gel apparatus placed in a fume hood, TEMED was then added to the solution, quickly mixed and poured between the glass plates to the pre marked line. Then 200μl of butanol was added on top of the gel to ensure the surface of the gel was flat. The gel was then left to set, using the excess resolving gel as a guide to when it was set, and the butanol was poured off. TEMED was then added to the 5% stacking gel and poured on top of the resolving gel to the edge of the glass plates and a 10-well or 12-well comb was inserted. Before loading the samples, the combs were removed and plates placed in sodium dodecyl sulphate-polyacrylamide gel electrophoresis (SDS-PAGE) apparatus, and running buffer added

(see recipe Table 2.8). The combs were removed and each well was flushed out using a pipette to remove excess gel.

### 2.8.2.3 SDS-PAGE

Polyacrylamide gels were set up in an SDS-PAGE Mini-Protean III apparatus rig (Bio-Rad) and 1X running buffer was added. Prepared protein samples (as described in section 2.8.2.1) were added to each well. 7µl of pre-stained full-range Rainbow molecular weight ladder (GE Healthcare) was added to one lane according to manufacturers' recommendations. The gels were then run at 120-200V until the dye front reached the end of the gel.

### 2.8.2.4 Protein transfer to nitrocellulose filter

After the proteins had been separated in the polyacrylamide gel, the gels were removed from glass plates and placed in transfer buffer (see recipe in Table 2.8), before cutting off the stacking gel. Amersham Hybond-ECL nitrocellulose filter (GE Healthcare) was cut to size and briefly soaked in transfer buffer, the nitrocellulose filter was placed on top of the polyacrylamide gel and was sandwiched between two sheets of 3MM blotting paper (Whatman) and sponge, each pre-soaked in transfer buffer. This 'sandwich' was then placed into plastic transfer supports, and placed into a transfer tank orientated so that the current runs through the gel towards the filter (- to +) in order to transfer the negatively charged proteins to the nitrocellulose filter. Transfer buffer was then added to the tank, and it was run at 100V for 1 hour. After transfer the nitrocellulose filter was carefully removed and placed in TBS/T (Tris Buffered Saline with 0.1% Tween, Sigma).

### 2.8.2.5 Antibody probing of filter

The nitrocellulose filter was first blocked for 1 hour in 5% [w/v] non-fat milk powder diluted in TBS/T with agitation. Agitation allowed total coverage of the filter with blocking solution and prevented the filter from drying out. The filter was then washed 3 times for 5 mins in TBS/T before addition of primary antibody, diluted in either 5% non-fat milk in TBS/T or 5% BSA in TBS/T (for antibody conditions see Table 2.9). The filter was incubated with the primary antibody either overnight at 4°C with agitation, or for 1 hour at room temperature with agitation (see Table 2.9), before washing 3 times for 5 mins in TBS/T. The filter was then incubated with HRP-linked secondary antibody diluted in 5% non-fat milk in TBS/T for 1 hour at room temperature

with agitation. The filter was then washed 3 times for 10 mins each time in TBS/T prior to signal detection.

### 2.8.2.6 Signal detection

The electrochemiluminescence (ECL) reagent kit (GE Healthcare) was used according to manufacturers' instructions for detection of antibody signal. These reagents utilise a chemifluorescent reaction catalysed by HRP to expose X-ray film. ECL reagents were prepared according to manufacturers' instructions just prior to use, filters were incubated with the reagents then excess solution removed. The filter was then taken to a dark room under safelight conditions, and X-ray film (Fujifilm Super RX, blue background) was exposed, and the film processed using an automatic processor (Xograph Compact X4 automatic X-ray film processor). A number of exposures of X-ray film for varying amounts of time were generated to produce clear images. These images were then overlaid on the filter in order to confirm the correct protein band size according to the prestained molecular weight ladder.

### 2.8.2.7 Confirmation of equal loading

Filters were reprobed with an antibody for β-actin (see Table 2.9 for conditions) to confirm that equal amounts of protein were added to each well. In order to confirm that increased presence of phospho-Akt and phospho-Erk was not due to higher abundance of unphosphorylated Akt and Erk protein in a particular sample, the same samples were run on two gels were run and one filter was probed with a total-Akt and total-Erk antibody, and the other with a phospho antibody (Table 2.9).

| 5% stacking polyacryalmide gel (2 gels) | 10% resolving polyacrylamide gel (2 gels) |
|---|---|
| 6.9ml Ultrapure double deionised H₂O<br><br>1.7ml 30% acrylamide/bisacrylamide (Sigma)<br><br>1.3ml 1M Tris-HCl pH6.8<br><br>100μl 10% [w/v] SDS (Sigma)<br><br>66μl 25% [w/v] Ammonium persulphate (Sigma)<br><br>13.2μl N,N,N',N'-teramethylethylenediamine(TEMED, Sigma) | 6.8ml Ultrapure double deionised H₂O<br><br>8.4ml 30% acrylamide/bisacrylamide (Sigma)<br><br>9.4ml 1M Tris-HCl pH8.8<br><br>250μl 10% [w/v] SDS (Sigma)<br><br>72μl 25% [w/v] Ammonium persulphate (Sigma)<br><br>13.2μl N,N,N',N'-teramethylethylenediamine(TEMED, Sigma) |
| **5X Running buffer (1L)** | **1X Transfer buffer (1L)** |
| 950ml deionised H₂O<br><br>15.1g Tris base (Sigma)<br><br>94g Glycine (Sigma)<br><br>50ml 10% [w/v] SDS (Sigma) | 800ml deionised H₂O<br><br>200ml Methanol (Fisher)<br><br>2.9g Tris base (Sigma)<br><br>14.5g Glycine (Sigma) |

Table 2.8 Recipes for various buffers used during protein analysis

| Primary Antibody | Manufacturer | Primary antibody conditions | Secondary antibody |
|---|---|---|---|
| Anti-Pten | Cell Signaling Technology #9559 | 1:1000 in 5% BSA in TBS/T, O/N @ 4°C | HRP-conjugated anti-rabbit (GE Healthcare) 1:2000 5% non fat milk in TBS/T, 1hr @ RT |
| Anti-phospho Akt (ser473) | Cell Signaling Technology #9275 | 1:1000 in 5% BSA in TBS/T, O/N @ 4°C | HRP-conjugated anti-rabbit (GE Healthcare) 1:2000 5% non fat milk in TBS/T, 1hr @ RT |
| Anti-Akt (total) | Cell Signaling Technology #9272 | 1:1000 in 5% BSA in TBS/T, O/N @ 4°C | HRP-conjugated anti-rabbit (GE Healthcare) 1:2000 5% non fat milk in TBS/T, 1hr @ RT |
| Anti-Erk (total) | Cell Signaling Technology #4695 | 1:1000 in 5% BSA in TBS/T, O/N @ 4°C | HRP-conjugated anti-rabbit (GE Healthcare) 1:2000 5% non fat milk in TBS/T, 1hr @ RT |
| Anti-phospho Erk (Thr202/Tyr204) | Cell Signaling Technology #4376 | 1:1000 in 5% BSA in TBS/T, O/N @ 4°C | HRP-conjugated anti-rabbit (GE Healthcare) 1:2000 5% non fat milk in TBS/T, 1hr @ RT |
| Anti-β Actin | Sigma #A5316 | 1:5000 in 5% non fat milk in TBS/T, 1 hr @ RT | HRP-conjugated anti-mouse (GE Healthcare) 1:2000 5% non fat milk in TBS/T, 1hr @ RT |

Table 2.9 Antibody conditions for western blot protein analysis

Key: BSA - Bovine Serum Albumin, TBS/T - Tris buffered saline with 0.1% Tween 20, RT - room temperature, O/N - overnight

## 2.9 RNA extraction and Gene Expression analysis

### 2.9.1 RNA isolation and quantification

RNA was isolated from epithelial cell pellets obtained from HBSS-EDTA epithelial cell extraction. The pellet was prepared as described in section 2.4.5.3 and stored at -20°C prior to RNA extraction.

#### 2.9.1.1 Homogenisation of epithelial cells

Epithelial cell pellets were frozen in Trizol (Invitrogen) in homogenising lysing matrix D tubes (MP Biomedicals), and were homogenised from frozen using a Precellys 24 Homogeniser (Bertin Technologies) at 6000RPM for 2 cycles of 25 seconds.

#### 2.9.1.2 Extraction and purification of RNA

Unless stated, all samples were kept on ice during RNA isolation. After homogenisation the whole solution was transferred to 2ml clean RNAse/DNAse free 1.5ml microcentrifuge tubes (Starlab) and centrifuged at 9500 x g for 10 mins at 4°C to pellet insoluble material. The supernatant was then transferred to a new 1.5ml microcentrifuge tube before adding 200µl of chloroform (Fisher) to each tube in a fume hood, the samples were then shaken vigorously by hand before being incubated at room temperature for 3 mins. The samples were then centrifuged at 9500 x g for 15 mins to separate the solution phases. 400µl of the aqueous phase was removed and added to 400µl of isopropanol (Fisher) in a clean 1.5ml microcentrifuge tube and mixed gently to precipitate RNA. The RNeasy Minikit (Qiagen) was then used to isolate and purify RNA. The RNA containing solution was added to RNeasy mini spin columns and centrifuged at 9500 x g for 30 secs at 4°C and the filtrate discarded. The RNA was now bound via adsorption to the silica-based column membrane, the RNA was DNase treated by incubating with DNase I (GE Healthcare) according to manufacturer's instructions for 10 mins at room temperature. The column was then washed by centrifugation of the column with 500µl of RPE buffer (RNeasy Mini Kit, Qiagen) once at 9500 x g for 30 secs at 4°C and filtrate discarded, then again at 9500 x g for 2 mins at 4°C and filtrate discarded. The column was finally centrifuged at 9500 x g for 1 min at 4°C without wash buffer to ensure the column contained no wash buffer.

The column was then incubated with 50µl RNase-free $H_2O$ (RNeasy Mini Kit, Qiagen) for 3 mins on ice. The column was then placed in a clean RNAse/DNAse free 1.5ml microcentrifuge tube and centrifuged at 9500 x g for 1 min at 4°C to elute the

RNA. The RNA was then aliquoted and stored at -80°C. The RNA was quantified in a 1μl sample using a NanoDrop 1000 (Thermo Scientific).

### 2.9.1.3 cDNA Synthesis

cDNA was prepared from 1μg of RNA using Superscript II reverse transcriptase (Invitrogen). Random hexamers (Invitrogen) were first annealed to the RNA. An annealing mixture solution was made up of RNA, random primers and dH₂O (outlined in Table 2.10) and was pipetted into strip tubes with appropriate caps (Greiner Bio-One). The samples were incubated at 70°C for 10 mins, 25°C for 10 mins and then stored at 4°C using a PTC-100 Peltier Thermocycler (MJ Research). A further 20μl of a reverse transcriptase enzyme mix (outlined in Table 2.11) was added to each sample whilst still in the thermocycler held at 4°C. Reverse transcription was carried out under the following conditions: 25°C for 10 mins, 37°C for 45 mins, 42°C for 45 mins, 70°C for 15 mins. After cDNA synthesis was complete 160μl of RNAse free water was added to each sample.

| Annealing mixture (per reaction) |
|---|
| 1μg RNA |
| 5μl Random hexamers (25ng/μl) (Invitrogen) |
| Make up to 20μl RNase free dH₂O |

Table 2.10 Annealing mixture per reaction

| Reverse transcription enzyme mix (per reaction) |
|---|
| 8μl 5x First stand buffer (Invitrogen) |
| 4μl Dithiothreitol (DDT) (Invitrogen) |
| 0.8μl dNTPs (25mM) (Bioline) |
| 1μl SuperScript II |
| 6.2μl RNAse free water |
| Total volume 40μl per reaction |

Table 2.11 Reverse transcription enzyme mixture per reaction

### 2.9.1.4 TaqMan Gene expression analysis

Quantification of gene expression of CBC stem cell markers Lgr5 and Ascl2 was carried out using TaqMan assays (Applied Biosystems). TaqMan assays involve the use of

three gene specific probes that allow sensitive quantification of genes expressed at low levels. Epithelial cell extracts from which RNA was extracted were made up of cells from the whole of the crypt-villus axis, so only a fraction of these cells would be stem cells. Thus, only a small proportion of the RNA extracted will represent mRNA transcribed from Lgr5 and Ascl2 genes. TaqMan assays are predesigned probes for various genes in various species. Each assay contains a forward and reverse primer for the gene of interest, and a probe complimentary to an internal region of the PCR product of these primers. The probe has a fluorescent molecule attached to the 5' end, and a quencher molecule attached to the 3' end. During the PCR reaction, the probe and primers bind to the DNA and when polymerisation occurs the Taq polymerase cleaves the fluorescent molecule from the probe (by 5'-3' nuclease activity of the enzyme) and releases it from its close position to the quencher molecule, allowing it to fluoresce.

As the relative abundance of stem cell marker cDNA is low in the intestinal epithelial cell cDNA samples, using traditional qRT-PCR reaction reagents such as Sybr green (which fluoresces when bound to double stranded DNA) can result in false positive readouts, as fluorescence from Sybr green binding to primer dimers that form may mask fluorescence from the PCR reaction.

### 2.9.1.5 Conditions for TaqMan gene expression analysis

qRT-PCR reactions were carried out in triplicate (including no DNA control wells), in MicroAmp 96-well PCR plates 0.1ml wells (Applied Biosystems), and sealed with MicroAmp heat activated optical adhesive film lids (Applied Biosystems). Each reaction contained 10ng of cDNA, 10μl TaqMan universal PCR mastermix (containing Taq polymerase, buffers and dNTPs) (Applied Biosystems), 1μl gene specific assay (supplied as a 20X stock, Applied Biosystems) and was made up to 25μl with PCR-grade $H_2O$. The assay mixes used for each gene of interest were as follows: Lgr5 (Assay I.D. mm00438890-m1, Applied Biosystems), Ascl2 (Assay I.D. mm01268891-g1, Applied Biosystems) and β-actin was used as an internal control. qRT-PCR reactions were carried out using the StepOne Plus Real-Time PCR System (Applied Biosystems), all reactions were carried out under the same cycling conditions (50°C for 2 min [for optimal uracil-N-glycosylase enzyme activity], 95°C for 10 min [for activation of the Taq DNA polymerase enzyme], then 40 cycles of: a denaturation step 95°C for 15 sec, and an annealing/elongation step – 60°C for 1 min). The data was collected automatically using StepOne software (Applied Biosystems).

## 2.9.1.6 Analysis of qRT-PCR data

The experimental data were collected automatically using StepOne software (Applied Biosystems). The data were examined prior to data analysis to ensure there were no fluorescent products in 'no cDNA' control wells, and that the fluorescence vs cycle plots for each replicate were comparable.

Differences in target gene expression between each cohort was assessed by comparing the changes in the number of cycles it takes for the fluorescence levels to reach the exponential phase, i.e. the higher the abundance of target gene cDNA the lower number of cycles it takes for the level of fluorescence to reach the exponential phase. Fluorescence vs cycle number plots were generated and thresholds sets automatically by the software, cycle time ($C_T$) and difference in cycle time ($\Delta C_T$) values were calculated between cohorts, normalising each reaction using the beta actin control. $C_T$ values were calculated automatically by the software and were verified by manual calculation from the raw data. The average $\Delta C_T$ was calculated for each cohort, $\Delta C_T$ means of each cohort were compared statistically using the Mann-Whitney U test to confirm significant changes in cycle time.

## 2.10 Assessment of recombination of genomic DNA

Assessment of recombination of loxP sites by cre recombinase was achieved by carrying out a PCR reaction that produced a PCR product only when loxP sites had recombined in the gDNA. Primers are designed so that they only come into close proximity in a gene when the loxP sites have been recombined and the DNA between them excised. A distinct PCR product can then be amplified (recombined band). gDNA was extracted from crude epithelial enriched samples obtained by scraping the intestinal mucosal surface with a scalpel as described in section 2.4.5.1. DNA was extracted using the same protocol used for extracting gDNA from ear biopsies outlined in section 2.3.1.

### 2.10.1 Recombined PCR reactions

The recombined PCR protocol was carried out in the same manner as described for the genotyping PCR in section 2.3.2. Both the Pten and Kras recombined PCRs could be multiplexed, combining the primers used to detect the presence of the WT and loxP targeted alleles with the primer used to generate the recombined or 'floxed' PCR product, so in these cases 2-3 PCR products were produced. The Apc and Cdh1 recombined PCRs yielded PCR products similar in size to the genotyping PCR products so these could not be multiplexed. The genotyping and recombined PCRs therefore had to be carried out separately. The primers required for recombined PCR of each allele are outlined in Table 2.12. The PCR reaction mixtures and cycling conditions for each allele are described in Table 2.13. The reaction mixtures for Pten and Kras PCRs are for the multiplex PCR, so will produce all relevant PCR products. The reaction mixtures for Apc and Cdh1 in Table 2.13 will only produce the PCR product for the recombined (floxed) allele so a separate genotyping PCR must be carried out to determine heterozygosity or homozygosity of the loxP flanked allele. These conditions and primers are described in Table 2.2 and Table 2.3.

### 2.10.2 Visualisation of PCR products

After recombined PCR reactions were carried out, PCR products were visualised in the same manner as described for visualisation of genotyping PCR products in section 2.3.3. The use of a 100bp ladder (Promega) as a marker of molecular weight of products allowed correct identification of PCR products only produced in recombined gDNA.

| Gene | Primers | Reference |
|------|---------|-----------|
| Pten | 1 Forward: 5'-GGCCTAGGACTCACTAGATAGC-3' <br> 2 Reverse: 5'-CTCCCACCAATGAACAAACAGT-3' <br> 3 Forward: 5'-GTGAAAGTGCCCCAACATAAGG-3' | Provided by Akira Suzuki, Akita University, Japan |
| Kras | 1 Forward: 5'-AGGGTAGGTGTTGGGATAGC-3' <br> 2 Reverse: 5'-CTCAGTCATTTTCAGCAGGC-3' <br> 3 Reverse: 5'-CTGCTCTTTACTGAAGGCTC-3' | (Guerra et al., 2003) |
| Apc | 1 Forward 5'-GTTCTGTATCATGGAAAGATAGGTGGTC-3' <br> 2 Reverse 5'-GAGTACGGGGTCTCTCTGTCTCAGTGAA-3' | (Shibata et al., 1997) |
| Cdh1 | 1 Forward 5'-ACATGTTTGTATCGATCTCAG-3' <br> 2 Reverse 5'-CCTGCCATGATTGTCATGGAC-3' | (Derksen et al., 2006) |

Table 2.12 Primers required for recombined PCR reactions

| | Pten Recombined | Apc Recombined | Kras Recombined | Cdh1 Recombined |
|---|---|---|---|---|
| PCR reaction mix | Multiplex PCR | | Multiplex PCR | |
| gDNA | 3µl | 2.5µl | 3µl | 2.5µl |
| PCR-grade water | 31.1µl | 31.7µl | 31.1µl | 31.7µl |
| GO Taq PCR buffer (5X) | 10µl | 10µl | 10µl | 10µl |
| MgCl$_2$ (25mM) | 5µl | 5µl | 5µl | 5µl |
| dNTPs (25mM) | 0.4µl | 0.4µl | 0.4µl | 0.4µl |
| Primer 1 (100mM) | 0.1µl | 0.1µl | 0.1µl | 0.1µl |
| Primer 2 (100mM) | 0.1µl | 0.1µl | 0.1µl | 0.1µl |
| Primer 3 (100mM) | 0.1µl | N/A | 0.1µl | N/A |
| Taq DNA polymerase | 0.2µl | 0.2µl | 0.2µl | 0.2µl |
| Brand of Taq polymerase | GoTaq | GoTaq | GoTaq | GO Taq |
| PCR cycling conditions | | | | |
| Initial denaturation | 5 min, 94°C | 3 min, 95°C | 5 min, 94°C | 2.5 min, 94°C |
| Cycle number | 35 cycles of: | 30 cycles of: | 30 cycles of: | 35 cycles of: |
| Step 1: denaturation | 1 min, 94°C | 30 sec, 95°C | 1 min, 94°C | 30 sec, 94°C |
| Step 2: annealing | 1 min, 58°C | 30 sec, 60°C | 1 min, 60°C | 30 sec, 60°C |
| Step 3: Extension | 1 min, 72°C | 1 min, 72°C | 1 min, 72°C | 1 min, 72°C |
| Final extension | 5 min, 72°C | 5 min, 72°C | 5 min, 72°C | 5 min, 72°C |
| | Hold at 15°C | Hold at 15°C | Hold at 15°C | Hold at 15°C |
| PCR product sizes | Targeted: 514bp Recombined: 705bp | Recombined: 258bp | WT band: 403bp Targeted stop cassette: 621bp Recombined: 669bp | Recombined: 320bp |

Table 2.13 Recombined PCR reaction mixtures, cycling conditions and product sizes

## 2.11 Data Analysis

### 2.11.1 Graphical representation of data

Raw data obtained from scoring, grading and quantitative PCR were inputted into Excel (Microsoft) spreadsheets. All means, standard deviations and sums were calculated using the calculator functions. Graphical representation of all data was also produced in Excel (Microsoft).

### 2.11.2 Comparison of means

The Minitab 15 (Minitab Inc.) statistical package was used to carry out normality tests of data (using the Andresson-Darling normality test) and comparison of means (using the Mann Whitney U test). Comparison of means analysis was carried out on cell scoring and $\Delta C_T$ data from qPCR using the Mann-Whitney U test, as all data collected was not normal.

### 2.11.3 Comparison of Cell Migration

BrdU positive cell positions were plotted as cumulative frequency curves, and were analysed using the Kolmologrov-Smirnov test using SPSS 16 (SPSS Inc.).

### 2.11.4 Survival Analysis

Survival data were analysed using MedCalc (MedCalc), Kaplan-Meier plots were used to present data, and significance was measured using the Log Rank test.

# Chapter 3: Analysing the short term intestinal phenotype of Pten loss and Kras activation

## 3.1 Introduction

PTEN (Phosphatase and tensin homolog deleted on chromosome ten) is a tumour suppressor gene that is a negative regulator of the PI3K pathway. In humans germline mutations of PTEN give rise to a group of inherited diseases collectively called PTEN hamartoma tumour syndromes, reviewed in (Blumenthal and Dennis, 2008), the most common of which being Cowden syndrome. Symptoms of this autosomal dominant disease include neural developmental defects (Padberg et al., 1991), and the formation of well-differentiated benign tumours called hamartomas found in multiple organs including the GI tract (Carlson et al., 1984, Merg and Howe, 2004). The individual is predisposed to cancer as these benign tumours are subject to malignant transformation. Somatic mutations in PTEN are commonly found in many sporadic cancers, examples include prostate (Feilotter et al., 1998, Wang et al., 1998), breast (Li et al., 1997, Saal et al., 2008), and endometrial cancer (Tashiro et al., 1997, Risinger et al., 1997). Due to PTEN's role in the development of benign tumours in the GI tract of Cowden syndrome patients, and its role in sporadic CRC, it is the subject of much research. For example in a study of CRC tumours, 40% harboured mutations in the PI3K pathway (including PTEN mutations), which would result in constitutive activation of the pathway (Parsons et al., 2005). Also, some studies have suggested that loss of PTEN expression is associated with poor clinical outcome of CRC patients (Jang et al., 2010, Li et al., 2009).

Another commonly mutated gene involved in both the PI3K pathway and the MAPK/Erk pathway is the oncogene KRAS. It is a member of the Ras family of small GTPases, and acts a signal transducer that activates both the p110 catalytic subunit of the PI3K protein (Rodriguez-Viciana et al., 1996), and the MAP kinase BRAF or CRAF. It is commonly mutated at codon 12 (glycine) which prevents association of guanine nucleotide exchange factor (GEF) and the subsequent dissociation of GTP, leaving Kras permanently bound to GTP and permanently in an 'on state'. The oncogenic form of KRAS is associated with many cancer types including lung (Mills et al., 1995), pancreatic (Almoguera et al., 1988, Smit et al., 1988) and colorectal cancer. KRAS has been found to be constitutively active in 40-50% of CRCs (Bos et al., 1987), its oncogenic activation constitutes one of the step-wise mutations required for the formation of colorectal cancer as described by (Fearon and Vogelstein, 1990).

Despite reports of intestinal neoplasia in a number of mouse models of Pten mutation (Di Cristofano et al., 1998, Podsypanina et al., 1999), and models of Kras activation (Calcagno et al., 2008, Janssen et al., 2002), other studies have reported that intestinal epithelial specific homozygous deletion of Pten (Marsh et al., 2008, Langlois et al., 2009) or inducible activation of Kras (Sansom et al., 2006, Haigis et al., 2008) alone do not result in tumour formation. As both PTEN and KRAS act within the same pathway, I hypothesise that there may be synergy between the two mutations in the context of murine intestinal neoplasia. Synergy between Pten and Kras has been noted in a number of tumour models including mouse models of endometrial, lung and pancreatic cancer (Dinulescu et al., 2005, Iwanaga et al., 2008, Hill et al., 2010). Unpublished data from the Clarke lab have also demonstrated synergy between Pten and Kras. These findings demonstrated that Pten deletion and activation of oncogenic Kras$^{G12V}$, result in the formation of both cholangio carcinoma and hyperplasia of the forestomach. Pten deletion and Kras activation was achieved by conditional transgenesis in this model, using the AhCre recombinase transgene. Expression of this transgene is driven by the Cyp1a1 promoter, which is induced by the presence of xenobiotics (Ireland et al., 2004). The AhCre transgene is expressed in a range of tissues including the epithelium of bile ducts, stomach, bladder, intestine and hepatocytes. Due to its wide range of expression, the effect of Pten deletion and Kras$^{G12V}$ activation on the intestinal epithelium was unable to be investigated using this cre recombinase transgene, as the onset of morbidity after induction of cre recombinase activity was rapid in these mice (around 40 days).

The following four chapters will address synergy between Pten and Kras in the small intestine at various time points after induction, both alone and in the context of Wnt activated tumourigenesis. In order to achieve intestinal specific recombination the VillinCreER$^T$ recombinase transgene was used, which is expressed throughout the intestinal epithelium (El Marjou et al., 2004). In this chapter I will investigate the short term effects of Pten loss and Kras activation alone, and with the addition of a heterozygous Apc mutation in the small intestine at day 15 post induction. Mice were generated bearing the VillinCreER$^T$ recombinase transgene and were homozygous for loxP flanked alleles of Pten (Suzuki et al., 2001), heterozygous for lox-stop-lox oncogenic Kras$^{G12V}$ (Kras$^{LSL/+}$) (Guerra et al., 2003) and with or without one loxP flanked allele of Apc (Shibata et al., 1997). Mice homozygous for oncogenic Kras are essentially Kras knockouts as the stop cassette inserted upstream of the gene prevents any expression, this lack of Kras expression causes homozygous embryos to die in utero, therefore oncogenic Kras heterozygotes are only available to study. VillinCreER$^T$-Pten$^{fl/fl}$

Kras$^{LSL/+}$ (hereafter referred to as Pten$^{fl/fl}$ Kras$^{LSL/+}$) and *Villin*CreER$^{T}$-Apc$^{fl/+}$ Pten$^{fl/fl}$ Kras$^{LSL/+}$ mice (hereafter referred to as Apc$^{fl/+}$ Pten$^{fl/fl}$ Kras$^{LSL/+}$) along with their appropriate controls were induced and sacrificed at 15 days post induction.

## 3.2 Results

### 3.2.1 Permanent recombination of loxP sites at the Apc, Pten and Kras locus is achieved in the intestinal epithelium

Mice were dissected and crude epithelial cell extracts were obtained from the small intestine by scraping the mucosal surface. To ascertain cre-mediated recombination of gDNA, gDNA was extracted from these samples and PCR for the recombined alleles of each of the loxP targeted genes was carried out. PCR was carried out on all samples to confirm recombination of the loxP sites. Figure 3.1 shows PCR products of representative samples of each of the cohorts induced.

*Villin*Cre recombinase is expressed in all intestinal epithelial cells, including stem cells, but can only enter the nucleus when tamoxifen is present and binds to its fused estrogen receptor. Recombination at each locus in the stem cell compartment allows permanent manipulation of the genome in cells that are maintained long term in the intestinal epithelium. The presence of a band corresponding to the recombined allele for each locus (a 705bp band for the Pten locus, 669bp band for Kras and a 258bp band for Apc), confirmed that the genes of interest had been successfully mutated. A PCR product for the recombined allele was present for each loxP flanked sample using DNA obtained from mice induced 15 days previously. Given that the intestinal epithelium renews itself every 2-3 days and mice were examined 15 days following induction, this strongly implies recombination has occurred within the stem cell population.
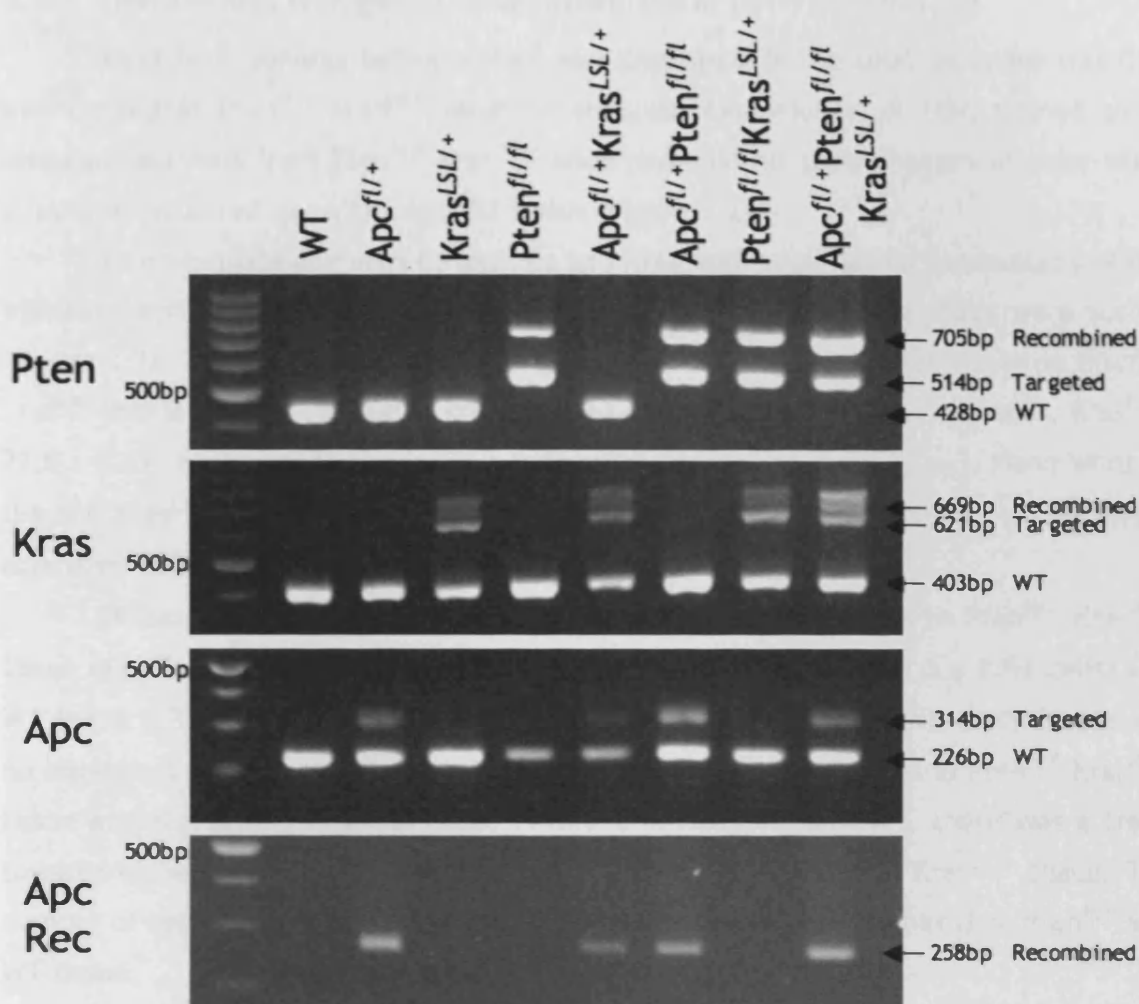
Figure 3.1 Recombined PCR confirmed that successful recombination at each loci was achieved and maintained at 15 days post induction

Recombination of loxP sites, and therefore gene mutation, was confirmed in each cohort by PCR carried out on gDNA from intestinal epithelial cells for the recombined allele. Primers are designed so that they only come into close proximity in a gene when loxP sites have been recombined and the DNA between them excised, a distinct PCR product can then be amplified (recombined band). Pten and Kras recombined PCRs could be multiplexed, whereas the recombined PCR for Apc was split due to similar product sizes. Pten: 705bp recombined band, 514bp loxP site targeted band, 428bp WT band. Kras: 669bp recombined band, 621bp loxP site targeted band, 403bp WT band. Apc: 314bp loxP site targeted band, 226bp WT band, Apc$^R$: 258bp recombined band.

### 3.2.2 Pten and Kras synergise to cause hyperplasia of the crypt-villus axis

Short term synergy between Pten and Kras alone in the small intestine was first investigated in Pten$^{fl/fl}$ Kras$^{LSL/+}$ mice. Histological examination of H&E stained small intestinal sections from Pten$^{fl/fl}$ Kras$^{LSL/+}$ mice revealed no gross changes in crypt-villus structure compared to control and WT tissue (Figure 3.2).

To investigate any effect Pten loss and Kras activation has on homeostasis of the intestinal epithelium, the number of cells per half crypt and half villus were scored (Figure 3.3). There were significantly higher numbers of cells per half crypt in Pten$^{fl/fl}$ Kras$^{LSL/+}$ tissue (30.7 ± 1.56 cells) compared to controls (Pten$^{fl/fl}$ 26 ± 1.84 cells, Kras$^{LSL/+}$ 27.8 ± 0.45 cells) and WT tissue (25 ± 2.42 cells) (p values = 0.0259, n≥3, Mann Whitney U test). Kras$^{LSL/+}$ control tissue also had a significantly higher number of cells per crypt compared to WT tissue (p value = 0.04, n≥3, Mann Whitney U test).

Similarly there were higher numbers of cells per half villus in Pten$^{fl/fl}$ Kras$^{LSL/+}$ tissue (129.5 ± 17.67 cells) compared to Pten$^{fl/fl}$ control tissue (104.3 ± 2.63 cells) and WT tissue (82.4 ± 6.93 cells) (p values = 0.0259, n≥3, Mann Whitney U test). There was no significant difference between the number of cells per half villus in Pten$^{fl/fl}$ Kras$^{LSL/+}$ tissue and the Kras$^{LSL/+}$ control tissue (118.9 ± 4.4 cells). However, there was a trend towards higher villus cell number in Pten$^{fl/fl}$ Kras$^{LSL/+}$ compared to Kras$^{LSL/+}$ tissue. The number of cells per half villus in Kras$^{LSL/+}$ tissue was significantly higher than Pten$^{fl/fl}$ and WT tissue.

Despite increases in crypt and villus cell number in Pten$^{fl/fl}$ Kras$^{LSL/+}$ tissue, they do not appear to be accompanied by an increase or decrease in apoptosis (Pten$^{fl/fl}$ Kras$^{LSL/+}$ = 0.06 ± 0.016, Pten$^{fl/fl}$ = 0.047 ± 0.064, Kras$^{LSL/+}$ = 0.047 ± 0.05, WT = 0.03 ± 0.02 apoptotic bodies) and mitosis (Pten$^{fl/fl}$ Kras$^{LSL/+}$ = 0.59 ± 0.17, Pten$^{fl/fl}$ = 0.61 ± 0.17, Kras$^{LSL/+}$ = 0.071 ± 0.15, WT = 0.52 ± 0.09 mitotic figures) or Ki67 positive cycling cells (Pten$^{fl/fl}$ Kras$^{LSL/+}$ = 27 ± 4.03, Pten$^{fl/fl}$ = 21.4 ± 1.81, Kras$^{LSL/+}$ = 24 ± 2.54, WT = 21.1 ± 1.5 cells). Thus, despite an increasing trend in Ki67 positive cells in Pten$^{fl/fl}$ Kras$^{LSL/+}$ and Kras$^{LSL/+}$ tissue compared to WT none of these changes were significant. However, Kras$^{LSL/+}$ tissue had a significantly higher abundance of mitotic figures (0.71 ± 0.15 cells) compared to WT tissue (0.52 ± 0.09) (p value = 0.0383, n≥3, Mann Whitney U test) (Figure 3.3, Figure 3.4).

Taken together, these data indicate that concomitant Pten loss and Kras activation disrupts normal intestinal homeostasis resulting in increased numbers of cells along the crypt-villus axis. Surprisingly, these changes in Pten$^{fl/fl}$ Kras$^{LSL/+}$ tissue were not accompanied by an increase in mitotic figures or Ki67 positive cycling cells.

**WT**    **Kras^{LSL/+}**

**Pten^{fl/fl}**    **Pten^{fl/fl}Kras^{LSL/+}**
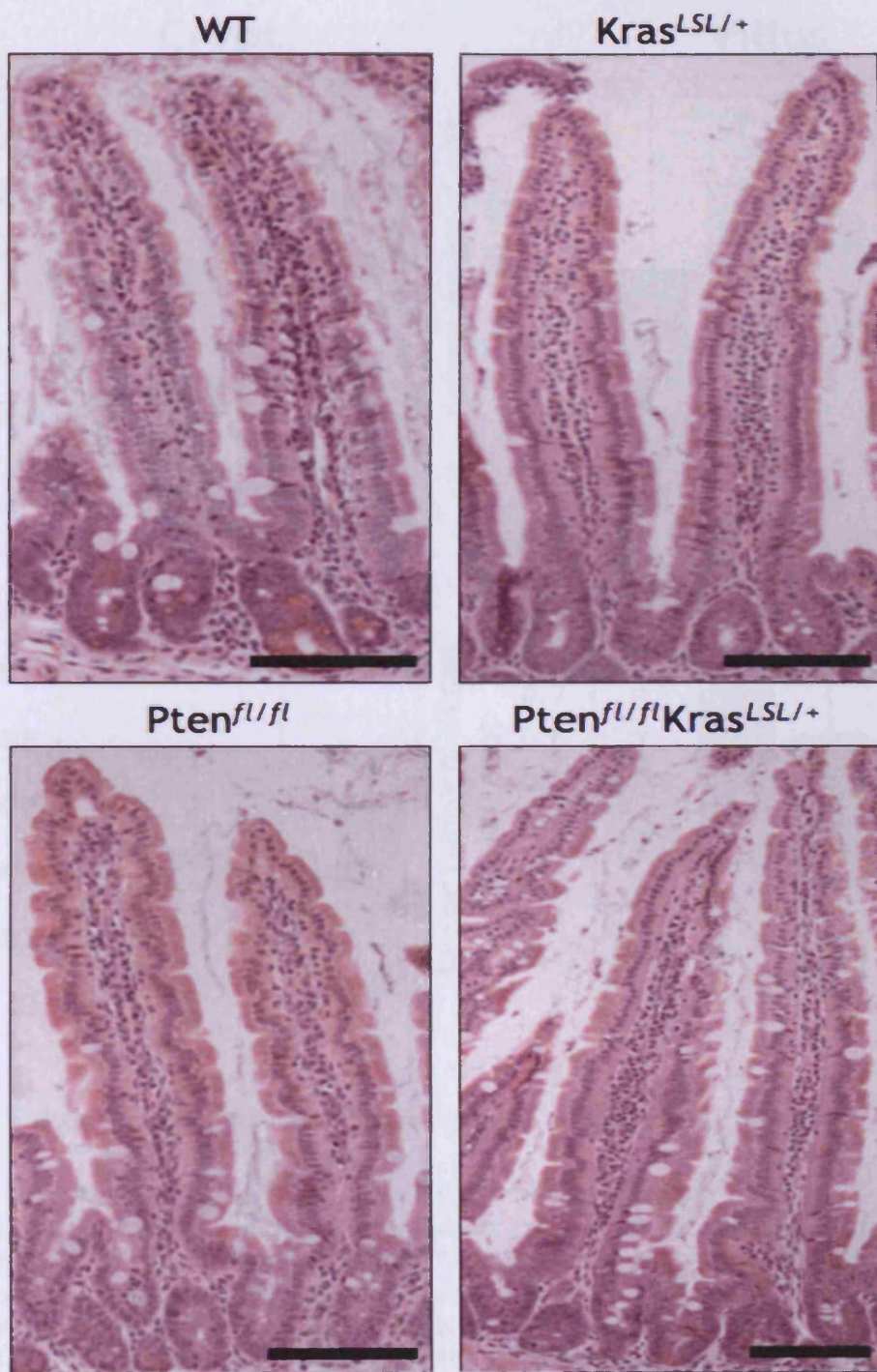
**Figure 3.2 Pten loss and Kras activation causes no gross alteration of the crypt-villus structure at day 15 post induction**

Histological examination of H&E stained small intestinal sections revealed no overt changes in crypt-villus structure of Pten^{fl/fl} Kras^{LSL/+} mice compared to the controls and WT tissue. Scale bars represent 200μm.
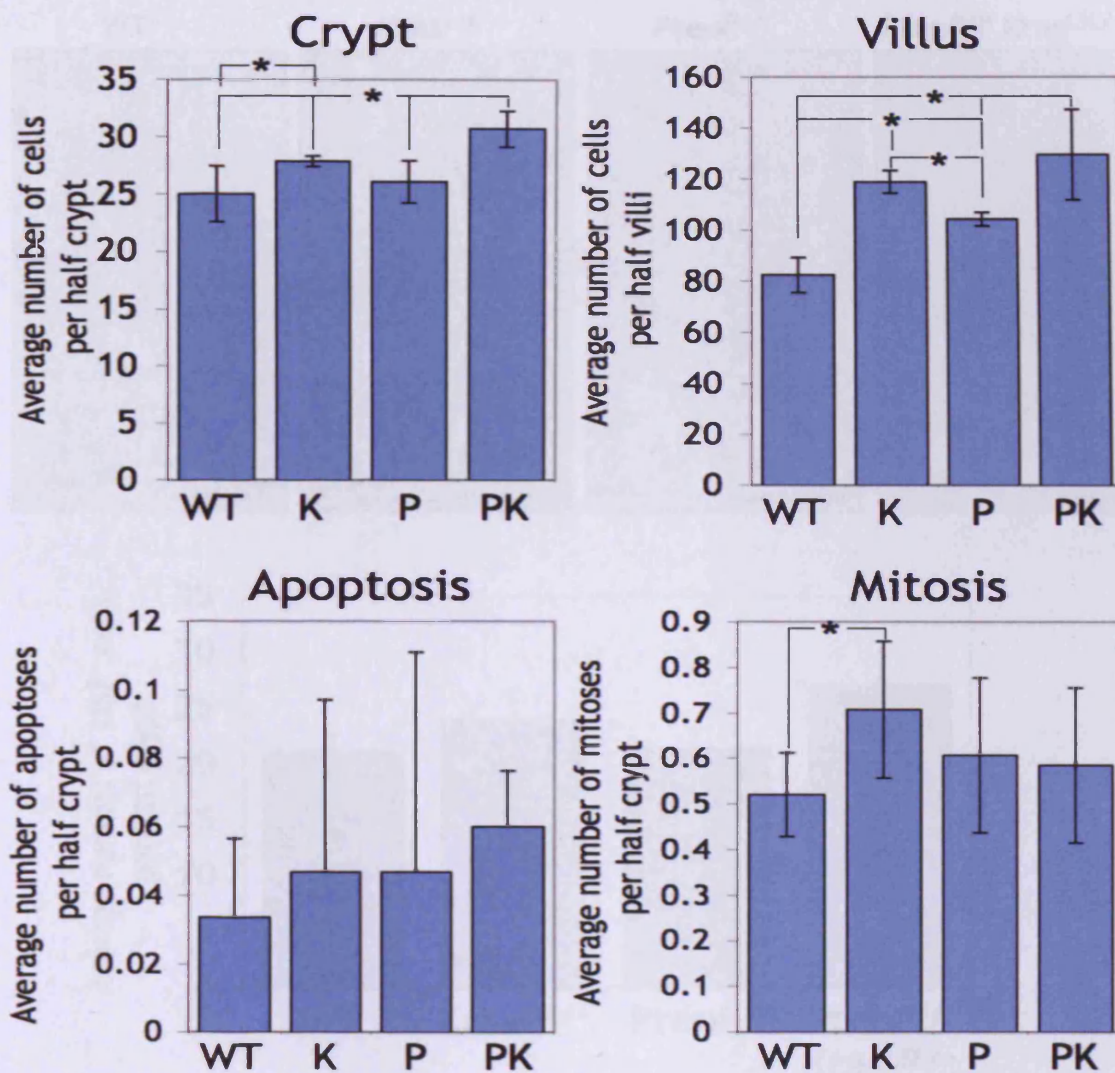
**Figure 3.3 Pten loss and Kras activation results in increased crypt and villus cell number**

Key: WT – Wild Type, K – Kras$^{LSL/+}$, P – Pten$^{fl/fl}$, PK – Pten$^{fl/fl}$ Kras$^{LSL/+}$

Crypt cell scoring revealed increased number of cells per half crypt in Pten$^{fl/fl}$ Kras$^{LSL/+}$ tissue compared to controls and WT tissue. The number of cells per half crypt in Kras$^{LSL/+}$ control tissue was also significantly higher compared to Pten$^{fl/fl}$ and WT tissue. Villus cell scoring revealed increased number of cells per half villus in Pten$^{fl/fl}$ Kras$^{LSL/+}$ tissue compared to Pten$^{fl/fl}$ and WT tissue (p value = 0.0259, n≥3, Mann Whitney U test). However Pten$^{fl/fl}$ Kras$^{LSL/+}$ villus cell number was not significantly different from Kras$^{LSL/+}$ tissue (p value = 0.1884, n≥3, Mann Whitney U test). Kras$^{LSL/+}$ tissue also had significantly higher numbers of cells per half villus compared to Pten$^{fl/fl}$ and WT tissue (*, p value <0.05, n≥3, Mann Whitney U test). There were no changes in the number of apoptotic bodies or mitotic figures as scored by H&E examination in Pten$^{fl/fl}$ Kras$^{LSL/+}$ tissue compared to controls and WT tissue (p values >0.05, n≥3, Mann Whitney U test), Kras$^{LSL/+}$ tissue had significantly higher number of mitotic figures compared to WT (*, p value = 0.0383, n≥3, Mann Whitney U test). Error bars indicate standard deviation.

| | WT | Kras$^{LSL/+}$ | Pten$^{fl/fl}$ | Pten$^{fl/fl}$ Kras$^{LSL/+}$ |
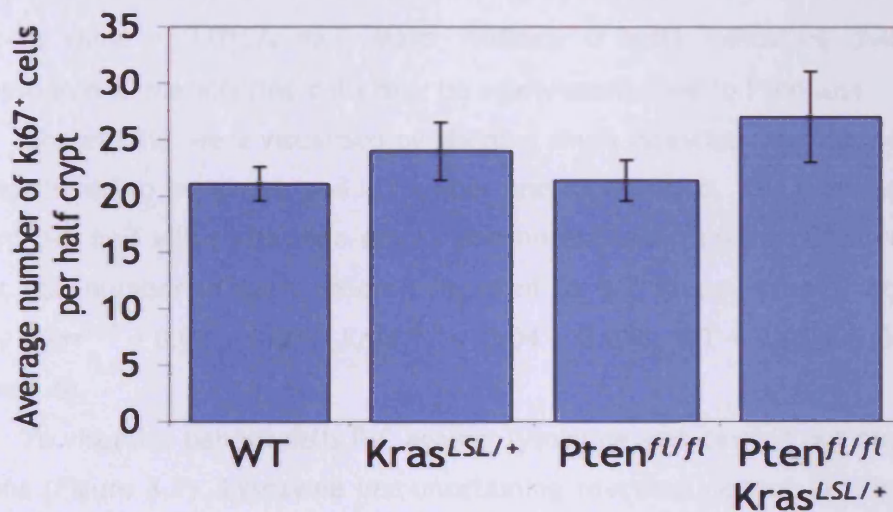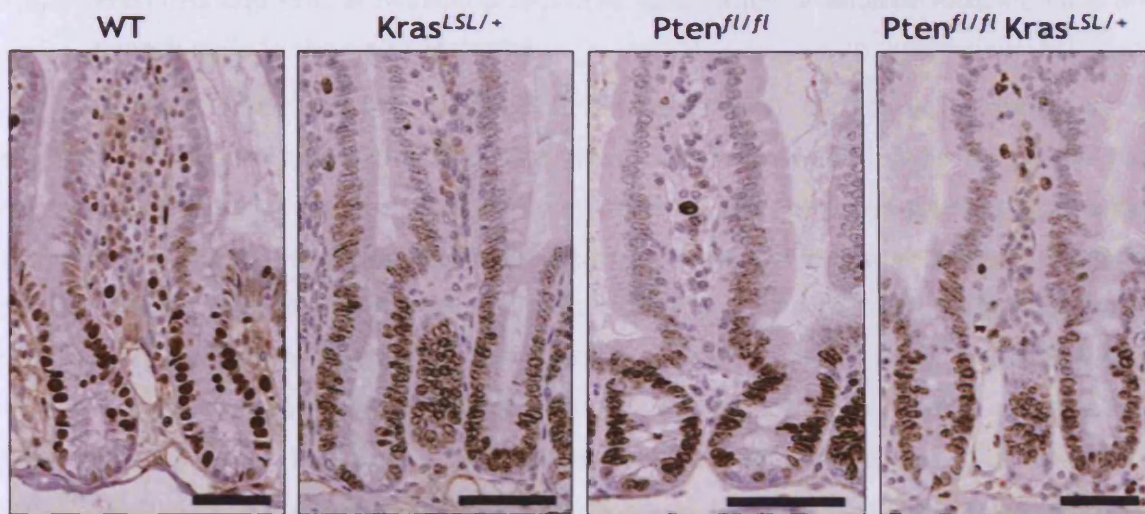
Figure 3.4 Pten loss and Kras activation does not affect the number of cycling cells present per half crypt

IHC against the cell cycle marker, Ki67, was carried out on small intestinal sections. There appeared to be no gross alteration in the positioning or abundance of Ki67 positive cells in Pten$^{fl/fl}$ Kras$^{LSL/+}$ tissue compared to controls and WT tissue, scale bars represent 50μm. This was confirmed by scoring the number of Ki67 positive cells per half crypt. There were no significant changes in the abundance of Ki67 positive cells (p values >0.05, n≥3, Mann Whitney U Test). However Pten$^{fl/fl}$ Kras$^{LSL/+}$ and Kras$^{LSL/+}$ tissue trended towards higher numbers of Ki67 positive cells compared to Pten$^{fl/fl}$ and WT tissue. Error bars indicate standard deviation.

### 3.2.3 Pten loss and Kras activation affects the abundance of enteroendocrine cells and paneth cells in the small intestine

As Pten loss and Kras activation disrupts small intestinal homeostasis, as evidenced by hyperplasia of the crypt and villus, the number and localisation of the four major small intestinal mature cell types was determined. Grimelius staining was carried out on small intestinal sections to mark enteroendocrine cells. Enteroendocrine scoring per half crypt-villus (and normalising for alterations in crypt-villus cell number) revealed significantly reduced numbers of enteroendocrine cells in $Pten^{fl/fl}$ $Kras^{LSL/+}$ tissue (0.0035 ± 0.0003 cells) compared to WT tissue (0.005 ± 0.0005 cells) (p value = 0.0404, n≥3, Mann Whitney U test) (Figure 3.5). The number of enteroendocrine cells present in $Pten^{fl/fl}$ tissue (0.004 ± 0.0005 cells) was also lower than WT tissue (p value = 0.0404, n≥3, Mann Whitney U test) but was not significantly different from $Pten^{fl/fl}$ $Kras^{LSL/+}$ tissue (p value = 0.0952, n≥3, Mann Whitney U test) indicating that the observed decrease in enteroendocrine cells may be solely attributed to Pten loss.

Goblet cells were visualised by staining small intestinal sections with alcian blue; they appeared to be unchanged in number and localisation. The number of goblet cells present per half villus was then scored and normalised. Scoring revealed no changes in goblet cell number in each cohort compared to WT tissue ($Pten^{fl/fl}$ $Kras^{LSL/+}$ = 0.05 ± 0.006, $Pten^{fl/fl}$ = 0.05 ± 0.004, $Kras^{LSL/+}$ = 0.04 ± 0.008, WT = 0.06 ± 0.006 goblet cells) (Figure 3.6).

To visualise paneth cells IHC against lysozyme was carried out on small intestinal sections (Figure 3.7). Lysozyme immunostaining revealed normal localisation of paneth cells (at the base of the crypt) in $Pten^{fl/fl}$ $Kras^{LSL/+}$ tissue. However, paneth cell scoring revealed that $Pten^{fl/fl}$ tissue had significantly lower numbers of paneth cells per crypt (3.12 ± 0.156 cells) compared to WT tissue (3.49 ± 0.117 cells) (p value = 0.0404, n≥3, Mann Whitney U test). Additional mutation of Kras in $Pten^{fl/fl}$ $Kras^{LSL/+}$ mice further enhances this phenotype, as $Pten^{fl/fl}$ $Kras^{LSL/+}$ tissue possessed significantly lower numbers of paneth cells (1.85 ± 0.306 cells) compared to $Pten^{fl/fl}$ tissue (3.12 ± 0.156 cells) as well as $Kras^{LSL/+}$ (2.96 ± 0.410 cells) and WT tissue (3.49 ± 0.117 cells) (p values = 0.0404, n≥3, Mann Whitney U test).

The localisation of alkaline phosphatase was visualised using a chromogenic substrate for alkaline phosphatase that is catalysed to produce a red stain. Small intestinal sections were incubated with the substrate. Alkaline phosphatase is normally expressed on the apical surface of enterocytes. The red stain therefore demarcates the apical surface of enterocytes and indicates the polarisation of the intestinal epithelium. Alkaline phosphatase staining revealed it to be localised to the apical/luminal surface of

the villus epithelium (Figure 3.8). Alkaline phosphatase is only present in differentiated enterocytes at the top of the crypt and along the length of the villus. There appeared to be no changes in alkaline phosphatase localisation in Pten$^{fl/fl}$ Kras$^{LSL/+}$ tissue compared to control and WT tissue.

In summary, staining for the various markers of each mature cell type confirmed the presence of each cell lineage and their normal localisation, in Pten$^{fl/fl}$ Kras$^{LSL/+}$ tissue and control tissue compared to WT. Pten loss appears to impact on enteroendocrine and paneth cell number. However Pten loss in concert with Kras activation causes a further reduction in paneth cells.

### 3.2.4 Concomitant mutations in Pten and Kras results in a subtle increase of phospho-Akt immunostaining

To investigate the mechanism through which mutations in Pten and Kras are synergising, IHC against the active form of the PI3K pathway effector protein Akt was carried out (Figure 3.9). Immunostaining revealed a subtle increase in the presence of the active form of Akt (pAkt [ser473]) in Pten$^{fl/fl}$ Kras$^{LSL/+}$ tissue compared to WT tissue. However, there also appeared to be a subtle elevation of pAkt present in the control tissue (both Pten$^{fl/fl}$ and Kras$^{LSL/+}$) compared to WT tissue. The subtle elevation of pAkt staining, and therefore PI3K pathway activation, presents a mechanism by which the phenotypes observed in Pten$^{fl/fl}$ Kras$^{LSL/+}$ and control tissue may be driven.

| WT | Kras$^{LSL/+}$ | Pten$^{fl/fl}$ | Pten$^{fl/fl}$ Kras$^{LSL/+}$ |
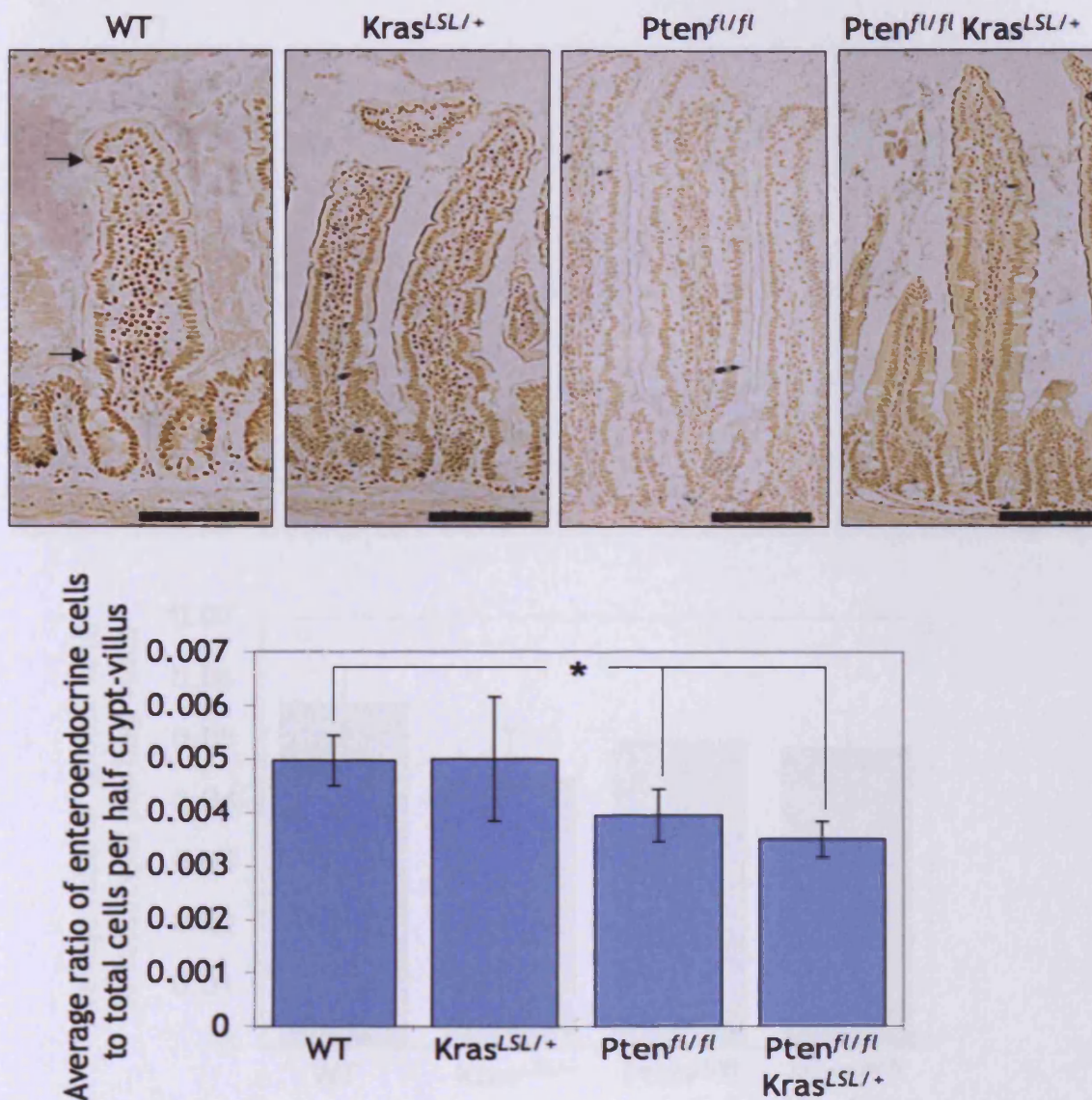
**Figure 3.5 Pten loss reduces the number of enteroendocrine cells present in the small intestine**

Grimelius staining of small intestinal sections to visualise the number of enteroendocrine cells present (indicated in WT intestine by arrows). Staining revealed normal localisation of enteroendocrine cells throughout the crypt-villus axis in Pten$^{fl/fl}$ Kras$^{LSL/+}$ tissue compared to control and WT tissue. Scale bars represent 100μm. The number of enteroendocrine cells present per half crypt-villus was scored and divided by the average number of cells per half crypt-villus, to normalise for the varying numbers of cells per half crypt-villus. Both experimental Pten$^{fl/fl}$ Kras$^{LSL/+}$ tissue and Pten$^{fl/fl}$ control tissue had significantly lower numbers of enteroendocrine cells per half crypt-villus compared to WT tissue (*, p values = 0.0404, n≥3, Mann Whitney U test). Error bars indicate standard deviation.

82

WT      Kras^{LSL/+}      Pten^{fl/fl}      Pten^{fl/fl} Kras^{LSL/+}
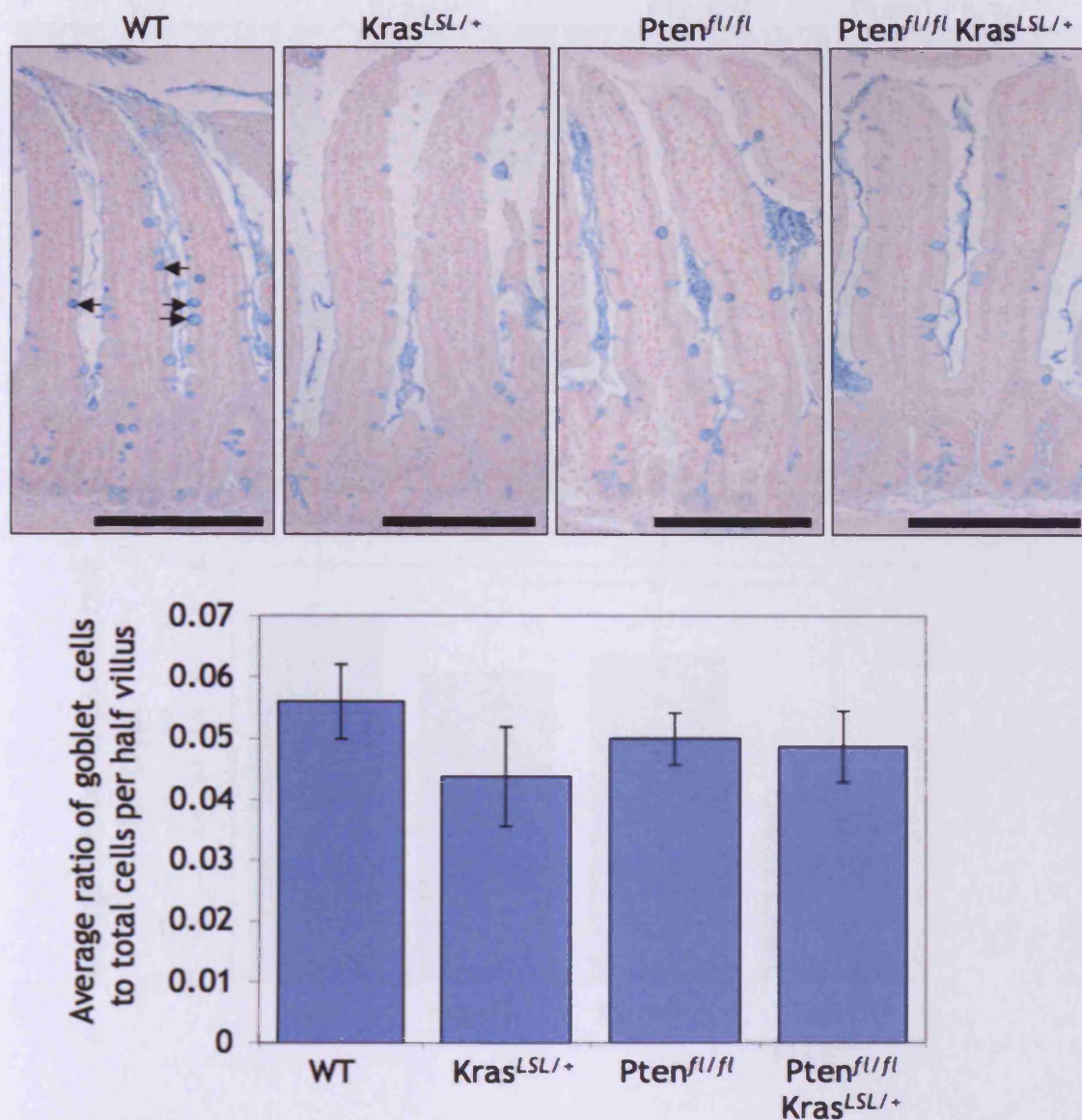
**Figure 3.6 Goblet cell number is unchanged in Pten^{fl/fl} Kras^{LSL/+} small intestine**

Small intestinal sections were stained with alcian blue in order to mark goblet cells (indicated in WT intestine by arrows). Staining revealed normal localisation of goblet cells throughout the crypt-villus axis in Pten^{fl/fl} Kras^{LSL/+} tissue compared to control and WT tissue. Scale bars represent 200μm. The number of goblet cells present per half villus were then scored and divided by the average number of cells per half villus, to normalise for varying villus cell number. There were no changes in goblet cell number in Pten^{fl/fl} Kras^{LSL/+} tissue compared to controls and WT (p values >0.05, n≥3, Mann Whitney U test). Error bars indicate standard deviation.
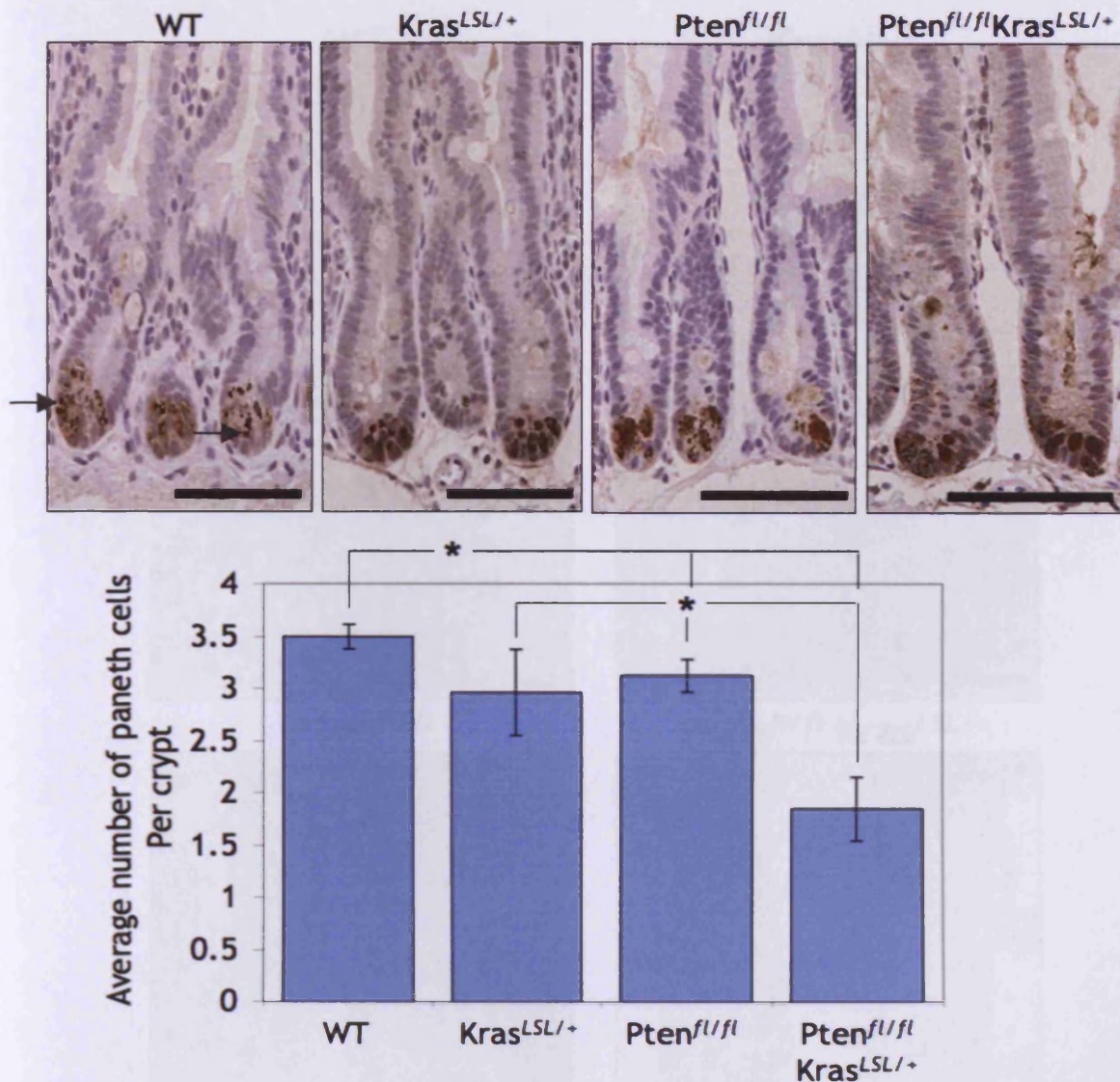
**Figure 3.7 Pten loss and Kras activation reduces the number of paneth cells present in small intestinal crypts**

IHC against lysozyme was carried out on small intestinal sections to indicate the presence and location of paneth cells, (indicated in WT intestine by arrows). Staining revealed normal localisation of paneth cells throughout the crypt in Pten$^{fl/fl}$ Kras$^{LSL/+}$ tissue compared to control and WT tissue. Scale bars represent 100μm. Subsequent scoring of paneth cells revealed that Pten loss causes a reduction in paneth cell number compared to WT tissue (*, p value <0.05, n≥3, Mann Whitney U test). The addition of a Kras mutation in Pten$^{fl/fl}$ Kras$^{LSL/+}$ compounds this effect, causing a significant decrease in the number of paneth cells present per crypt compared to both controls and WT tissue (*, p values <0.05, n≥3, Mann Whitney U test). Error bars indicated standard deviation.
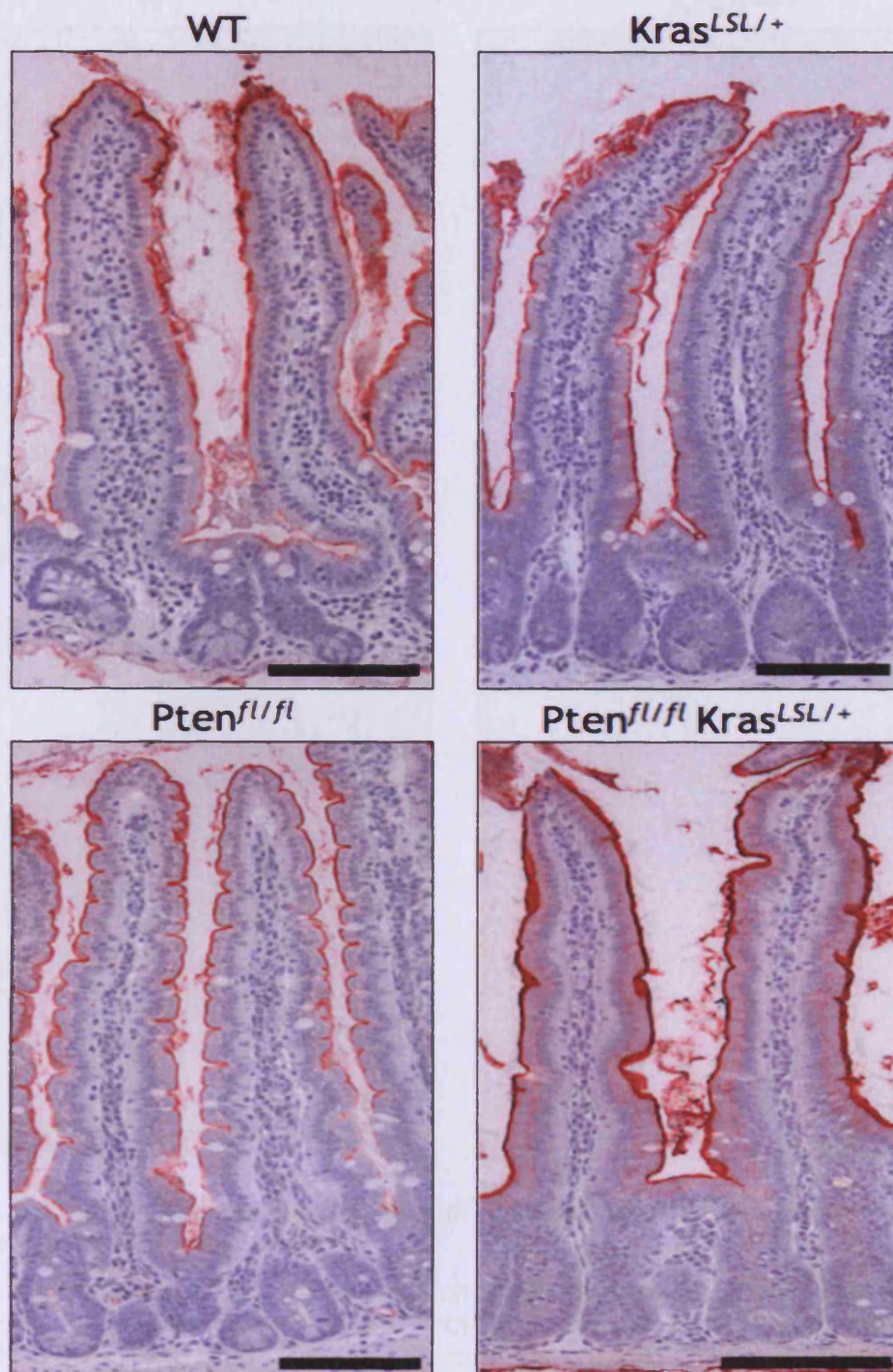
**Figure 3.8 Alkaline phosphatase remained localised to the apical membrane of differentiated enterocytes**

Small intestinal sections were incubated with a chromogenic substrate for alkaline phosphatase (catalysed to produce a red stain). Alkaline phosphatase is normally expressed on the apical membrane of differentiated enterocytes. Staining revealed normal localisation of alkaline phosphatase and therefore intact polarisation of the intestinal epithelium in Pten$^{fl/fl}$ Kras$^{LSL/+}$ and control tissue. Scale bars represent 100μm.

**WT**　　　　　　**Kras**$^{LSL/+}$

**Pten**$^{fl/fl}$　　　　　　**Pten**$^{fl/fl}$**Kras**$^{LSL/+}$
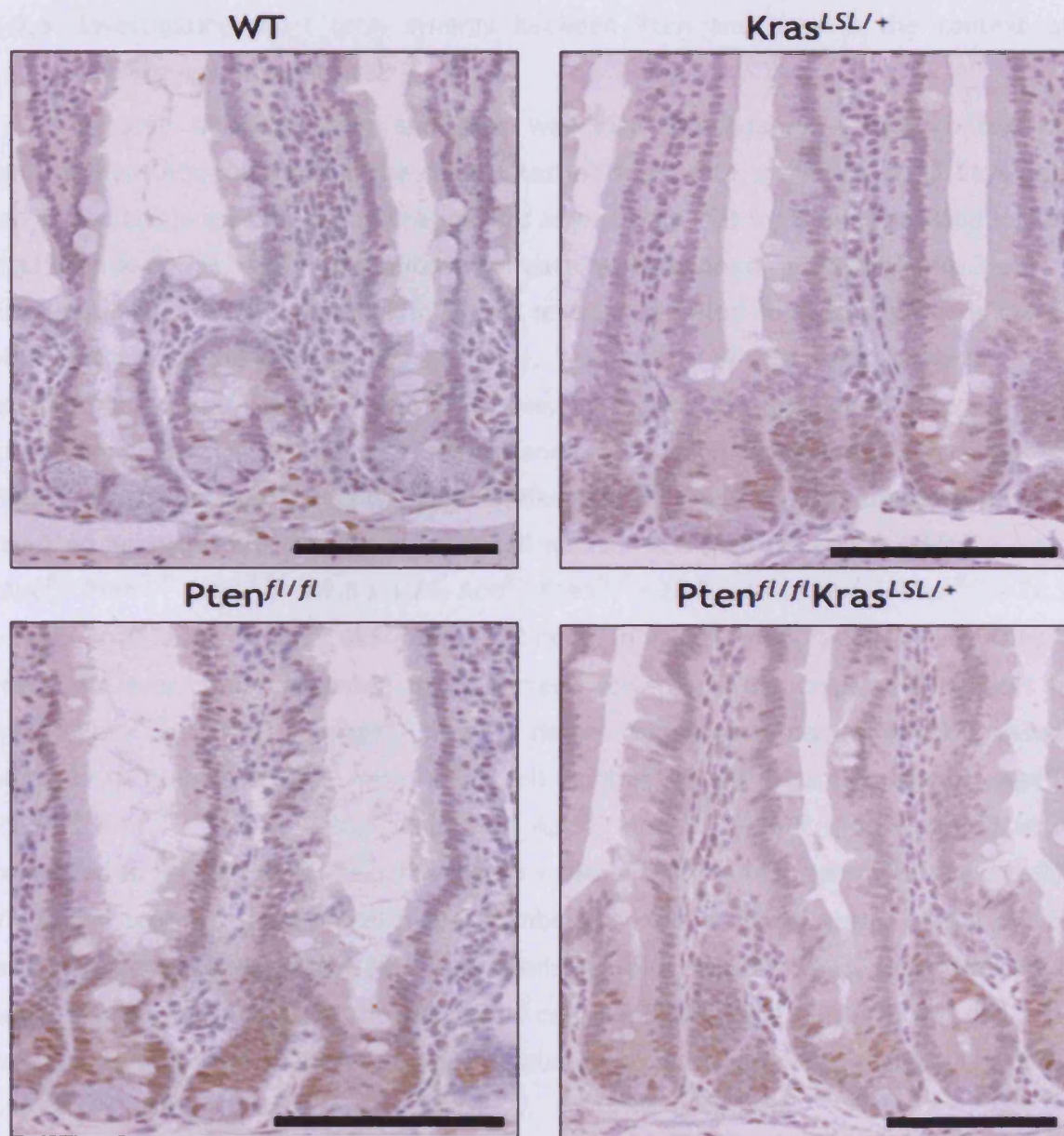
**Figure 3.9 Loss of Pten and activation of Kras alone and concomitantly, subtly enhances the level of phospho-Akt**

IHC against pAkt (Ser473) was carried out on small intestinal sections. Examination of the sections revealed a subtle increase in cytoplasmic and nuclear immunostaining in Pten$^{fl/fl}$ Kras$^{LSL/+}$ tissue and also in the control tissues compared to WT tissue. Immunostaining in both Pten$^{fl/fl}$ Kras$^{LSL/+}$ and control tissue is predominantly found in the crypt region. Scale bars represent 100μm.

### 3.2.5 Investigating short term synergy between Pten and Kras in the context of heterozygous Apc deletion

Synergy between Pten and Kras was also investigated in the context of heterozygous Apc mutation in the small intestine from mice sacrificed at 15 days post induction. Locus-specific recombination was assessed by PCR for the recombined loci of Apc, Pten and Kras, confirming mutation of each of the genes of interest (Figure 3.1). Examination of H&E stained small intestinal sections revealed no overt changes in crypt-villus structural morphology (Figure 3.10). Assessment of histological changes was carried out on $Apc^{fl/+}$ $Pten^{fl/fl}$ $Kras^{LSL/+}$ tissue, by scoring the number of cells per half crypt-villus and levels of apoptosis, mitosis and proliferation as previously carried out on $Pten^{fl/fl}$ $Kras^{LSL/+}$ tissue in section 3.2.2. Unlike $Pten^{fl/fl}$ $Kras^{LSL/+}$ mice, crypt cell scoring revealed no significant changes in crypt cell number in any of the cohorts (Figure 3.11) ($Apc^{fl/+}$ $Pten^{fl/fl}$ $Kras^{LSL/+}$ = 29.8 ± 3.26, $Apc^{fl/+}$ $Pten^{fl/fl}$ = 26.7 ± 2.71, $Apc^{fl/+}$ $Kras^{LSL/+}$ = 28.9 ± 5.15, $Apc^{fl/+}$ = 26.1 ± 0.36, WT = 25 ± 2.42 cells) (p values >0.05, n≥3, Mann Whitney U test). However, there appeared to be a trend towards higher crypt cell numbers in $Apc^{fl/+}$ $Pten^{fl/fl}$ $Kras^{LSL/+}$ and $Apc^{fl/+}$ $Kras^{LSL/+}$ tissues compared to control and WT tissue. Similarly to $Pten^{fl/fl}$ $Kras^{LSL/+}$ mice, villus cell number was significantly higher in $Apc^{fl/+}$ $Pten^{fl/fl}$ $Kras^{LSL/+}$ (134.2 ± 20.6 cells) and $Apc^{fl/+}$ $Kras^{LSL/+}$ (120.5 ± 10.9 cells) tissue compared to WT tissue (82.4 ± 6.93 cells) (p values = 0.0259, n≥3, Mann Whitney U test). Villus cell scoring also revealed higher numbers of cells in $Apc^{fl/+}$ tissue (104.5 ± 7.67 cells) compared to WT tissue (82.4 ± 6.93 cells) (p value = 0.0404, n≥3, Mann Whitney U test). Despite an increasing trend in villus cell number in $Apc^{fl/+}$ $Pten^{fl/fl}$ $Kras^{LSL/+}$ and $Apc^{fl/+}$ $Kras^{LSL/+}$ tissue compared to $Apc^{fl/+}$ tissue it was not significant (p values = 0.0558, n≥3, Mann Whitney U test) (Figure 3.11).

Levels of cell death and proliferation in $Apc^{fl/+}$ $Pten^{fl/fl}$ $Kras^{LSL/+}$ tissue was assessed by scoring apoptotic bodies and mitotic figures present in H&E stained sections. Proliferation was further assessed by scoring the number of Ki67 positive cycling cells per half crypt. There were no significant changes in apoptosis, mitosis and Ki67 positive cells in $Apc^{fl/+}$ $Pten^{fl/fl}$ $Kras^{LSL/+}$ tissue compared to controls and WT tissue. Apoptosis: $Apc^{fl/+}$ $Pten^{fl/fl}$ $Kras^{LSL/+}$ = 0.09 ± 0.044, $Apc^{fl/+}$ $Pten^{fl/fl}$ = 0.06 ± 0.057, $Apc^{fl/+}$ $Kras^{LSL/+}$ = 0.11 ± 0.116, $Apc^{fl/+}$ = 0.14 ± 0.072, WT = 0.03 ± 0.023 apoptotic bodies. Mitosis: $Apc^{fl/+}$ $Pten^{fl/fl}$ $Kras^{LSL/+}$ = 0.57 ± 0.139, $Apc^{fl/+}$ $Pten^{fl/fl}$ = 0.7 ± 0.085, $Apc^{fl/+}$ $Kras^{LSL/+}$ = 0.74 ± 0.141, $Apc^{fl/+}$ = 0.49 ± 0.095, WT = 0.52 ± 0.092 mitotic figures. Ki67 positive proliferating cells: $Apc^{fl/+}$ $Pten^{fl/fl}$ $Kras^{LSL/+}$ = 21.9 ± 2.71, $Apc^{fl/+}$ $Pten^{fl/fl}$ = 21.8 ± 1.66, $Apc^{fl/+}$ $Kras^{LSL/+}$ = 25.1 ± 1.68, $Apc^{fl/+}$ = 22.5 ± 0.65, WT = 22.5 ± 0.64 Ki67 positive cells,

(p values >0.05, n≥3, Mann Whitney U test) (Figure 3.11, Figure 3.12). However, there were some significant changes within the control groups.

Heterozygous Apc loss alone resulted in a significant increase in the number of apoptotic bodies per half crypt (0.14 ± 0.072 cells) compared to WT tissue (0.03 ± 0.023 cells) (p value = 0.0383, n≥3, Mann Whitney U test). Apoptosis levels in $Apc^{fl/+}$ $Pten^{fl/fl}$ $Kras^{LSL/+}$, $Apc^{fl/+}$ $Kras^{LSL/+}$ and $Apc^{fl/+}$ $Pten^{fl/fl}$ tissue were not significantly altered from the WT (p values >0.05, n≥3, Mann Whitney U test). Therefore suggesting additional mutation of either Pten or Kras alone, or both together suppresses the apoptotic effects of heterozygous Apc deletion. Data obtained from mitosis and Ki67 scoring revealed significant increases in mitotic bodies only in $Apc^{fl/+}$ $Pten^{fl/fl}$ tissue (0.70 ± 0.085 mitoses) compared to $Apc^{fl/+}$ (0.49 ± 0.095 mitoses) and WT tissue (0.52 ± 0.092 mitoses) (p value = 0.0249, n≥3, Mann Whitney U test), and $Apc^{fl/+}$ $Kras^{LSL/+}$ tissue has significantly higher numbers of Ki67 positive cells (25.1 ± 1.68 positive cells) compared to WT tissue (21.1 ± 1.50 cells) (p value = 0.0404, n≥3, Mann Whitney U test).

Taken together these data suggest that there is synergy in the small intestinal epithelium between Pten and Kras in the context of heterozygous Apc deletion. This was evidenced by an increase in villus cell number. This phenotype may be driven by Pten loss and Kras activation alone, as the number of cells per half villus in $Apc^{fl/+}$ $Pten^{fl/fl}$ $Kras^{LSL/+}$ mice (134.2 ± 20.6 cells) was not significantly altered from the number of cells per half villus in $Pten^{fl/fl}$ $Kras^{LSL/+}$ mice (129.5 ± 17.67 cells, p value = 0.4426, n≥3, Mann Whitney U test). However, an increase in the number of crypt cells was not observed in $Apc^{fl/+}$ $Pten^{fl/fl}$ $Kras^{LSL/+}$ mice unlike $Pten^{fl/fl}$ $Kras^{LSL/+}$ mice, suggesting that additional mutation of Apc rescues this phenotype.
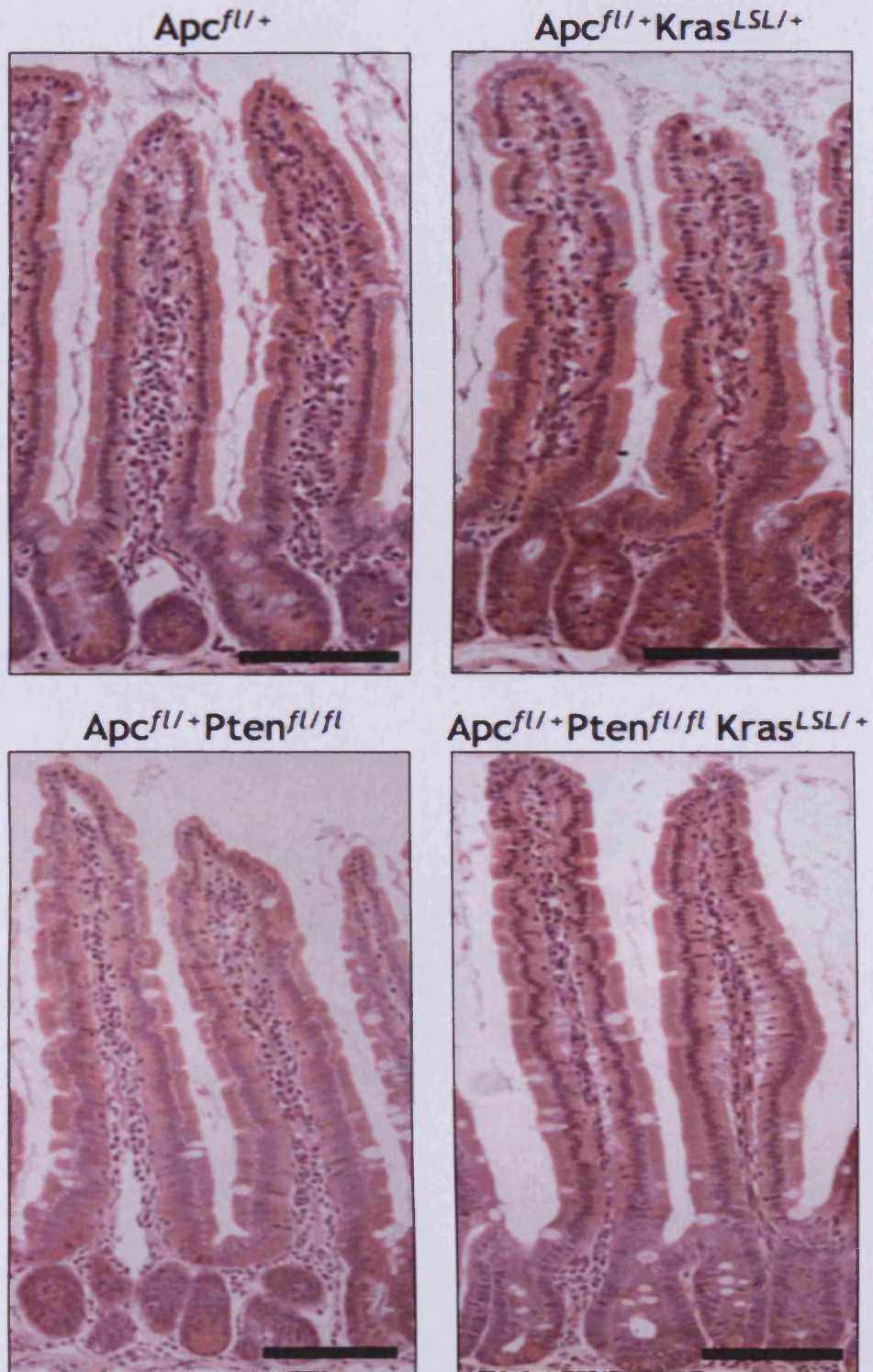
**Figure 3.10 Pten loss and Kras activation causes no gross alteration of the crypt-villus structure in the context of a heterozygous Apc deletion**

H&E stained small intestinal sections revealed no gross changes in crypt-villus structure in Apc$^{fl/+}$ Pten$^{fl/fl}$ Kras$^{LSL/+}$ tissue compared to control and WT tissue. Scale bars represent 200μm.
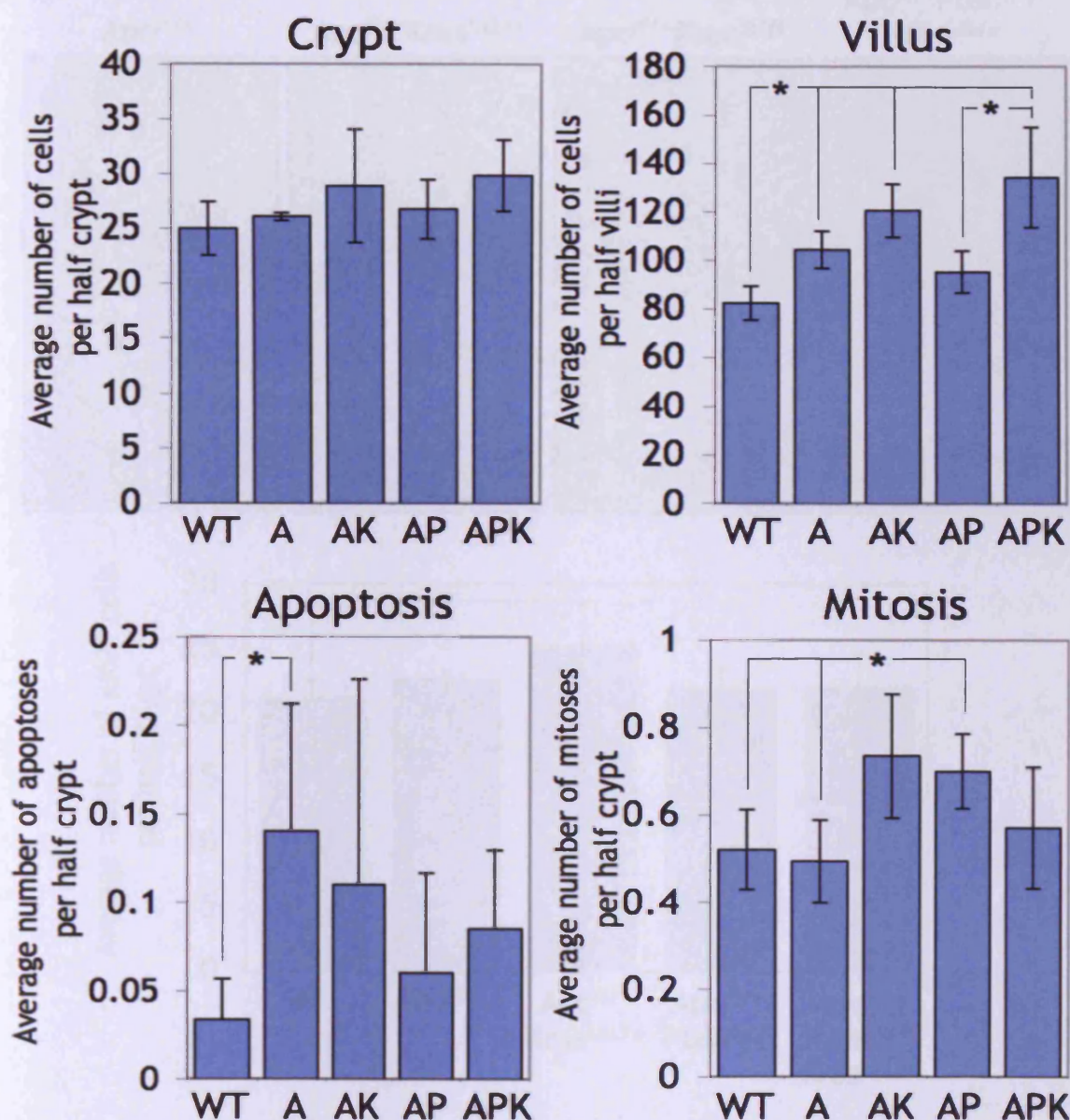
**Figure 3.11 Pten loss and Kras activation in the context of a heterozygous Apc mutation results in increased villus cell number**

Key: WT – Wild Type, A - Apc$^{fl/+}$, AK – Apc$^{fl/+}$ Kras$^{LSL/+}$, AP – Apc$^{fl/+}$ Pten$^{fl/fl}$, APK – Apc$^{fl/+}$ Pten$^{fl/fl}$ Kras$^{LSL/+}$

Crypt cell scoring revealed no significant changes in crypt cell number in Apc$^{fl/+}$ Pten$^{fl/fl}$ Kras$^{LSL/+}$ tissue compared to control and WT tissue. However, villus cell scoring revealed increased number of cells per half villus in Apc$^{fl/+}$ Pten$^{fl/fl}$ Kras$^{LSL/+}$ tissue compared to Apc$^{fl/+}$ Pten$^{fl/fl}$ and WT tissue (*, p values <0.05, n≥3, Mann Whitney U test). There were no changes in the number of apoptotic bodies or mitotic figures as scored by H&E examination in Apc$^{fl/+}$ Pten$^{fl/fl}$ Kras$^{LSL/+}$ tissue compared to controls and WT tissue (p values >0.05, n≥3, Mann Whitney U test). However Apc$^{fl/+}$ control tissue had higher levels of apoptosis compared to WT tissue. Apc$^{fl/+}$ Pten$^{fl/fl}$ control tissue had significantly higher levels of mitosis than both Apc$^{fl/+}$ and WT tissue (*, p values <0.05, n≥3, Mann Whitney U test). Error bars indicate standard deviation.
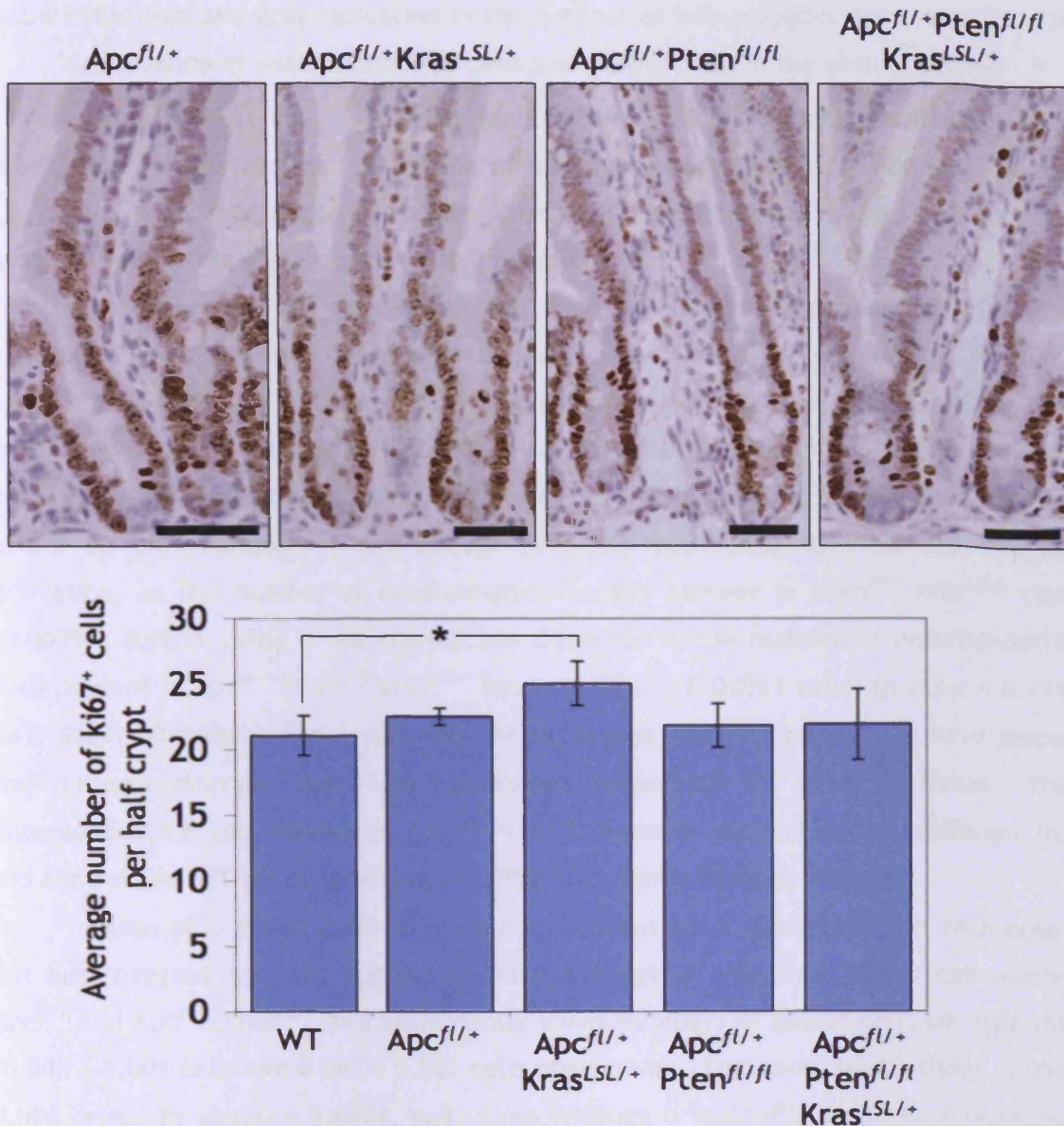
Figure 3.12 Simultaneous Pten loss and Kras activation causes no changes in the number of cycling cells in the context of a heterozygous Apc deletion

IHC against cell cycle marker, Ki67, was carried out on small intestinal sections. There appeared to be no gross alteration in the positioning or abundance of Ki67 positive cells in Apc$^{fl/+}$ Pten$^{fl/fl}$ Kras$^{LSL/+}$ tissue compared to controls and WT tissue. Scale bars represent 50μm. This was confirmed by scoring the number of Ki67 positive cells per half crypt. There were no significant changes in the abundance of Ki67 positive cells in Apc$^{fl/+}$ Pten$^{fl/fl}$ Kras$^{LSL/+}$ tissue compared to controls and WT tissue (p values >0.05, n≥3, Mann Whitney U Test). However, Apc$^{fl/+}$ Kras$^{LSL/+}$ control tissue had significantly higher numbers of Ki67 positive cells per half crypt compared to WT tissue (*, p value <0.05, n≥3, Mann Whitney U test). Error bars indicate standard deviation.

### 3.2.6 Pten loss and Kras activation in the context of heterozygous Apc loss affects the abundance of enteroendocrine cells and paneth cells in the small intestine

Alterations in cell lineage in $Apc^{fl/+}$ $Pten^{fl/fl}$ $Kras^{LSL/+}$ mice were assessed by scoring the number and/or localisation of mature cell types along the crypt-villus axis, i.e. goblet cells, enteroendocrine cells, paneth cells and the brush border of enterocytes as described for $Pten^{fl/fl}$ $Kras^{LSL/+}$ tissue in section 3.2.3.

Grimelius staining revealed normal localisation of enteroendocrine cells in all cohorts. Lower numbers of enteroendocrine cells were observed in $Apc^{fl/+}$ $Pten^{fl/fl}$ $Kras^{LSL/+}$ tissue ($0.0028 \pm 0.00061$ cells) compared to the $Apc^{fl/+}$ ($0.0046 \pm 0.00027$ cells) and $Apc^{fl/+}$ $Kras^{LSL/+}$ ($0.0046 \pm 0.00008$ cells) controls and WT tissue ($0.005 \pm 0.00047$ cells) (p values = 0.0404, n≥3, Mann Whitney U Test) (Figure 3.13). It is likely that this effect on enteroendocrine cell lineage is solely attributed to Pten loss and Kras activation, as the number of enteroendocrine cells present in $Pten^{fl/fl}$ $Kras^{LSL/+}$ tissue ($0.0035 \pm 0.0003$ cells) is not statistically different to the number of enteroendocrine cells present in $Apc^{fl/+}$ $Pten^{fl/fl}$ $Kras^{LSL/+}$ tissue ($0.0028 \pm 0.00061$ cells) (p value = 0.1914, n≥3, Mann Whitney U Test). However, heterozygous Apc loss appears to have rescued the enteroendocrine cell loss phenotype observed in $Pten^{fl/fl}$ tissue. Thus, enteroendocrine cell number in $Apc^{fl/+}$ $Pten^{fl/fl}$ tissue is not statistically different from the control and WT tissue (p values = 0.0952, n≥3, Mann Whitney U test).

Alcian blue staining revealed normal localisation of goblet cells in each cohort, but heterozygous Apc loss appears to have a negative effect on goblet cell number. $Apc^{fl/+}$ and $Apc^{fl/+}$ $Kras^{LSL/+}$ had significantly lower numbers of goblet cells per half villus ($0.045 \pm 0.001$ cells and $0.042 \pm 0.002$ cells respectively) compared to WT tissue ($0.056 \pm 0.006$ cells), (p values = 0.0404, n≥3, Mann Whitney U test) (Figure 3.14). Interestingly this phenotype is rescued by Pten loss and Kras activation, as goblet cell number in $Apc^{fl/+}$ $Pten^{fl/fl}$ $Kras^{LSL/+}$ ($0.049 \pm 0.006$ cells) was not significantly altered from WT tissue (p values = 0.1914, n≥3, Mann Whitney U test).

Lysozyme immunostaining revealed normal localisation of paneth cells in $Apc^{fl/+}$ $Pten^{fl/fl}$ $Kras^{LSL/+}$ tissue, at the base of the crypt (Figure 3.15). However, paneth cell scoring revealed a reduction in the abundance of paneth cells in $Apc^{fl/+}$ $Pten^{fl/fl}$ $Kras^{LSL/+}$ ($2.75 \pm 0.43$ cells), $Apc^{fl/+}$ $Kras^{LSL/+}$ ($2.75 \pm 0.43$ cells) and $Apc^{fl/+}$ $Pten^{fl/fl}$ ($2.86 \pm 0.242$ cells) tissue compared to WT tissue ($3.49 \pm 0.117$ cells) (p values <0.05, n≥3, Mann Whitney U test) (Figure 3.15). Heterozygous loss of Apc alone ($Apc^{fl/+}$) had no effect on paneth cell number (p value = 0.0606, n≥3, Mann Whitney U test).

Alkaline phosphatase staining was used to demarcate the brush border of mature enterocytes as described for $Pten^{fl/fl}$ $Kras^{LSL/+}$ tissue in section 3.2.3. Alkaline

phosphatase staining revealed normal staining localised to the apical/luminal surface of the villus epithelium in Apc$^{fl/+}$ Pten$^{fl/fl}$ Kras$^{LSL/+}$ tissue. There appeared to be no changes in alkaline phosphatase localisation in Apc$^{fl/+}$ Pten$^{fl/fl}$ Kras$^{LSL/+}$ tissue compared to control and WT tissue (Figure 3.16).

In summary the alterations in the abundance of mature cell types observed in Pten$^{fl/fl}$ Kras$^{LSL/+}$ mice remain the same in Apc$^{fl/+}$ Pten$^{fl/fl}$ Kras$^{LSL/+}$ mice i.e. a reduction in enteroendocrine and paneth cells, and no changes in goblet cell number compared to WT. Additionally, the decrease in enteroendocrine cell number appears to be driven by Pten loss and Kras activation alone, as the figures observed in Apc$^{fl/+}$ Pten$^{fl/fl}$ Kras$^{LSL/+}$ tissue are not significantly altered from those observed in Pten$^{fl/fl}$ Kras$^{LSL/+}$ tissue (p value = 0.1914, n≥3, Mann Whitney U test). Heterozygous loss of Apc decreases goblet cell number shown in Figure 3.14, Pten loss and Kras activation rescues this phenotype to bring goblet cell numbers back to normal WT levels. The loss in paneth cells observed in Apc$^{fl/+}$ Pten$^{fl/fl}$ Kras$^{LSL/+}$ and Pten$^{fl/fl}$ Kras$^{LSL/+}$ tissue does appear to be rescued partially by heterozygous Apc loss, as Apc$^{fl/+}$ Pten$^{fl/fl}$ Kras$^{LSL/+}$ tissue has significantly higher numbers of paneth cells compared to Pten$^{fl/fl}$ Kras$^{LSL/+}$ tissue (2.75 ± 0.43 cells vs 1.85 ± 0.306 cells, p value = 0.0404, n≥3, Mann Whitney U test). However, paneth cell number is not restored to normal WT levels (Figure 3.15).

### 3.2.7 Concomitant mutations in Pten and Kras in a context of a heterozygous Apc mutation result in a subtle increase of phospho-Akt immunostaining

The level of pAkt immunostaining was again assessed to investigate synergy through the PI3K pathway, as in section 3.2.4. Immunostaining of pAkt in Apc$^{fl/+}$ Pten$^{fl/fl}$ Kras$^{LSL/+}$ tissue was substantially increased compared to control tissue (Figure 3.17), unlike what was observed in Pten$^{fl/fl}$ Kras$^{LSL/+}$ tissue in Figure 3.9. There appeared to be no overt differences in pAkt immunostaining in control tissue, pAkt was found within the cytoplasm of cells in the crypt region. Mutations in Pten and Kras appear to be synergising through the PI3K pathway in the Apc$^{fl/+}$ Pten$^{fl/fl}$ Kras$^{LSL/+}$ model.
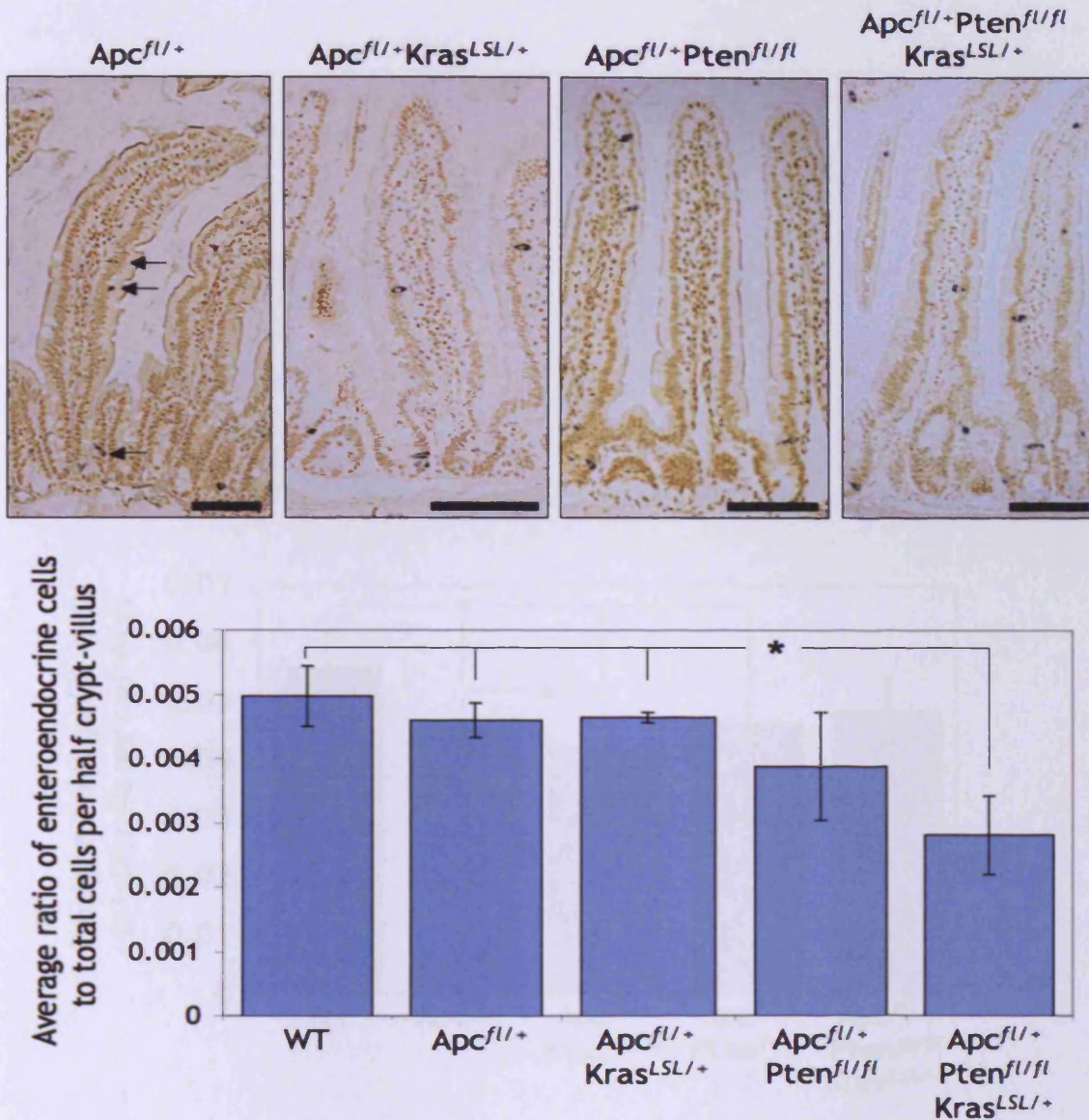
**Figure 3.13 Pten loss and Kras activation in the context of heterozygous Apc loss reduces the number of enteroendocrine cells present in the small intestine**

Grimelius staining of enteroendocrine cells was carried out on small intestinal sections to visualise the number of enteroendocrine cells present (indicated in Apc$^{fl/+}$ tissue by arrows). Staining revealed normal localisation of enteroendocrine cells throughout the crypt-villus axis in Apc$^{fl/+}$ Pten$^{fl/fl}$ Kras$^{LSL/+}$ tissue compared to control and WT tissue. Scale bars represent 100µm. The number of enteroendocrine cells present per half crypt-villus was scored and divided by the average number of cells per half crypt-villus, to normalise for the varying numbers of cells per half crypt-villus. Apc$^{fl/+}$ Pten$^{fl/fl}$ Kras$^{LSL/+}$ tissue had significantly lower numbers of enteroendocrine cells per half crypt-villus compared to Apc$^{fl/+}$, Apc$^{fl/+}$ Kras$^{LSL/+}$ control and WT tissue (*, p values = 0.0404, n≥3, Mann Whitney U test), in a similar manner to what was observed in Pten$^{fl/fl}$ Kras$^{LSL/+}$ tissue. Unlike Pten$^{fl/fl}$ tissue, enteroendocrine cell number in Apc$^{fl/+}$ Pten$^{fl/fl}$ tissue is not statistically different from the control and WT tissue (p values = 0.0952, n≥3, Mann Whitney U test). Error bars indicate standard deviation.
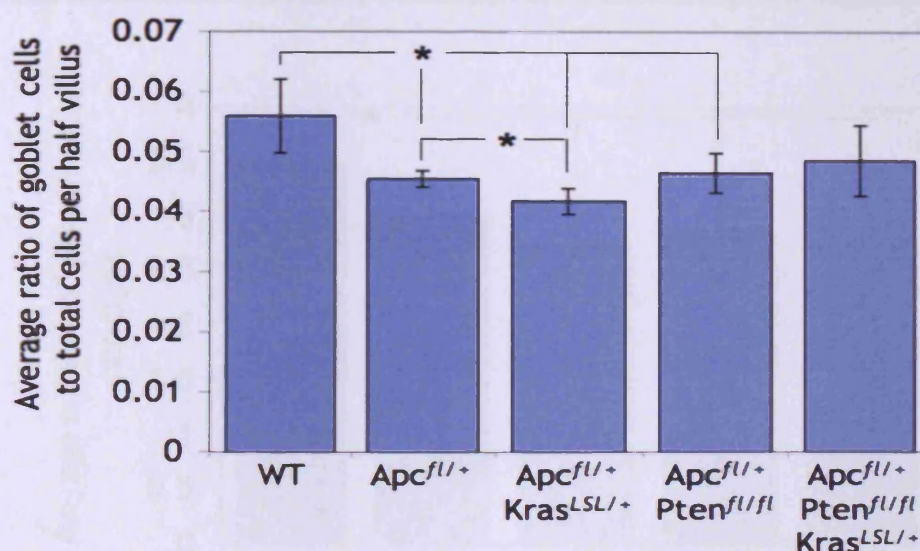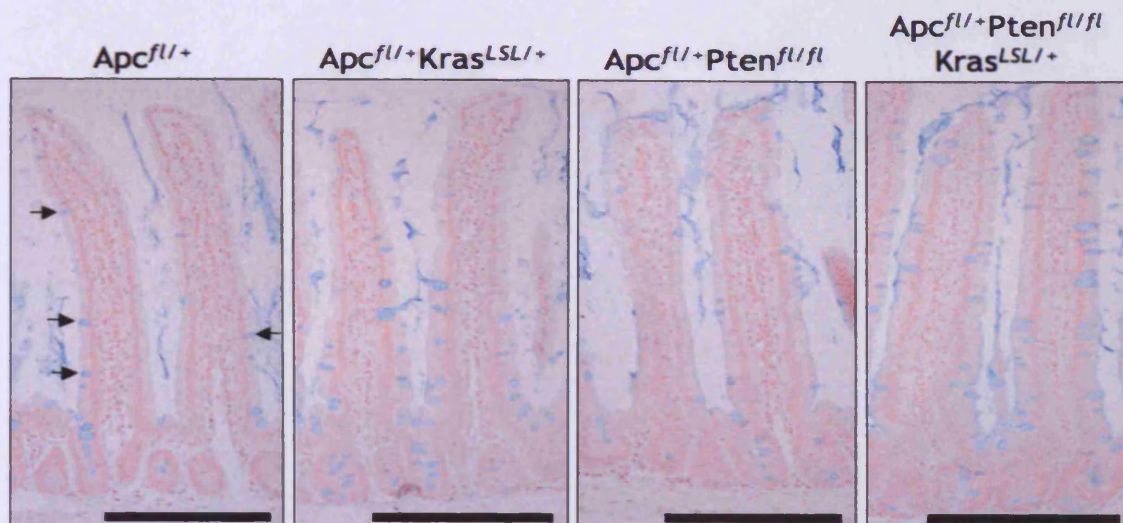
**Figure 3.14 Pten and Kras synergise to rescue goblet cell decrease caused by heterozygous Apc loss**

Small intestinal sections were stained with alcian blue in order to mark goblet cells (indicated in Apc$^{fl/+}$ tissue by arrows). Staining revealed normal localisation of goblet cells throughout the crypt-villus axis in Apc$^{fl/+}$ Pten$^{fl/fl}$ Kras$^{LSL/+}$ tissue compared to control and WT tissue. Scale bars represent 200μm. The number of goblet cells present per half villus was then scored and divided by the average number of cells per half villus, to normalise for varying villus cell number. Heterozygous Apc loss appears to negatively affect the goblet cell lineage resulting in decreased numbers per half villus compared to WT (p value = 0.0404, n≥3, Mann Whitney U test). This effect is further compounded by activation of oncogenic Kras (p value = 0.0404, n≥3, Mann Whitney U test). Addition of Pten loss appears to rescue this phenotype, however despite a trend towards higher numbers of goblet cells, Apc$^{fl/+}$ Pten$^{fl/fl}$ is significantly lower than WT (p value = 0.0404, n≥3, Mann Whitney U test). Goblet cell number in Apc$^{fl/+}$ Pten$^{fl/fl}$ Kras$^{LSL/+}$ mice is not significantly altered from the WT (p value = 0.1914, n≥3, Mann Whitney U test). Error bars indicate standard deviation.
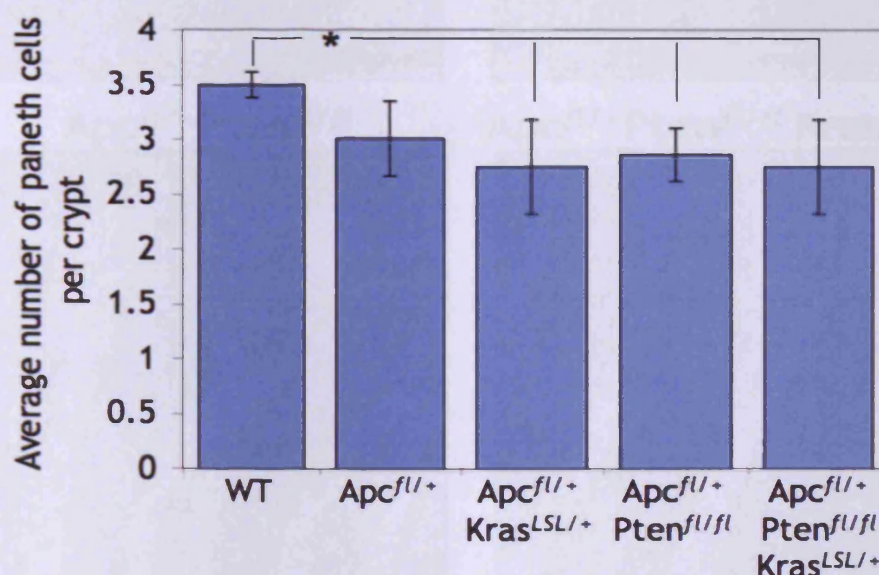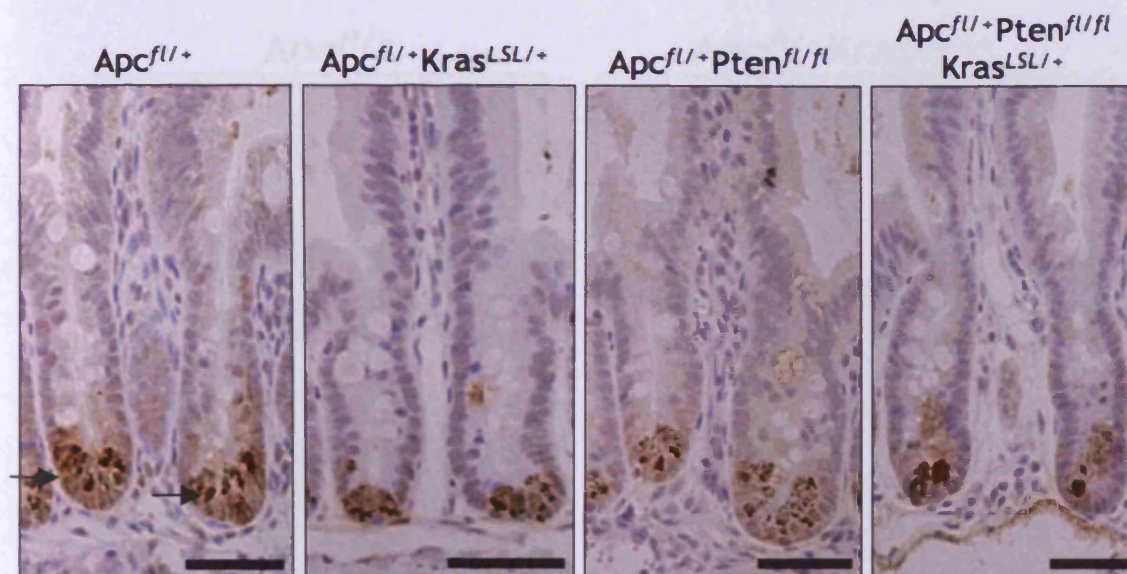
**Figure 3.15 Paneth cell scoring revealed a reduction in abundance in all Apc$^{fl/+}$ cohorts**

IHC against lysozyme was carried out on small intestinal sections to indicate the presence of paneth cells (indicated in Apc$^{fl/+}$ tissue by arrows). Immunostaining revealed normal localisation of paneth cells in the base of the crypt in Apc$^{fl/+}$ Pten$^{fl/fl}$ Kras$^{LSL/+}$ tissue compared to control and WT tissue. Scale bars represent 50μm. Subsequent scoring of lysozyme positive paneth cells revealed that additional mutation of Pten loss or Kras activation both individually or together in Apc$^{fl/+}$ mice significantly reduces the abundance of paneth cells compared to WT tissue (p values <0.05, n≥3, Mann Whitney U test). Error bars indicate standard deviation.
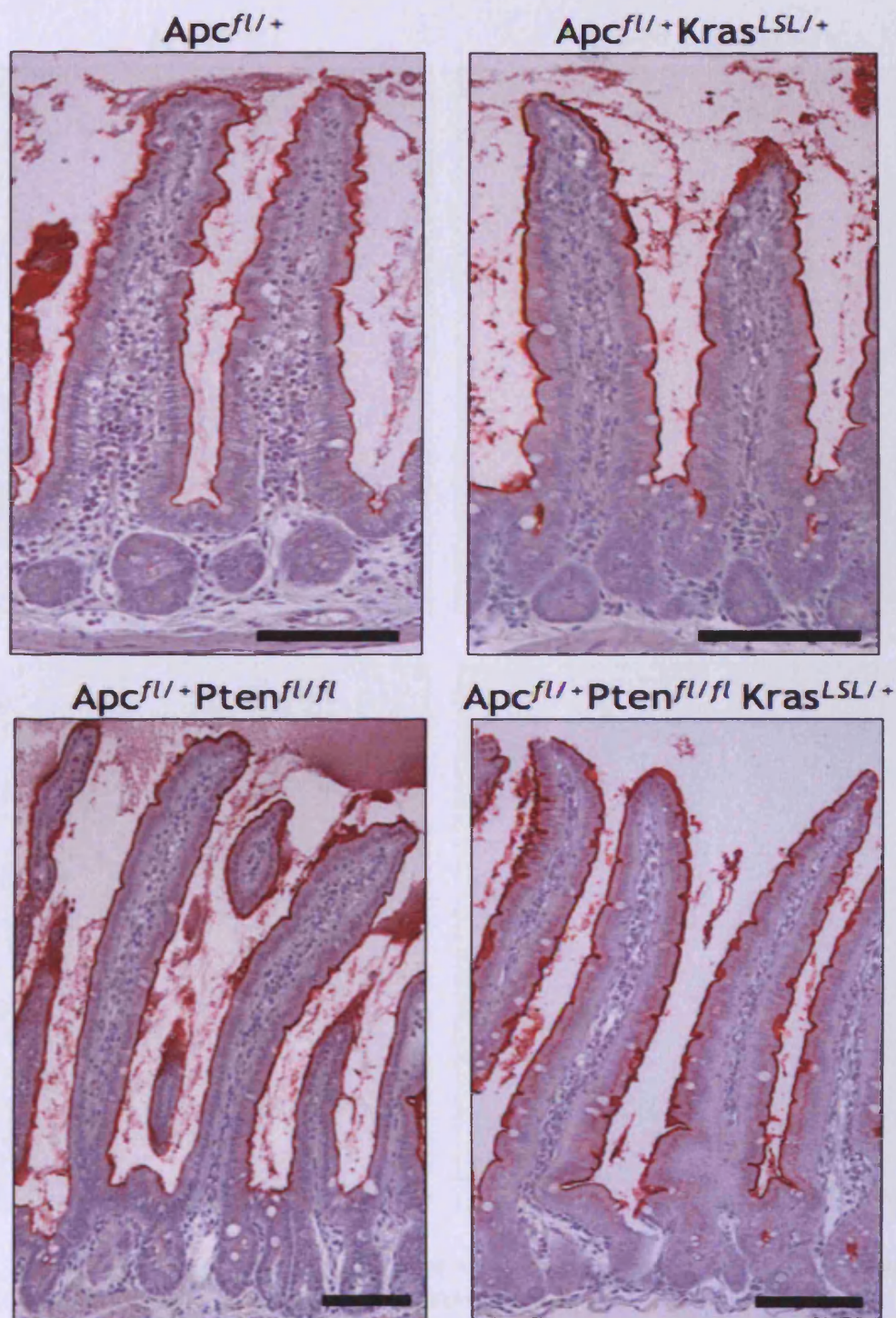
**Figure 3.16 Alkaline phosphatase remained localised to the apical membrane of differentiated enterocytes**

Small intestinal sections were incubated with a chromogenic substrate for alkaline phosphatase (catalysed to produce a red stain). Alkaline phosphatase is normally expressed on the apical membrane of differentiated enterocytes. Staining revealed normal localisation of alkaline phosphatase and therefore intact polarisation of the intestinal epithelium in $Apc^{fl/+} Pten^{fl/fl} Kras^{LSL/+}$ and control tissue. Scale bars represent 100μm.
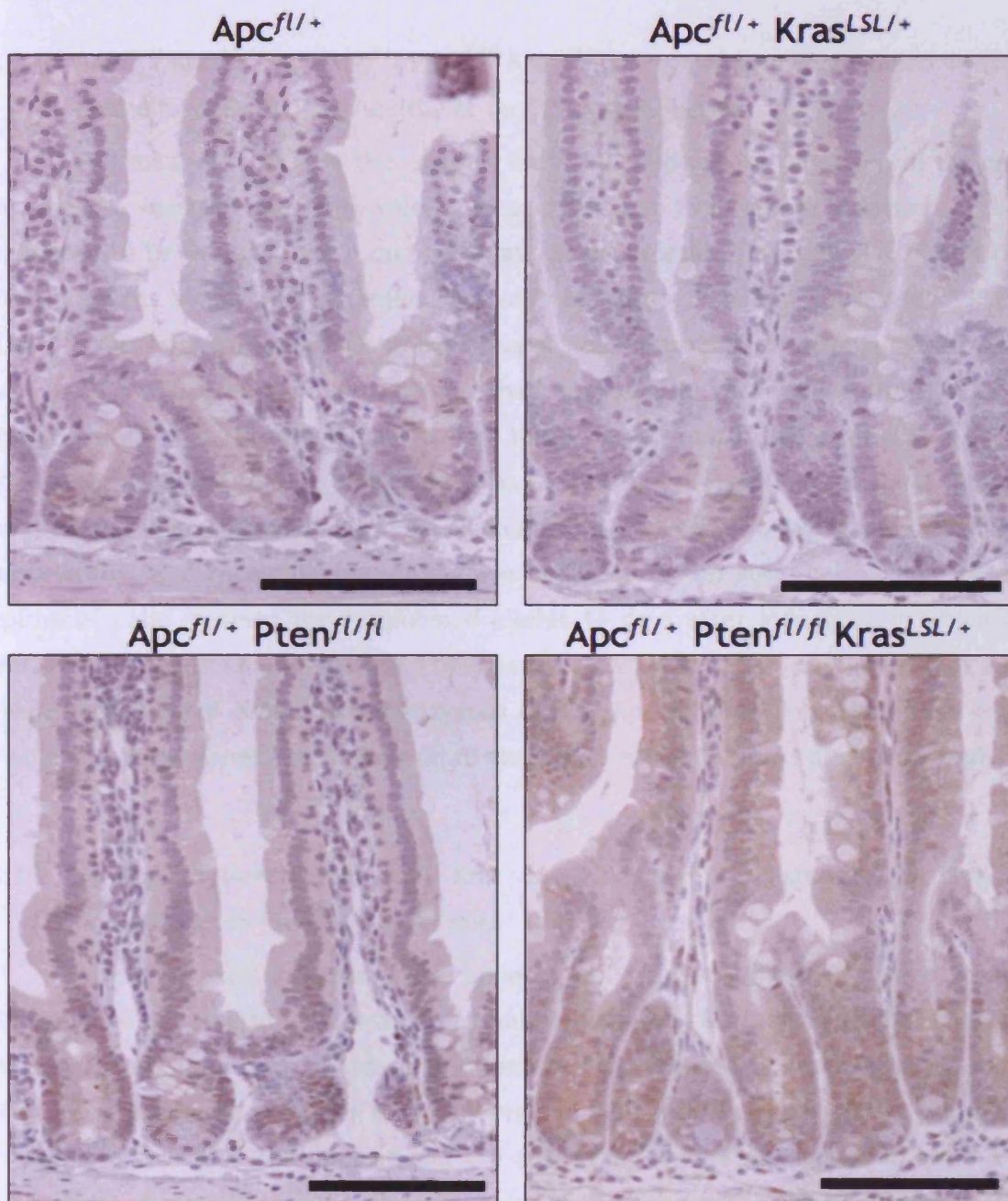
**Figure 3.17 Loss of Pten and activation of Kras in the context of a heterozygous Apc mutation enhances phospho-Akt immunostaining**

IHC against pAkt (Ser473) was carried out on small intestinal sections. Examination of the sections revealed increased immunostaining of pAkt in Apc$^{fl/+}$ Pten$^{fl/fl}$ Kras$^{LSL/+}$ tissue compared to control tissue. pAkt immunostaining remains localised to the crypt region in the control tissues as was observed in the Apc and WT controls in Figure 3.9. Scale bars represent 100μm.

## 3.3 Discussion

### 3.3.1 Pten$^{fl/fl}$ Kras$^{LSL/+}$ and Apc$^{fl/+}$ Pten$^{fl/fl}$ Kras$^{LSL/+}$ mice maintain recombined intestinal epithelial cells and are healthy at day 15 post induction

The mice described in this chapter were induced via i.p. injection of tamoxifen at around 6 weeks of age. They were then sacrificed at 15 days post induction. All mice appeared to be in good health up to 15 days post induction. In particular, mutation of Pten and Kras alone, and in conjunction with Apc (Pten$^{fl/fl}$ Kras$^{LSL/+}$ and Apc$^{fl/+}$ Pten$^{fl/fl}$ Kras$^{LSL/+}$ mice) appeared to have no overt impact on mouse health at this timepoint.

To confirm that cre recombinase had successfully recombined the DNA at the loxP sites and that this recombination had taken place in intestinal epithelial cells, PCR for the recombined alleles of interest was carried out on gDNA from small intestinal epithelial cells. Recombined PCR indicated that each allele had recombined successfully, and recombination must have occurred in the stem cell compartment as epithelial cells retained the recombined alleles 15 days after induction, in which time the intestinal epithelium has turned over at least two times. This confirmed that loss of Pten, activation of Kras and heterozygous loss of Apc in small intestinal stem cells is viable and these genetically manipulated stem cells remain 15 days after induction.

### 3.3.2 Synergy between Pten and Kras is evidenced by disruption of intestinal homeostasis in Pten$^{fl/fl}$ Kras$^{LSL/+}$ mice

At day 15 post induction there appears to be active synergy between Pten and Kras, evidenced by disrupted small intestinal homeostasis. Despite no obvious changes in the structural morphology of the small intestinal crypt-villus axis, histological analysis of the tissue revealed hyperplasia of the crypts and villi. Numerous changes in cell number including crypt-villus cell number and the alterations in the abundance of various cell types were observed. Both the crypts and villi of Pten$^{fl/fl}$ Kras$^{LSL/+}$ mice contained greater number of cells compared to WT tissue (Figure 3.3). Mutation of Pten and Kras alone disrupts intestinal homeostasis in some cases for example, Kras activation alone results in an increased abundance of cells in the crypt. However, when combined with a mutation in Pten, this phenotype is further enhanced, evidenced by a significant increase in the number of crypt cells in Pten$^{fl/fl}$ Kras$^{LSL/+}$ tissue compared to Kras$^{LSL/+}$ tissue. Thus, indicating synergy between Pten and Kras mutations.

Surprisingly, despite an increase in crypt and villus cell number, there was no statistical significance between the number of the Ki67 positive cells in Pten$^{fl/fl}$ Kras$^{LSL/+}$ tissue and WT tissue (Figure 3.4), which suggests that this phenotype is not driven by an

increase in proliferating cells. Therefore, one possible hypothesis to how Pten loss and Kras activation are driving the disruption of intestinal homeostasis may not be by an increase in cell proliferation but by a decrease in apoptosis at the tip of the villus. If cells are not undergoing apoptosis and are not sloughed from the villus tip then a build up of cells would ensue, resulting in increased number of cells occupying the crypt-villus axis. One possible mechanism for this may be through the subtle accumulation of pAkt in control and experimental intestine (Figure 3.9). A number of pro-apoptotic factors are inactivated by pAkt, such as Bad, Bim and Bax, which are all involved in the intrinsic apoptotic pathway. Activation of pAkt has been shown to reduce apoptosis in colorectal cancer cell lines (Itoh et al., 2002). Additionally, this has also been shown *in vivo* in a number of mouse models of intestinal mucosal barrier damage. In these models, intestinal mucosal barrier damage is alleviated by a reduction in apoptosis mediated by upregulation of PI3K signalling (Huang et al., 2011, Chen et al., 2010, Qiu et al., 2010). Accumulation of pAkt cannot be correlated with a reduction in apoptosis in this study, as no changes in the level of apoptosis in the crypt were observed. However, the number of apoptotic events in normal intestinal tissue is very low, and perhaps the effect of pAkt on apoptosis levels is only evident in instances when the intestine is undergoing high levels of cell death, such as mucosal barrier damage.

Disruption of small intestinal homeostasis was also evident when scoring differentiated cell types in $Pten^{fl/fl}$ $Kras^{LSL/+}$ tissue. There was a reduction in enteroendocrine and paneth cells in $Pten^{fl/fl}$ $Kras^{LSL/+}$ and $Pten^{fl/fl}$ tissue compared to WT tissue (Figure 3.5, Figure 3.7), but there was no alteration in the abundance of goblet cells and enterocytes appeared to be differentiating normally as assessed by alkaline phosphatase staining (Figure 3.6, Figure 3.8). Synergy between Pten and Kras appears to preferentially affect the differentiation of enteroendocrine and paneth cells. Both enteroendocrine and paneth cells are secretory cells, and the fate of secretory cell lineages is in part dependent upon the Notch signalling pathway. Activation of the Notch pathway maintains intestinal epithelial cells in an undifferentiated state, thus activation is highest in the intestinal crypts. Inappropriate activation of the pathway in mice leads to the loss of all secretory cell types and conversion of the differentiated epithelia to immature progenitor cells (Fre et al., 2005, van Es et al., 2005). Activation of mTOR may present as a possible mechanism of modulation of Notch signalling in these mouse models. Activation of mTOR in mouse embryonic fibroblasts blocks cellular differentiation via upregulation of Notch signalling (Ma et al., 2010).

### 3.3.3 Synergy between Pten and Kras is observed in $Apc^{fl/+}$ $Pten^{fl/fl}$ $Kras^{LSL/+}$ tissue, similar to that observed in $Pten^{fl/fl}$ $Kras^{LSL/+}$ tissue

Scoring of crypt-villus cell number and differentiated cell types in $Apc^{fl/+}$ $Pten^{fl/fl}$ $Kras^{LSL/+}$ yielded overall similar results to those observed in $Pten^{fl/fl}$ $Kras^{LSL/+}$ tissue. $Apc^{fl/+}$ $Pten^{fl/fl}$ $Kras^{LSL/+}$ mice had significantly more cells per half villus, but this was not accompanied by an increase in crypt cell number (Figure 3.11). $Apc^{fl/+}$ $Pten^{fl/fl}$ $Kras^{LSL/+}$ mice also had lower numbers of enteroendocrine and paneth cells, and no changes in goblet cell number or alkaline phosphatase localisation (section 3.2.6). As the phenotypes are similar one would assume the pathways governing them in $Pten^{fl/fl}$ $Kras^{LSL/+}$ mice are the same in $Apc^{fl/+}$ $Pten^{fl/fl}$ $Kras^{LSL/+}$ mice. In most cases the changes observed in cell abundance in $Apc^{fl/+}$ $Pten^{fl/fl}$ $Kras^{LSL/+}$ tissue, were not significantly altered from the similar changes observed in $Pten^{fl/fl}$ $Kras^{LSL/+}$ mice, suggesting that many of the phenotypes observed in $Apc^{fl/+}$ $Pten^{fl/fl}$ $Kras^{LSL/+}$ mice could be attributed to Pten and Kras synergy alone.

Interestingly in some incidences heterozygosity of Apc also appeared to impact on intestinal homeostasis. $Apc^{fl/+}$ mice have significantly higher numbers of cells per half villus and increased levels of apoptosis compared to WT (Figure 3.11). This is consistent with observed increases in villus length that has previously been shown in the normal mucosa of $Apc^{Min}$ mice (You et al., 2006). However, an increase in cell number does not necessarily equate to an increase in villus length. $Apc^{fl/+}$ mice also have lower numbers of goblet cells per crypt-villus, which is subsequently rescued by Pten loss and Kras activation (Figure 3.14). These findings suggest that at short time points, prior to loss of heterozygosity and formation of Wnt driven lesions, heterozygosity of Apc can impact upon intestinal homeostasis. You et al suggest that the changes observed in the normal tissues of $Apc^{Min}$ mice are a result of excess β-catenin and enhanced Wnt signalling (You et al., 2006). This hypothesis could be plausible as acute activation of Wnt signalling in the intestine leads to increased proliferation, and loss of differentiation (Sansom et al., 2004). Thus one may postulate that haploinsufficiency of Apc may result in 'chronic' or 'higher than baseline' activation of Wnt signalling which may give rise to the phenotypes observed here and by You et al. However, the level of canonical-Wnt pathway activation was not assessed in $Apc^{fl/+}$ intestine, so it cannot be confirmed if the phenotypes observed are attributed to this.

## 3.4 Summary

Taken together, the histological data from $Pten^{fl/fl}$ $Kras^{LSL/+}$ and $Apc^{fl/+}$ $Pten^{fl/fl}$ $Kras^{LSL/+}$ mice provide evidence that even at a short time point after induction there is synergy between Pten and Kras, resulting in disrupted intestinal homeostasis and hyperplasia of the crypt-villus possibly driven by activation of the PI3K pathway. It also appears that most of the phenotypes observed in $Apc^{fl/+}$ $Pten^{fl/fl}$ $Kras^{LSL/+}$ mice are independent of Apc heterozygosity and are attributed to Pten and Kras synergy alone.

## 3.5 Further Work

In order to deduce a mechanism by which Pten and Kras give rise to the resulting phenotypes, it would be useful to assess the level of Notch pathway and mTOR activation in $Pten^{fl/fl}$ $Kras^{LSL/+}$ and $Apc^{fl/+}$ $Pten^{fl/fl}$ $Kras^{LSL/+}$ intestine. As Apc haploinsufficiency results in an intestinal phenotype, it would be interesting to assess the level of canonical-Wnt pathway activation in $Apc^{fl/+}$ cohorts.

As there is genetic evidence that knockout/in of the genes of interest is achieved and maintained in both $Pten^{fl/fl}$ $Kras^{LSL/+}$ and $Apc^{fl/+}$ $Pten^{fl/fl}$ $Kras^{LSL/+}$ mice up until at least day 15 post induction, and it has no immediate effect on mouse health, it will be next investigated how these genetic alterations effect mouse lifespan and intestinal tumourigenesis in chapters 4 and 6. Further characterisation of synergy between Pten and Kras independently of Apc heterozygosity is carried out in chapter 5.

# Chapter 4: Investigating synergy between Pten and Kras in an intestinal tumour model

## 4.1 Introduction

Mice that are heterozygous for Apc, whether constitutive ($Apc^{Min}$) or conditional ($Apc^{fl/+}$), are commonly used to study the effects a particular drug, gene or substance has on intestinal tumourigenesis, as Apc heterozygous mice are predisposed to the formation of adenomas in the intestinal tract via loss of heterozygosity of Apc (Moser et al., 1992, Shibata et al., 1997). Apc heterozygous mice develop benign intestinal tumours that do not progress to invasive, advanced tumours. The development of mouse models of CRC that recapitulate more advanced stages of disease are therefore needed to enhance our understanding of tumour progression, metastasis, and for preclinical testing of new therapeutics.

Marsh et al have generated a mouse model of advanced intestinal tumourigenesis. They showed that conditional homozygous loss of Pten ($Pten^{fl/fl}$) promotes tumour progression in conditional Apc heterozygous mice ($Apc^{fl/+}$ $Pten^{fl/fl}$ mice) through upregulation of PI3K pathway activation, to give rise to intestinal adenocarcinoma with smooth muscle invasion. However, none of the tumours observed progressed to metastatic carcinoma (Marsh et al., 2008). As progression of the tumours occurred through increased activation of the PI3K pathway, it was postulated that the additional mutation of Kras may allow 'hyperactivation' of the PI3K pathway and promote tumour metastasis. As previously described, KRAS is an oncogene that can activate both the MAPK/Erk pathway and the PI3K pathway (through association with the p110 subunit of the PI3K protein), and activating mutations in KRAS are commonly associated with human CRC (Bos et al., 1987, Fearon and Vogelstein, 1990). Synergy between Kras and Pten has previously been observed in other tumour mouse models including lung, pancreas and endometrium (Dinulescu et al., 2005, Hill et al., 2010, Iwanaga et al., 2008).

The addition of a Kras mutation to the $Apc^{fl/+}$ $Pten^{fl/fl}$ model was first investigated in the Clarke lab utilising the AhCre recombinase transgene to drive recombination in epithelial tissues, as was used in the Marsh et al study. AhCre recombinase is expressed in an array of tissues including, bile ducts, stomach epithelium, intestine and liver. Unpublished data from the Clarke lab have demonstrated that Pten and Kras mutations synergise, in the context of a heterozygous Apc mutation, to cause the formation of cholangio carcinoma and hyperplasia of the forestomach. These non-intestinal

phenotypes caused rapid morbidity, primarily owing to large tumours blocking the stomach. These data demonstrate that the *Ah*Cre transgene was not useful to investigate the potential synergy of a Kras mutation with Pten loss in the context of Wnt-driven intestinal tumours, owing to the short mouse survival time after induction. To circumvent this the *Villin*Cre recombinase transgene was used in replacement of AhCre, as *Villin*Cre is expressed specifically in the intestinal epithelium (El Marjou et al., 2004).

As shown in chapter 3, there is evidence of synergy between Pten and Kras mutations in the context of a heterozygous Apc mutation in the intestine at day 15 post induction. In this chapter I will investigate the long term effects of deleting Pten in conjunction with Kras activation in a mouse model predisposed to Wnt driven intestinal tumours ($Apc^{fl/+}$ mouse model). *Villin*CreER$^T$-$Apc^{fl/+}$ $Pten^{fl/fl}$ $Kras^{LSL/+}$ mice (hereafter referred to as $Apc^{fl/+}$ $Pten^{fl/fl}$ $Kras^{LSL/+}$ mice) were generated and induced along with the appropriate controls. They were then sacrificed when they became symptomatic of disease.

## 4.2 Results

### 4.2.1 Pten and Kras synergise to significantly shorten $Apc^{fl/+}$ mouse survival time post induction

$Apc^{fl/+}Pten^{fl/fl}Kras^{LSL/+}$ mice and controls were induced and culled when they became symptomatic of disease, i.e. intestinal prolapse, pale feet, blood in faeces, swelling of the abdomen. Mice were dissected, and the small intestine and colon were either fixed in formalin in preparation for IHC or fixed in methacarn in preparation for H&E staining.

$Apc^{fl/+}$ $Pten^{fl/fl}$ $Kras^{LSL/+}$ mice had a significantly shorter life span compared to controls (median of 41 days post induction, p value <0.001, Log Rank test) (Figure 4.1, A). $Apc^{fl/+}$ $Pten^{fl/fl}$ mice had a median survival of 73 days post induction, $Apc^{fl/+}$ $Kras^{LSL/+}$ mice 196 days post induction and $Apc^{fl/+}$ mice 282 days post induction. The number of tumours present at death was scored from H&E stained sections of the whole small intestine for each cohort (Figure 4.1, B). $Apc^{fl/+}$ $Pten^{fl/fl}$ $Kras^{LSL/+}$ mice possessed a larger number of tumours (average of 50 tumours per section, n=10) compared to the $Apc^{fl/+}$ $Pten^{fl/fl}$ (average of 12 tumours per section, n=6) and $Apc^{fl/+}$ (average of 18 tumours per section, n=3), which potentially accounts for the difference in survival times between the cohorts. However, $Apc^{fl/+}$ $Pten^{fl/fl}$ $Kras^{LSL/+}$ mice had a similar tumour burden to the $Apc^{fl/+}$ $Kras^{LSL/+}$ control cohort (average of 60 tumours per section, n=7),

despite the difference in survival times between the two cohorts (41 days and 196 days respectively). Interestingly, $Apc^{fl/+}$ $Pten^{fl/fl}$ mice possessed a smaller number of tumours compared to $Apc^{fl/+}$ $Kras^{LSL/+}$ mice, yet had a much shorter survival time post induction.

### 4.2.2 Pten and Kras synergise to promote progression of tumours in $Apc^{fl/+}$ mice

To try to understand why $Apc^{fl/+}$ $Pten^{fl/fl}$ $Kras^{LSL/+}$ had a shorter life span compared to $Apc^{fl/+}$ $Kras^{LSL/+}$ mice, despite them both possessing similar number of tumours, H&E stained sections were again scored for the number of tumours present but the tumours were also given a grade corresponding to the level of progression (tumours were graded according to the criteria outlined in chapter 2: materials and methods section 2.6.5). Tumours were graded as follows: microadenomas were given a score of 1, benign adenomas with no evidence of invasion – 2, adenocarcinoma with evidence of invasion into the submucosa – 3, and adenocarcinoma with evidence of invasion through the smooth muscle wall and underlying serosa – 4 (Figure 4.2).

Grading of tumours revealed that, despite $Apc^{fl/+}$ $Pten^{fl/fl}$ $Kras^{LSL/+}$ and $Apc^{fl/+}$ $Kras^{LSL/+}$ mice possessing a similar tumour burden (when the number of tumours per section was scored [Figure 4.1, B]), the tumours observed in $Apc^{fl/+}$ $Pten^{fl/fl}$ $Kras^{LSL/+}$ mice were more advanced than those observed in $Apc^{fl/+}$ $Kras^{LSL/+}$ mice. $Apc^{fl/+}$ $Pten^{fl/fl}$ $Kras^{LSL/+}$ mice had an average tumour distribution of 41.5 microadenomas (grade 1), 5.1 adenomas (grade 2), 3.1 adenocarcinomas with submucosal invasion (grade 3) and 0.5 adenocarcinomas with smooth muscle invasion per section (grade 4) (n=10) (Figure 4.2), whereas $Apc^{fl/+}$ $Kras^{LSL/+}$ mice predominantly bore microadenomas, adenomas and the rare tumour with submucosal and smooth muscle invasion (0.4 and 0.1 tumours per section respectively). $Apc^{fl/+}$ $Pten^{fl/fl}$ mice possessed an average tumour distribution of 12 tumours per section yet had a median life span of 73 days post induction (Figure 4.1). Tumour grading revealed that a significant proportion of these tumours (25%), were large adenocarcinomas with submucosal invasion – grade 3 (Figure 4.2). Despite these mice possessing a smaller number of tumours, a larger proportion of these tumours were more advanced and invasive, resulting in morbidity of the mouse.

### 4.2.3 Evidence of smooth muscle invasion was only observed in $Apc^{fl/+}$ $Pten^{fl/fl}$ $Kras^{LSL/+}$ mice

H&E stained sections of the most advanced tumours found in each cohort are shown in Figure 4.3. Microadenomas and adenomas were the only tumours observed in $Apc^{fl/+}$ mice, an average of 18 tumours per section were observed. However, none of

these tumours possessed evidence of invasion, despite some of them becoming very large (an example of a large adenoma observed in $Apc^{fl/+}$ mice is shown in Figure 4.3). $Apc^{fl/+}$ $Kras^{LSL/+}$ mice possessed a substantially higher tumour burden than $Apc^{fl/+}$ mice and therefore had a shorter life span. Of the 420 tumours scored from H&E stained sections in the $Apc^{fl/+}$ $Kras^{LSL/+}$ cohort (n=7), only three tumours showed evidence of invasion into the submucosa and one through the smooth muscle wall. On average 3 tumours per section in $Apc^{fl/+}$ $Pten^{fl/fl}$ mice were classed as grade 3, adenocarcinoma with invasion into the submucosa, as shown in Figure 4.3. Here the tumour remains confined to the intestine, as no infiltration of the smooth muscle boundary is observed. Evidence of tumour progression to adenocarcinoma with smooth muscle wall invasion is frequently observed in $Apc^{fl/+}$ $Pten^{fl/fl}$ $Kras^{LSL/+}$ mice. An average of 0.5 tumours per section in $Apc^{fl/+}$ $Pten^{fl/fl}$ $Kras^{LSL/+}$ mice had progressed to invade through the smooth muscle wall, which is likely to be the cause of morbidity in these mice and led to a significantly shortened life span. Despite evidence of the adenocarcinoma breaking through the confines of the small intestinal smooth muscle wall, no evidence of metastasis was observed.

A



B
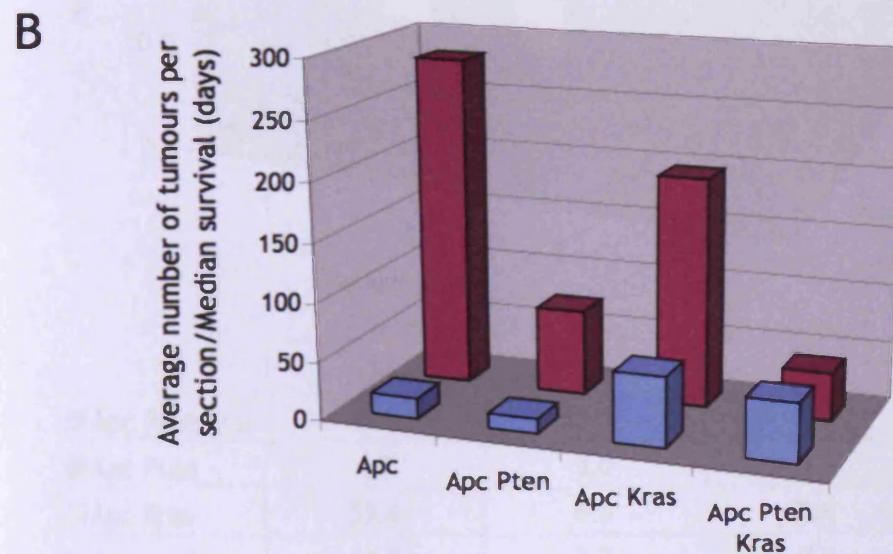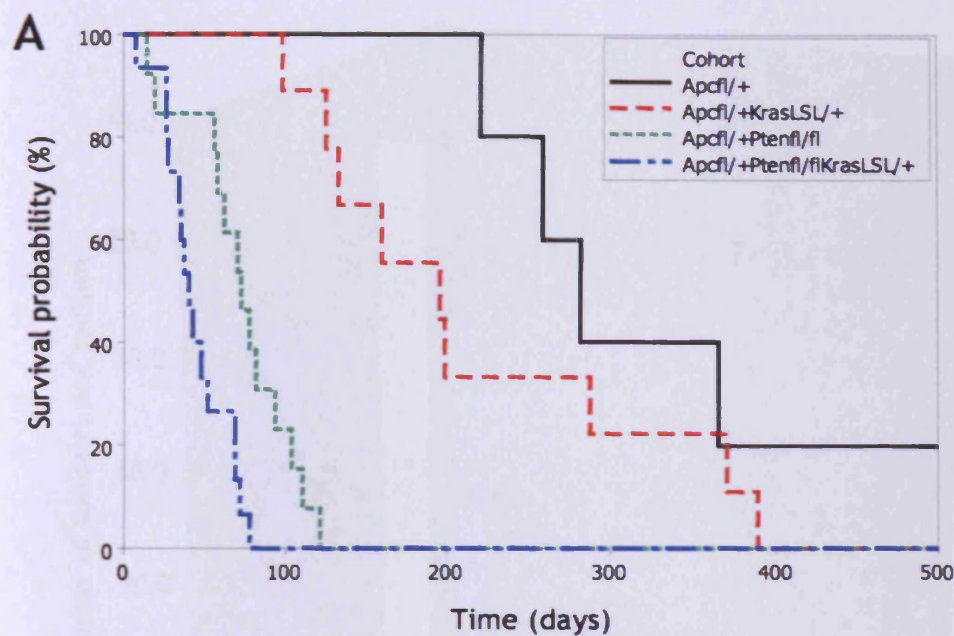
| | Apc | Apc Pten | Apc Kras | Apc Pten Kras |
|---|---|---|---|---|
| ■ Average number of tumours per section | 18 | 12 | 60 | 50 |
| ■ Median Survival | 282 | 73 | 196 | 41 |

**Figure 4.1 Apc$^{fl/+}$Pten$^{fl/fl}$Kras$^{LSL/+}$ mice have a significantly shorter lifespan than controls, but a similar tumour number to Apc$^{fl/+}$Kras$^{LSL/+}$ mice**

(A) Apc$^{fl/+}$Pten$^{fl/fl}$Kras$^{LSL/+}$ mice have a significantly shorter lifespan compared to all Apc$^{fl/+}$ controls (p value <0.001, Log Rank test). Apc$^{fl/+}$Pten$^{fl/fl}$Kras$^{LSL/+}$ mice lived to a median time of 41 days post induction, Apc$^{fl/+}$Pten$^{fl/fl}$ -median 81 days, Apc$^{fl/+}$Kras$^{LSL/+}$ - median 192 days and Apc$^{fl/+}$ - median 282 days. (B) Key: blue bars – average number of tumours per section, red bars – median survival. The number of tumours per H&E section were scored for each cohort. Despite Apc$^{fl/+}$Pten$^{fl/fl}$Kras$^{LSL/+}$ mice having a shorter life span than Apc$^{fl/+}$Kras$^{LSL/+}$ mice, they possessed a similar number of tumours.
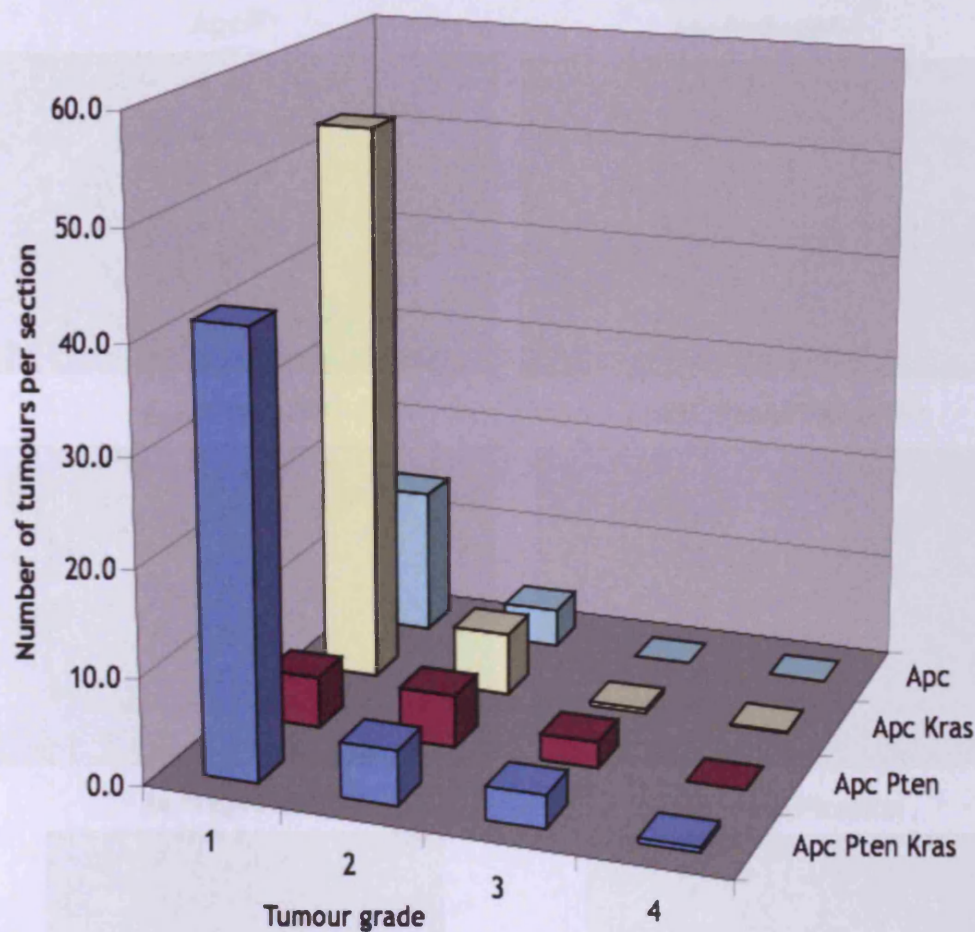
| | 1 | 2 | 3 | 4 |
|---|---|---|---|---|
| ■ Apc Pten Kras | 41.5 | 5.1 | 3.1 | 0.5 |
| ■ Apc Pten | 4.8 | 5.0 | 2.5 | 0.0 |
| □ Apc Kras | 53.4 | 6.0 | 0.4 | 0.1 |
| □ Apc | 14.0 | 3.7 | 0.0 | 0.0 |

**Figure 4.2 Grading of tumours revealed that tumours in Apc$^{fl/+}$ Pten$^{fl/fl}$ Kras$^{LSL/+}$ mice are the most invasive, invading through the smooth muscle wall**

Tumours present in H&E stained small intestinal sections for each cohort were scored and graded according to the level of invasiveness. Grading revealed that Apc$^{fl/+}$ Pten$^{fl/fl}$ Kras$^{LSL/+}$ mice (dark blue bars) possessed the most invasive tumours, an average of 0.5 tumours per section were classed as adenocarcinomas with smooth muscle invasion (grade 4). Tumours observed in Apc$^{fl/+}$ Kras$^{LSL/+}$ mice (yellow bars) were predominantly early stage tumours (grade 1 and 2), which would account for the longer survival time of this cohort compared to Apc$^{fl/+}$ Pten$^{fl/fl}$ Kras$^{LSL/+}$ mice, which have a similar overall number of tumours. Despite having an overall lower tumour number compared to the other cohorts, Apc$^{fl/+}$ Pten$^{fl/fl}$ mice (red bars) possessed higher numbers of adenocarcinomas with submucosal invasion (grade 3) compared to Apc$^{fl/+}$ Kras$^{LSL/+}$ and Apc$^{fl/+}$ cohorts.
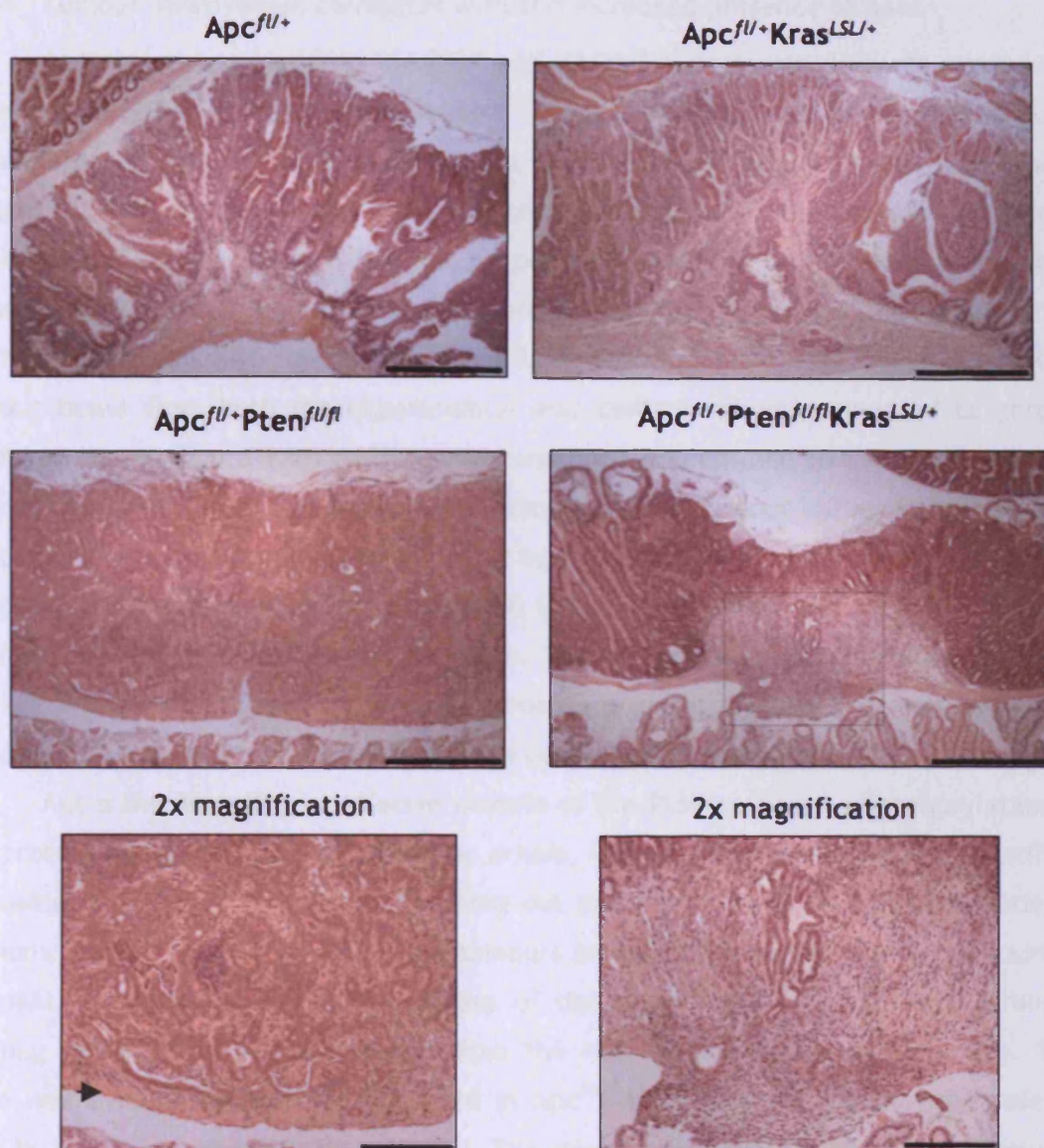
**Figure 4.3 H&E stained sections of the most advanced tumours in each cohort**

Apc$^{fl/+}$ mice predominantly bore microadenomas and adenomas, none of which showed any signs of invasiveness. Apc$^{fl/+}$ Kras$^{LSL/+}$ mice also predominantly bore microadenomas and adenomas but at a much higher frequency than Apc$^{fl/+}$ mice, some of these tumours possessed invasive characteristics (i.e. submucosal invasion), but this was a rare event. Apc$^{fl/+}$ Pten$^{fl/fl}$ mice had the lowest tumour number but a large proportion of these tumours had invaded into the submucosa. The arrow indicates the intact smooth muscle wall boundary in the magnified Apc$^{fl/+}$ Pten$^{fl/fl}$ tumour. There was frequent evidence of tumours that had invaded through the smooth muscle wall and invaded into the peritoneal cavity in Apc$^{fl/+}$ Pten$^{fl/fl}$ Kras$^{LSL/+}$ mice. However, metastasis was not observed. Scale bars represent 500μm, magnified images scale bars represent 200μm.

### 4.2.4 Tumour invasiveness correlates with the increased presence of pAkt

As Kras impinges on both the PI3K and MAPK/Erk pathways, IHC was carried out on intestinal tissue and tumours from $Apc^{fl/+}$ $Pten^{fl/fl}$ $Kras^{LSL/+}$ mice and control cohorts for markers of pathway activation. MEK is a kinase that is part of the MAP Kinase cascade; it acts downstream of Kras and phosphorylates Erk, the protein that elicits the effects of the pathway. MEK must be phosphorylated in order to become active. Immunostaining for phosphorylated MEK (pMEK) therefore indicates activation of the MAPK/Erk pathway. IHC against pMEK (ser221) revealed increased levels of pMEK in tumour tissue from both the experimental and control cohorts compared to normal intestinal tissue (Figure 4.4). pMEK immunostaining was confined to the crypt region of normal intestinal tissue, but staining was homogenous in tumour tissue, indicating that tumour cells are perhaps in an immature progenitor-like state. However, there was no discernable difference in the level of pMEK immunostaining in $Apc^{fl/+}$ $Pten^{fl/fl}$ $Kras^{LSL/+}$ tumours compared to the control tumours. Therefore it can be concluded that the MAPK/Erk pathway is upregulated in all tumours initiated by Apc loss, and additional mutation of Pten and Kras does not enhance activation of the pathway.

Akt is the downstream effector protein of the PI3K pathway; phosphorylation of the protein by PDK1 allows it to become active. IHC against pAkt (ser473) and pmTOR (a downstream target of pAkt) was carried out on normal intestine and tumour tissue sections (Figure 4.5, Figure 4.6). Most tumours in $Apc^{fl/+}$ mice had little or no staining for pAkt. In some tumour sections areas of the tumour appeared to have stronger staining (particularly in the nucleus) than the rest of the tumour (Figure 4.5). The same was evident for tumours observed in $Apc^{fl/+}$ $Kras^{LSL/+}$ mice, despite the role of Kras in activation of the PI3K pathway. The nuclear localisation of pAkt is likely to coincide with areas of the tumour that are proliferating, as nuclear pAkt was also observed in the normal tissue in cells undergoing mitosis. There was strong immunostaining for pAkt in all tumours in $Apc^{fl/+}$ $Pten^{fl/fl}$ $Kras^{LSL/+}$ and $Apc^{fl/+}$ $Pten^{fl/fl}$ mice, particularly in the tumours with evidence of invasion. pAkt appeared to be localised to the membrane as well as the cytoplasm, membrane associated staining of pAkt is thought to be a marker of high activity of the protein (Mende et al., 2001). pmTOR (a downstream target of pAkt) immunostaining correlates with the staining of pAkt i.e. strong staining in $Apc^{fl/+}$ $Pten^{fl/fl}$ $Kras^{LSL/+}$ and $Apc^{fl/+}$ $Pten^{fl/fl}$ tissue compared to $Apc^{fl/+}$ tumour tissue (Figure 4.6). However, unlike pAkt, pmTOR immunostaining in $Apc^{fl/+}$ $Kras^{LSL/+}$ tumours is relatively strong and comparable to $Apc^{fl/+}$ $Pten^{fl/fl}$ $Kras^{LSL/+}$ and $Apc^{fl/+}$ $Pten^{fl/fl}$ tissue.

### 4.2.5 No evidence of epithelial-to mesenchymal transition observed in invasive tumours

E-cadherin forms cell-to-cell junctions called adherens junctions between epithelial cells. It is a membrane spanning protein that forms homodimers with E-cadherin protein found on the surface of neighbouring epithelial cells. The loss of membrane associated E-cadherin is a marker of cells undergoing epithelial-to-mesenchymal transition (EMT), which is thought to occur at the leading edge of tumours and is associated with increased invasiveness (Vleminckx et al., 1991).

IHC against E-cadherin was carried out on tumour tissue sections. E-cadherin was membrane bound in all tumours found in each cohort (Figure 4.7). E-cadherin staining does not appear as strong in tumours from $Apc^{fl/+}$ $Kras^{LSL/+}$, $Apc^{fl/+}$ $Pten^{fl/fl}$ and $Apc^{fl/+}$ $Pten^{fl/fl}$ $Kras^{LSL/+}$ mice, due to the large stromal component that makes up a proportion of these tumours. The tumour cells that are invading into the submucosa and the smooth muscle wall still maintain membrane associated E-cadherin.

**Normal Tissue**     **Apc$^{fl/+}$**     **Apc$^{fl/+}$ Kras$^{LSL/+}$**

**Apc$^{fl/+}$ Pten$^{fl/fl}$**     **Apc$^{fl/+}$ Pten$^{fl/fl}$ Kras$^{LSL/+}$**
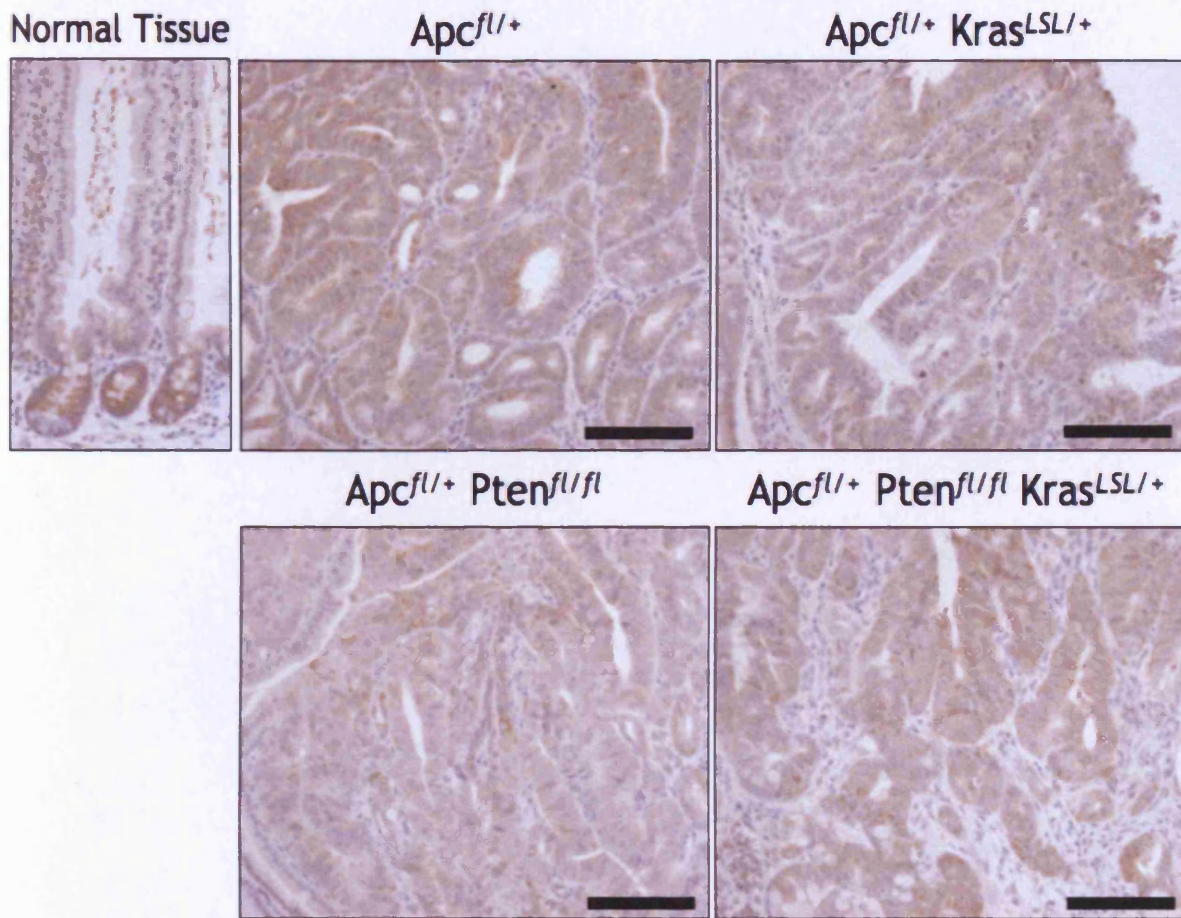
**Figure 4.4 pMEK immunostaining revealed no overt variations in staining intensity between tumours from each cohort**

IHC against pMEK (ser221) was carried out on tumour and normal tissue sections from Apc$^{fl/+}$ Pten$^{fl/fl}$ Kras$^{LSL/+}$ mice and controls. MEK is a MAP kinase protein that is downstream of Kras in the MAPK/Erk signalling pathway. The phosphorylated form of the protein is the active form, so therefore the presence of pMEK indicates activation of the MAPK/Erk pathway. pMEK immunostaining of the tumour sections from all cohorts revealed a subtle increase in the presence of staining compared to normal tissue. However, there appeared to be no increase in staining intensity in Apc$^{fl/+}$ Pten$^{fl/fl}$ Kras$^{LSL/+}$ tumours compared to controls. Scale bars represent 100μm.
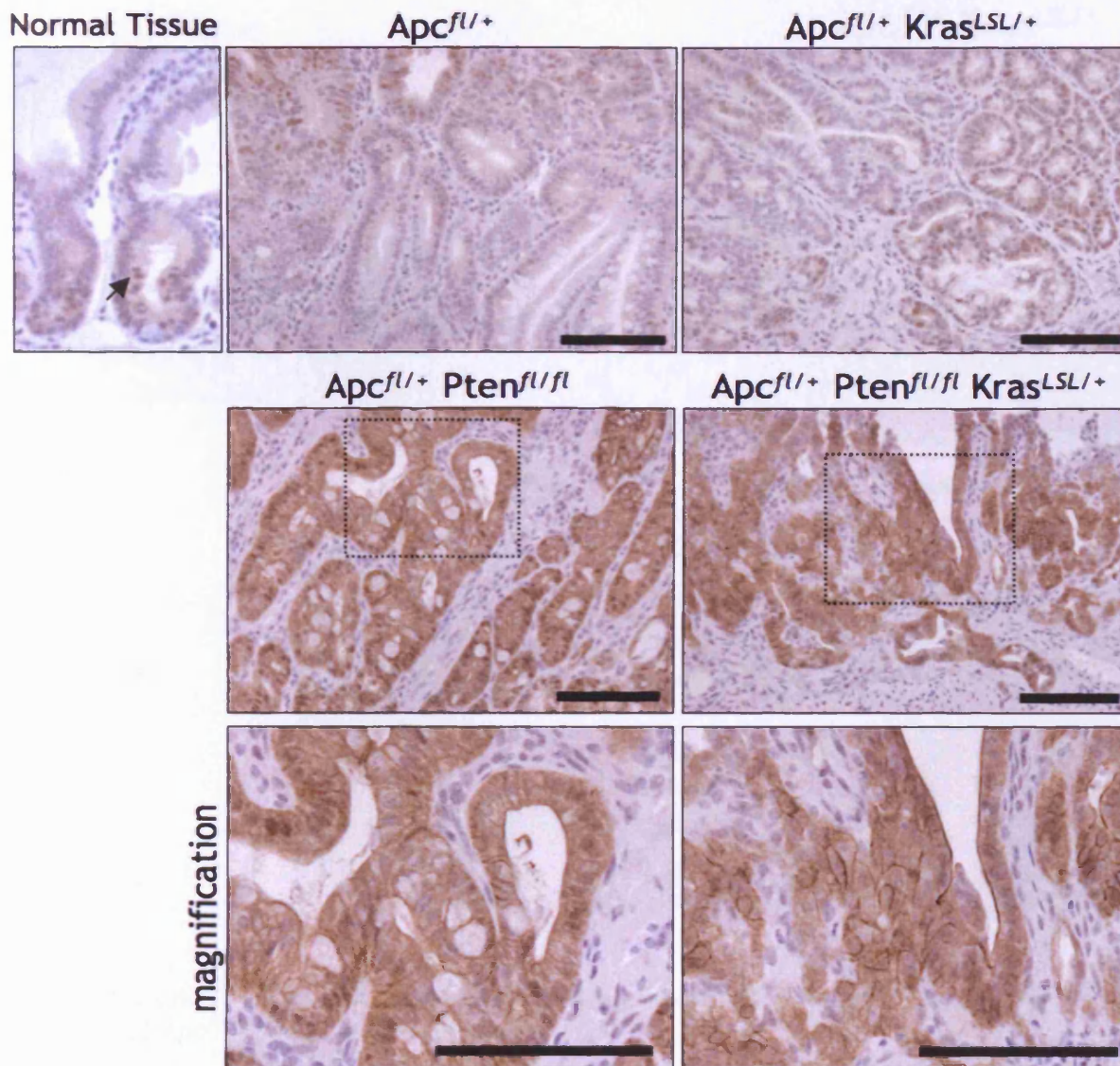
**Figure 4.5 Presence of pAkt as assessed by IHC staining, correlates with tumour invasiveness**

IHC against pAkt (ser473) was carried out on tumour and normal tissue sections from Apc$^{fl/+}$ Pten$^{fl/fl}$ Kras$^{LSL/+}$ mice and controls. Immunostaining for pAkt in Apc$^{fl/+}$ and Apc$^{fl/+}$ Kras$^{LSL/+}$ tumours appeared to be no stronger than that of normal tissue, some areas of the tumours appeared to stain stronger and in particular the staining was nuclear. This nuclear staining is likely to correlate with a more proliferative part of the tumour, as cells that are undergoing mitosis in the normal tissue also have stronger nuclear staining (arrow). Staining in all tumours from Apc$^{fl/+}$ Pten$^{fl/fl}$ Kras$^{LSL/+}$ and Apc$^{fl/+}$ Pten$^{fl/fl}$ mice, and particularly in the tumours with evidence of invasion, was markedly stronger than the staining seen in both control tumours and normal tissue. This staining was both cytoplasmic and membrane bound (as shown in the magnified image), membrane localisation of pAkt is thought to indicate strong activation of the PI3K pathway. Scale bars represent 100μm.

113
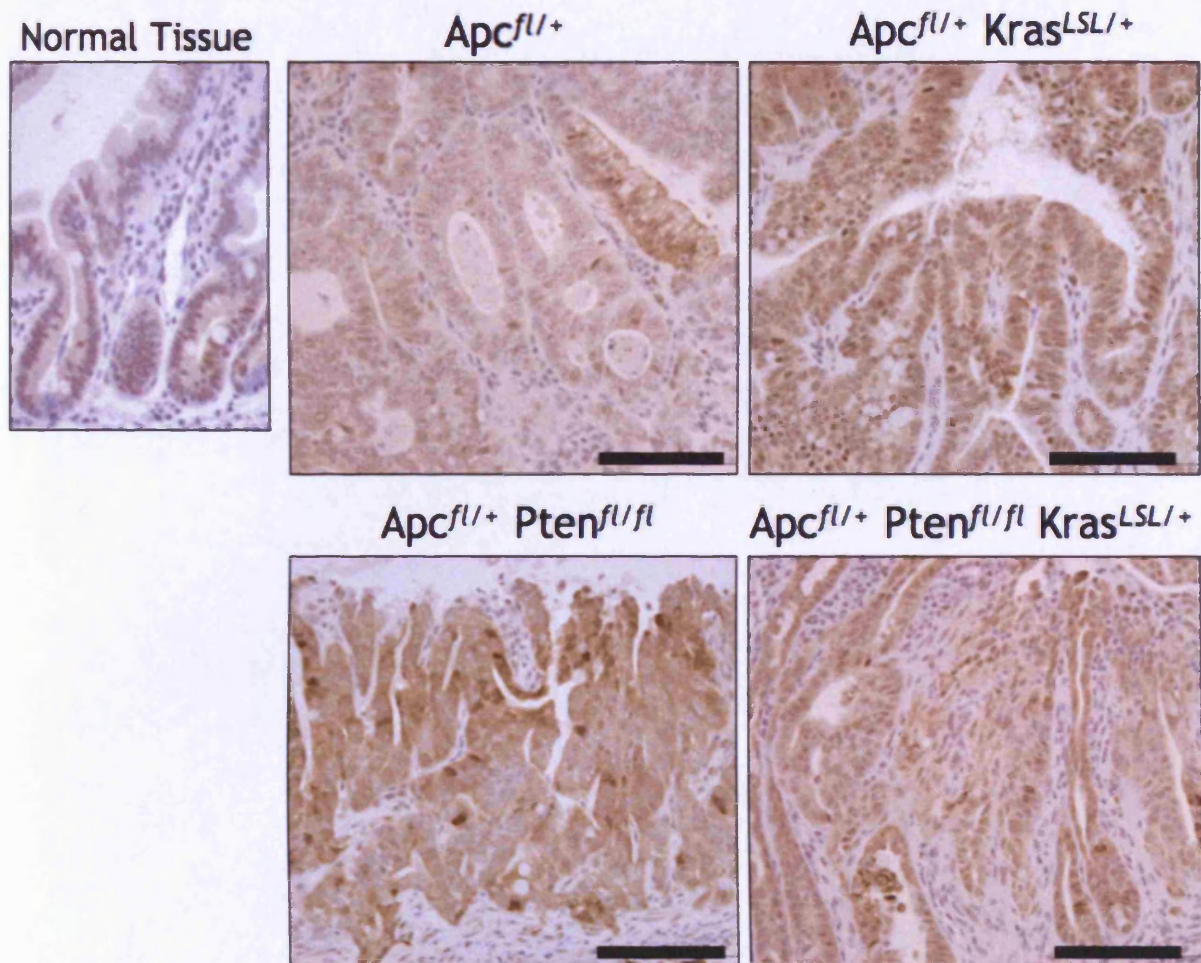
**Figure 4.6 pmTOR immunostaining revealed no overt differences between Apc$^{fl/+}$ Pten$^{fl/fl}$ and Apc$^{fl/+}$ Pten$^{fl/fl}$ Kras$^{LSL/+}$ tumours**

IHC against the activated form of mTOR, pmTOR (ser2448), was carried out on tumour and normal tissue sections from Apc$^{fl/+}$ Pten$^{fl/fl}$ Kras$^{LSL/+}$ mice and controls. mTOR is activated by pAkt, and therefore is a useful marker of its downstream activity. pmTOR immunostaining appears stronger in Apc$^{fl/+}$ Pten$^{fl/fl}$ Kras$^{LSL/+}$ tissue and in the Apc$^{fl/+}$ Pten$^{fl/fl}$ and Apc$^{fl/+}$ Kras$^{LSL/+}$ controls compared to Apc$^{fl/+}$ tissue. However, there is no overt difference between the staining in any of these tumours, so is not a useful marker in determining hyperactivation of Akt and the PI3K pathway. Scale bars represent 100μm.
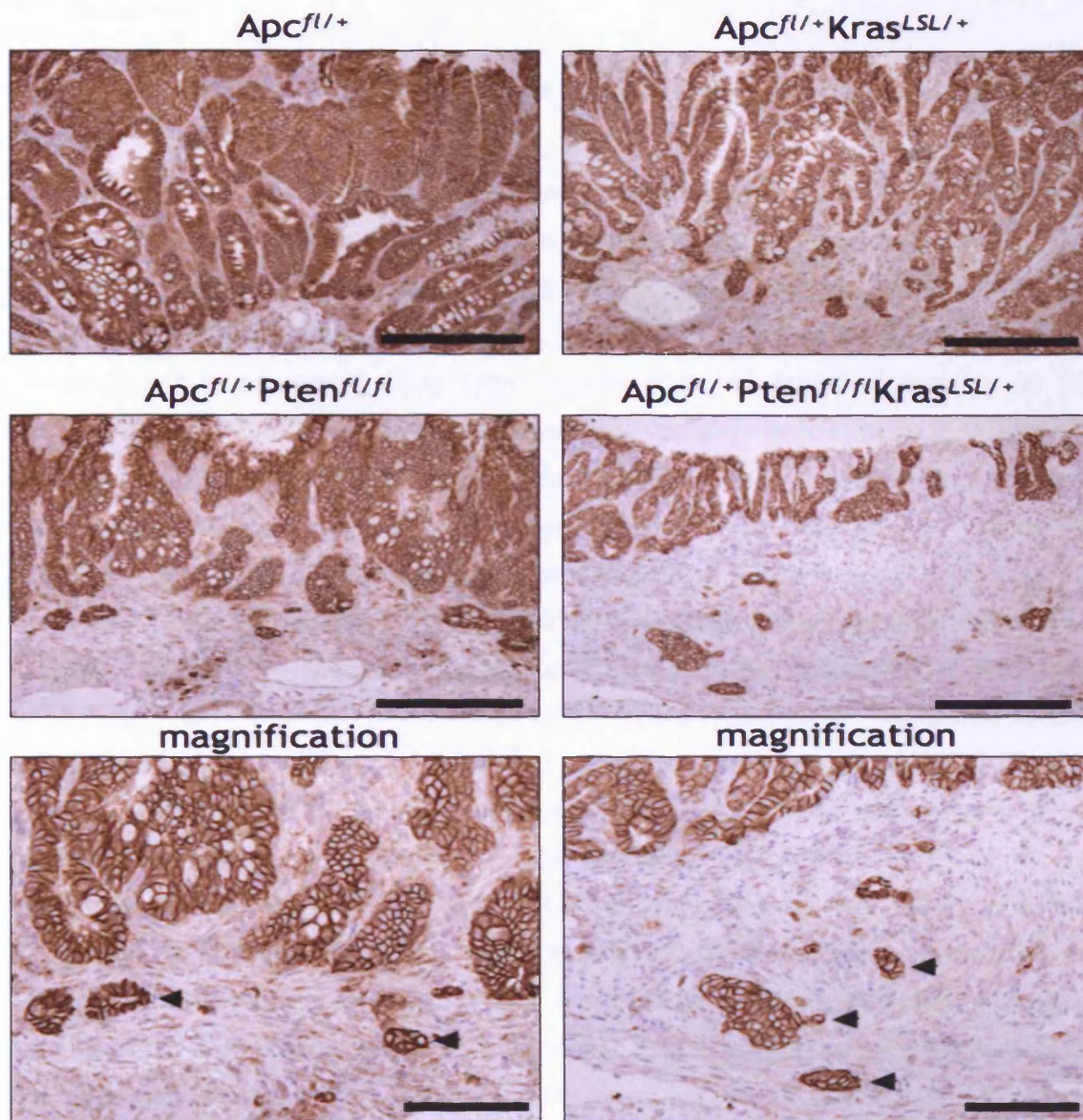
**Figure 4.7 Invasive tumours still possess membrane bound E-cadherin**

IHC against E-cadherin was carried out on small intestinal tumour tissue sections from each cohort. Staining revealed that the epithelial component of all tumours from benign adenomas in $Apc^{fl/+}$ mice to invasive adenocarcinomas in $Apc^{fl/+}$ $Pten^{fl/fl}$ $Kras^{LSL/+}$ mice, maintain membrane associated E-cadherin. Arrow heads indicate that the invasive components of tumours still maintain membrane localised E-cadherin immunostaining. Scale bars represent 200μm, magnified images 100μm.

## 4.3 Discussion

### 4.3.1 Pten and Kras synergise to reduce mouse life span in the context of an intestinal tumour model

As previously introduced, the *Ah*Cre recombinase transgene had first been implemented to investigate synergy between Pten and Kras mutations in the context of intestinal tumourigenesis. However, these mice rapidly succumbed to cholangio carcinoma (neoplasia of the gall bladder and bile ducts) and benign forestomach hyperplasia, thus preventing long term investigation of potential synergy in an intestinal setting. To circumvent this, an intestinal-specific cre recombinase (*Villin*Cre) was used to drive recombination. Experimental (*Villin*Cre-Apc$^{fl/+}$ Pten$^{fl/fl}$ Kras$^{LSL/+}$) and control groups (*Villin*Cre-Apc$^{fl/+}$, *Villin*Cre-Apc$^{fl/+}$ Kras$^{LSL/+}$ and *Villin*Cre-Apc$^{fl/+}$ Pten$^{fl/fl}$) were generated, induced and culled when symptomatic of disease.

Apc$^{fl/+}$ Pten$^{fl/fl}$ Kras$^{LSL/+}$ mice had a significantly shorter survival time post induction compared to the control cohorts (Figure 4.1, A). Interestingly, *Villin*Cre-Apc$^{fl/+}$ Pten$^{fl/fl}$ mice survived to a median of 78 days post induction, compared to the previously published *Ah*Cre-Apc$^{fl/+}$ Pten$^{fl/fl}$ mice, which survived to a median of 99 days post induction (Marsh et al., 2008). Despite morbidity in these mice being caused by an intestinal tumour phenotype, the difference in lifespan is likely to be attributed to differences in experimental strategy. *Ah*CreER$^{T}$ was used in this model and cre recombinase is activated at lower levels in the intestinal epithelium compared to *Villin*Cre due to the requirement of both a xenobiotic and tamoxifen being present to allow its activation. Therefore, in *Ah*Cre mice a lower proportion of intestinal cells undergo mutation of Apc, Pten and Kras. This lower activity of *Ah*Cre is evident when the number of tumours were scored; *Ah*Cre-Apc$^{fl/+}$ Pten$^{fl/fl}$ mice bore an average of 7 intestinal tumours, whereas *Villin*Cre-Apc$^{fl/+}$ Pten$^{fl/fl}$ mice bore an average of 12.

Scoring of the number of tumours present in H&E stained sections revealed that Apc$^{fl/+}$ Pten$^{fl/fl}$ Kras$^{LSL/+}$ mice bore a large number of tumours (average of 50 per section) (Figure 4.1, B), which could be responsible for the low mortality rate of the cohort. The number of tumours scored in Apc$^{fl/+}$ Pten$^{fl/fl}$ Kras$^{LSL/+}$ mice was higher than those scored in Apc$^{fl/+}$ Pten$^{fl/fl}$ mice, suggesting that Pten and Kras synergise to enhance initiation of tumourigenesis. However, Apc$^{fl/+}$ Kras$^{LSL/+}$ mice possessed an average of 60 tumours per section, a higher tumour number than Apc$^{fl/+}$ Pten$^{fl/fl}$ Kras$^{LSL/+}$ mice, yet these mice had a median survival time of 196 days post induction (Figure 4.1,B), thus suggesting, that the short survival time of Apc$^{fl/+}$ Pten$^{fl/fl}$ Kras$^{LSL/+}$ mice cannot not be solely attributed to tumour number.

### 4.3.2 Loss of Pten alone and in conjunction with Kras activation promotes tumour invasiveness in Apc$^{fl/+}$ mice

The level of tumour invasiveness was scored in each cohort. This revealed that only Apc$^{fl/+}$ Pten$^{fl/fl}$ Kras$^{LSL/+}$ and Apc$^{fl/+}$ Pten$^{fl/fl}$ mice possessed advanced tumours that had progressed from benign adenomas and become invasive (Figure 4.2, Figure 4.3). Apc$^{fl/+}$ Kras$^{LSL/+}$ mice were predominantly predisposed to the formation of microadenomas and adenomas, and these tumours rarely progressed to invade the submucosa or smooth muscle. However, the addition of a Kras mutation enhances tumour initiation in Apc$^{fl/+}$ mice, which is consistent with other studies (Janssen et al., 2006, Luo et al., 2009, Sansom et al., 2006). The level of tumour progression in both Apc$^{fl/+}$ Pten$^{fl/fl}$ Kras$^{LSL/+}$ and Apc$^{fl/+}$ Pten$^{fl/fl}$ mice is likely to be the cause of reduced lifespan in both these cohorts compared to controls.

Again there were differences between the tumours observed in VillinCre-Apc$^{fl/+}$ Pten$^{fl/fl}$ mice and those in AhCre-Apc$^{fl/+}$ Pten$^{fl/fl}$ mice. The tumours in AhCre-Apc$^{fl/+}$ Pten$^{fl/fl}$ mice were also invasive, and a proportion of these tumours (21.5%) had infiltrated through the smooth muscle wall (Marsh et al., 2008). Adenocarcinoma with smooth muscle invasion was not observed in VillinCre-Apc$^{fl/+}$ Pten$^{fl/fl}$ mice, only in VillinCre-Apc$^{fl/+}$ Pten$^{fl/fl}$ Kras$^{LSL/+}$ mice. The lower efficiency of recombination in AhCre mice compared to VillinCre mice, may offer explanation as to why adenocarcinomas with smooth muscle invasion are not observed in VillinCre-Apc$^{fl/+}$ Pten$^{fl/fl}$ mice. The lower number of tumours arising in AhCre-Apc$^{fl/+}$ Pten$^{fl/fl}$ mice due to lower DNA recombination efficiency, allows these mice to live longer. Therefore, the tumours present have a longer period in which to progress and invade further into the smooth muscle. VillinCre-Apc$^{fl/+}$ Pten$^{fl/fl}$ mice succumb to an earlier death due to a higher tumour number, so these tumours do not have adequate time to invade further into the smooth muscle.

### 4.3.3 Comparison of Apc$^{fl/+}$ Pten$^{fl/fl}$ Kras$^{LSL/+}$ and Apc$^{fl/+}$ Pten$^{fl/fl}$ models

IHC against pAkt (ser473) indicated that the PI3K pathway was being highly activated in tumours in VillinCre-Apc$^{fl/+}$ Pten$^{fl/fl}$ Kras$^{LSL/+}$ and VillinCre-Apc$^{fl/+}$ Pten$^{fl/fl}$ mice compared to tumours arising in control mice (Figure 4.5). The observed association of strong immunostaining for pAkt with highly invasive tumours in both VillinCre-Apc$^{fl/+}$ Pten$^{fl/fl}$ Kras$^{LSL/+}$ and VillinCre-Apc$^{fl/+}$ Pten$^{fl/fl}$ mice is consistent with the AhCre-Apc$^{fl/+}$ Pten$^{fl/fl}$ mouse model (Marsh et al., 2008) and other studies, which

have implicated the PI3K pathway in neoplastic progression (Rychahou et al., 2006, Samuels et al., 2005). These studies have demonstrated that activation of the PI3K pathway increases the propensity of CRC cell lines to invade in *in vitro* assays, and form metastases *in vivo* when injected into nude mice (Rychahou et al., 2006, Samuels et al., 2005).

As the tumours found in *Villin*Cre-$Apc^{fl/+}$ $Pten^{fl/fl}$ $Kras^{LSL/+}$ mice had invaded through the smooth muscle wall of the small intestine, and tumours found in *Villin*Cre-$Apc^{fl/+}$ $Pten^{fl/fl}$ mice were confined to the small intestine, one would assume that the PI3K pathway is being activated more strongly in the tumours found in *Villin*Cre-$Apc^{fl/+}$ $Pten^{fl/fl}$ $Kras^{LSL/+}$ mice. However, despite there being an overt difference in the level of invasiveness of the tumours from *Villin*Cre-$Apc^{fl/+}$ $Pten^{fl/fl}$ $Kras^{LSL/+}$ and *Villin*Cre-$Apc^{fl/+}$ $Pten^{fl/fl}$ mice, hyperactivation of pAkt was unable to be determined in *Villin*Cre-$Apc^{fl/+}$ $Pten^{fl/fl}$ $Kras^{LSL/+}$ tumours. IHC against the active form of mTOR (pmTOR), a downstream target of pAkt, was carried out to assess any possible increase in the downstream activity of pAkt in *Villin*Cre-$Apc^{fl/+}$ $Pten^{fl/fl}$ $Kras^{LSL/+}$ mice (Figure 4.6). pmTOR immunostaining proved not to be a useful marker of the downstream activity of pAkt and the PI3K pathway, as there were no overt differences between the tumours. Surprisingly, the level of pmTOR immunostaining in $Apc^{fl/+}$ $Kras^{LSL/+}$ tumours also appeared elevated, despite low levels of pAkt activation. Interestingly, the MAPK pathway did not appear to be more active in tumours bearing Kras mutations (Figure 4.4), and therefore it appears to not play a role in tumour progression.

IHC proved not be useful in discerning the level of PI3K activation in the tumours from each cohort. However, as the tumours arising in these mice possess a large stromal component, it would be difficult to obtain a homogenous sample of tumour epithelial cells needed for protein extraction and quantification of protein levels. Due to the heterogeneous nature of the tumours, IHC proves to be the most useful method for indicating pathway activation, specifically in tumour cells. As IHC is purely qualitative, it is difficult to determine levels of pathway activation.

Despite being unable to prove that the PI3K pathway is hyperactivated in tumours of *Villin*Cre-$Apc^{fl/+}$ $Pten^{fl/fl}$ $Kras^{LSL/+}$ mice, an argument for synergy between Pten and Kras through the PI3K pathway can be made when comparing the tumours observed in *Villin*Cre-$Apc^{fl/+}$ $Pten^{fl/fl}$ $Kras^{LSL/+}$mice and *Ah*Cre-$Apc^{fl/+}$ $Pten^{fl/fl}$ mice. In both these models, adenocarcinoma with smooth muscle invasion is observed, it can be argued that as *Ah*Cre-$Apc^{fl/+}$ $Pten^{fl/fl}$ mice live longer post induction, the tumours have additional time to accumulate pAkt, and therefore enhance activation of the PI3K pathway. As *Villin*Cre-$Apc^{fl/+}$ $Pten^{fl/fl}$ $Kras^{LSL/+}$ mice have the same observed tumour

phenotype but do not live as long, it can be postulated that these tumours therefore have enhanced activation of pAkt at earlier time points, driven by activation of Kras and the combined loss of negative regulation of PI3K via Pten loss.


## 4.4 Summary

Pten loss and Kras activation act synergistically in the context of a *Villin*Cre-Apc$^{fl/+}$ intestinal tumour model to promote tumour initiation and progression, which is likely to be driven by hyperactivation of the PI3K pathway. However, addition of an oncogenic allele of Kras did not promote tumour progression through to metastasis as was hypothesised.

## 4.5 Further Work

Loss of Pten and activation of Kras promotes tumour progression, which appears to be driven by activation of the PI3K pathway. However, there are many downstream targets of PI3K, and so therefore it would be useful to determine which of these targets promotes tumour progression and invasion for potential therapeutic targeting. One potential target may be the forkhead transcription factors (FKHR). Some studies have shown that inactivation of FKHR via pAkt mediated phosphorylation, reduced the tumourigenic potential and invasiveness of colorectal cancer cell lines (Khaleghpour et al., 2004, Samuels et al., 2005). Therefore, it would be interesting to assess the level of FKHR phosphorylation in tumours arising in Apc$^{fl/+}$ Pten$^{fl/fl}$ Kras$^{LSL/+}$ mice.

The large number of tumours, invasiveness of the tumours observed and its well-defined survival curve, make the *Villin*CreER$^{T}$-Apc$^{fl/+}$ Pten$^{fl/fl}$ Kras$^{LSL/+}$ intestinal tumour model a good candidate for testing the efficacy of anti-cancer drugs on intestinal tumours.

As E-cadherin expression was maintained in invasive tumours in both Apc$^{fl/+}$ Pten$^{fl/fl}$ Kras$^{LSL/+}$ and Apc$^{fl/+}$ Pten$^{fl/fl}$ mice, further work on the loss of E-cadherin and its role in promoting invasion of tumours will be investigated in the context of tumours arising in Apc$^{fl/+}$ Pten$^{fl/fl}$ mice in Chapter 7.

# Chapter 5: Investigating short term synergy between Pten and Kras in the intestinal epithelium

## 5.1 Introduction

Pten acts as a negative regulator of the PI3K pathway, and Kras can cause activation of the PI3K pathway through its interaction with the p110 catalytic subunit of the PI3K protein. Mutations in Pten and Kras, causing loss of function and constitutive activation of the proteins respectively, may act synergistically through the PI3K pathway. Loss of Pten alone would cause elevation of the active form of the downstream PI3K effector protein Akt. However, additional mutation of Kras may result in hyperactivation of the PI3K pathway causing further accumulation of active Akt.

Findings in chapter 3 suggested that mutations in Pten and Kras synergise, to give rise to hyperplasia of the small intestinal epithelium, and a decrease in the abundance of differentiated cell types. There was a subtle increase in PI3K pathway activity in the small intestines of mice that bore mutations in Pten and Kras either alone or concomitantly in chapter 3. I have also demonstrated that mutations in Pten and Kras synergise in the context of tumourigenesis to promote tumour progression and decrease mouse survival.

Further to the finding that Pten loss and Kras activation disrupts small intestinal homeostasis in the mouse at day 15 post induction (outlined in chapter 3), I wished to investigate potential synergy between Pten and Kras mutations in normal small intestine at longer time points after induction. $VillinCreER^T$-$Pten^{fl/fl}$ $Kras^{LSL/+}$ mice (hereafter referred to as $Pten^{fl/fl}$ $Kras^{LSL/+}$ mice) and the appropriate controls, ($VillinCreER^T$-$Pten^{+/+}$ $Kras^{LSL/+}$ [$Kras^{LSL/+}$] and $VillinCreER^T$-$Pten^{fl/fl}$ $Kras^{+/+}$ [$Pten^{fl/fl}$] and $VillinCreER^T$-$Pten^{+/+}$ $Kras^{+/+}$ [WT]) were generated, induced and sacrificed at 50 days post induction. At least 8 mice were induced in each cohort and were given either a 2 hour or 48 hour pulse of BrdU prior to sacrifice.

## 5.2 Results

### 5.2.1 Recombination of loxP sites at the Pten and Kras locus is maintained at 50 days post induction

*Villin*Cre recombinase is expressed in all small intestinal epithelial cells including the stem cell compartment. Therefore, due to recombination of DNA in the stem cells, presence of the recombined allele is maintained long term throughout the small intestine epithelium. A multiplex PCR for the recombined alleles of Pten and Kras was carried out on gDNA extracted from intestinal epithelial cell enriched samples, obtained from scrapings of the mucosal surface of the intestine at day 50 post induction. PCR showed that the recombined alleles of Pten and Kras were still present at day 50 post induction (Figure 5.1, A). Another epithelial enriched sample was obtained from the small intestines of day 50 mice using the HBSS-EDTA epithelial isolation method. Inverted small intestinal samples were shaken in a solution of HBSS-EDTA and centrifuged to obtain a cleaner epithelial cell sample, suitable for the extraction of protein and RNA. Protein was extracted from these epithelial enriched samples and western blot was carried out against the Pten protein. Western blotting showed that Pten had been lost at the protein level (Figure 5.1, B).

### 5.2.2 Pten loss and Kras activation results in gross alteration of villus structure at 50 days post induction

The intestines from mice sacrificed at day 50 post induction were dissected, a 10cm section of the small intestine was fixed and processed for H&E staining, and a 1cm section of the small intestine was prepared for visualisation by SEM. The same region of the intestine (relative to the stomach) was dissected each time.

Examination of the intestine at day 50 post induction by H&E section revealed a high proportion of villi to be bifurcated or branched in $Pten^{fl/fl}$ $Kras^{LSL/+}$ mice, but not in controls (Figure 5.2, left panel). 3-dimensional imaging of the mucosal surface of the small intestine by SEM confirmed these morphological changes of the villus structure. It would appear that the synergy between Pten and Kras that drives hyperplasia of the small intestine evident at day 15 post induction, becomes more pronounced at later stages, evidenced by gross alterations of the villus structure at day 50 post induction.
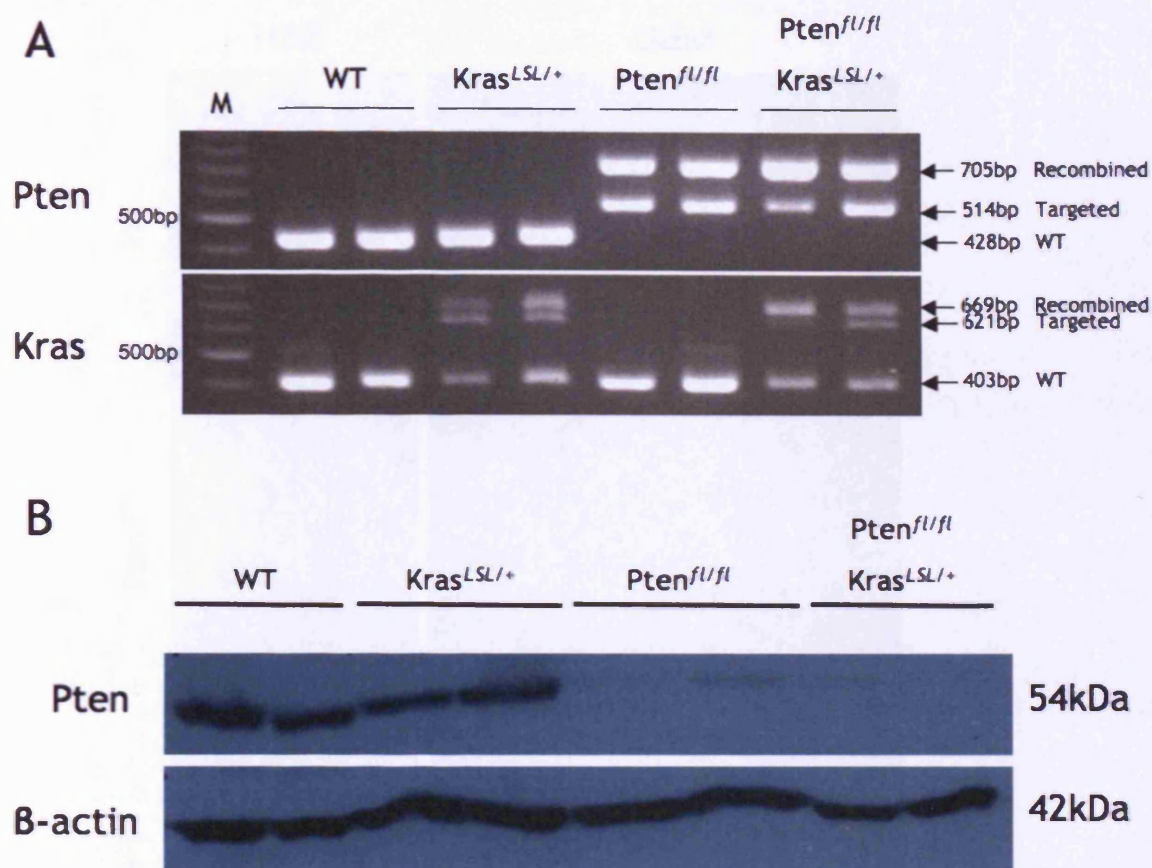
**Figure 5.1 Recombined PCR for the Pten and Kras locus, and loss of Pten protein prove maintenance of the recombined alleles in the intestinal epithelium at day 50 post induction**

(A) Key: M = DNA marker, 100kb ladder. Multiplex PCRs for the recombined alleles of Pten and Kras showed the presence of a recombined band for Pten (upper panel) and Kras (lower panel) in Pten*fl/fl* Kras*LSL/+* mice. The correct recombined bands were seen for each of the controls. PCR carried out on DNA samples from both Pten*fl/fl* Kras*LSL/+* and Pten*fl/fl* mice yielded products for the targeted unrecombined allele. This is likely to be a result of DNA from unrecombined epithelial cells and non epithelial cells (i.e. stromal cells where *Villin*CreER$^T$ is not expressed) being present in the epithelial cell samples. (B) Western blot for Pten revealed a significant reduction of Pten protein in Pten*fl/fl* and Pten*fl/fl* Kras*LSL/+* samples compared to controls. However, there are some faint bands visible in the Pten*fl/fl* samples, which are again likely to be caused by underlying intestinal stromal cells or unrecombined epithelial cells.
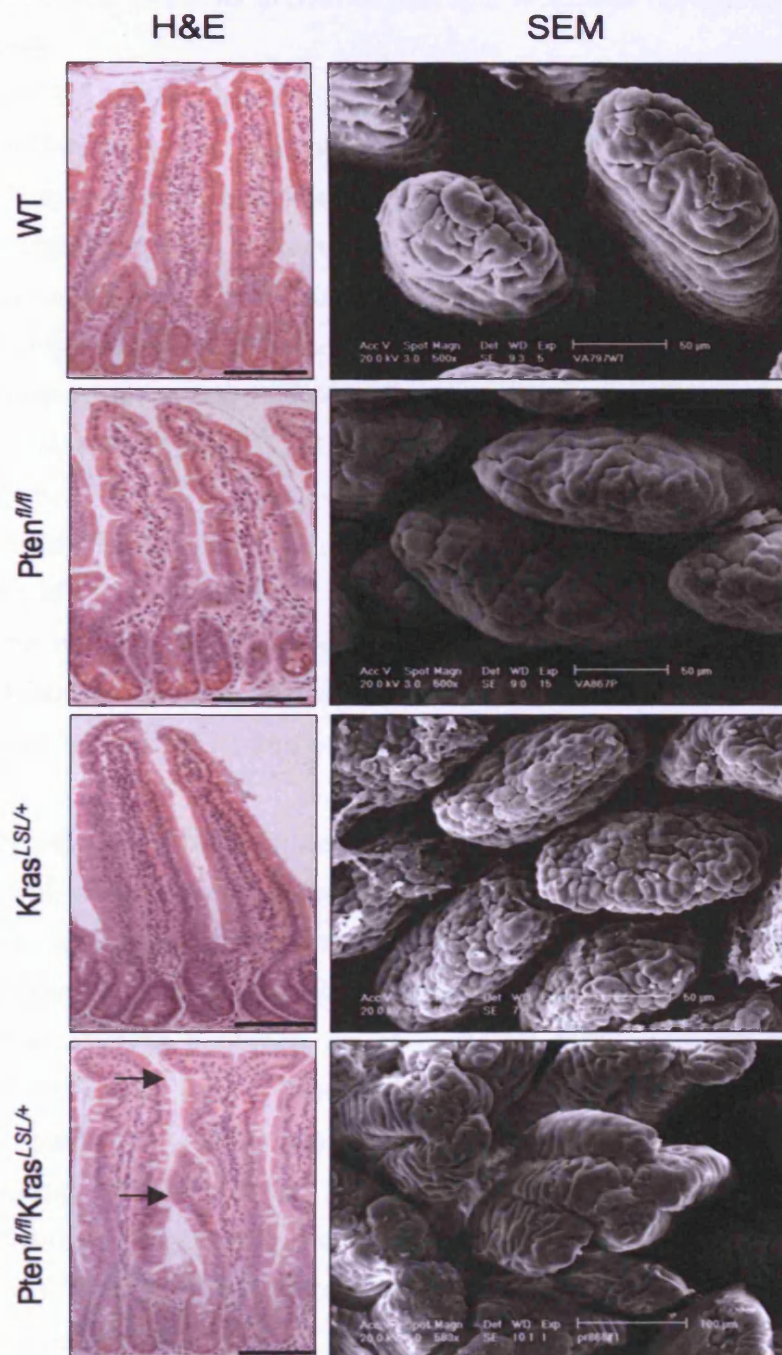
**Figure 5.2 Gross alterations in villus morphology were evident in both H&E sections and in SEM images.**

H&E sections in the left panel reveal changes in villus structure in $Pten^{fl/fl}$ $Kras^{LSL/+}$ small intestine compared to the controls (scale bars represent 200μm). Villi appeared to be bifurcating and branching (arrows), and there are no longer finger-like projections. This finding was confirmed by SEM (right panel), which shows clearly that the villi in $Pten^{fl/fl}$ $Kras^{LSL/+}$ small intestine are made up of a number of projections from a common base compared to the WT and controls.

123

### 5.2.3 Pten loss and Kras activation disrupts intestinal homeostasis at the histological level

H&E stained small intestinal sections were scored for the number of cells per half crypt and the number of cells per half villus. 50 half crypt-villus structures were scored for each mouse in both experimental ($Pten^{fl/fl} Kras^{LSL/+}$) and control cohorts.

Histological analysis revealed a significant increase in the number of cells per half crypt and villus in $Pten^{fl/fl} Kras^{LSL/+}$ mice compared to WT and controls (p value <0.05 for both crypt and villus length, Mann Whitney-U test, n=4) (Figure 5.3). $Pten^{fl/fl} Kras^{LSL/+}$ mice possessed an average of 40 ± 3 cells per half crypt, compared to $Pten^{fl/fl}$ (32 ± 4 cells per half crypt), $Kras^{LSL/+}$ (33 ± 2 cells per half crypt) and WT (32 ± 4 cells per half crypt). $Pten^{fl/fl} Kras^{LSL/+}$ mice possessed an average of 124 ± 18 cells per half villus, compared to $Pten^{fl/fl}$ (83 ± 14 cells per half villus), $Kras^{LSL/+}$ (94 ± 10.6 cells per half villus) and WT (74 ± 16 cells per half villus).

The number of apoptotic bodies and mitotic figures per half crypt was scored from H&E stained small intestinal sections as described in the methods chapter. 50 half crypts were scored for each mouse in both experimental ($Pten^{fl/fl} Kras^{LSL/+}$) and control cohorts.

Despite an increase in both crypt and villus cell number, statistical comparisons of the level of apoptosis and mitosis in $Pten^{fl/fl} Kras^{LSL/+}$ tissue revealed no significant differences compared to control and WT tissue, and within controls (p values >0.05, Mann-Whitney U test, n=4) (Figure 5.4). Apoptosis scoring of $Pten^{fl/fl} Kras^{LSL/+}$ tissue revealed an average apoptotic count of 0.06 ± 0.06 apoptotic bodies per half crypt, compared to $Pten^{fl/fl}$ (0.05 ± 0.06 apoptotic bodies per half crypt), $Kras^{LSL/+}$ (0.11 ± 0.05 apoptotic bodies per half crypt) and WT (0.06 ± 0.04 apoptotic bodies per half crypt). Mitosis scoring of $Pten^{fl/fl} Kras^{LSL/+}$ tissue revealed an average mitotic count of 0.63 ± 0.2 mitotic figures per half crypt, compared to $Pten^{fl/fl}$ (0.42 ± 0.13 mitotic figures per half crypt), $Kras^{LSL/+}$ (0.54 ± 0.25 mitotic figures per half crypt) and WT (0.06 ± 0.04 mitotic figures per half crypt).
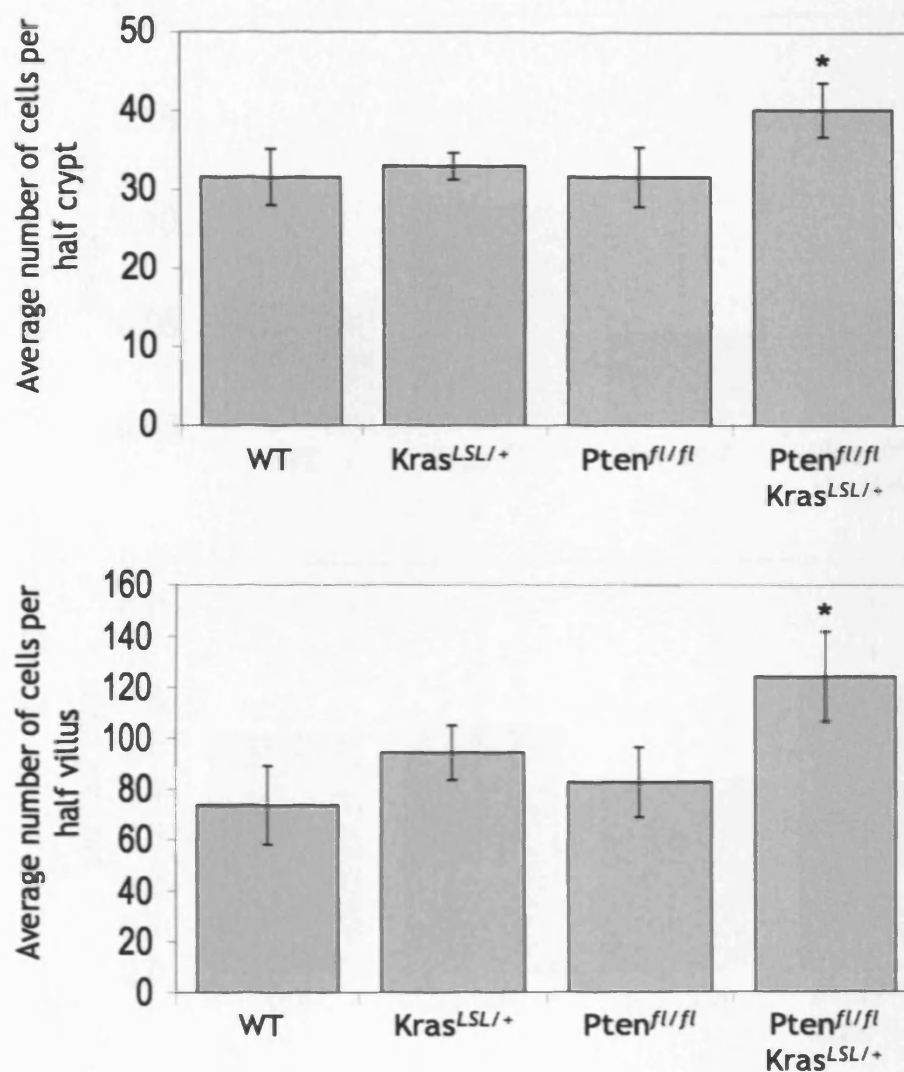
**Figure 5.3 Crypt and villus scoring revealed significantly more cells per half crypt-villus in Pten$^{fl/fl}$ Kras$^{LSL/+}$ intestine compared to controls**

Crypt size (upper panel) and villus size (lower panel) was determined by scoring the number of cells per half crypt and villus on H&E stained intestinal sections of experimental (Pten$^{fl/fl}$ Kras$^{LSL/+}$) and control mice. Scoring revealed that Pten$^{fl/fl}$ Kras$^{LSL/+}$ mice had significantly higher numbers of cells along crypt-villus axis compared to controls and WT mice (*, p values <0.05, n=4, Mann Whitney U Test). Error bars indicate standard deviation.
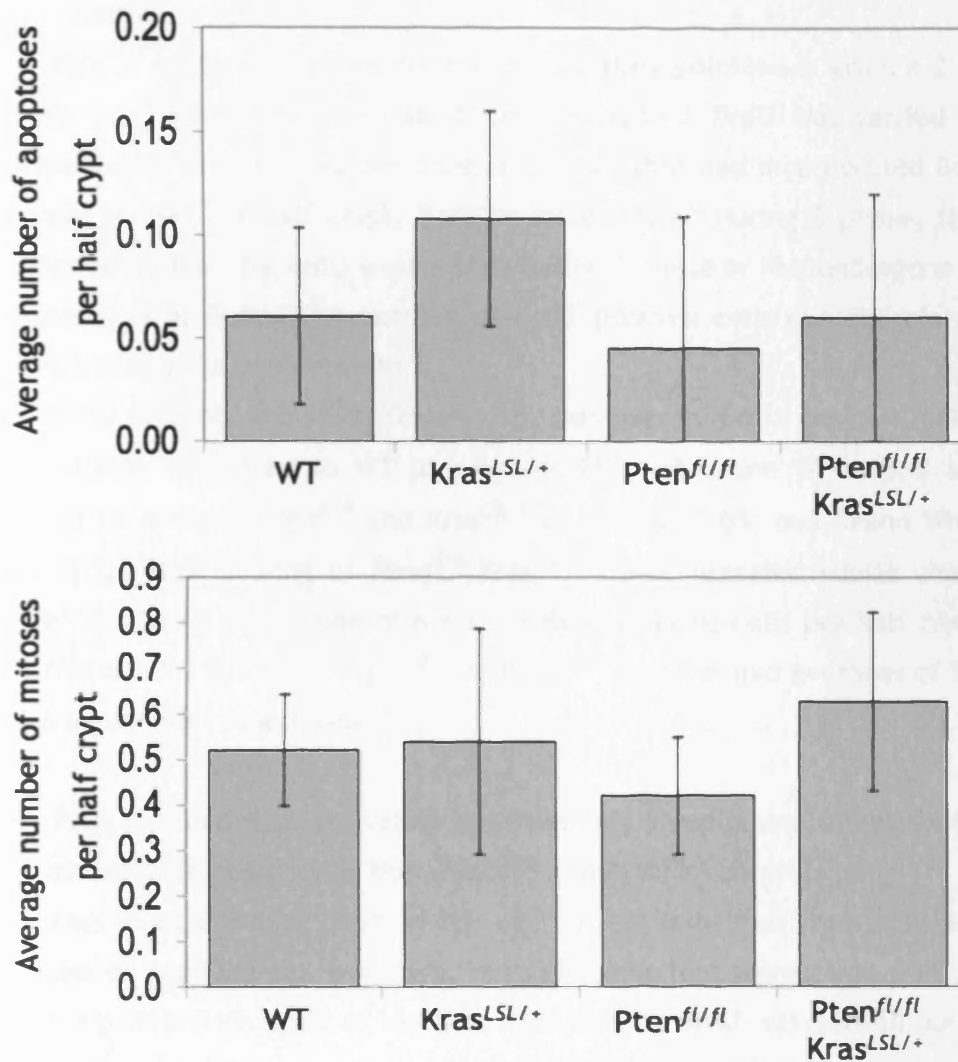
Figure 5.4 Apoptosis and mitosis scoring per half crypt revealed no changes in Pten$^{fl/fl}$ Kras$^{LSL/+}$ tissue compared to control

Number of apoptotic bodies per half crypt (upper panel) and mitotic figures per half crypt (lower panel) was determined by scoring H&E stained intestinal sections of experimental (Pten$^{fl/fl}$ Kras$^{LSL/+}$) and control mice. Scoring revealed that there were no changes in apoptotic or mitotic levels in Pten$^{fl/fl}$ Kras$^{LSL/+}$ mice compared to controls and WT, neither was there any changes between the control cohorts (Pten$^{fl/fl}$ and Kras$^{LSL/+}$) compared to WT tissue (p values >0.05, n=4, Mann Whitney U Test). Error bars indicate standard deviation.

### 5.2.4 Pten loss and Kras activation causes a subtle increase in proliferation in the intestinal crypts

Half of all the mice used for the day 50 time point were given a 2 hour pulse of BrdU via i.p. injection prior to sacrifice. IHC against BrdU was carried out on small intestinal tissue sections and the number of cells that had incorporated BrdU into their DNA were scored per half crypt. BrdU is incorporated during S phase, therefore cells that stained positive for BrdU were either within S phase or had undergone S phase after administration of BrdU. The number of BrdU positive cells can therefore be used to quantify the level of proliferation.

BrdU scoring analysis revealed an increase in BrdU positive cells in $Pten^{fl/fl}$ $Kras^{LSL/+}$ tissue compared to WT (p value <0.05, n≥3, Mann Whitney U test), but not compared to controls $Pten^{fl/fl}$ and $Kras^{LSL/+}$ (p values >0.05, n≥3, Mann Whitney U test) (Figure 5.5). BrdU scoring of $Pten^{fl/fl}$ $Kras^{LSL/+}$ tissue revealed subtle changes in BrdU positive cells, with an average of 6.4 ± 0.9 BrdU positive cells per half crypt, compared to WT tissue 5.1 ± 0.5 cells, $Pten^{fl/fl}$ and $Kras^{LSL/+}$ controls had averages of 5.0 ± 0.7 cells and 5.6 ± 0.9 cells respectively.

### 5.2.5 Pten loss and Kras activation together has a compound effect on the migratory phenotypes observed in both $Pten^{fl/fl}$ and $Kras^{LSL/+}$ controls

Half of all the mice used for the day 50 post induction time point were given a 2 hour pulse of BrdU via i.p. injection, the remaining half were given a 48 hour pulse of BrdU via i.p. injection prior to sacrifice. IHC against BrdU was carried out on intestinal tissue sections and the number and position of positive cells along the crypt-villus axis were scored per half crypt-villus. The cumulative position of BrdU positive cells along the crypt-villus after 2 and 48 hours was compared in a cumulative frequency curve (Figure 5.6).

The cumulative frequency of BrdU positive cell position after a 2 hour pulse of BrdU revealed that positive cells were found in lower and higher cell positions along the crypt-villus axis in $Pten^{fl/fl}$ $Kras^{LSL/+}$ tissue compared to WT (p value <0.05, Kolmologrov-Smirnov test). The proliferative zone is therefore expanded in these mice. BrdU positive cells labeled significantly lower positions in the crypt in $Pten^{fl/fl}$ control tissue compared to WT tissue (p value <0.05, Kolmologrov-Smirnov test) (Figure 5.6, A). Cumulative frequency of BrdU positive cell position after a 48 hour pulse of BrdU revealed that in both experimental ($Pten^{fl/fl}$ $Kras^{LSL/+}$) and control ($Kras^{LSL/+}$ and $Pten^{fl/fl}$) tissue BrdU positive cells were found higher up the crypt-villus axis after 48 hours compared to WT tissue (p values <0.001, Kolmologrov-Smirnov test) (Figure 5.6, B). Therefore, the cells

have migrated faster up the crypt-villus axis. Synergy between Pten and Kras is evident as increases in cell migration in control cohorts appear to be compounded in the experimental cohort, as the Pten$^{fl/fl}$ Kras$^{LSL/+}$ cumulative frequency curve is significantly shifted from control cohorts (p value <0.001, Kolmologrov-Smirnov test).

### 5.2.6 Increases in the abundance of proliferative cells and the proliferative zone are not attributed to an increase in intestinal stem cell number

Significant increases in the number of proliferative cells per half crypt (see section 5.2.4), and an expansion of the proliferation zone in the crypt (see section 5.2.5) of Pten$^{fl/fl}$ Kras$^{LSL/+}$ mice may be driven by an expansion in the number of stem cells. As a surrogate marker of relative stem cell abundance, RNA was extracted from epithelial cell enriched pellets and the corresponding cDNA was synthesised, qRT-PCR was carried out using the TaqMan assay for the small intestinal CBC stem cell markers Lgr5 and Ascl2. TaqMan assay was used to ensure accurate readouts of stem cell marker expression as their endogenous expression level is very low.

Quantification of Lgr5 and Ascl2 expression revealed no changes in relative expression levels in Pten$^{fl/fl}$ Kras$^{LSL/+}$ small intestine compared to control and WT tissue (Figure 5.7). The average $\Delta C_T$ for Lgr5 expression in Pten$^{fl/fl}$ Kras$^{LSL/+}$ intestinal tissue was 12.64 ± 1.03, compared to the averages of Pten$^{fl/fl}$ (12.58 ± 0.78), Kras$^{LSL/+}$ (12.24 ± 0.63) and WT (12.02 ± 1.02). The average $\Delta C_T$ for Ascl2 expression in Pten$^{fl/fl}$ Kras$^{LSL/+}$ intestinal tissue was 13.36 ± 1.22, compared to the averages of Pten$^{fl/fl}$ (12.81 ± 0.64), Kras$^{LSL/+}$ (13.25 ± 0.33) and WT (12.34 ± 0.79). The average $\Delta C_T$ for each cohort was compared using the Mann Whitney U test. Statistical analysis revealed that there was no significant changes in average $\Delta C_T$ value for both Lgr5 and Ascl2 in Pten$^{fl/fl}$ Kras$^{LSL/+}$ mice compared to controls and WT. Therefore, increases in the number of proliferative cells in Pten$^{fl/fl}$ Kras$^{LSL/+}$ tissue may be attributed to expansion of transit-amplifying (TA) cell number, but is not a result of stem cell expansion.
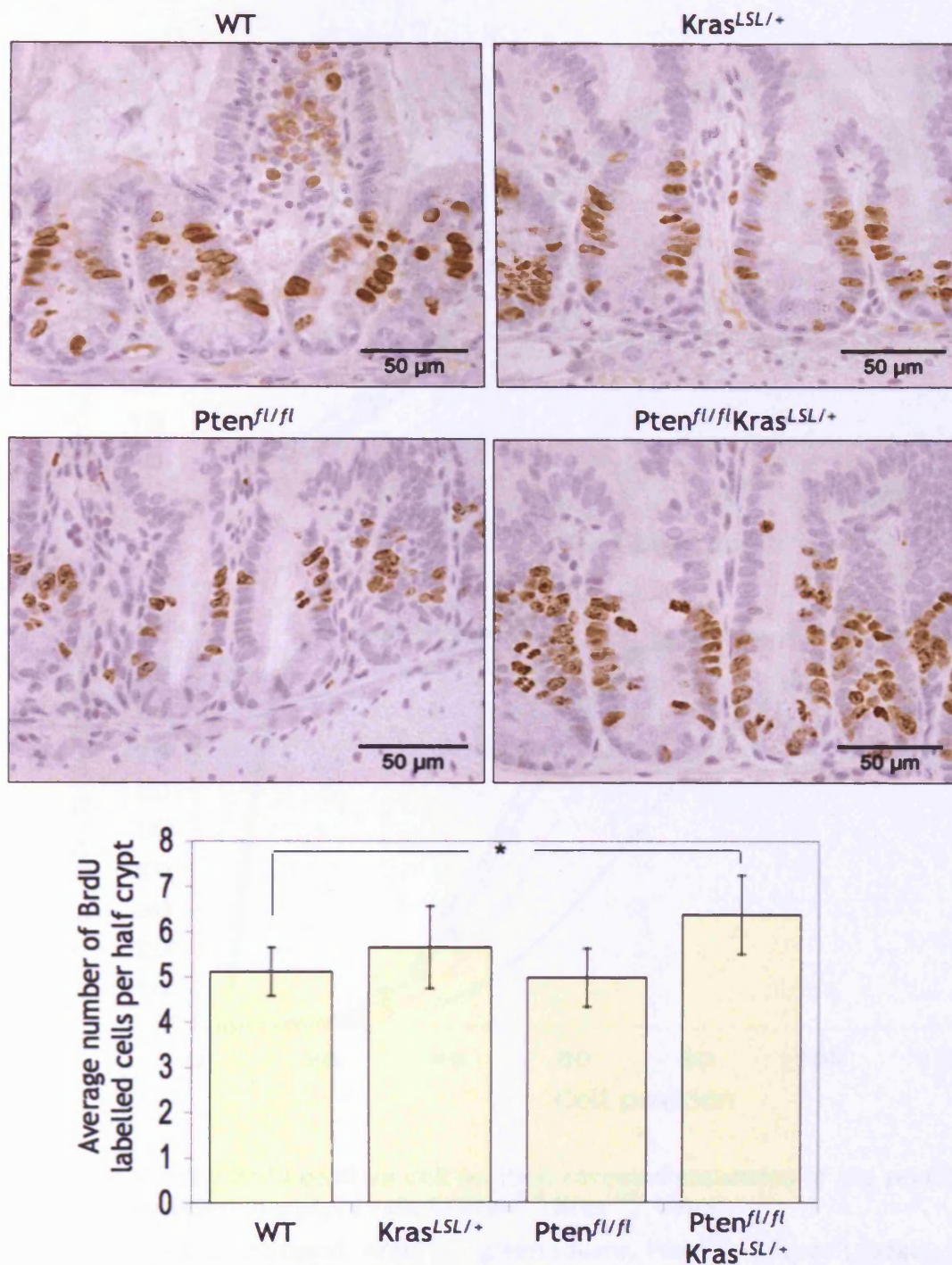
**Figure 5.5 BrdU scoring revealed a subtle proliferative phenotype in Pten$^{fl/fl}$ Kras$^{LSL/+}$ compared to WT**

IHC against BrdU (upper panel) suggests there may be an increase in the number of BrdU cells in Pten$^{fl/fl}$ Kras$^{LSL/+}$. Scoring of BrdU positive cells per half crypt revealed that there is only a significant increase in Pten$^{fl/fl}$ Kras$^{LSL/+}$ tissue compared to WT tissue (*, p value <0.05, n≥3, Mann Whitney U test). There was no significant difference between Pten$^{fl/fl}$ Kras$^{LSL/+}$ and controls (Pten$^{fl/fl}$ and Kras$^{LSL/+}$). Error bars indicate standard deviation.
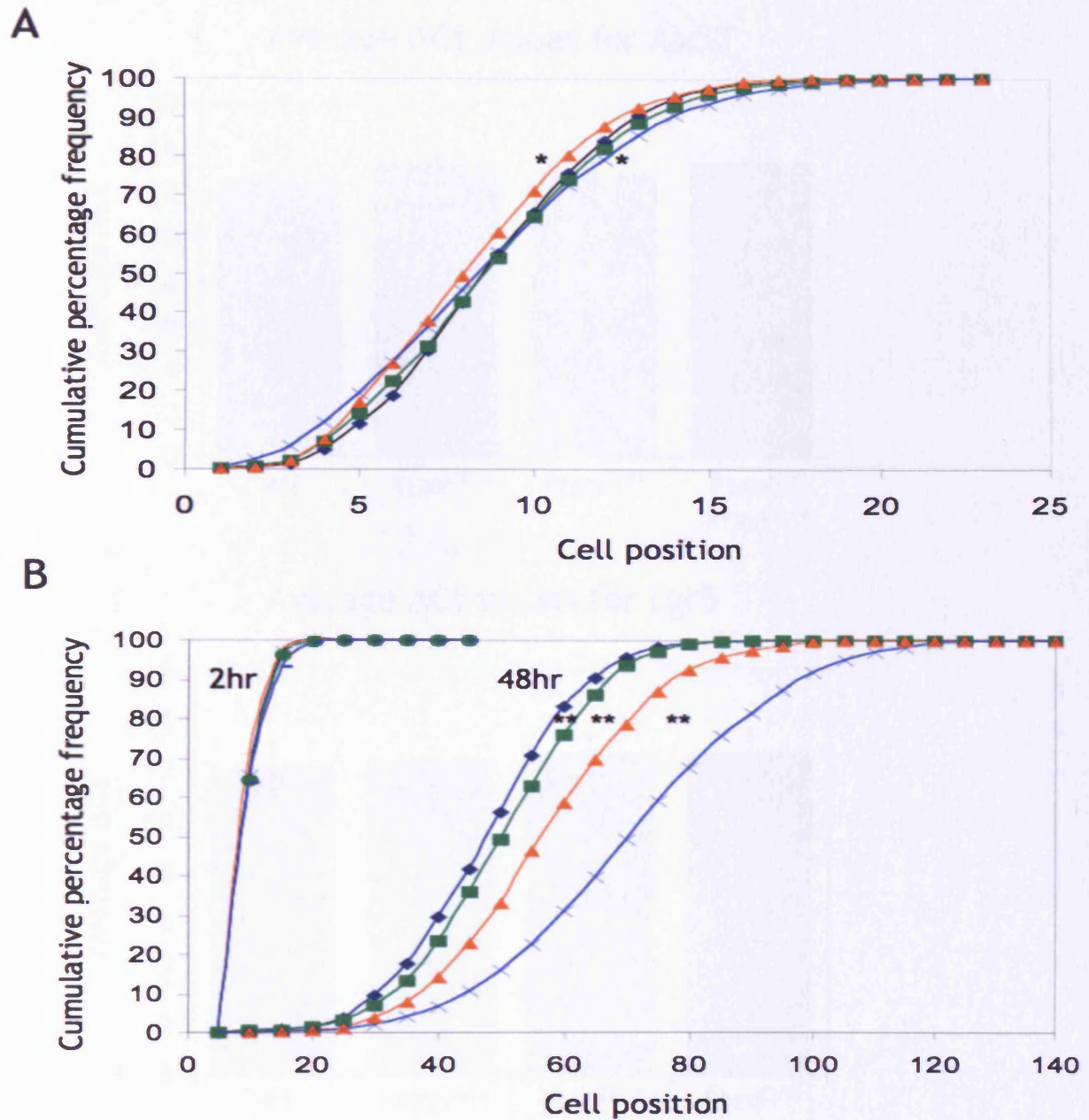
**Figure 5.6 Scoring BrdU positive cell position revealed expansion of the proliferative zone and increased migratory rate in Pten$^{fl/fl}$ Kras$^{LSL/+}$ tissue**

Key: WT - dark blue diamond, Kras$^{LSL/+}$ - green square, Pten$^{fl/fl}$ - orange triangle, Pten$^{fl/fl}$ Kras$^{LSL/+}$ - light blue crosses

(A) Cumulative position of BrdU positive cells per half crypt after a 2 hour pulse of BrdU revealed lower and higher positioning of proliferative cells in Pten$^{fl/fl}$ Kras$^{LSL/+}$ tissue compared to WT, suggesting an increase in proliferative zone. Positioning of proliferative cells in Pten$^{fl/fl}$ control tissue was significantly lower compared to WT (*, p value <0.05, Kolmologrov-Smirnov test). (B) Cumulative position of BrdU positive cells per half crypt after a 48 hour pulse of BrdU revealed that cells in Pten$^{fl/fl}$ Kras$^{LSL/+}$ and control tissues positioned significantly higher than WT tissue (**, p value <0.001, Kolmologrov-Smirnov test). Therefore the rate of migration was increased in experimental and control tissues compared to WT.

## Average ΔCt values for Ascl2

## Average ΔCt values for Lgr5
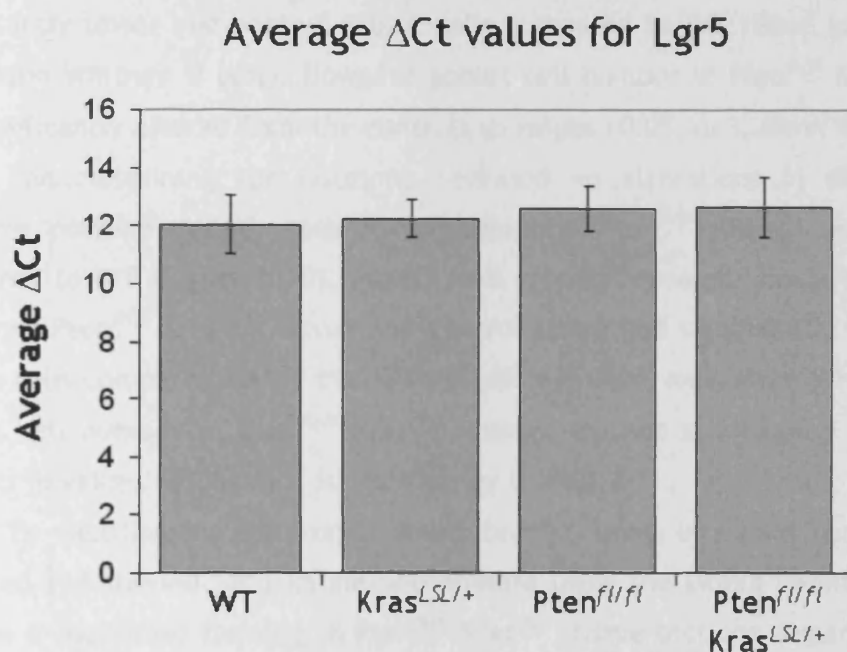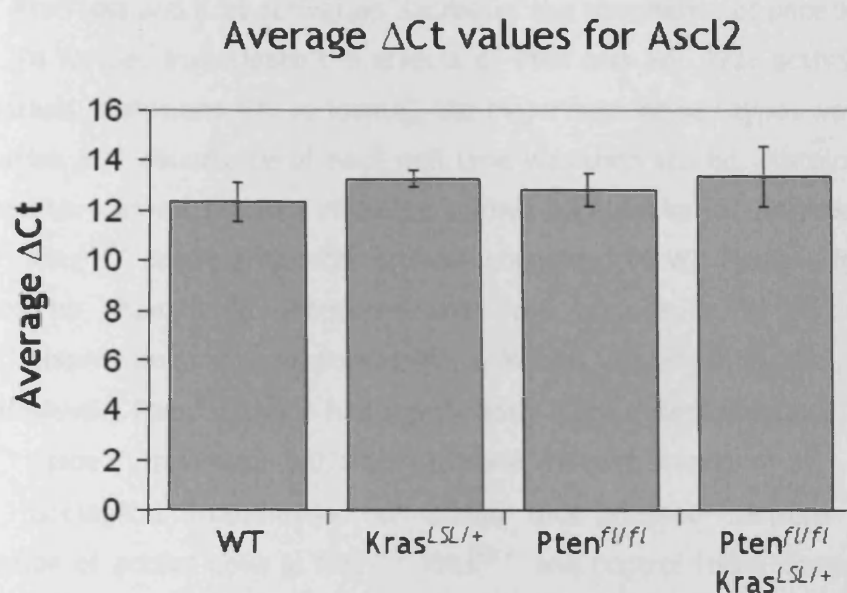
**Figure 5.7 qRT-PCR expression analysis of stem cell markers Ascl2 and Lgr5 revealed no changes in expression levels in Pten$^{fl/fl}$ Kras$^{LSL/+}$ small intestine**

The expression of intestinal stem cell specific markers Ascl2 (upper panel) and Lgr5 (lower panel) was quantified by qPCR to ascertain the number of stem cells present in the small intestine in each cohort. There was no change in the average $\Delta C_T$ value in Pten$^{fl/fl}$ Kras$^{LSL/+}$ tissue compared to control and WT samples for both Ascl2 and Lgr5 (p value >0.05, Mann Whitney U test).

### 5.2.7 Pten loss and Kras activation decreases the abundance of paneth and goblet cells

To further investigate the effects of Pten loss and Kras activation on intestinal homeostasis, stains and IHC to identify the major mature cell types was carried out. The localisation and abundance of each cell type was then scored. Histological examination of grimelius stained sections revealed normal localisation of enteroendocrine cells in $Pten^{fl/fl}$ $Kras^{LSL/+}$ tissue and control tissue compared to WT tissue (Figure 5.8). Scoring revealed no changes in enteroendocrine cell abundance in experimental ($Pten^{fl/fl}$ $Kras^{LSL/+}$ tissue) and controls compared to WT (p values >0.05, n≥3, Mann Whitney U test). However, $Pten^{fl/fl}$ tissue had significantly more enteroendocrine cells than $Pten^{fl/fl}$ $Kras^{LSL/+}$ tissue (*, p value = 0.0204, n≥3, Mann Whitney U test).

Histological examination of alcian blue stained sections revealed normal localisation of goblet cells in $Pten^{fl/fl}$ $Kras^{LSL/+}$ and control tissue compared to WT tissue (Figure 5.9). Scoring revealed that both $Pten^{fl/fl}$ $Kras^{LSL/+}$ tissue and control tissue had significantly lower numbers of goblet cells compared to WT tissue (p values = 0.0404, n≥3, Mann Whitney U test). However goblet cell number in $Pten^{fl/fl}$ $Kras^{LSL/+}$ tissue was not significantly altered from the controls (p values >0.05, n≥3, Mann Whitney U test).

Immunostaining for lysozyme revealed no alterations in the localisation of lysozyme positive paneth cells in experimental $Pten^{fl/fl}$ $Kras^{LSL/+}$ and control tissue compared to WT (Figure 5.10). Paneth cell scoring revealed, similarly to goblet cells, that both $Pten^{fl/fl}$ $Kras^{LSL/+}$ tissue and control tissue had significantly lower numbers of paneth cells compared to WT tissue (p values = 0.0404, n≥3, Mann Whitney U test), but paneth cell number in $Pten^{fl/fl}$ $Kras^{LSL/+}$ tissue was not significantly altered from the controls (p values >0.05, n≥3, Mann Whitney U test).

To visualise the enterocyte brush border, small intestinal tissue sections were prepared and stained for alkaline phosphatase using the Liquid Permanent red system. Alkaline phosphatase staining on $Pten^{fl/fl}$ $Kras^{LSL/+}$ tissue sections demarcated the luminal surface of enterocytes revealing the presence of mature enterocytes and that the polarisation of the epithelial sheet was comparable to control and WT tissue (Figure 5.11).

### 5.2.8 The intestinal phenotypes caused in $Pten^{fl/fl}$ $Kras^{LSL/+}$ mice are likely to be driven by hyperactivation of pAkt

As Kras has dual roles in controlling the activity of both the PI3K and MAPK pathways, IHC and western blotting was carried out to quantify the levels of downstream markers of the PI3K and MAPK pathway, pAkt (ser473) and pErk

(Thr202/Tyr204) respectively (Figure 5.12). The phosphorylated forms of these proteins represent the active state of the protein.

IHC for pAkt indicated that there was a subtle increase in staining intensity in Pten$^{fl/fl}$ Kras$^{LSL/+}$ tissue and Pten$^{fl/fl}$ control tissue compared to WT and the Kras$^{LSL/+}$ control (Figure 5.12, A). Western blot for pAkt confirmed that loss of Pten alone results in accumulation of pAkt, and this accumulation is enhanced when Pten loss is combined with Kras activation (Figure 5.12, B). However, IHC and western blot for pErk revealed normal localisation and abundance of the active form of the protein in experimental samples compared to control and WT samples (Figure 5.12). The accumulation of pAkt and therefore activation of the PI3K pathway is associated with no obvious phenotypes in Pten$^{fl/fl}$ mice apart from increased epithelial cell migration, whereas higher accumulation of pAkt and therefore hyperactivation of the PI3K pathway in Pten$^{fl/fl}$ Kras$^{LSL/+}$ mice is associated with overt changes to villus morphology and intestinal homeostasis as well as enhanced epithelial cell migration.
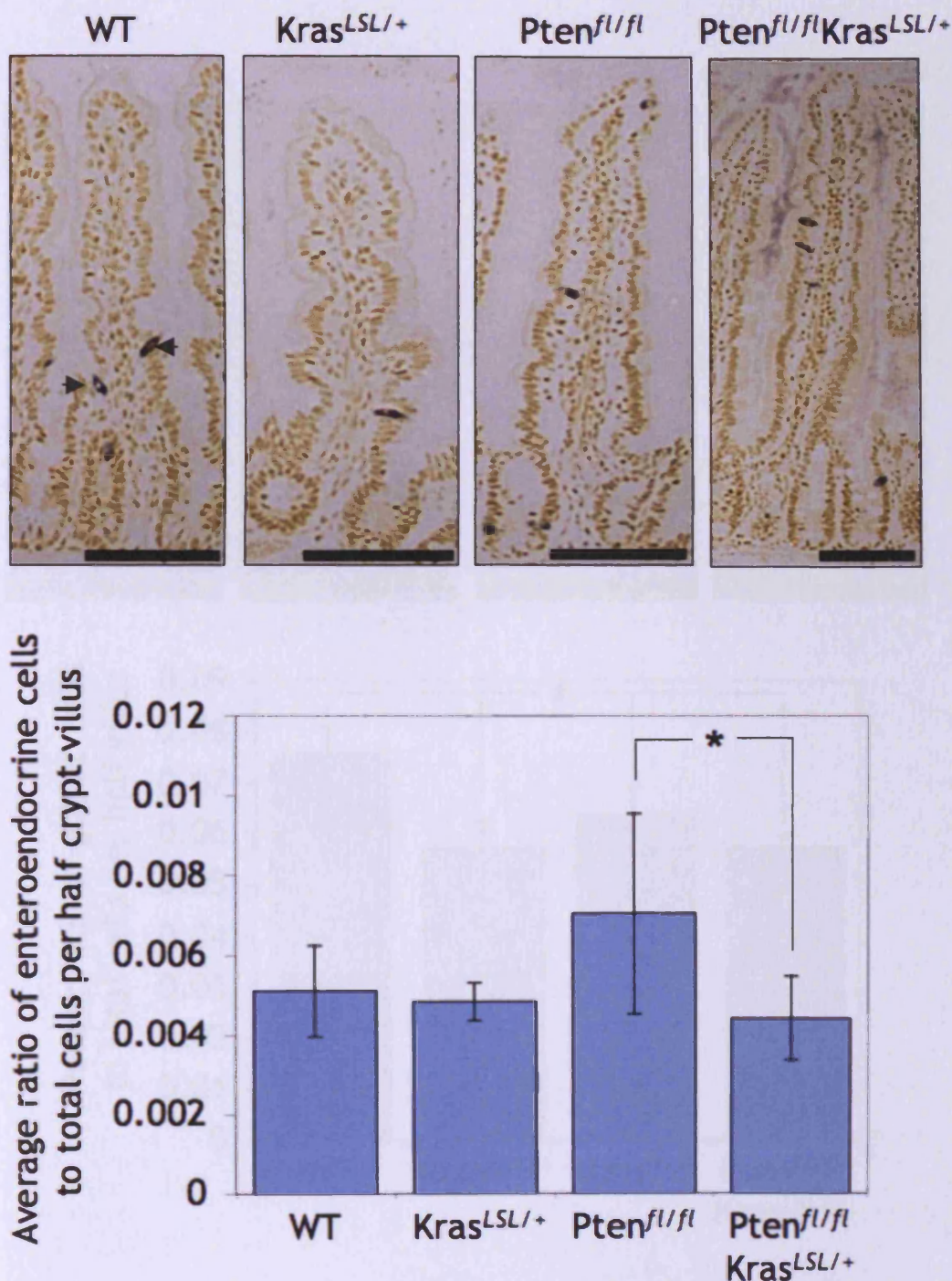
**Figure 5.8 Pten loss and Kras activation has no effect on enteroendocrine cell number**

Grimelius staining revealed normal localisation of enteroendocrine cells in each cohort. Arrows indicate enteroendocrine cells in WT tissue. Scale bars represent 200μm. Enteroendocrine cells were scored and normalised to account for changes in crypt-villus cell number. Scoring revealed that enteroendocrine cell number in $Pten^{fl/fl}$ $Kras^{LSL/+}$ tissue and the controls was not significantly altered from WT tissue (p values >0.05, n≥3, Mann-Whitney U test). $Pten^{fl/fl}$ tissue trended towards higher enteroendocrine cell number but was only significantly higher than $Pten^{fl/fl}$ $Kras^{LSL/+}$ tissue (*, p value = 0.0204, n≥3, Mann Whitney U test). Error bars indicate standard deviation.
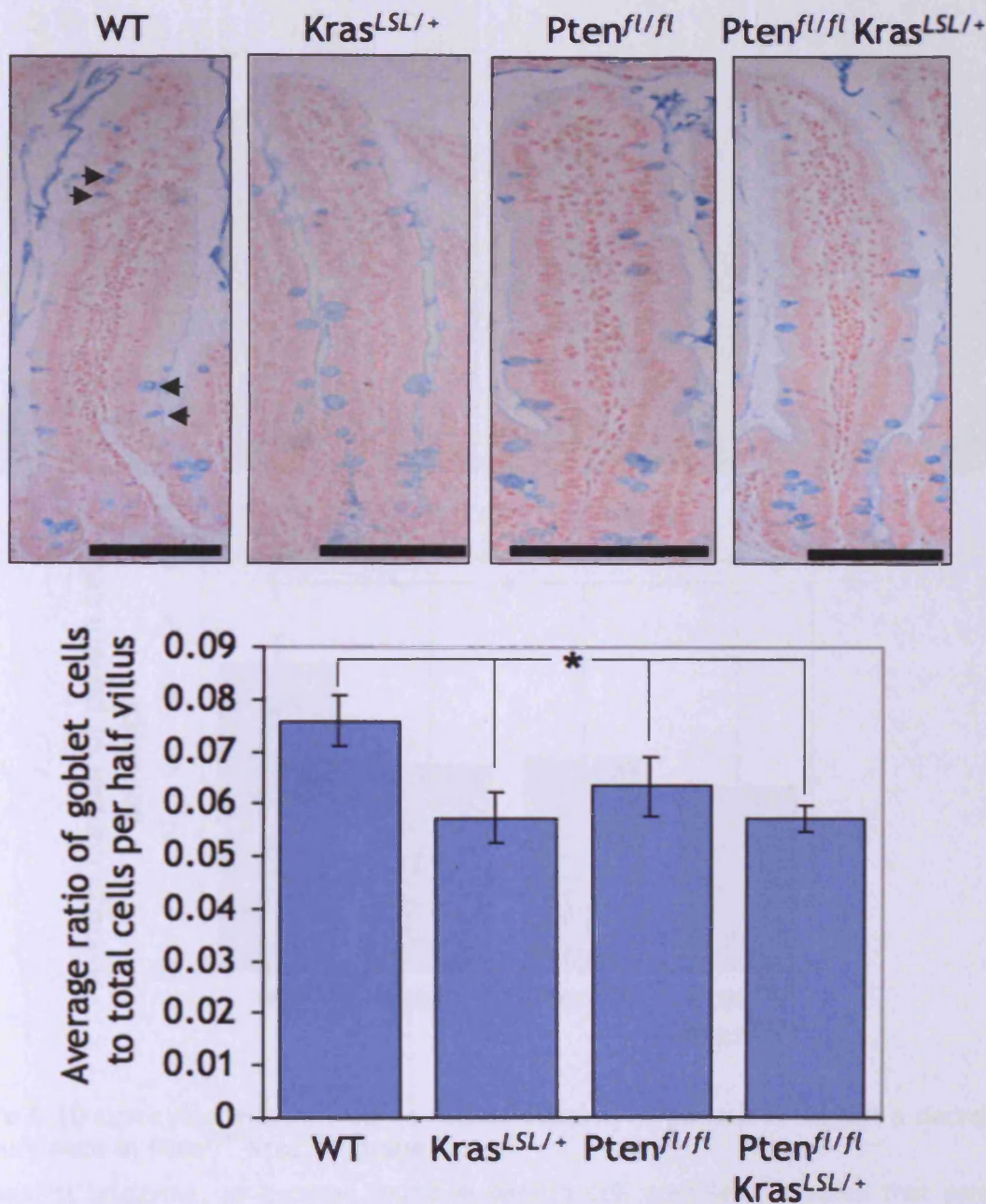
**Figure 5.9 Pten loss and Kras activation causes a reduction in goblet cell number**

Small intestinal sections were stained with alcian blue that stains the mucins present in goblet cells. Staining revealed no changes in localisation of the goblet cells. They were distributed normally throughout the crypt-villus. Arrows indicate goblet cells in WT tissue. Scale bars represent 200µm. Goblet cells were scored and normalised to account for changes in villus cell number. Scoring revealed that there was a significant reduction in Pten$^{fl/fl}$ Kras$^{LSL/+}$ tissue and control tissue compared to WT tissue (*, p values = 0.0404, n≥3, Mann Whitney U test). Experimental and control scores were not significantly altered from each other. Error bars indicate standard deviation.
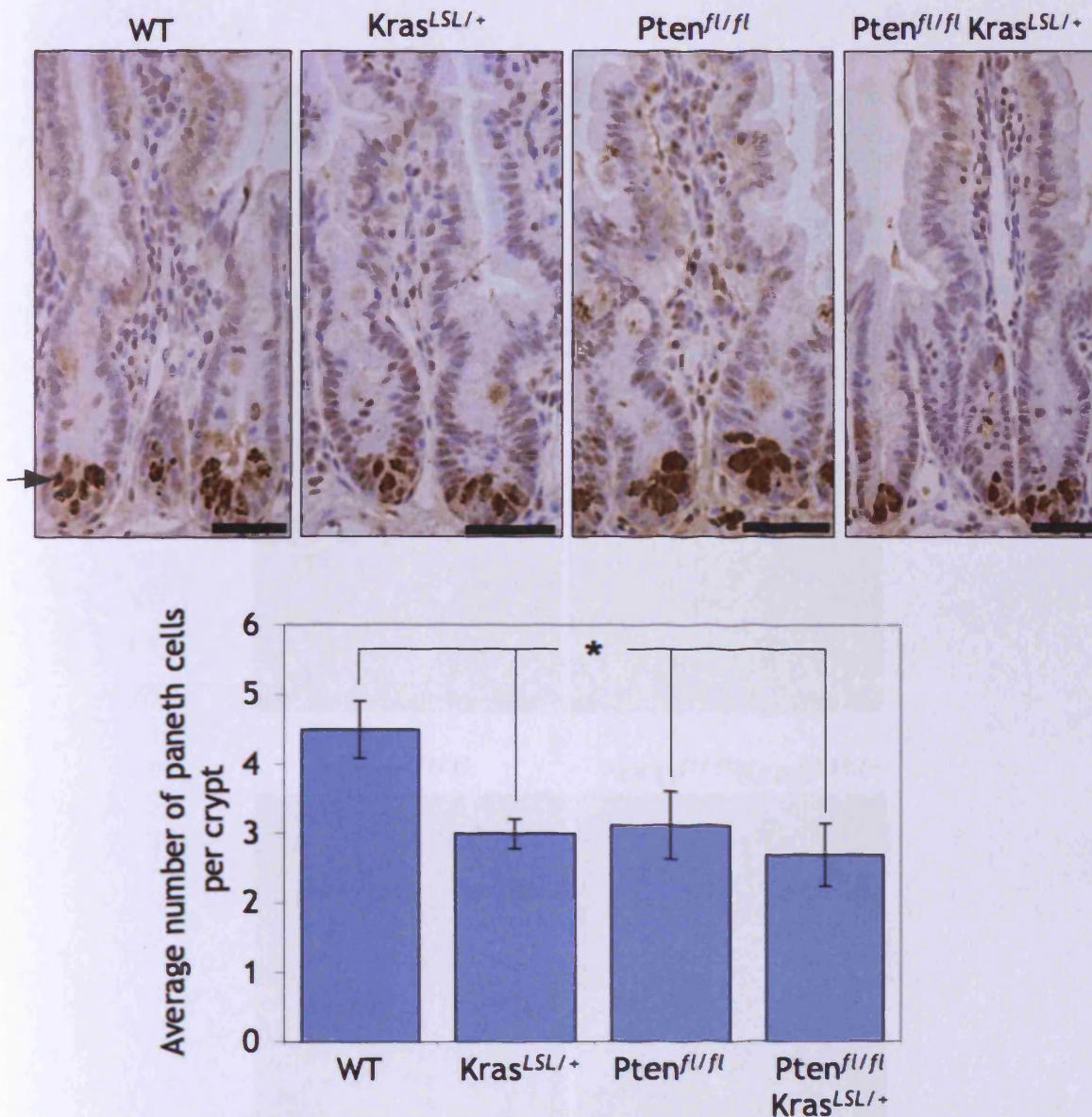
**Figure 5.10 Lysozyme IHC showed no mislocalisation of paneth cells, but a decrease in abundance in Pten$^{fl/fl}$ Kras$^{LSL/+}$ tissue**

IHC against lysozyme, an enzyme found in paneth cell granules, revealed that paneth cells remained localised to the base of the crypt in Pten$^{fl/fl}$ Kras$^{LSL/+}$ and control tissue compared to WT (arrow shows normal position of a lysozyme stained paneth cell). Scale bars represent 100μm. Paneth cell scoring revealed a significantly lower abundance of paneth cells in Pten$^{fl/fl}$ Kras$^{LSL/+}$ tissue and control tissue compared to WT (*, p values = 0.0404, n≥3, Mann Whitney U test). Error bars indicate standard deviation.

**WT**    **Kras$^{LSL/+}$**

**Pten$^{fl/fl}$**    **Pten$^{fl/fl}$Kras$^{LSL/+}$**
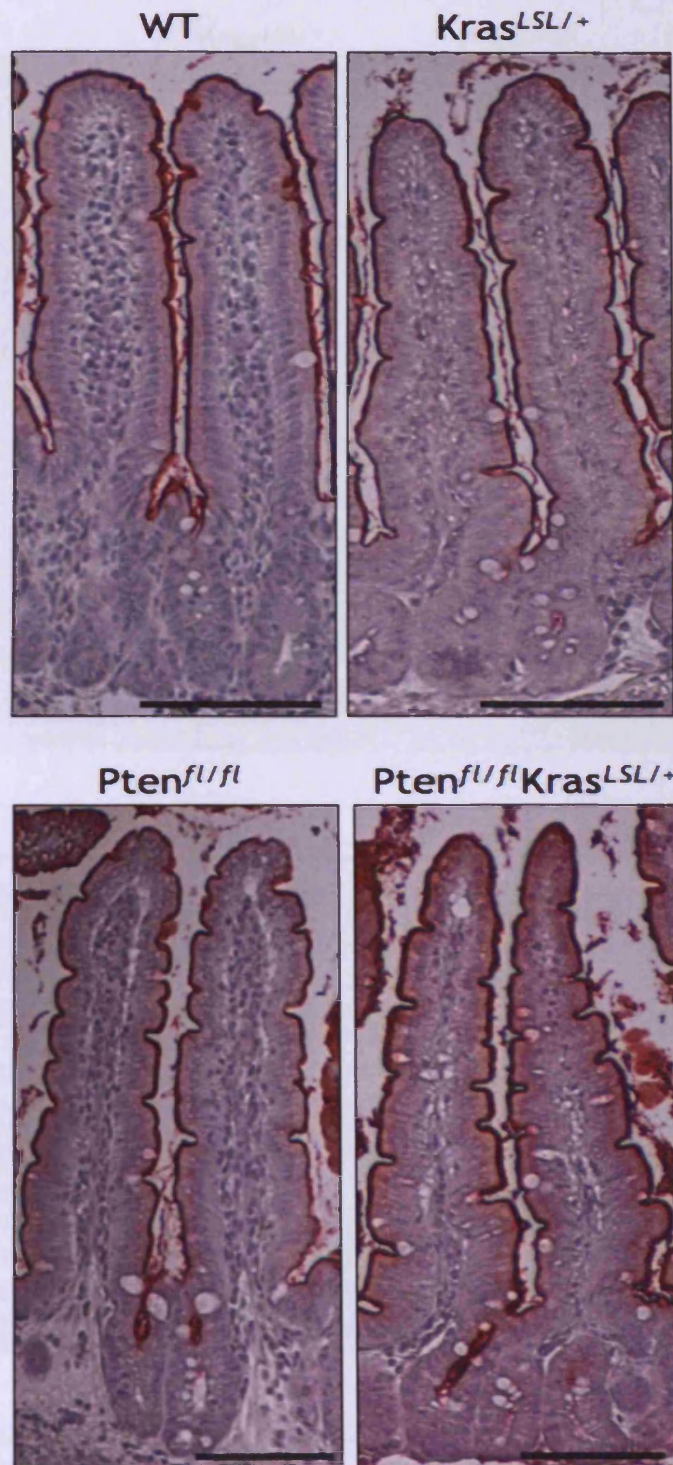
**Figure 5.11 Alkaline phosphatase staining revealed no apparent changes enterocyte maturation**

Alkaline phosphatase staining revealed no changes in the localisation of staining, expression was maintained on the luminal surface of the enterocytes in Pten$^{fl/fl}$ Kras$^{LSL/+}$ and controls compared to WT tissue. Therefore indicating enterocytes were differentiating normally. Scale bars represent 100µm.
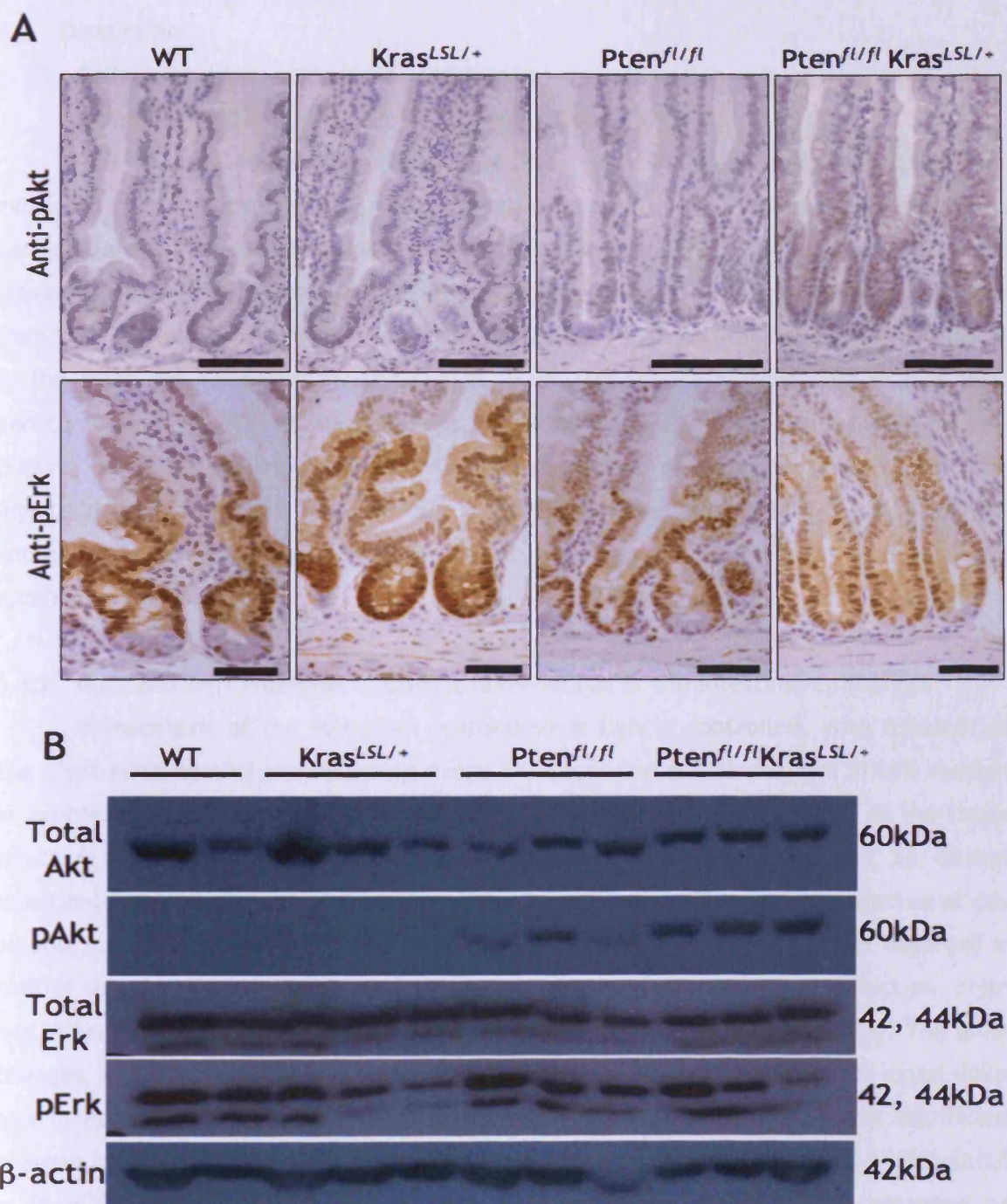
**Figure 5.12 IHC and western blot for pAkt confirmed activation of PI3K pathway in Pten*fl/fl* Kras*LSL/+* intestinal tissue**

(A) IHC against pAkt (ser473) revealed accumulation of pAkt in Pten*fl/fl* Kras*LSL/+* and to a lesser extent Pten*fl/fl* tissue compared to WT and Kras*LSL/+* tissue. Scale bars represent 100μm. IHC against pErk (Thr202/Tyr204) revealed no overt differences between experimental and control tissues. Scale bars represent 50μm. (B) Western blot for pAkt (ser473) confirmed the presence of pAkt in Pten*fl/fl* Kras*LSL/+* and Pten*fl/fl* tissue. Hyperactivation of pAkt was evident in Pten*fl/fl* Kras*LSL/+* samples compared to the Pten*fl/fl* control samples. Western blot confirmed that pErk (Thr202/Tyr204) levels were no higher than WT in experimental samples.

## 5.3 Discussion

### 5.3.1 Cells that have undergone conditional recombination are maintained in the intestinal epithelium at day 50 post induction

PCR for the recombined alleles of Pten and Kras was carried out on DNA extracted from intestinal epithelial cell samples to confirm that the intestinal stem cells had undergone cre mediated DNA recombination, and the recombined stem cells were retained in the small intestinal epithelium at day 50 post induction. Unpublished data from the Clarke lab has shown that some mutations, such as Stat3 and Brg1, are lethal to the stem cell following recombination, with subsequent replacement with a 'WT' unrecombined cell. PCR products for the Pten and Kras recombined alleles were present (Figure 5.1), confirming that $VillinCreER^T$ mediated recombination occurs in the intestinal stem cell, that the stem cell is able to survive concomitant deletion of Pten and activation of Kras, and is further able to populate the entire crypt-villus axis with recombined cells.

### 5.3.2 Pten and Kras synergise to disrupt homeostasis of the intestinal epithelium

Homeostasis of the intestinal epithelium is tightly controlled, with turnover of the crypt-villus epithelium occurring every 2-3 days, and subtle changes in cell number or proliferation can have a significant effect on the overall maintenance of the tissue structure. Pten loss and Kras activation appears to synergistically act to disrupt intestinal homeostasis, as evidenced by villus branching or bifurcations, observed at day 50 post induction (Figure 5.2). The increases in crypt and villus cell number observed in control tissue at day 15 post induction are not observed at day 50 post induction, crypt and villus hyperplasia is only observed in $Pten^{fl/fl} Kras^{LSL/+}$ tissue (Figure 5.3). The gross changes in villus morphology and increase in abundance of cells along the crypt-villus axis in $Pten^{fl/fl} Kras^{LSL/+}$ mice at day 50 confirm that the more subtle, yet significant changes in crypt-villus cell number (hinting at early alterations in intestinal homeostasis) in $Pten^{fl/fl} Kras^{LSL/+}$ mice at day 15 post induction were unable to be controlled by compensatory mechanisms at later time points, but homeostasis was able to be restored in the control mice.

Villus branching has previously been observed in mouse models of intestinal specific inhibition of Hedgehog signalling. These branches appear to be driven by proliferating cells along the crypt-villus axis that form ectopic crypts (Madison et al., 2005). The villus bifurcations or 'branches' observed in the $Pten^{fl/fl} Kras^{LSL/+}$ small intestine, are not the result of ectopic crypt formation, as proliferation is confined to the crypt (as assessed by BrdU incorporation Figure 5.5). Branching therefore may be the

result of an 'overflow mechanism' to compensate for the large increases in cell number along the crypt-villus axis (Figure 5.3). One could hypothesise that normal migration and sloughing off of cells from the tip of the villus is no longer able to balance out the increasing number of cells being generated through increased proliferation, and so therefore the crypt and villus become elongated. Once these extended villi have reached a point where it was logistically impossible to extend further in length, due to restriction of lumen width, the cells then exude from the central villus structure and form branches to alleviate the build up of cells migrating from the crypt. This, as suggested in chapter 3, may be a result of decreased apoptosis at the villus tip. Apoptosis of cells at the villus tip is thought to account for the majority of cell loss from the villus and regulation of cell number (Hall et al., 1994). A decrease in apoptosis may be caused by the increased activation of the PI3K pathway, confirmed by increased abundance of pAkt in $Pten^{fl/fl}$ $Kras^{LSL/+}$ mice (Figure 5.12). Upregulation of pAkt, and therefore PI3K signalling, has been shown to be associated with a decrease in apoptosis in colorectal cancer cell lines (Itoh et al., 2002). Apoptosis scoring has only been carried out in the crypts in this study; no significant changes in the level of apoptosis were observed in $Pten^{fl/fl}$ $Kras^{LSL/+}$ mice (Figure 5.4). However, apoptosis levels are low in tissues that have not undergone cellular damage, so therefore it may be difficult to observe a decrease in apoptosis.

Alterations in crypt and villus cell number in $Pten^{fl/fl}$ $Kras^{LSL/+}$ small intestine is also accompanied by a decrease in goblet and paneth cell number (Figure 5.9, Figure 5.10), suggesting that concurrent Pten loss and Kras activation negatively impacts on differentiation of these two cell types, resulting in their lower abundance. This effect was also observed in both $Kras^{LSL/+}$ and $Pten^{fl/fl}$ control tissue, but this decrease was not compounded in $Pten^{fl/fl}$ $Kras^{LSL/+}$ tissue suggesting that the two mutations do not synergise in the context of differentiation. As previously mentioned in chapter 3, activation of the PI3K pathway may be responsible for alterations in differentiated cell types, as mTOR (a downstream target of pAkt) plays a role in activation of Notch signalling which is responsible for the differentiation of secretory cell types (Ma et al., 2010). Some of these findings are in contrast to the findings in $Pten^{fl/fl}$ $Kras^{LSL/+}$ mice sacrificed at day 15 post induction. There were no changes in the number of enteroendocrine cells present in the small intestine at day 50, as was observed at day 15 post induction, and at day 50 post induction $Pten^{fl/fl}$ $Kras^{LSL/+}$ mice have significantly lower numbers of goblet cells than WT tissue, which was not observed at day 15 post induction. It is unclear why some of the early phenotypes appear to have been

circumvented at later timepoints, however it is clear that mutations in both Pten and Kras negatively affect intestinal secretory cell differentiation.

### 5.3.3 Pten loss and Kras activation does not cause expansion of the stem cell compartment

Loss of Pten in the murine small intestine has been associated with an expansion in stem cell number (He et al., 2007). Increases in crypt cell number and proliferation along with expansion of the proliferative zone in Pten$^{fl/fl}$ Kras$^{LSL/+}$ mice (Figure 5.3, Figure 5.5 and Figure 5.6, A), led to the hypothesis that the phenotypes observed in Pten$^{fl/fl}$ Kras$^{LSL/+}$ mice may be the result of an increase in stem cell number. Expression levels of intestinal CBC stem cell markers Lgr5 and Ascl2 were unchanged in Pten$^{fl/fl}$ Kras$^{LSL/+}$ tissue compared to control and WT tissue (Figure 5.7). The observed increases in crypt length and proliferation may therefore be attributed to an increase in transit amplifying progenitor cells. Pten loss and Kras activation must therefore be enhancing the activity of the stem cell or progenitor cell compartment driving proliferation, resulting in an increase in progenitor cells. Increased proliferation observed in Pten$^{fl/fl}$ Kras$^{LSL/+}$ mice, correlated with increased activation of the PI3K pathway (as indicated by accumulation of pAkt, Figure 5.12). Wnt pathway activation controls small intestinal proliferation and loss of Pten has previously been shown to drive activation of the Wnt pathway by inactivation of GSK-3β, through PI3K pathway activation (Persad et al., 2001). Therefore, it could be possible that Wnt pathway activation may be responsible for increased proliferation in these mice. However, the CBC stem cell markers Lgr5 and Ascl2 are also Wnt pathway transcriptional targets, so therefore expression of these genes would be upregulated if the Wnt pathway was being activated in these mice. It is therefore more likely that proliferation is driven by phosphorylation of downstream targets of Akt resulting in increased proliferation. Such targets include phosphorylation and inactivation of GSK-3β that normally results in degradation of the cell cycle promoter, cyclin D1 (Diehl et al., 1998), and phosphorylation of cell cycle inhibitor p21$^{Cip}$ (Li et al., 2002).

Synergy between Pten and Kras mutations through upregulation of proliferation has previously been noted in a mouse model of pancreatic specific Pten loss and Kras activation. The two mutations were shown to synergise in metaplastic tissue and tumours to result in higher numbers of proliferating cells, compared to metaplasia and tumours that arises in mice with Kras activation alone (Hill et al., 2010). This study also observed accumulation of pAkt and other active downstream targets of the PI3K

pathway in tumours but not metaplastic tissue that possess both Pten and Kras mutations (Hill et al., 2010).

### 5.3.4 Concomitant Pten loss and Kras activation causes hyperactivation of Akt

Synergy between Pten and Kras appears to manifest through activation of the PI3K pathway, which may be driving the observed phenotypes. IHC for pAkt indicated that there was a subtle increase in staining intensity in $Pten^{fl/fl}$ $Kras^{LSL/+}$ intestine compared controls and WT (Figure 5.12, A). Western blot for pAkt revealed that loss of Pten alone results in accumulation of pAkt and this accumulation is enhanced when Pten loss is combined with Kras activation (Figure 5.12, B). Loss of Pten results in a subtle migratory phenotype that is accompanied by low levels of pAkt accumulation (Figure 5.12, B). Loss of Pten together with activation of Kras results in a range of phenotypes including villus bifurcation, increased proliferation a much more severe migratory phenotype. Taken together these data suggest that varying levels of pAkt, and hence PI3K pathway stimulation, directly correlates with phenotype severity. These findings provide evidence that activation of the PI3K pathway in the intestine is not binary, and simply 'switching-on' the pathway by Pten deletion is not sufficient to affect intestinal homeostasis. Only when the pathway is hyperactivated, by additional activation of Kras in concert with Pten deletion, is evidence of disrupted homeostasis observed. The finding that elevated levels of pAkt are associated with hyperplasia, enhanced proliferation and increased migratory rate of intestinal epithelial cells in the mouse small intestine is consistent with other studies that show PI3K signalling plays a role in intestinal cell migration *in vitro* (Dise et al., 2008), and promotes proliferation *in vivo* (Sheng et al., 2003).

Synergy between Pten loss and Kras activation through PI3K has been shown in some tumour models. Hill et al showed that Pten and Kras mutations synergised through the PI3K pathway and to a lesser extent MAPK/Erk pathways to promote pancreatic tumourigenesis (Hill et al., 2010). A study by Miller et al showed that Pten and Kras mutations synergise through the PI3K pathway to promote thyroid tumourigenesis. Inhibition of the PI3K pathway conferred a survival advantage on these mice. However, unlike the findings I observed in this chapter, Miller et al also demonstrated that activation of the PI3K pathway was necessary for activation of the MAPK/Erk pathway in the thyroid model, and inhibition of the PI3K pathway also resulted in inhibition of the MAPK pathway (Miller et al., 2009).

### 5.4 Summary

Pten loss and Kras activation acts synergistically to disrupt intestinal homeostasis at day 50 post induction. Hyperproliferation of the crypt and villus is observed, along with enhanced migration and the formation of villus bifurcations. The phenotypes observed at this time point are accompanied by hyperactivation of Akt. Activation of Akt is likely to be driving these phenotypes, as the PI3K pathway promotes proliferation by inhibition of a number of cell cycle regulators, and promotes migration.

### 5.5 Further Work

I have proposed that hyperactivation of pAkt and hence, PI3K pathway activation, drives the phenotypes observed in $Pten^{fl/fl}$ $Kras^{LSL/+}$ mice. To mechanistically prove this, it would be useful to treat $Pten^{fl/fl}$ $Kras^{LSL/+}$ mice with a PI3K inhibitor at day 50 post induction for a fixed period of time, for example 2 weeks, to see if the changes observed in cell proliferation and migration are restored to WT levels and villus bifurcations are lost. To also prove that a decrease in apoptosis at the villus tip is driving villus bifurcation, it would be insightful to score the level of apoptosis observed at the villus tip via H&E scoring and caspase 3 scoring.

$Pten^{fl/fl}$ $Kras^{LSL/+}$ mice maintained good health throughout the duration of this experiment, despite major changes in mucosal architecture of the small intestine. In light of this, further to this day 50 time point a number of $Pten^{fl/fl}$ $Kras^{LSL/+}$ mice were induced and aged to assess synergy between the genes in the long term. The results from this experiment are discussed in chapter 6.

# Chapter 6: Investigating the long term effects of Pten loss and Kras activation on the intestinal epithelium

## 6.1 Introduction

Previously the Clarke lab and others have shown that Pten loss alone does not cause tumour formation, despite mutation of Pten underlying a number of familial intestinal tumour syndromes (Marsh et al., 2008, Langlois et al., 2009). Similarly, the Clarke lab and others have shown that activation of oncogenic Kras does not result in tumour formation in the intestine (Haigis et al., 2008, Sansom et al., 2006). These studies also showed that, in the context of Wnt initiated tumours, addition of Kras and Pten alone both promote initiation and progression of Wnt activated tumours. Data in chapter 4 provided evidence of synergy between Pten and Kras in the context of a Wnt initiated tumour model (*Villin*CreER$^T$-Apc$^{fl/+}$ Pten$^{fl/fl}$ Kras$^{LSL/+}$ mice). Pten loss and Kras activation together promotes both initiation of tumours, and progression of adenomas through to adenocarcinoma.

Despite Pten and Kras impinging on the same pathway, a number of mouse models have shown synergy between mutations in the two genes. This synergy was evidenced by increased tumourigenecity and tumour progression in the endometrium, lung, thyroid and pancreas (Miller et al., 2009, Dinulescu et al., 2005, Iwanaga et al., 2008, Hill et al., 2010). Unpublished data from the Clarke lab has also demonstrated synergy between Pten and Kras mutations, in both the gall bladder and stomach, giving rise to cholangio carcinoma and forestomach hyperplasia respectively. I have shown evidence in chapters 3 and 5 that Pten loss and Kras activation, without an Apc mutation, has a synergistic effect on the small intestine, resulting in disrupted homeostasis in the short term (day 15 and 50 post induction). Disrupted homeostasis observed in *Villin*CreER$^T$-Pten$^{fl/fl}$ Kras$^{LSL/+}$ mice was evidenced by hyperplasia at day 15 post induction, and the formation of villus bifurcations at day 50 post induction. The observation that Pten loss and Kras activation causes disruption of intestinal homeostasis and the formation of epithelial aberrations at short time points after induction, leads to the hypothesis that these mutations together may give rise to intestinal neoplasms in the long term. To address this question, in this chapter I will investigate the effect of long term Pten loss and Kras activation in the murine small intestine.

*Villin*CreER$^T$-Pten$^{fl/fl}$ Kras$^{LSL/+}$ (hereafter referred to as Pten$^{fl/fl}$ Kras$^{LSL/+}$) mice and the appropriate controls (*Villin*CreER$^T$-Pten$^{fl/fl}$ Kras$^{+/+}$ [hereafter referred to as Pten$^{fl/fl}$], *Villin*CreER$^T$-Pten$^{+/+}$ Kras$^{LSL/+}$ [hereafter referred to as Kras$^{LSL/+}$] and *Villin*CreER$^T$-Pten$^{+/+}$

Kras$^{+/+}$ [hereafter referred to as WT]), were induced at 6-12 weeks of age and sacrificed when they became symptomatic of disease.

## 6.2 Results

### 6.2.1 Intestinal Pten loss and Kras activation together significantly reduces mouse life span

Pten$^{fl/fl}$ Kras$^{LSL/+}$ mice had a significantly shortened lifespan (median survival 280 days) compared to control and WT mice, most of which were sacrificed at day 550 post induction, the experimental endpoint (Figure 6.1, A). A number of the control mice had to be sacrificed before the experimental endpoint, mainly due to the development of lymphoma, which is reasonably common in ageing mice. Further to this, one Kras$^{LSL/+}$ mouse had developed ill health as a consequence of intussusception. Pten$^{fl/fl}$ Kras$^{LSL/+}$ mice were sacrificed either because of colonic ischemia and resultant colon blockage, or because of tumour burden.

When Pten$^{fl/fl}$ Kras$^{LSL/+}$ mice were dissected it was noted that 25% (9/36) of the mice appeared to have a large blockage of compacted faeces and blood in the colon (Figure 6.1, B). This blockage was always found in mice that also had evidence of intussusception (where the intestine has inverted or 'turned-in on itself'), either at the ileal-caecal or the colonic-caecal junction. It would appear that the intussusception was restricting the blood supply of the colon and causing ischemia, resulting in colonic blockage. The cause of the intussusception was likely to be linked to the hyperproliferation of the epithelium, i.e. rapid proliferation forces the supporting stroma upwards and could potentially pull the smooth muscle up with it, causing intussusception. Mice with intussusception had a median survival time of 160 days post induction. Some of these mice also possessed benign sessile serrated adenomas (see below) but none had evidence of carcinoma.

The remaining 75% (27/36) of the Pten$^{fl/fl}$ Kras$^{LSL/+}$ cohort had a median survival time of 344 days post induction and were sacrificed due to tumour burden. A number of small intestinal tumours at differing stages were observed in the remaining cohort of Pten$^{fl/fl}$ Kras$^{LSL/+}$ mice: 30% (8/27) of the mice possessed hyperplastic polyps, 78% (21/27) of the possessed benign sessile serrated adenomas, 44% (12/27) had adenocarcinoma and a further 41% (11/27) had metastatic carcinoma (Figure 6.1, C). Intestinal tumours were not observed in WT or Kras$^{LSL/+}$ mice. However some Pten$^{fl/fl}$ mice possessed benign tumours. It is of note that villus bifurcations are still frequently observed in aged Pten$^{fl/fl}$ Kras$^{LSL/+}$ mice, indicating that once the structures are formed they are unable to be reversed in a Pten negative Kras activated setting.
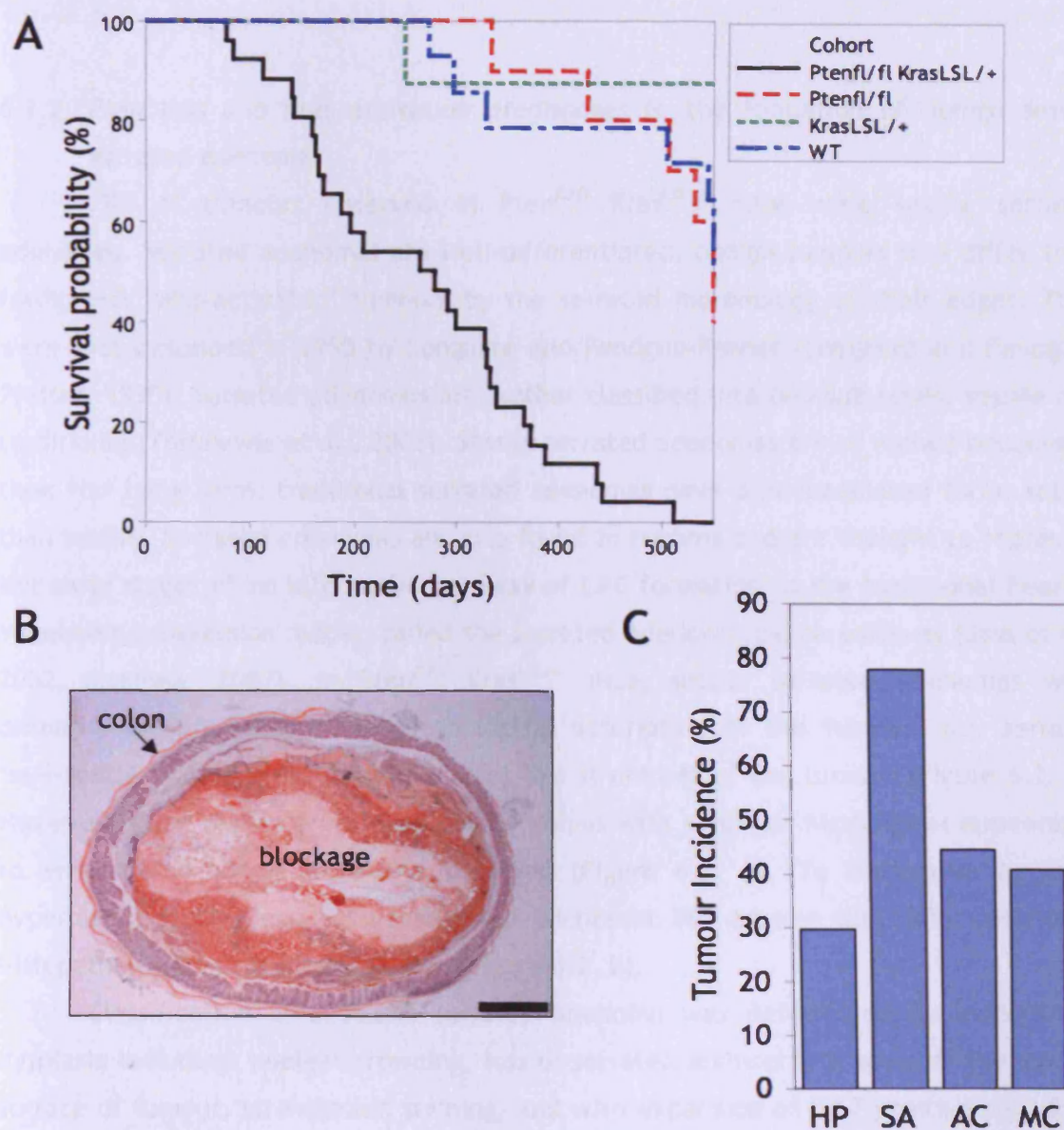
**Figure 6.1 Pten$^{fl/fl}$ Kras$^{LSL/+}$ mice have a significantly shorter lifespan compared to controls due to colonic ischemia and tumour burden**

(A) Survival plot of Pten$^{fl/fl}$ Kras$^{LSL/+}$ mice and controls, Pten$^{fl/fl}$ Kras$^{LSL/+}$ mice have a significantly shorter lifespan compared to control and WT mice (p values <0.001, both Log-Rank and Wilcoxon test). The ageing experiment was conducted until 550 days post induction. (B) 25% of the Pten$^{fl/fl}$ Kras$^{LSL/+}$ ageing cohort were found to have a large blockage in the colon caused by restriction of the colonic blood supply (colonic ischemia), which was in turn caused by intussusception of the intestine at the ileal-caecal or the colonic-caecal junction. Scale bar represents 1000μm. (C) A spectrum of intestinal tumour types was observed in the remaining Pten$^{fl/fl}$ Kras$^{LSL/+}$ ageing cohort. The incidence of these tumour types was as follows: 30% - hyperplastic polyps (HP), 78% - sessile serrated adenomas (SA), 44% - adenocarcinomas (AC) and 41% - metastatic carcinoma (MC).

## 6.2.2 Pten loss and Kras activation predisposes to the formation of benign sessile serrated adenomas

78% of tumours observed in $Pten^{fl/fl}$ $Kras^{LSL/+}$ mice were sessile serrated adenomas. Serrated adenomas are well-differentiated, benign tumours that differ from traditional 'Wnt-activated' tumours by the serrated morphology of their edges. They were first described in 1990 by Longacre and Fenoglio-Preiser (Longacre and Fenoglio-Preiser, 1990). Serrated adenomas are further classified into two sub-types: sessile and traditional (Torlakovic et al., 2003). Sessile serrated adenomas are so named because of their flat lying form, traditional serrated adenomas have a pedunculated form, rather than sessile. Serrated adenomas are also found in humans and are thought to represent the early stages of an alternative pathway of CRC formation to the traditional Fearon-Vogelstein progression model, called the Serrated Adenocarcinoma pathway (Jass et al., 2002, Makinen, 2007). In $Pten^{fl/fl}$ $Kras^{LSL/+}$ mice, sessile serrated adenomas were primarily distinguished by histopathological description of the tumour, i.e. serrated 'saw-tooth' like appearance of the crypt-like structures of the tumour (Figure 6.2, A). However, some earlier stage hyperplastic polyps with a similar histological appearance to serrated adenomas were also observed (Figure 6.2, A). To distinguish between hyperplastic polyps and sessile serrated adenomas IHC against Ki67 and descriptive histopathological criteria were used[1] (Figure 6.2, B).

Classification of a sessile serrated adenoma was determined by evidence of dysplasia including: nuclear crowding, loss of serrated architecture towards the luminal surface of tumour, strong eosin staining, and with expansion of Ki67 positive cells from the crypt towards the periphery of the tumour (Figure 6.2). Conversely hyperplastic polyps showed no evidence of dysplasia, and Ki67 positive cells were confined to the crypts at the base of the tumour.

Interestingly, sessile serrated adenomas were observed in 40% (4/10) of the $Pten^{fl/fl}$ control mice that had survived over 500 days post induction. This suggests that long term loss of Pten alone, can lead to tumour formation in the mouse. Addition of a Kras activating mutation synergises with Pten loss to accelerate formation of sessile serrated adenomas, as they are observed in $Pten^{fl/fl}$ $Kras^{LSL/+}$ mice at a higher incidence

---

[1] Histopathological description of the tumours observed was provided by Prof. Geraint Williams, Heath Park Campus, Cardiff University, Cardiff

than in Pten$^{fl/fl}$ mice and at earlier times post induction. Sessile serrated adenomas were observed as early at 113 days post induction in Pten$^{fl/fl}$ Kras$^{LSL/+}$ mice.

### 6.2.3 Sessile serrated adenomas arise independently of Wnt signalling

As Pten and Kras both impinge on the PI3K pathway, and Kras also activates the MAPK pathway, IHC for markers of PI3K activation, phospho-Akt(ser473) (pAkt) and MAPK pathway activation, phospho-p44/42 MAPK(Thr202/Tyr204) (pErk) and phospho-MEK1/2(Ser221) (pMEK) was carried out on tumour sections and adjacent normal intestinal tissue. Sessile serrated adenomas stained strongly for pErk, pMEK and pAkt compared to the adjacent normal tissue, indicating activation of the MAPK and PI3K pathways in the tumour (Figure 6.3).

Activation of the Wnt pathway (by mutation of Apc for example) is commonly regarded to be the initiating mutation of all intestinal tumours according to the Fearon-Vogelstein step-wise model of CRC progression. Serrated adenomas are thought to arise from either BRAF or KRAS mutations in humans, hence IHC for the surrogate marker of Wnt activation, β-catenin, was carried out to determine its cellular localisation. Staining revealed basolateral localisation of β-catenin confirming that the canonical Wnt pathway was not being activated in these tumours, and therefore these tumours were forming independently of mutations in the Wnt pathway (Figure 6.3).

### 6.2.4 Pten loss and Kras activation results in a number of intestinal phenotypes

Within the Pten$^{fl/fl}$ Kras$^{LSL/+}$ cohort there was a 44% incidence of intestinal adenocarcinoma with smooth muscle invasion, and a 41% incidence of metastatic carcinoma of the small intestine (Figure 6.1, C). These advanced tumours were frequently found in addition to, and alongside, benign sessile serrated adenomas. They also possessed serrated features (i.e. saw-tooth like morphology of the epithelial component of the tumour), despite overall changes in tumour morphology compared to sessile serrated adenomas (Figure 6.4). This evidence of serration in adenocarcinoma, carcinoma and metastases leads to the hypothesis that the sessile serrated adenomas are precursor lesions that progress into carcinomas. Evidence of the range of benign through to metastatic tumours found in Pten$^{fl/fl}$ Kras$^{LSL/+}$ mice is shown in Figure 6.5, with the most compelling piece of evidence in support of progression from sessile serrated adenoma, being a sessile serrated adenoma with areas of the tumour invading into the submucosa - potentially representing the step from benign to invasive tumour. The Pten$^{fl/fl}$ Kras$^{LSL/+}$ mouse model therefore represents a model of the serrated adenocarcinoma pathway.
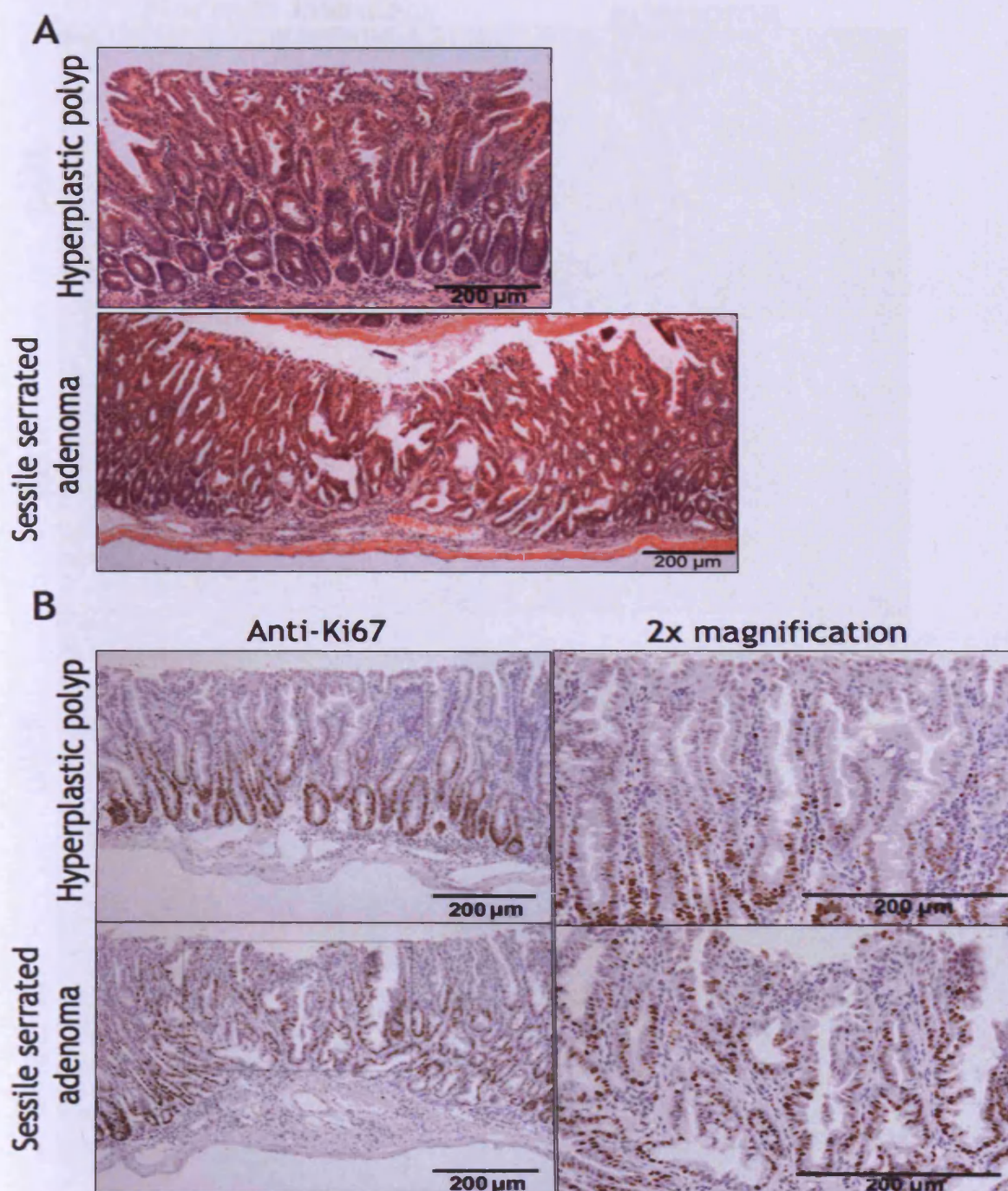
**Figure 6.2 Pten^{fl/fl} Kras^{LSL/+} mice were predisposed to sessile serrated adenomas**

(A) Benign hyperplastic polyps and sessile serrated adenomas were observed in Pten^{fl/fl} Kras^{LSL/+} mice. Both had a 'sawtooth-like' serrated appearance to the crypts. Sessile serrated adenomas could be distinguished from hyperplastic polyps by evidence of strong eosin staining, and dysplasia such as nuclear overcrowding. (B) IHC against Ki67 helped to further distinguish between hyperplastic polyps and sessile serrated adenomas. Immunostaining remained confined to crypts in hyperplastic polyps, but was found throughout the sessile serrated adenoma and towards the luminal surface of the tumour. Scale bars represent 200μm.
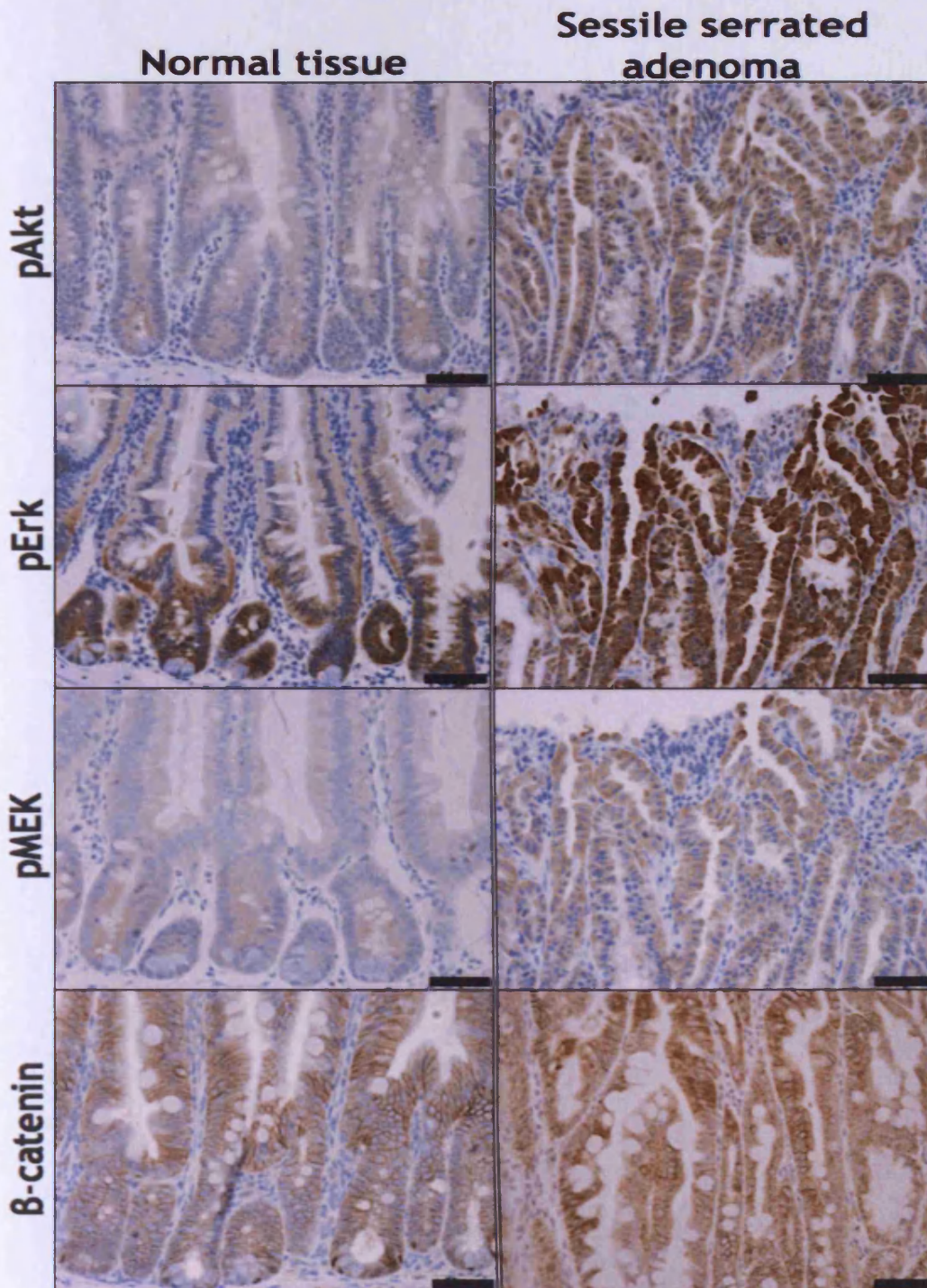
**Figure 6.3 IHC staining revealed that sessile serrated adenomas arise independently of Wnt activation and have evidence of PI3K and MAPK pathway activation**

IHC staining against the phosphorylated forms of Akt (phospho-Akt ser473), Erk (phospho-p44/42 MAPK, Thr202/Tyr204) and MEK (phospho-MEK1/2, Ser221) revealed stronger staining in sessile serrated adenomas compared to the adjacent tissue. IHC staining against β-catenin revealed basolateral localisation of the protein, indicating that the Wnt pathway was not being activated in these tumours. Scale bars represent 100μm.
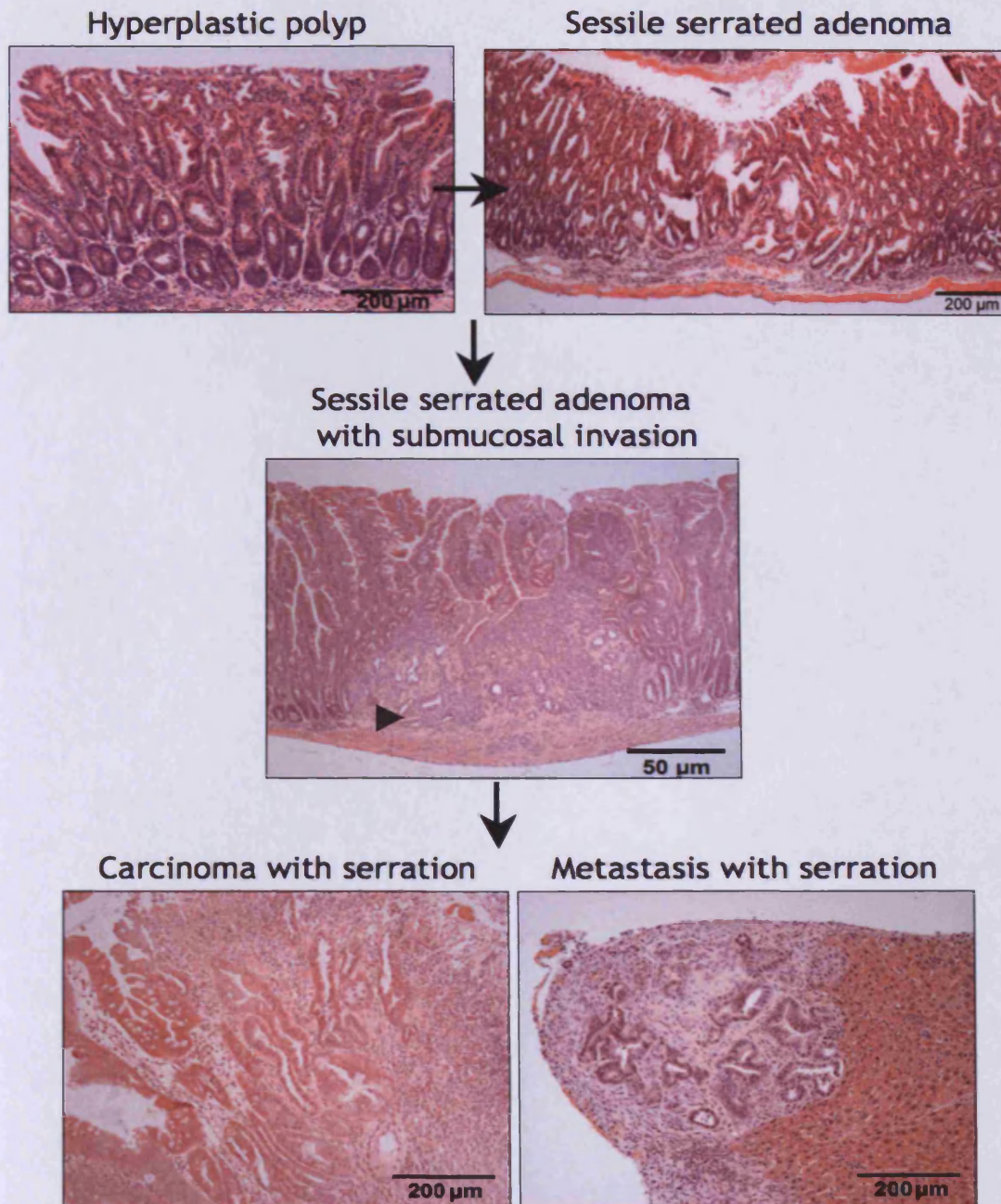
**Figure 6.4 Progression of hyperplastic polyp to metastatic carcinoma**

Pten$^{fl/fl}$ Kras$^{LSL/+}$ mice developed a spectrum of tumours at different stages of tumour progression, from hyperplastic polyp to metastatic carcinoma. However, all these tumours possessed 'serrated-morphology' of the epithelial component, suggesting that the sessile serrated adenomas observed in these mice are the precursor lesions that develop into metastatic carcinoma. The likely pathway of progression from benign serrated adenoma to metastatic carcinoma is depicted here. (Arrow head shows the region of a sessile serrated adenoma that is beginning to invade into the submucosa and become more aggressive). Scale bars represent 200µm and 50µm.

## 6.2.5 Carcinomas in Pten$^{fl/fl}$ Kras$^{LSL/+}$ mice frequently metastasise to the liver

41% of Pten$^{fl/fl}$ Kras$^{LSL/+}$ mice developed metastatic carcinoma. The primary tumour shown in Figure 6.5 is a typical large carcinoma observed in these mice. There was a large stromal component to all carcinomas, making up the bulk of the tumour, and the epithelial component possessed serrated morphology as shown in Figure 6.4.

The sites of metastasis in these mice were scored (11 mice had metastatic carcinoma, some with more than one site of metastasis), the sites of metastasis included the liver (7/11 mice had metastases to the liver), pancreas (3/11), lung (1/11) (Figure 6.5), and the lymph nodes (2/11). Some metastases occurred in the peritoneum associated with the kidneys (1/11), epididymal fat pads and mesenteric connective tissue (7/11). Metastases into the peritoneum and pancreas are likely to be the result of direct invasion from the primary carcinoma. However, liver and lymph node metastases are highly likely to have seeded there through the blood and lymphatic vessels, and lung metastases are only able to travel there via the blood stream. Serial sectioning through the liver revealed the presence of 'micro-metastases' found deep within the tissue, which could have only seeded there via blood bourne metastasis.

## 6.2.6 The canonical Wnt pathway is activated in all invasive adenocarcinomas and carcinomas in Pten$^{fl/fl}$ Kras$^{LSL/+}$ mice

PI3K, MAPK and canonical-Wnt pathway activation status was determined by IHC. Immunostaining of metastatic carcinoma tissue sections for pAkt (PI3K), pErk and pMEK (MAPK), β-catenin and CD44 (Wnt) was carried out. As observed in sessile serrated adenomas, the carcinomas and metastases stained strongly for pErk, pMEK and pAkt compared to normal adjacent mucosa, indicating MAPK and PI3K pathway activation (Figure 6.6). However, there was also accumulation of nuclear β-catenin and strong staining for canonical Wnt target gene CD44 in both carcinoma and metastases (Figure 6.6), indicating that the canonical Wnt pathway was also being activated in these tumours. As both the normal mucosa and the benign serrated adenomas in Pten$^{fl/fl}$ Kras$^{LSL/+}$ do not show evidence of nuclear β-catenin (and therefore Wnt activation), one can postulate that a spontaneous somatic Wnt activating mutation must have occurred during progression of the tumour. Interestingly, nuclear accumulation of β-catenin was present in all observed carcinomas and invasive adenocarcinomas suggesting that a Wnt activating mutation is necessary for tumour progression.
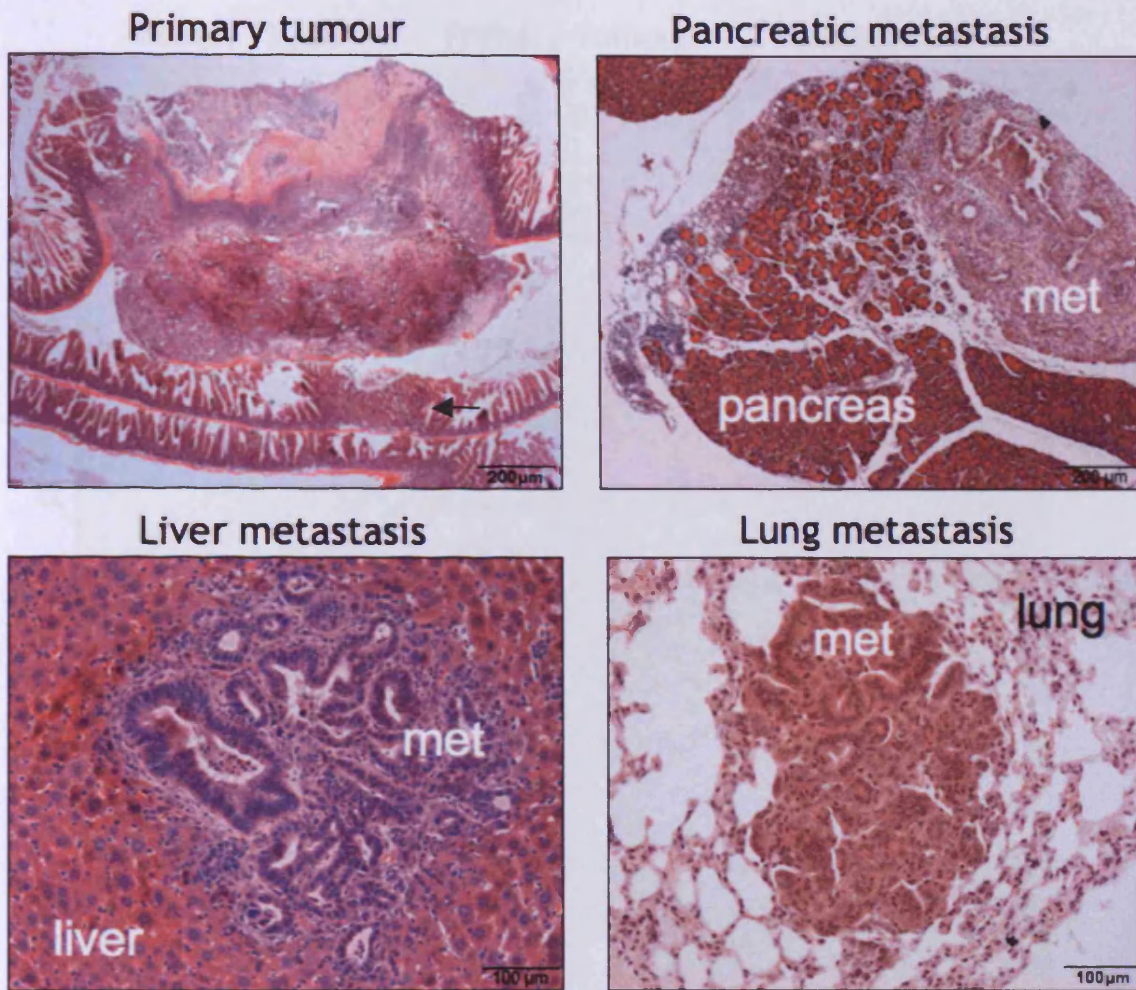
**Figure 6.5 Sites of metastasis of carcinomas found in Pten$^{fl/fl}$ Kras$^{LSL/+}$ mice**

Top left image shows a typical primary tumour found in Pten$^{fl/fl}$ Kras$^{LSL/+}$ mice (arrow shows sessile serrated adenoma also observed in this mouse, scale bar represents 200μm). Metastases were predominantly found in the pancreas (n=3/11) (top right image, scale bar represents 200μm) and liver (n=7/11) (bottom left image, scale bar represents 100μm). There was also evidence of metastases to the lung (n=1/11) (bottom right image, scale bar represents 100μm).
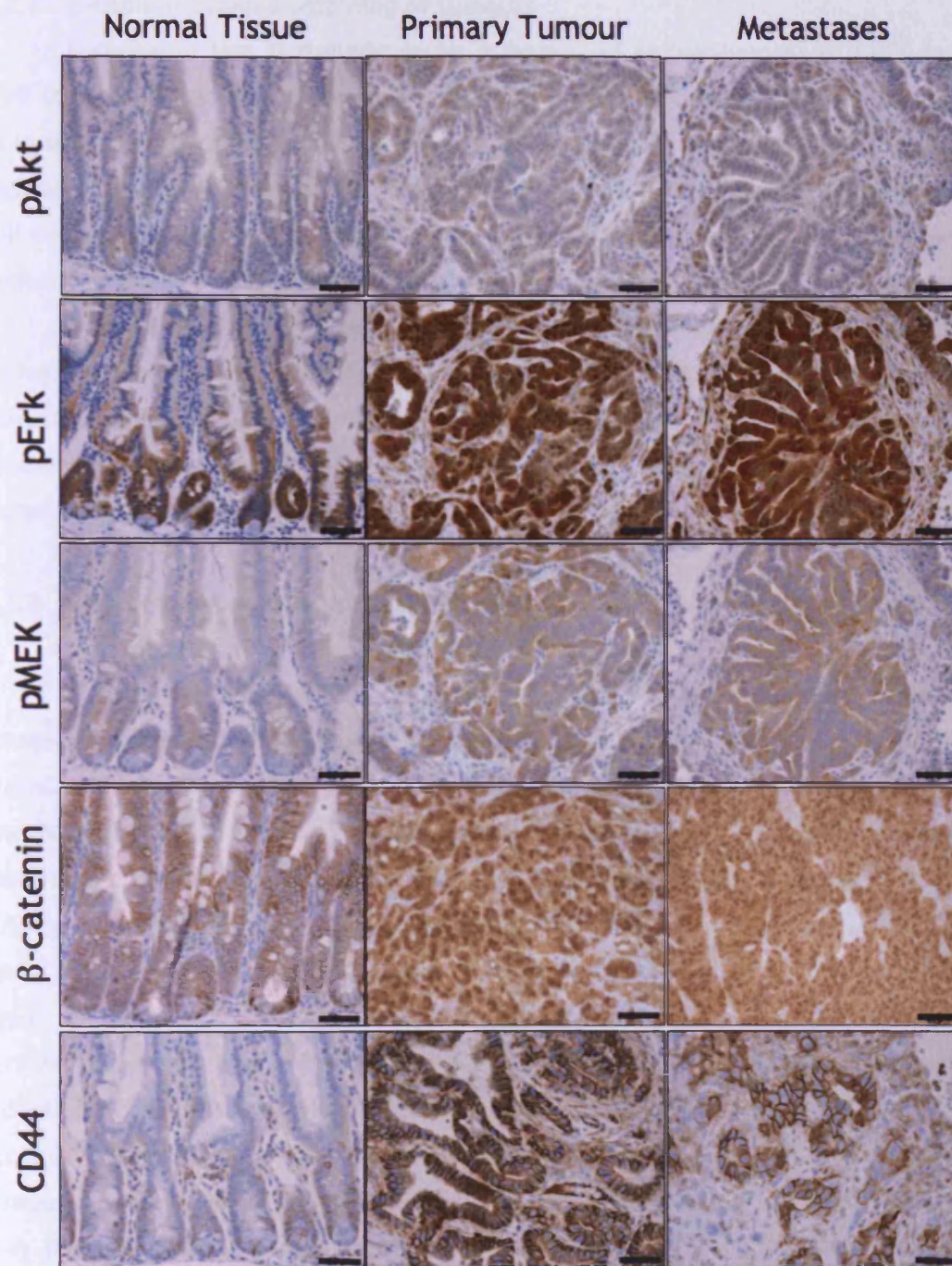
**Figure 6.6 IHC indicated activation of the PI3K and MAPK pathways in metastatic carcinoma, as well as activation of the Wnt pathway**

IHC for pAkt (ser473), pErk (Thr202/Tyr204) and pMEK (Ser221) indicated stronger staining for each, in both carcinomas and metastases, compared to normal intestinal mucosal staining – indicating activation of the PI3K and MAPK pathways. However, IHC staining for β-catenin revealed its subcellular localisation to be nuclear in the carcinoma and metastases, compared to basolateral staining in the normal intestinal tissue. Therefore, the canonical Wnt pathway was being activated in these advanced tumours, further confirmed by intense staining for Wnt target gene CD44 in the carcinomas and metastases. Scale bars represent 50μm.

### 6.2.7 E-cadherin immunostaining of tumours

E-cadherin loss is thought to be a marker of aggressiveness of CRCs in humans, with loss of E-cadherin expression associated with increased propensity of the tumours to invade and metastasise (Dorudi et al., 1995, Karamitopoulou et al., 2011). Loss of E-cadherin expression induces EMT, and it is this change in morphology, along with loss of cell-to-cell contacts that is thought to be the cause of increased tumour invasiveness. E-cadherin was visualised by IHC, which was carried out on tumour tissue sections

Despite tumours in $Pten^{fl/fl}$ $Kras^{LSL/+}$ mice progressing to metastasis, IHC for E-cadherin revealed no changes in E-cadherin expression in both carcinomas and metastases (Figure 6.7). There were no areas of tumour that appeared to have lost E-cadherin expression, and all cells within the tumours still appeared to possess epithelial morphology.

### 6.2.8 Reduced cre expression in $Apc^{fl/+}$ $Pten^{fl/fl}$ $Kras^{LSL/+}$ mice decreases tumour number but does not give rise to metastatic carcinomas

Despite all adenocarcinomas and carcinomas present in $Pten^{fl/fl}$ $Kras^{LSL/+}$ mice possessing evidence of canonical Wnt pathway activation, no Wnt driven tumours in $VillinCreER^T$-$Apc^{fl/+}$ $Pten^{fl/fl}$ $Kras^{LSL/+}$ mice became metastatic, described in chapter 4. One possible reason for this may be that as the levels of cre expression and subsequent DNA recombination are high, the mouse has a large number of tumours that progress quickly to adenocarcinoma and cause rapid morbidity. To circumvent this, a cohort of $Apc^{fl/+}$ $Pten^{fl/fl}$ $Kras^{LSL/+}$ were induced with a 10x lower dose of tamoxifen (8mg/kg) and aged. As predicted, they survived to a median of 324 days compared to the median survival time of mice induced with 80mg/kg doses of tamoxifen of 41 days post induction. This longevity was due to the decrease in tumour number caused by lower cre recombination. 8mg/kg (low dose) $Apc^{fl/+}$ $Pten^{fl/fl}$ $Kras^{LSL/+}$ mice had an average of 3.3 tumours per section, compared to 80mg/kg (normal dose) $Apc^{fl/+}$ $Pten^{fl/fl}$ $Kras^{LSL/+}$ mice that possessed an average of 50 tumours per section. All low dose mice possessed invasive adenocarcinomas, 6 out of 7 mice possessed one adenocarcinoma that had invaded through the smooth muscle into the peritoneal cavity, but none of these mice showed evidence of metastasis (Figure 6.8). These data therefore suggest that a Wnt activating mutation is an obligate event for metastasis in $Pten^{fl/fl}$ $Kras^{LSL/+}$ mice, and they do not arise out of a Wnt initiated adenoma.

**Normal Tissue**   **Primary Tumour**

**Liver Metastasis**
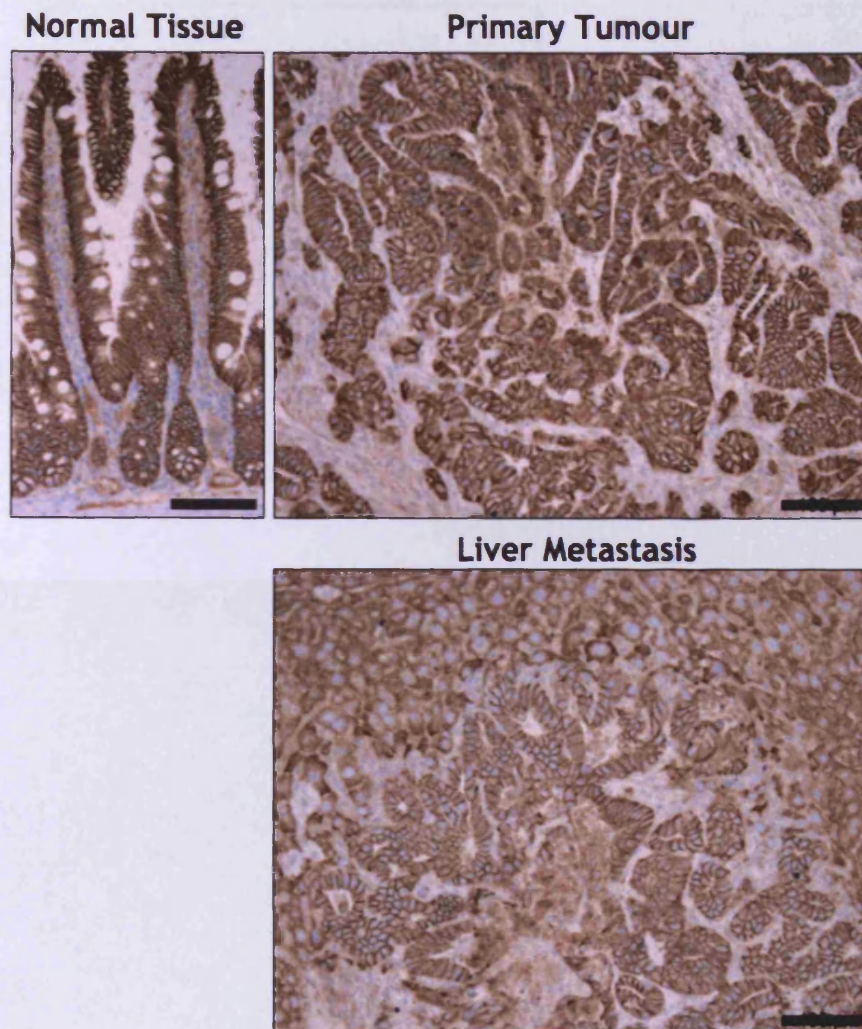
**Figure 6.7 IHC reveals no changes in expression of E-cadherin in metastatic carcinomas**

IHC against E-cadherin revealed no overt loss of expression of the protein, the cells maintained basolateral localisation in both the primary tumours and metastases. E-cadherin loss is associated with increased invasion, but there was no evidence of loss of E-cadherin in all the tumours observed in Pten$^{fl/fl}$ Kras$^{LSL/+}$ mice. Scale bars represent 100μm.

**A**
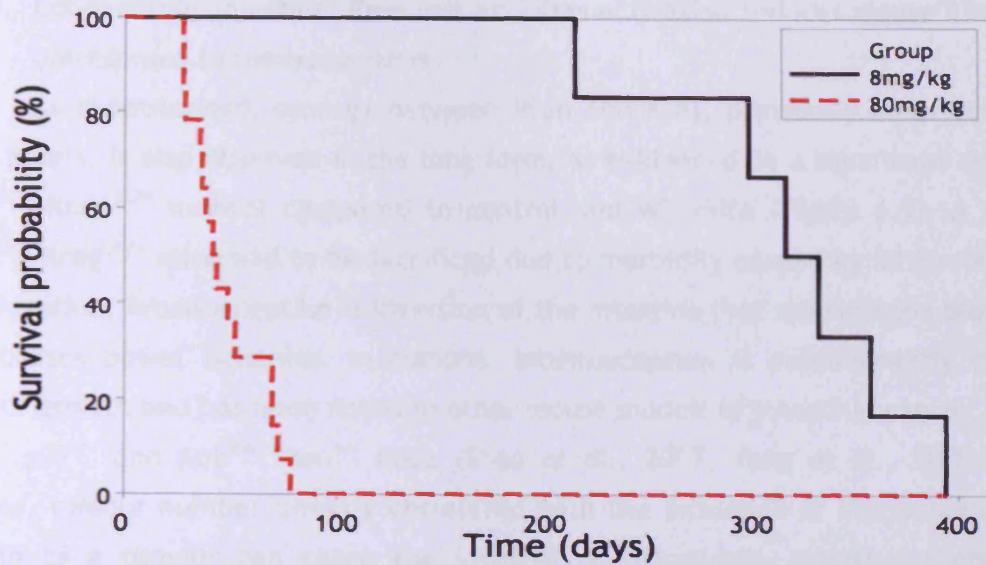
**B**
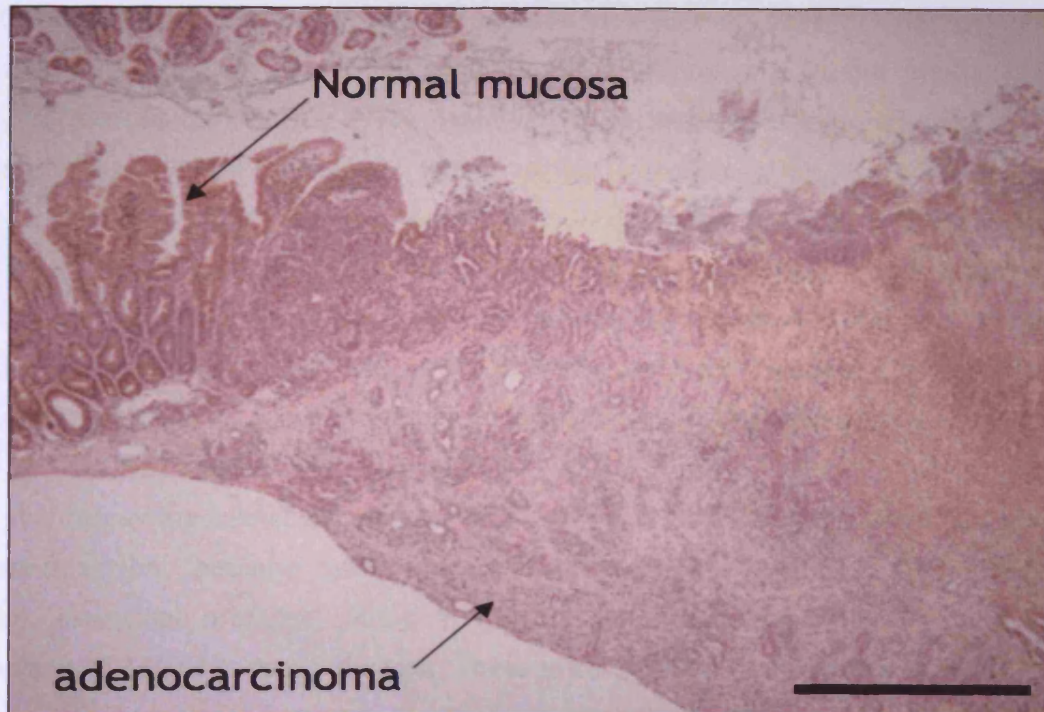
Figure 6.8 Tumours in low recombination Apc*fl/+* Pten*fl/fl* Kras*LSL/+* mice do not progress to metastasis

(A) Apc*fl/+* Pten*fl/fl* Kras*LSL/+* mice that were given a 10x lower dose of tamoxifen have a significantly longer lifespan than those given a normal dose (p value < 0.001, Log-Rank test). They have a median survival time of 324 days, compared to the 80mg/kg cohort that survived until a median of 41 days post induction.

(B) An example of an adenocarcinoma with smooth muscle invasion observed in low dose Apc*fl/+* Pten*fl/fl* Kras*LSL/+* mice. All of the low dose Apc*fl/+* Pten*fl/fl* Kras*LSL/+* mice developed invasive adenocarcinoma, 6 out of the 7 mice developed invasive adenocarcinoma that infiltrated the smooth muscle wall and underlying serosa, but none developed metastasis. Scale bar represents 500μm.

## 6.3  Discussion

### 6.3.1  Concomitant intestinal Pten loss and Kras activation reduces mouse lifespan and predisposes to tumourigenesis

As hypothesised, synergy between Pten and Kras, previously observed at short time points, is also observed in the long term, as evidenced by a significant decrease in $Pten^{fl/fl}$ $Kras^{LSL/+}$ survival compared to control and WT mice (Figure 6.1). A subset of $Pten^{fl/fl}$ $Kras^{LSL/+}$ mice had to be sacrificed due to morbidity caused by intussusception of the intestine, intussusception is inversion of the intestine that restricts the blood supply and causes bowel ischemia. In humans, intussusception is predominantly caused by tumour growth and has been noted in other mouse models of intestinal cancer, including $Apc^{+/-}$ $p27^{-/-}$ and $Apc^{Min}$ $Pten^{+/-}$ mice (Shao et al., 2007, Yang et al., 2005). In both studies, tumour number directly correlated with the incidence of intussusception. The growth of a tumour can cause the intestine to invaginate. However there was no evidence of tumours at the site of intussusception in $Pten^{fl/fl}$ $Kras^{LSL/+}$ mice. Intussusception can also be caused by bacterial infection due to the production of lipopolysaccharides (Lin et al., 1998). However, if bacterial infection was the cause of intussusception in these mice, one would expect intussusception to be observed in control littermates and it was not. Bacterial induced intussusception is thought to be caused by intestinal motility dysfunction, which may be the cause of intussusception in $Pten^{fl/fl}$ $Kras^{LSL/+}$ mice – motility may be reduced by hyperplasia of the mucosal epithelium. As previously stated the action of increased proliferation and migration may cause intussusception by forcing the supporting stroma upwards and pulling the smooth muscle up with it, allowing it to invaginate.

The remaining subset of the $Pten^{fl/fl}$ $Kras^{LSL/+}$ mice induced that did not succumb to intussusception, become symptomatic of an intestinal tumour burden (swollen abdomen, intestinal prolapse, blood in faeces, anaemia), and were sacrificed at a median time of 344 days post induction. These mice displayed spectrum of tumours from benign sessile serrated adenomas to metastatic carcinoma (Figure 6.4). The $Pten^{fl/fl}$ $Kras^{LSL/+}$ mouse model is one of the few examples of an intestinal tumour model that doesn't require a Wnt activating mutation to drive tumourigenesis. Some of these models include Smad4 deletion (Hohenstein et al., 2003), Braf activation (Carragher et al., 2010) and TGFβR deletion with Kras activation (Trobridge et al., 2009). It is also consistent with mouse models in which an activating Kras mutation, in concert with another (non-Wnt activating) mutation, drives intestinal tumourigenesis (Bennecke et al., 2010, Trobridge et al., 2009).

### 6.3.2 Sessile serrated adenomas appear to be driven by PI3K and MAPK activation and arise independently of Wnt activation

Sessile serrated adenomas are also observed in the human colon. They are early stage tumours, regarded to be precursors of CRC that form via an alternative pathway to the Fearon-Vogelstein pathway of CRC progression (Huang et al., 2004, Makinen et al., 2001, Makinen, 2007). Serrated adenomas were first described by Longacre & Fenoglio-Preiser after re-examination of a large number of tumours originally classified as hyperplastic polyps (Longacre and Fenoglio-Preiser, 1990). Hyperplastic polyps are considered benign, and are usually not resected during routine colonoscopy. However, serrated adenomas are thought to have the propensity to progress to carcinoma, and as hypermethylation is common in these tumours, they may be the precursor lesions to CpG island methylator phenotype (CIMP) colorectal cancers (Jass, 2005). Serrated adenomas were further classified into two sub-types: sessile and traditional. Sessile describing flat tumours, and traditional describing pedunculated or stalked tumours (Torlakovic et al., 2003). The main morphological and histological differences between serrated adenomas and 'traditional 'Wnt-initiated' adenomas' are that serrated adenomas have a 'saw-tooth appearance' to the edges of the tumour, they appear more eosinophillic (i.e. appear to stain darker with eosin) to the surrounding normal epithelium, the tumours are well defined in structure and consist of well differentiated cells (sometimes rich in goblet cells). Whereas, traditional 'Wnt-initiated' adenomas are made up of more immature 'progenitor-like' cells (Figure 6.9). The sessile serrated adenomas observed in Pten$^{fl/fl}$ Kras$^{LSL/+}$ mice were morphologically distinct from traditional 'Wnt-driven' adenomas and possessed no evidence of Wnt pathway activation, as there was a lack of nuclear β-catenin (a surrogate marker of Wnt activation, Figure 6.3). Strong immunostaining for pAkt, pErk and pMEK (active PI3K and MAPK pathway downstream effectors respectively), indicated that these tumours are likely to be driven by these pathways.

The observation that Pten and Kras mutations synergise to promote Wnt-independent tumour formation is consistent with the evidence in humans that serrated adenomas arise via a Wnt-independent mechanism, namely mutations in KRAS or BRAF (Chan et al., 2003, Higashidani et al., 2003, Kambara et al., 2004). However, it appears from aged control cohorts that loss of Pten in the mouse may be sufficient for initiation of sessile serrated adenomas, and additional Kras mutation further promotes this initiation. Sessile serrated adenomas were not observed in Kras$^{LSL/+}$ control mice. Contrary to the human situation, the Pten$^{fl/fl}$ Kras$^{LSL/+}$ mouse model gives rise to sessile serrated adenomas, linking a Kras mutation with this subtype of serrated adenoma. In

humans BRAF is commonly associated with sessile serrated adenomas, and KRAS with traditional serrated adenomas (Chan et al., 2003, Higashidani et al., 2003, Kambara et al., 2004). Interestingly, Carragher et al have recently shown that Braf mutations in the mouse intestine give rise to traditional serrated adenomas (Carragher et al., 2010), concluding that in mice, Kras mutations are associated with sessile serrated adenomas, and Braf mutations with traditional serrated adenomas, in contrast to the findings in human tumours.

## Traditional 'Wnt-driven' adenoma
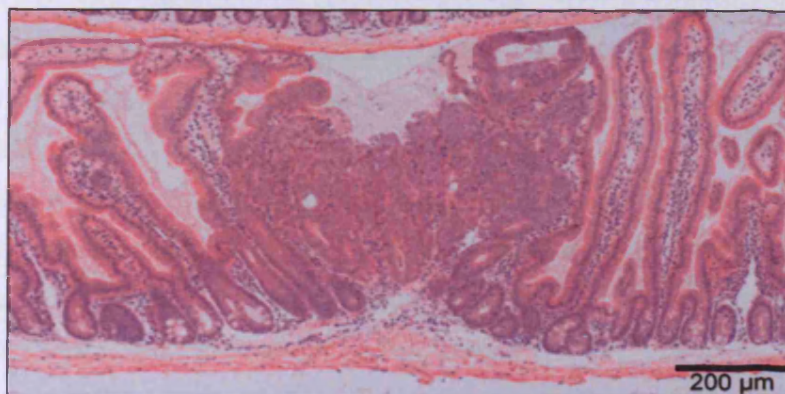


## Sessile serrated adenoma
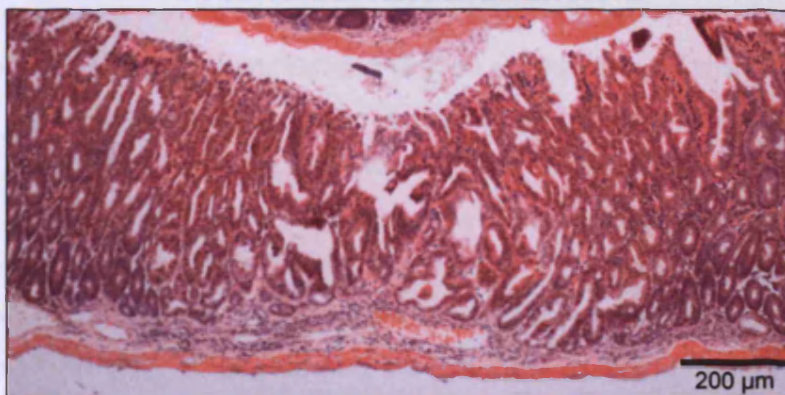


**Figure 6.9 Traditional Wnt driven adenoma vs Wnt independent sessile serrated adenoma**

Traditional 'Wnt-initiated' adenomas are easily distinguished from other types of adenoma, such as the serrated adenoma or hyperplastic polyp, simply by their morphology. Wnt-initiated adenomas lose normal crypt-villus morphology and the cells resemble immature progenitor cells. Serrated adenomas maintain crypt-like structures but individual villi are usually not discernable. The crypt-like structures forming the adenoma take on a serrated 'saw-tooth' appearance to their edges.

### 6.3.3 Pten loss and Kras activation also predisposes to the development of Wnt-activated metastatic intestinal carcinomas

Pten$^{fl/fl}$ Kras$^{LSL/+}$ mice were also predisposed to the formation of invasive intestinal adenocarcinomas that had infiltrated the smooth muscle wall, and intestinal carcinomas that had metastasised. Similarly to the sessile serrated adenomas, these late stage tumours show strong immunostaining for markers of PI3K and MAPK pathway activation. However, immunostaining for β-catenin and Wnt target gene CD44 indicate that the Wnt pathway is also active in these tumours (Figure 6.6). As the surrounding normal tissue or the benign sessile serrated adenomas do not show any evidence of elevated activity of Wnt signalling, it could be assumed that a spontaneous somatic Wnt activating mutation must have occurred at some stage in these tumours. It therefore appears that in order for a tumour to become invasive and metastasise, it must acquire Wnt pathway activation.

There are two possible hypotheses as to when Wnt activating mutations are acquired and how the late stage tumours arise in these mice (also outlined in Figure 6.10):

1. A spontaneous Wnt activating mutation occurs within the benign sessile serrated adenoma, which then progresses to carcinoma

2. A spontaneous Wnt activating mutation occurs in the mucosa deficient for Pten and activated for Kras, which then gives rise to a tumour that progresses to carcinoma

Neither hypothesis can be conclusively proven within the constraints of the mouse models used in this study. However, there is evidence in favour of the latter hypothesis. Apc$^{fl/+}$ Pten$^{fl/fl}$ Kras$^{LSL/+}$ mice that received a ten times lower dose of tamoxifen developed one or two large adenocarcinomas that invaded through the smooth muscle wall and underlying serosa per mouse, but none of these tumours progressed to metastasis – suggesting that an initiating Wnt mutation does not necessarily give rise to metastasis even when given a long latency period (Figure 6.8). In Pten$^{fl/fl}$ Kras$^{LSL/+}$ mice, invasive adenocarcinomas and metastatic carcinomas were frequently observed with sessile serrated adenomas (Figure 6.5). This finding, taken together with the observations that some sessile serrated adenomas had evidence of invasion, and carcinomas and metastases displaying serrated morphology (Figure 6.4) gives strong evidence in favour of the first hypothesis. Further evidence to support the hypothesis that sessile serrated adenomas are the precursor lesions to the carcinomas observed in Pten$^{fl/fl}$ Kras$^{LSL/+}$ mice through a Wnt-activating mutation, comes from the observation that some sessile serrated adenomas have evidence of nuclear β-catenin in humans (Wu et al., 2008, Yachida et al., 2009). This also supports the notion that a Wnt-activating

mutation can promote tumour progression, as well as initiation. In humans, serrated adenomas have high levels of methylation, and it is the methylation of tumour suppressor promoters that is thought to be the driver of progression tumour progression (Jass, 2005). However, the level of methylation in the tumours arising in Pten$^{fl/fl}$ Kras$^{LSL/+}$ mice was not investigated, so it cannot be ascertained whether it is indeed methylation that is driving loss of expression of additional tumour suppressors.
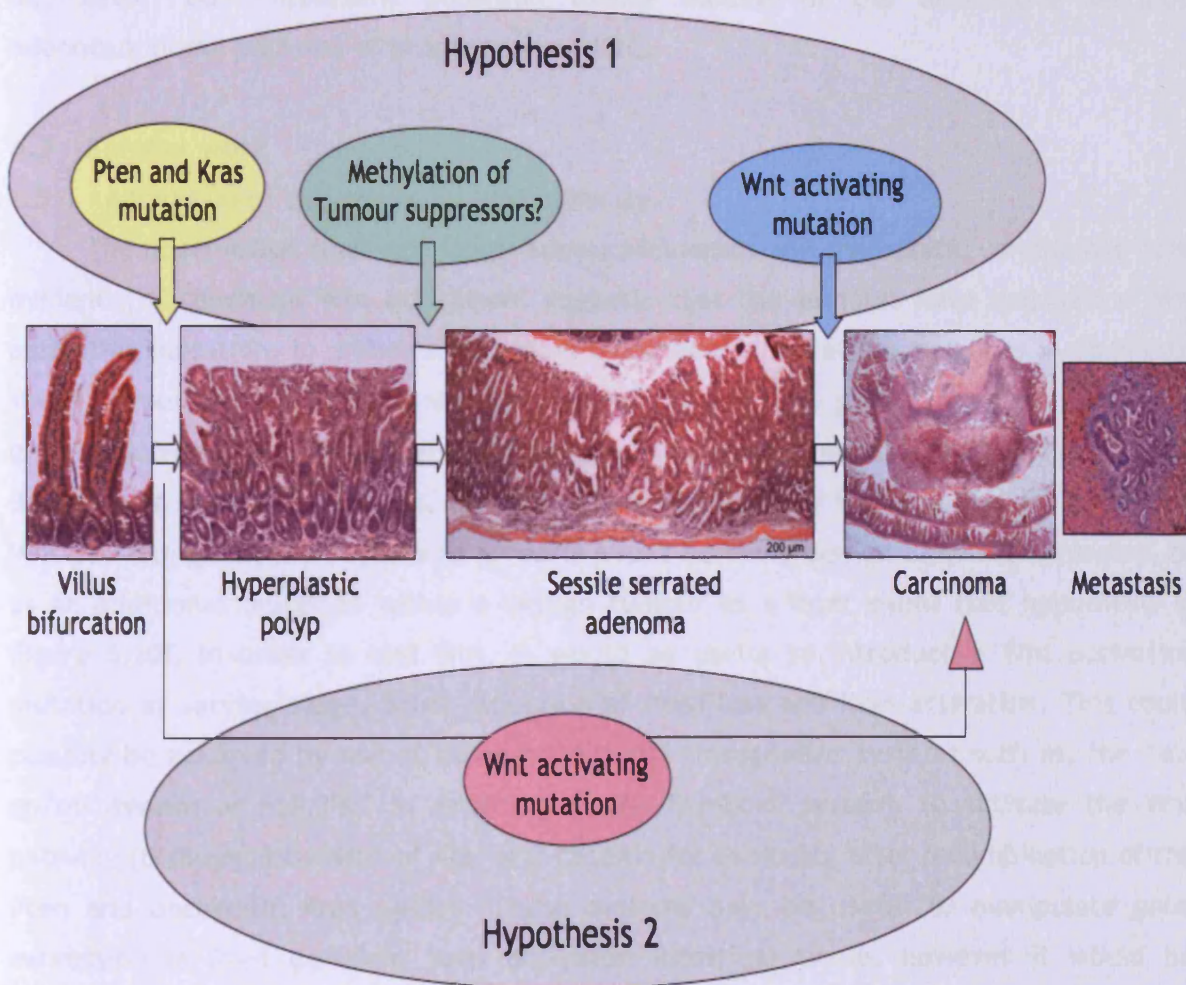


**Figure 6.10 The two possible proposed pathways of tumour progression in Pten$^{fl/fl}$ Kras$^{LSL/+}$ mice**

The metastatic carcinomas may arise in two ways in Pten$^{fl/fl}$ Kras$^{LSL/+}$ mice. The first being a progression from a non Wnt-initiated benign sessile serrated adenoma through to metastatic carcinoma by a series of mutations including mutation mechanisms such as methylation of various tumour suppressors and a proven Wnt activating mutation. The second possible pathway may arise from a the acquisition of a Wnt initiating mutation in the epithelium that is deficient for Pten and has activated Kras, which then progresses to metastatic carcinoma. In the latter hypothesis sessile serrated adenomas would arise independently of this pathway and remain benign.

## 6.4 Summary

The Pten$^{fl/fl}$ Kras$^{LSL/+}$ mouse model is one of the few models of serrated adenomas. Other published models implicate TGF-β, Kras and Braf activation in the formation of these tumours (Bennecke et al., 2010, Hohenstein et al., 2003, Carragher et al., 2010). Both the Pten$^{fl/fl}$ Kras$^{LSL/+}$ mouse model described here, and a mouse model described by Bennecke et al in which Kras$^{G12D}$ is activated along with concomitant Ink4a/Arf deletion, give rise to serrated adenomas and metastatic carcinoma in the intestine (Bennecke et al., 2010). Both represent potential mouse models of the alternative serrated adenocarcinoma pathway of progression to CRC.

## 6.5 Further work

### 6.5.1 Activation of the canonical Wnt pathway

The observation that late stage adenocarcinomas and metastatic carcinomas have evidence of canonical Wnt activation, suggests that the tumours have acquired a Wnt activating mutation. In order to ascertain whether the mutations acquired in each late stage tumour are the same, it would be useful to sequence gDNA from the tumours for genes involved in the canonical-Wnt pathway that are commonly mutated i.e. Apc and β-catenin to look for mutations. Further to this, it is unclear from my findings whether a Wnt activating mutation occurs as an early event before a benign tumour has formed, or as an additional mutation within a benign tumour as a later event (see hypothesis in Figure 6.10). In order to test this, it would be useful to introduce a Wnt activating mutation at varying stages after induction of Pten loss and Kras activation. This could possibly be achieved by use of other conditional transgenesis systems such as, the Tet-on/off system or FLP/FRT in addition to the Cre-LoxP system, to activate the Wnt pathway (through activation of Apc or β-catenin for example) after recombination of the Pten and oncogenic Kras alleles. These systems may be useful to manipulate gene expression in Pten deficient Kras activated intestinal tissue, however it would be difficult to test whether a Wnt activating mutation must occur within a sessile serrated adenoma to progress to carcinoma using these systems.

### 6.5.2 Methylation of DNA in sessile serrated adenomas

Increased methylation of tumour suppressors is observed in human serrated adenomas, however I have not addressed whether increased methylation is observed in the sessile serrated adenomas in Pten$^{fl/fl}$ Kras$^{LSL/+}$ mice. I could assess the level of methylation in sessile serrated adenomas by carrying out IHC against DNA-(cytosine-5)-methyltransferase 3 beta, which carries out *de novo* methylation so may be upregulated

in these tumours. Methyl specific PCR could also be carried out on the promoter regions of genes commonly methylated in human sessile serrated adenomas.

# Chapter 7:    Investigating the role of E-cadherin in the intestinal epithelium

## 7.1    Introduction

The integrity of epithelial cell layers is maintained by cell-to-cell and cell-to-matrix contacts. Adherens junctions, tight junctions and desmosomes are the three major types of cell-to-cell contacts that mediate epithelial cell layer integrity. Maintenance of these junctions is paramount to the successful functioning of the epithelial cell layer. In the intestine, cell-to-cell contacts prevent diffusion of molecules and microbes between epithelial cells, give stability to the epithelial layer and help maintain apical and basal polarisation of the cells. The cadherin superfamily of proteins contributes to the formation of cell-to-cell adhesions, specifically adherens junctions and desmosomes. Epithelial-cadherin (E-cadherin) is the prototypic cadherin. It is a transmembrane glycoprotein that mediates the formation of adherens junctions by forming $Ca^{2+}$ dependent homodimers between adjacent epithelial cells. Adherens junctions form a circumferential belt around epithelial cells, but are also found along the lateral surface of the cells. In an adherens junction, E-cadherin is the membrane spanning protein that forms homodimers with E-cadherin molecules on the cell surface of neighbouring cells. The cytoplasmic domain of E-cadherin binds to β-catenin and p120-catenin which in turn bind α-catenin that links to the actin cytoskeleton. The role of E-cadherin and adhesion is reviewed in (Wijnhoven et al., 2000).

Downregulation or loss of E-cadherin has been associated with a number of epithelial cancers including colorectal cancer (CRC). Reduction in E-cadherin expression in CRCs has been associated with disease progression (Dorudi et al., 1993, Karamitopoulou et al.), and a reduction in patient survival time (Dorudi et al., 1995). E-cadherin's key role in tumour invasion has been demonstrated by the reintroduction of E-cadherin into a number of E-cadherin negative cancer cell lines causing a reduction of their capacity to invade (Vleminckx et al., 1991). E-cadherin loss may promote tumourigenesis and progression through its involvement in cell signalling, either through its cellular association with β-catenin (Morin et al., 1997), or through facilitation of juxtacrine signalling by maintaining cell-to-cell contacts. Loss of E-cadherin and therefore loss of cell adhesions may also promote easier detachment of cells within a tumour, thereby promoting metastasis or through induction of EMT, which is thought to be a key event that occurs before a neoplastic cell can become metastatic (Huber et al., 2005, Hay, 1995, Takeichi, 1993).

A number of studies have shown that deletion of E-cadherin in *in vivo* tumour models of breast and pancreatic cancers enhances the phenotype, promoting tumour progression and invasion (Perl et al., 1998, Derksen et al., 2006). In the intestine, one study has reported the effects of constitutive heterozygous deletion of E-cadherin in the Apc$^{1638N}$ intestinal adenoma model (Smits et al., 2000). In this model, loss of E-cadherin promoted adenoma formation but failed to enhance progression, therefore suggesting that E-cadherin loss may only be important at later stages of disease and so would not promote progression in this early tumour model. To address this question I crossed conditional Cdh1 (E-cadherin) floxed mice (Derksen et al., 2006) with *Villin*CreER$^T$ Apc$^{fl/+}$Pten$^{fl/fl}$ mice, which are a model of invasive intestinal adenocarcinoma that bear more advanced intestinal tumours than Apc heterozygous mice as described in chapter 4.

I also generated *Villin*CreER$^T$-Cdh1$^{fl/fl}$ and *Villin*CreER$^T$-Cdh1$^{fl/+}$ mice to investigate the role of the E-cadherin in normal adult mouse intestinal epithelium. Schneider et al recently described the phenotype of homozygous Cdh1 loss in the mouse intestine. They showed that mice that have lost both alleles of Cdh1 succumb to rapid morbidity due to disruption of the colonic epithelial barrier (Schneider et al., 2010). In this chapter I will also investigate homozygous Cdh1 loss and heterozygous Cdh1 loss, and compare my findings to the Schneider et al findings.

## 7.2   Results

### 7.2.1   Homozygous E-cadherin loss causes rapid mouse mortality

E-cadherin null mice are inviable and embryos die at pre-implantation stage (Riethmacher et al., 1995). So to investigate the effects of E-cadherin loss alone in the intestine, the cre loxP conditional knockout system was used. E-cadherin floxed mice were obtained (Cdh1$^{fl/fl}$) and crossed to the intestinal specific cre recombinase, *Villin*CreER$^T$. *Villin*CreER$^T$-Cdh1$^{fl/fl}$ mice (herein referred to as Cdh1$^{fl/fl}$) were generated along with the appropriate controls (Cdh1$^{fl/+}$ and Cdh1$^{+/+}$ [or WT]) induced and sacrificed when they became sick.

Cdh1$^{fl/fl}$ mice have loxP sites flanking exons 4-15 in the Cdh1 gene. Recombination of the DNA at these sites results in a functional null allele (Derksen et al., 2006). Cdh1$^{fl/fl}$ mice survived until a maximum of 4 days post induction, whereas Cdh1$^{fl/+}$ and WT mice remained healthy and were sacrificed at the end of the experiment at 346 days post induction (Figure 7.1, A). No intestinal tumour phenotype was evident in the aged Cdh1$^{fl/+}$ cohort, and histological examination revealed no

differences from WT tissues. By day 4 post induction Cdh1$^{fl/fl}$ mice were hunched, dehydrated and had diarrhea. When dissected out, the small intestine was considerably shorter than the age matched Cdh1$^{fl/+}$ control and WT small intestine (Figure 7.1, B). However, colon length appeared normal in each cohort. Cdh1$^{fl/fl}$ small intestine had an average length of 22.6 ± 5.5 cm, compared to the Cdh1$^{fl/+}$ average small intestinal length of 45.3 ± 5.7 cm and the WT average of 45.8 ± 4.3 cm. Cdh1$^{fl/fl}$ small intestines were significantly shorter than both Cdh1$^{fl/+}$ control and WT intestines (p values <0.001, n≥3, Mann Whitney U test). There was no statistical difference in Cdh1$^{fl/+}$ small intestinal length compared to the WT (p value 0.894, n≥3, Mann Whitney U test).

## 7.2.2 Homozygous E-cadherin loss causes loss of integrity of the intestinal epithelium

gDNA was extracted from crudely enriched small intestinal epithelial cell samples and PCR for the recombined allele was carried out to ensure that intestinal epithelial DNA had undergone recombination. Presence of the band corresponding to the recombined allele confirmed disruption of the Cdh1 gene in both Cdh1$^{fl/+}$ and Cdh1$^{fl/fl}$ mice (Figure 7.2, A). The targeted (unrecombined) bands present in the Cdh1$^{fl/fl}$ samples are presumed to arise from gDNA from unrecombined epithelial cells and stromal cells that do not express cre recombinase, which contaminate the sample due to the crude nature of enrichment.

Examination of H&E stained sections of small intestinal tissue revealed loss of epithelial sheet integrity in Cdh1$^{fl/fl}$ mice, and loss of defined crypt-villus structure (Figure 7.2, B). The arrows in Figure 7.2, B indicate the remaining crypt and villus-like structures. The stromal cells that support the epithelium remained but formed no defined structure. There was also evidence of expansion of the submucosal layer indicated by the dashed line in Figure 7.2, B. There appeared to be no apparent changes in Cdh1$^{fl/+}$ small intestine compared to WT intestine.

## 7.2.3 E-cadherin deficient intestinal epithelial cells detach from the epithelial sheet

IHC against E-cadherin was carried out on small intestinal tissue sections to assess the extent of E-cadherin loss. IHC revealed no obvious changes in E-cadherin expression in Cdh1$^{fl/+}$ tissue compared to WT tissue (Figure 7.3), indicating that the presence of one intact allele of Cdh1 is sufficient to maintain E-cadherin expression and cell-to-cell adhesions. IHC for E-cadherin in Cdh1$^{fl/fl}$ tissue surprisingly revealed the presence of membrane bound E-cadherin on the remaining 'crypt-villus-like' structures, but there was no evidence of the darker band of E-cadherin between cells at the

basolateral surface (arrow in the WT IHC image in Figure 7.3) and uniform expression of E-cadherin along the apical membrane as observed in WT tissue. Despite the presence of E-cadherin immunostaining in $Cdh1^{fl/fl}$ tissue, higher power images revealed that the cells that had maintained E-cadherin expression no longer possessed the morphological features of normal intestinal epithelial cells, and as expected, the cells that were detaching from the epithelial sheet no longer expressed E-cadherin (Figure 7.3, lower panel).

### 7.2.4 E-cadherin loss causes morphological changes and apoptosis of intestinal epithelial cells

High power images of H&E stained intestinal sections further confirmed the changes in cell morphology observed in E-cadherin immunostained sections. Loss of E-cadherin disrupts the cell-to-cell adhesions and in turn the cells lose polarity. Normal intestinal epithelial cells form polarised epithelial sheets (Figure 7.4, left panel), the cells are columnar in shape and the nuclei are aligned at the basal surface of the cell, the nuclei are uniform in shape and cytoplasm occupies the majority of the cell. Cells that have lost E-cadherin in $Cdh1^{fl/fl}$ mice lose the uniform structure of the epithelium, with each epithelial cell differing in morphology to its neighbour (Figure 7.4, right panel). The cells have a more rounded shape compared to the normal columnar morphology epithelial cells possess. The nuclei also appear larger and more round, and the cytoplasm of the cells appears to have been depleted.

IHC against cleaved caspase 3 (which is only present in cells undergoing apoptosis) revealed the presence of many apoptotic cells in $Cdh1^{fl/fl}$ tissue (Figure 7.5). Many of these cleaved caspase 3 positive cells appear to have been shed from the crypt-villus epithelium, suggesting that loss of contact of neighbouring epithelial cells initiates anoikis (the apoptotic program triggered by loss of cell-to-cell contact). There also appeared to be higher numbers of caspase 3 positive cells in $Cdh1^{fl/+}$ small intestinal tissue compared to WT. This will be investigated further in section 7.2.6.

### 7.2.5 E-cadherin deficiency induces subtle changes in colonic epithelium at day 3 post induction

The morbidity seen at around day 3 post induction in $Cdh1^{fl/fl}$ is likely to be caused by the severe small intestinal phenotype. The absence of any identifiably normal crypt-villus structures is likely to cause the mouse to become rapidly dehydrated and malnourished. However, as *VillinCre* recombinase is also expressed in the colon,

investigation of any overt changes in the colon was carried out. H&E stained colon sections revealed that heterozygous loss of E-cadherin (Cdh1$^{fl/+}$) does not alter colonic epithelial morphology compared to WT (Cdh1$^{+/+}$) tissue (Figure 7.6). Homozygous loss of E-cadherin (Cdh1$^{fl/fl}$) does appear to subtly alter colonic morphology compared to control and WT tissue (Figure 7.6). Much like the cell morphology changes observed in small intestinal tissue, Cdh1$^{fl/fl}$ luminal epithelium appears to have lost polarity. The cells no longer possess a columnar morphology and uniform localisation of the nuclei near the basal surface of the cell appears to be disrupted (Figure 7.6, arrow head).

IHC against E-cadherin was carried out on colon tissue sections. Immunostaining revealed that the epithelial cells present in the colon maintained some E-cadherin expression (Figure 7.7). However, this staining appeared reduced compared to control and WT tissue and some luminal epithelial cells appeared to have lost membrane localisation of E-cadherin (Figure 7.7, inset images). There also appeared to be an increase in the abundance of stromal cells in Cdh1$^{fl/fl}$ tissue (which is more evident in the E-cadherin stained colon tissue sections).
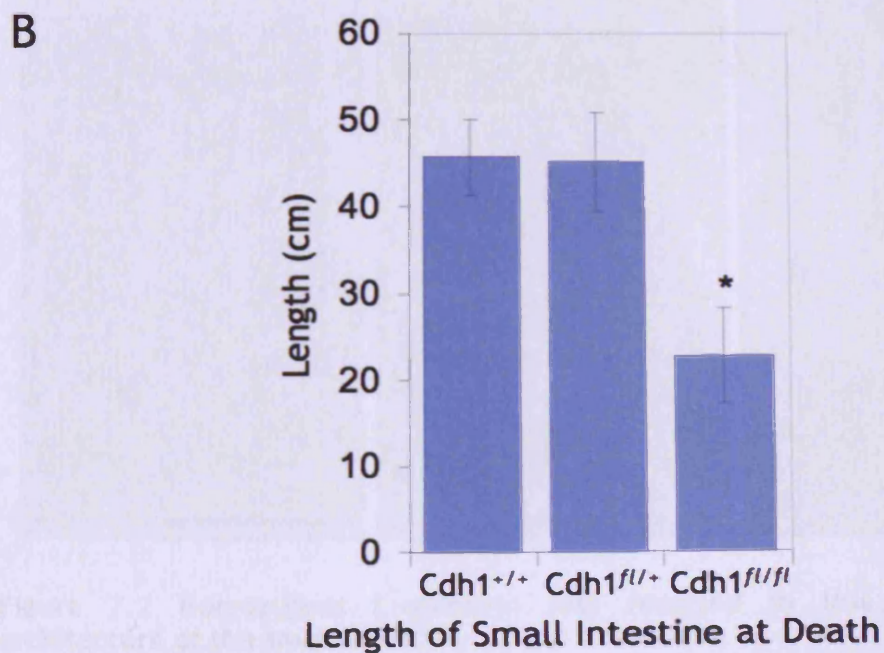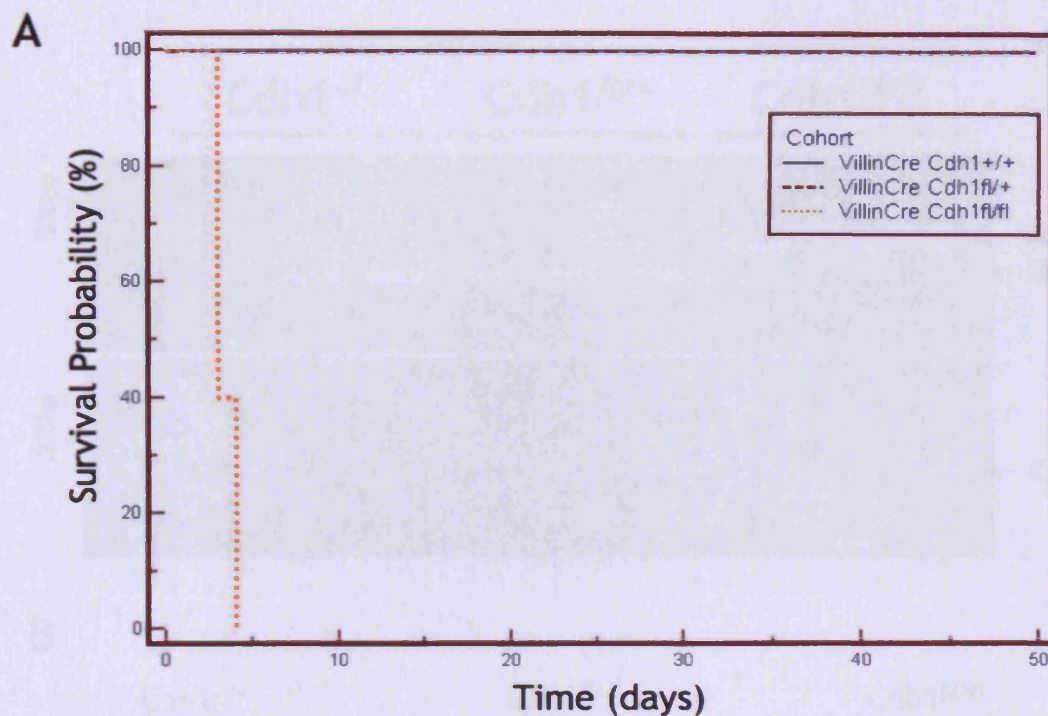
Figure 7.1 Homozygous loss of E-cadherin specifically in the intestinal epithelium leads to rapid death

(A) Cdh1$^{fl/fl}$ mice rapidly die after induction of gene deletion, surviving only 3-4 days after induction, Cdh1$^{fl/+}$ and Cdh1$^{+/+}$ mice however survive beyond 50 days post induction. (B) Cdh1$^{fl/fl}$ had significantly shorter small intestines compared to Cdh1$^{fl/+}$ and WT mice at day 3 post induction (*, p value <0.001, n≥3, Mann Whitney U test). Error bars indicate standard deviation.
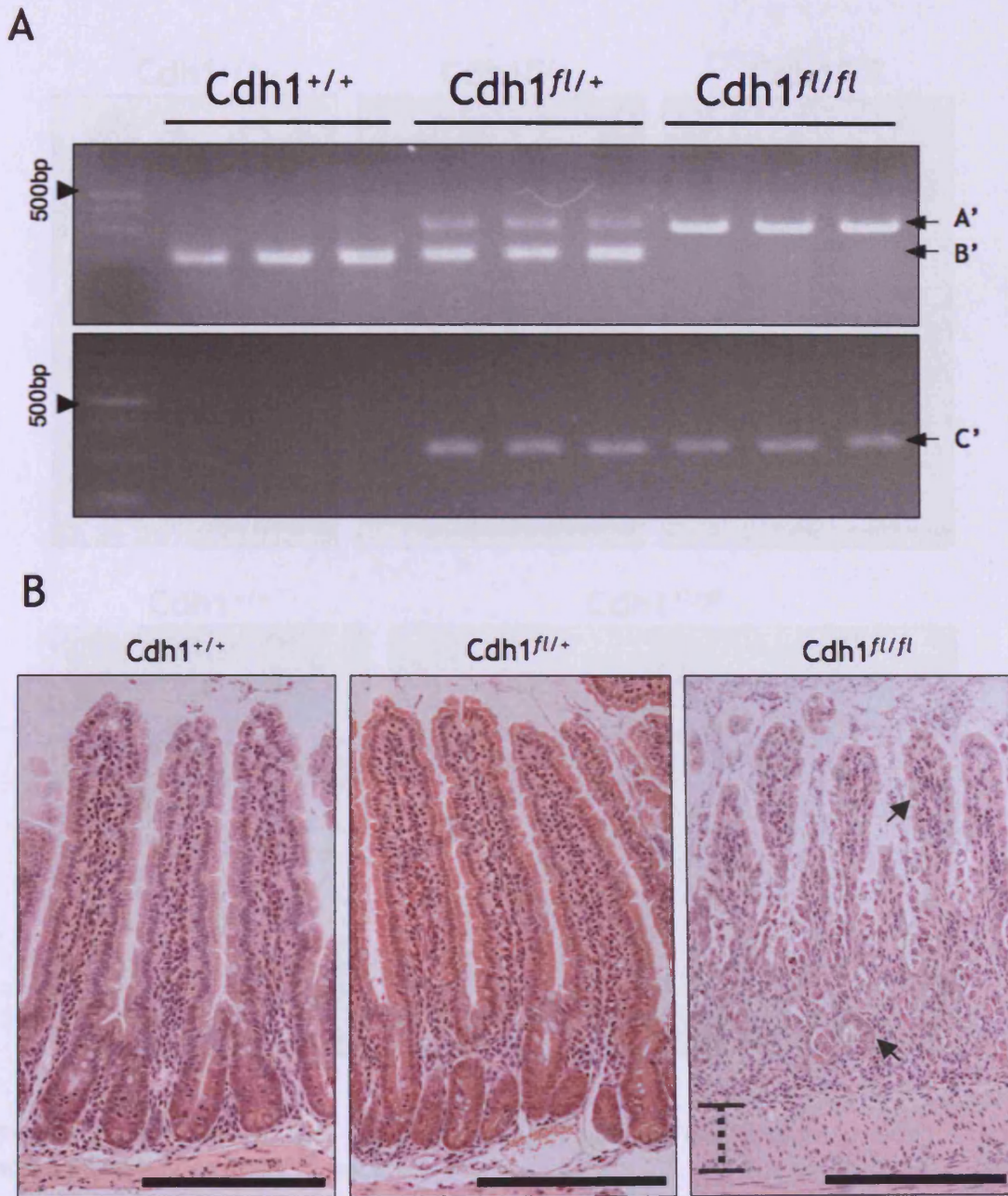
**Figure 7.2 Homozygous E-cadherin loss resulted in loss of the crypt-villus architecture of the small intestine**

(A) PCR for the recombined allele, revealed presence only in Cdh1$^{fl/+}$ and Cdh1$^{fl/fl}$ samples. Upper panel – genotyping PCR, A' – band corresponding to targeted allele (330bp), B' – band corresponding to (WT) untargeted band (200bp). Lower panel – recombined PCR, C' – band corresponding to recombined (floxed) band (320bp). (B) Histological examination of Cdh1$^{fl/fl}$ small intestinal tissue and controls at day 3 post induction revealed extensive loss of crypt-villus architecture due to apparent loss of epithelial cells (arrows indicate remaining 'crypt' and 'villus' structures, dashed line indicates submucosal layer). However, Cdh1$^{fl/+}$ tissue appeared identical to Cdh1$^{+/+}$ tissue. Scale bars represent 200μm.
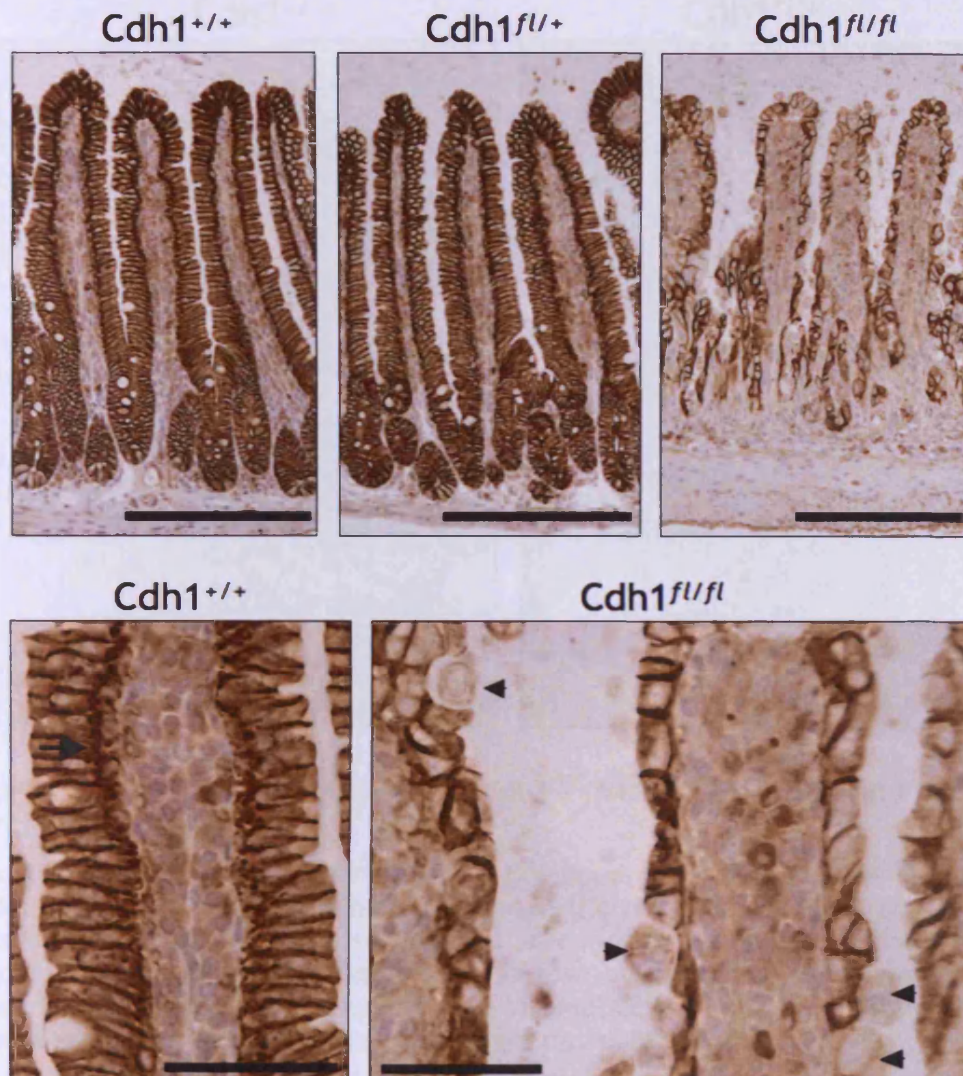
**Figure 7.3 E-cadherin IHC staining revealed normal expression in Cdh1$^{fl/+}$ mice and sparse staining in Cdh1$^{fl/fl}$ mice**

Upper panel, IHC against E-cadherin revealed no overt changes in abundance of E-cadherin in Cdh1$^{fl/+}$ tissue compared to WT. E-cadherin staining in Cdh1$^{fl/fl}$ tissue was only present in cells that formed the only discernible crypt-villus structures, scale bars represent 100μm.

Lower panel, magnified images of E-cadherin stained Cdh1$^{fl/fl}$ tissue revealed that the cells that had lost E-cadherin expression (arrow heads) also appeared to be detaching from the villus structure, whereas the cells that maintained some E-cadherin expression remained attached to neighbouring cells forming a 'villus-like' structure. However, darker staining at the basolateral surface as shown by an arrow in WT tissue was not present in Cdh1$^{fl/fl}$ tissue, scale bars represent 50μm.
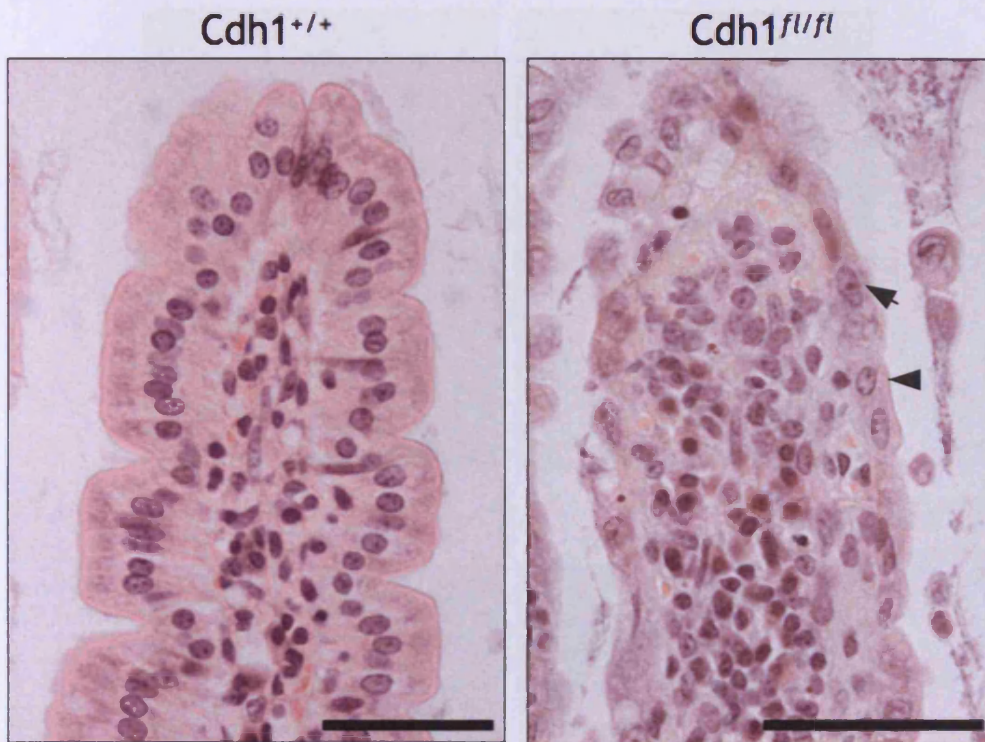
**Figure 7.4 Intestinal epithelial cells in Cdh1$^{fl/fl}$ mice lose polarity and their columnar morphology**

Normal intestinal epithelial cells form a polarised sheet of columnar cells, with their nuclei positioned towards the basal surface of the cell (left panel). E-cadherin deficient cells lose polarity and have no defined morphology, taking on a rounded or more cuboidal shape causing the epithelium to lose uniformity (arrow heads). There also appears to be an increased abundance of stromal cells in Cdh1$^{fl/fl}$ tissue, which is likely to be a result of villus shortening. Scale bars represent 50µm.
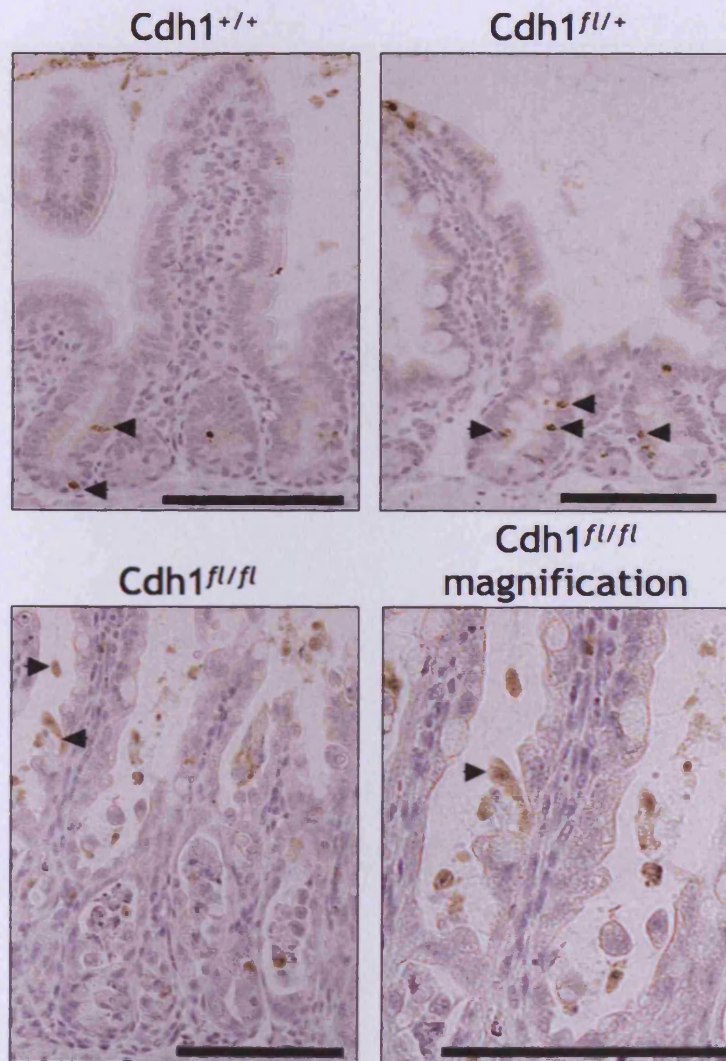
**Figure 7.5 E-cadherin loss increased the incidence of caspase 3 positive apoptotic cells**

IHC against cleaved caspase 3 (Asp175) was carried out on small intestinal tissue sections. Staining revealed many positive apoptotic cells (arrow heads) compared to WT tissue in both Cdh1$^{fl/+}$ tissue, which had maintained normal intestinal morphology, and in Cdh1$^{fl/fl}$ tissue, which had lost normal intestinal morphology. Scale bars represent 100μm.
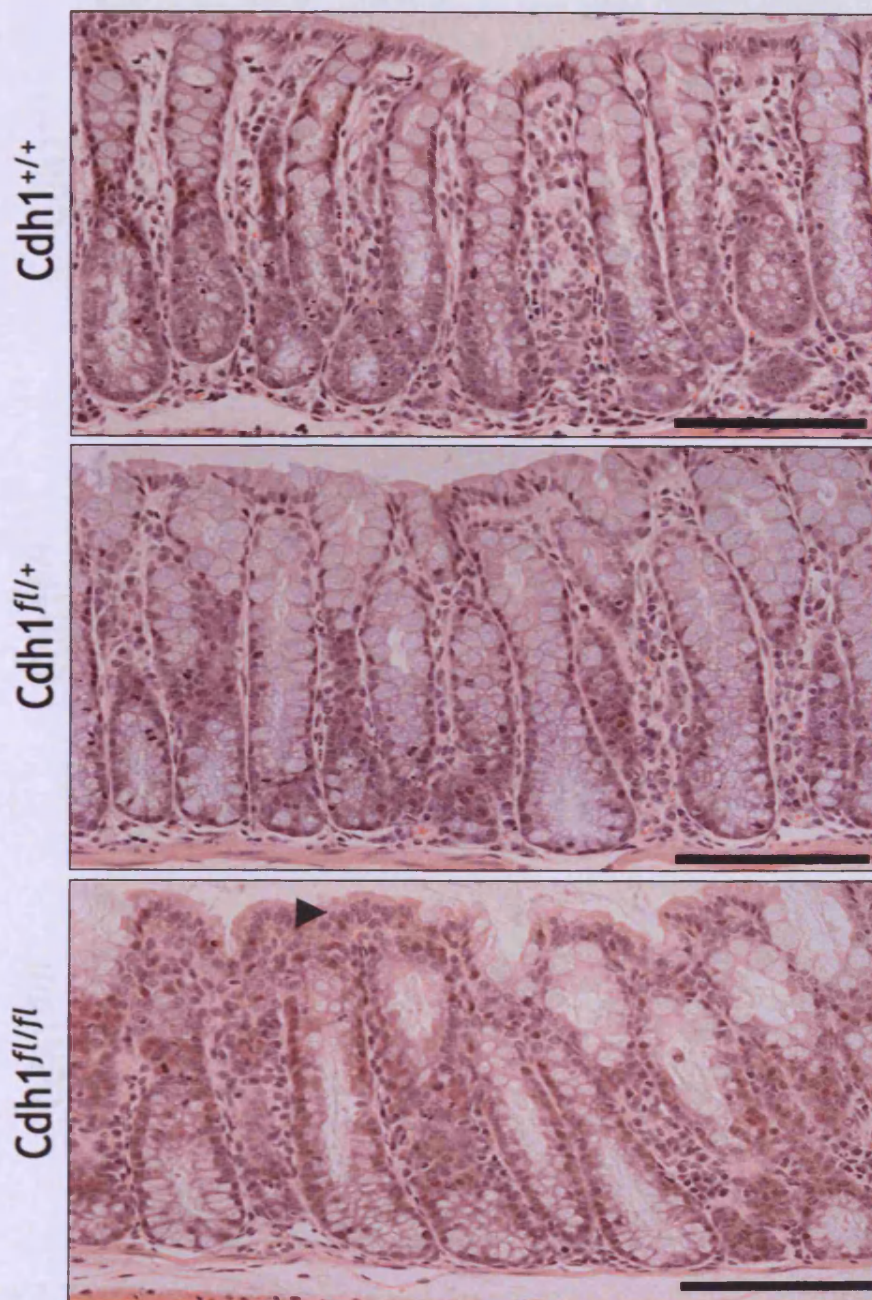
**Figure 7.6 E-cadherin deficiency resulted in subtle disruption of colonic epithelium**

There appeared to be no differences in Cdh1$^{fl/+}$ epithelium compared to WT. However, there was evidence of subtle disruption of the colonic epithelium in Cdh1$^{fl/fl}$ mice. The luminal epithelium had begun to lose polarity as evidenced by changes in morphology of epithelial cells (arrow head). There also appeared to be depletion of goblet cells within the crypts. Scale bars represent 100μm.
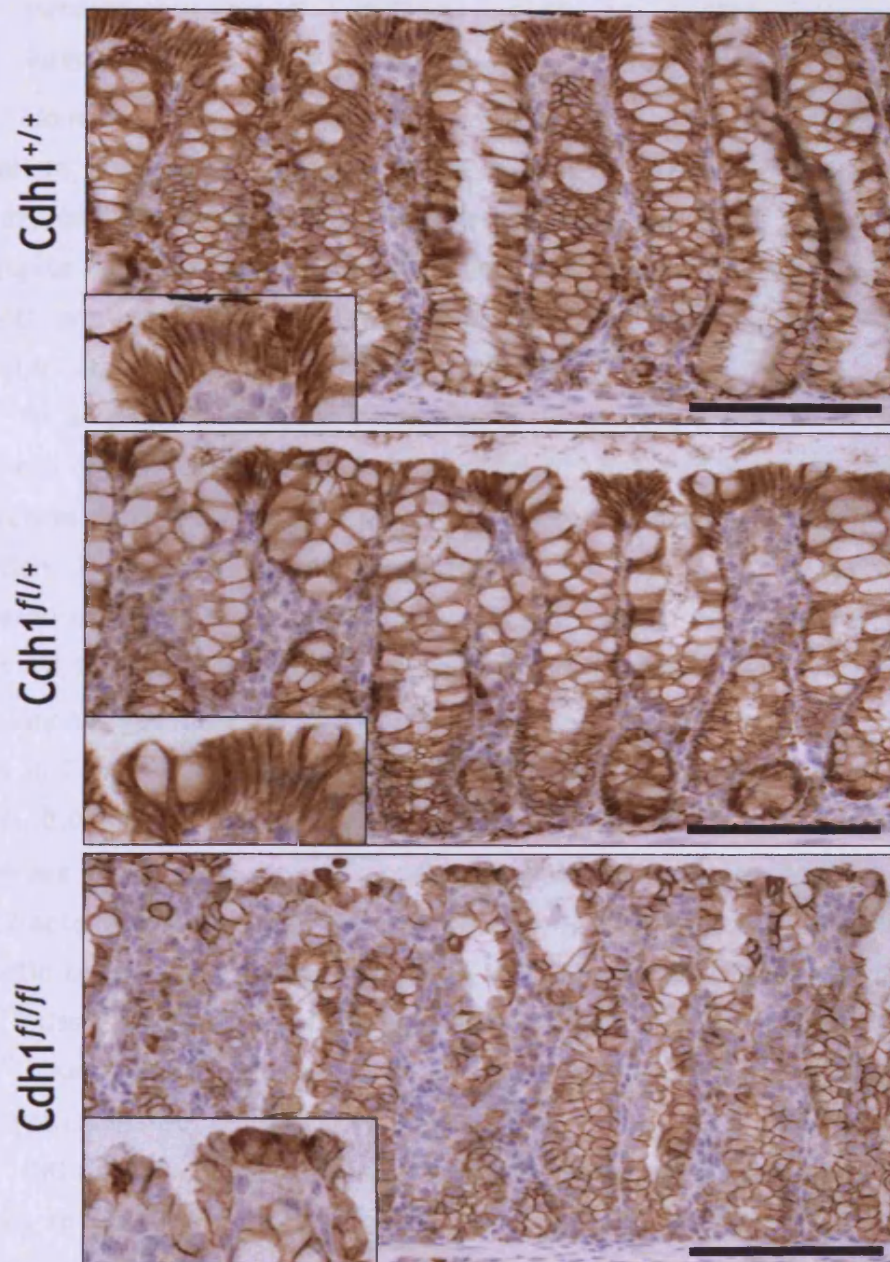
**Figure 7.7 IHC revealed reduction of E-cadherin in Cdh1$^{fl/fl}$ colonic epithelium**

IHC against E-cadherin revealed reduction of expression in the colonic epithelium, much like what was observed in the small intestinal epithelium. Some cells in Cdh1$^{fl/fl}$ colonic tissue appeared to have lost expression of E-cadherin (inset magnified images), whereas some cells still appeared to have E-cadherin present but the morphology of these cells and pattern of expression was not uniform as observed in Cdh1$^{fl/+}$ and WT tissue. An increase in the presence of stromal cells in Cdh1$^{fl/fl}$ tissue compared to Cdh1$^{fl/+}$ and WT tissue is also evident in these images. Scale bars represent 100μm.

### 7.2.6 Heterozygous loss of E-cadherin induces an apoptotic response in the small intestine

Homozygous loss of E-cadherin causes catastrophic loss of the small intestinal epithelium resulting in morbidity of the animal at days 3-4 post induction. However, heterozygous loss of E-cadherin appears to have no overt phenotype. To further investigate heterozygous loss of E-cadherin in the small intestine, Cdh1$^{fl/+}$ mice were induced and sacrificed at day 3 and day 15 post induction and phenotypic characterisation of the small intestine was carried out.

As an overt increase in the presence of caspase 3 positive apoptotic cells was evident in Cdh1$^{fl/+}$ tissue at day 3 post induction, scoring of apoptotic bodies and mitotic figures was carried out on H&E stained tissue sections taken at day 3 and day 15 post induction. There were no changes in the number of mitotic figures in Cdh1$^{fl/+}$ tissue compared to WT at both day 3 and day 15 post induction (Figure 7.8, lower panel) (p values = 0.3313 (day 3), 0.5 (day 15), n≥3, Mann Whitney U test). However, at both day 3 and day 15 post induction there was a significant increase in the number of apoptotic bodies in Cdh1$^{fl/+}$ tissue compared to WT (Figure 7.8, upper panel) (p values = 0.0404 (day 3), 0.0383 (day 15), n≥3, Mann Whitney U test). At day 3 post induction there was an average of 1.7 ± 0.3 apoptotic bodies per half crypt, compared to the WT average of 1 ± 0.2 apoptotic bodies per half crypt. At day 15 post induction the average number of apoptotic bodies was reduced compared to the score at day 3 post induction in both Cdh1$^{fl/+}$ tissue and WT, but there was still a significant increase in apoptotic score in Cdh1$^{fl/+}$ tissue. Cdh1$^{fl/+}$ tissue had an average score of 0.43 ± 0.31 apoptotic bodies per half crypt compared to 0.03 ± 0.02 in WT tissue.

IHC against cleaved caspase 3 (Asp175) was carried out on small intestinal tissue sections to visualise cells undergoing apoptosis and positive cells were scored. The increase in apoptosis in the crypts of Cdh1$^{fl/+}$ tissue at day 3 and day 15 post induction scored from H&E sections was confirmed by cleaved caspase 3 scoring (Figure 7.9) (p values = 0.0404 and 0.0383 respectively, n≥3, Mann Whitney U test). This increase in apoptosis was only evident in the crypts; there was no difference in the number of cleaved caspase 3 positive cells present in the villi (p values = 0.1914 (day 3), 0.092 (day 15), n≥3, Mann Whitney U test).

The level of apoptosis observed in Cdh1$^{fl/+}$ and WT tissue at day 3 post induction in both H&E stained and caspase 3 immunostained sections was higher than the level of apoptosis observed at day 15 post induction. The higher levels of apoptosis at day 3 post induction is likely to be attributed to the toxic effects of the tamoxifen present

systemically in the mouse at this timepoint, due to the 4 day induction regime of $Villin$CreER$^T$ recombinase.

### 7.2.7 Heterozygous loss of E-cadherin does not alter crypt-villus cell number

As there appeared to be an increase in cell death in Cdh1$^{fl/+}$ tissue (Figure 7.5) the number of cells per half crypt-villus were scored in order to assess whether this apparent increase in cell death altered intestinal homeostasis (Figure 7.10). At day 3 post induction crypt scoring revealed no significant difference between Cdh1$^{fl/+}$ and WT tissue (p values >0.05, Mann Whitney U test). Cdh1$^{fl/+}$ tissue had an average of 23 cells ± 1.6 per crypt compared to WT tissue which had an average of 22 cells ± 2.2, and villus scoring revealed that Cdh1$^{fl/+}$ tissue had an average of 78 cells ± 10.6 per villus compared to WT tissue which had an average of 80 cells ± 7.6. Crypt-villus scoring was also carried out on tissue samples taken from mice sacrificed at day 15 post induction, scoring again revealed no significant difference between Cdh1$^{fl/+}$ and WT tissue (p values >0.05, Mann Whitney U test). Cdh1$^{fl/+}$ tissue had an average of 27 cells ± 3.3 per crypt compared to WT tissue which had an average of 25 cells ± 2.4, and villus scoring revealed that Cdh1$^{fl/+}$ tissue had an average of 90 cells ± 12.5 per villus compared to WT tissue which had an average of 82 cells ± 6.9.

### 7.2.8 BrdU positive cells are found in lower crypt positions in Cdh1$^{fl/+}$ mice

Cdh1$^{fl/+}$ and WT mice were induced and at day 3 post induction given a pulse of BrdU via i.p. injection and sacrificed at either 2 hours or 24 hours after BrdU injection. IHC against BrdU was carried out on small intestinal tissue sections in order to visualise the cells that had incorporated BrdU into their DNA, and had hence gone through S phase of the cell cycle (Figure 7.11). The position of BrdU positive cells along the half crypt-villus axis was then scored in 50 half crypt-villi per mouse, n=4 (number of mice per cohort) as well as the number of BrdU positive cells in tissues that had received both a 2 hour and a 24 hour pulse of BrdU.

There was no significant difference between the number of BrdU positive cells per crypt-villus in Cdh1$^{fl/+}$ tissue compared to WT in both mice that had received a 2 hour and a 24 hour pulse of BrdU (Figure 7.11) (p values >0.05, Mann Whitney U test). The most frequently labeled positions of BrdU positive cells after a 2 hour and a 24 hour pulse of BrdU could be visualised by plotting the cumulative frequency of BrdU positive cells at each position along the crypt-villus axis, the resultant curves for Cdh1$^{fl/+}$ and WT positioning could then be compared to each other statistically using the Kolmologrov-

178

Smirnov test. The cumulative frequency plot of the position of BrdU positive cells after a 2 hour pulse of BrdU revealed overall lower positioning of cycling cells in $Cdh1^{fl/+}$ crypts compared to WT (Figure 7.12, upper panel) (p value <0.001, Kolmologrov-Smirnov test). The cumulative frequency plot of the position of BrdU positive cells after 24 hours allows analysis of the migration of the BrdU labeled cells up the crypt villus axis (as BrdU is only bioavailable for 2 hours, so only the cells labeled within the 2 hour period will remain labeled). After a 24 hour pulse of BrdU the cumulative frequency curve for $Cdh1^{fl/+}$ tissue was not significantly shifted from the WT curve (p value >0.05, Kolmologrov-Smirnov test), so BrdU labeled cells are found in the same positions in $Cdh1^{fl/+}$ tissue as WT tissue. These data suggest that the intestinal epithelial cells in $Cdh1^{fl/+}$ tissue migrate faster up the crypt villus axis, given that after a 2 hour pulse of BrdU labeled cells are found in significantly lower positions in the crypt compared to WT tissue. However, after 24 hours the cumulative positions of BrdU labeled cells are not significantly different from the positions of BrdU positive cells in WT tissue, suggesting that the cells must migrate faster to maintain normal cell positioning.

### 7.2.9 Apoptosis frequently occurs in the lower portion of the crypt in $Cdh1^{fl/+}$ mice

Quantification of the cumulative positioning of BrdU labeled cells after a 2 hour pulse of BrdU revealed that the cycling cells were frequently found at lower positions in the crypt compared to WT tissue (Figure 7.12). This finding could not be explained by shortening of the crypt, as crypt cell scoring revealed no changes in the number of cells per crypt compared to WT tissue (section 7.2.7). However, heterozygous loss of E-cadherin enhances the level of apoptosis in the crypt as described in section 7.2.6. Similarly to scoring the position of BrdU labeled cells, the position of caspase 3 positive cells along the crypt length was scored in $Cdh1^{fl/+}$ tissue. This scoring revealed that the positions that were most frequently occupied by caspase 3 positive apoptotic cells (cell positions 5-7), were also the most frequent positions to be occupied by BrdU labeled cycling cells (Figure 7.13). There are two possible hypotheses to explain why BrdU positive cells are found lower in the crypt in $Cdh1^{fl/+}$ mice. The first being that the proliferating cells are actively migrating downwards in order to compensate for the frequent loss of cells via apoptosis in the lower portion of the crypts, therefore those positions will also frequently be labeled by BrdU. The second possibility is that as there are frequently more instances of apoptosis at these positions in the crypt, therefore cells undergoing proliferation are also frequently found in this position to compensate

for a loss of cells. This in turn would result in a higher cumulative frequency of BrdU positive cells being found in the lower portion of the crypt.
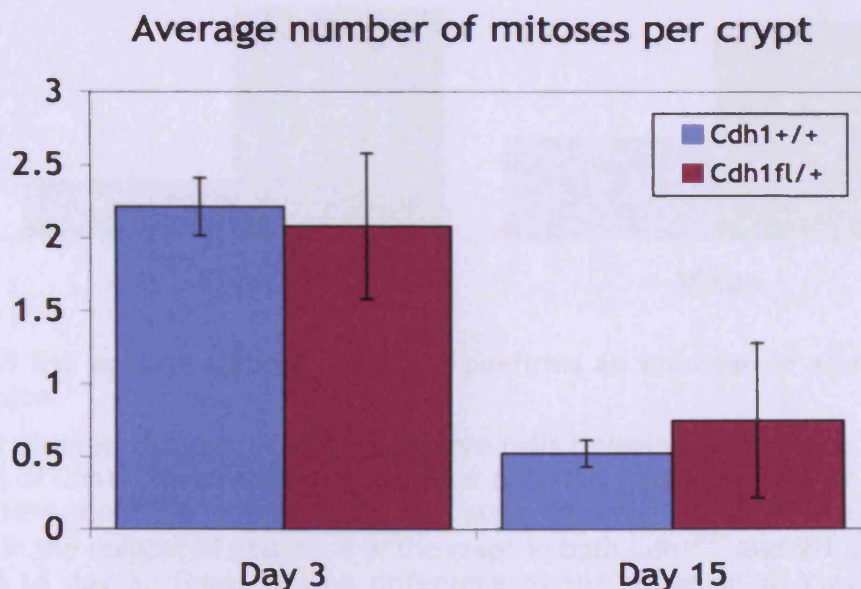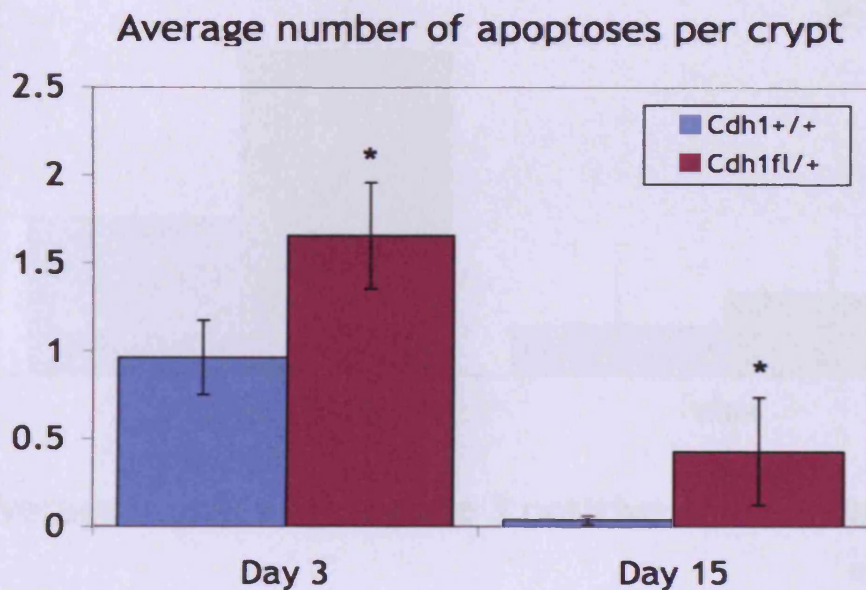




**Figure 7.8 Heterozygous E-cadherin loss increases the number of apoptotic bodies per half crypt compared to WT, but does not effect the number of mitotic figures**

Scoring of apoptotic bodies in H&E stained sections revealed an increase in Cdh1$^{fl/+}$ tissue compared to WT at both day 3 and day 15 post induction (* p values 0.0404 and 0.0383 respectively, n≥3, Mann Whitney U test). However, there was an overall decrease in the level of apoptosis at day 15 compared to day 3 post induction. Scoring of mitoses revealed no changes between Cdh1$^{fl/+}$ and WT tissue. Error bars indicate standard deviation.

## Average number of caspase 3 positive cells at day 3
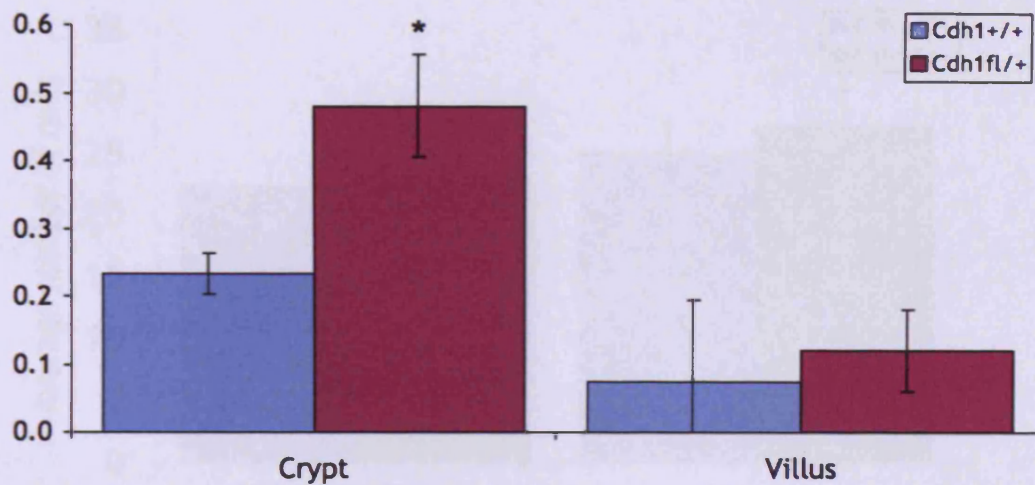


## Average number of caspase 3 positive cells at day 15
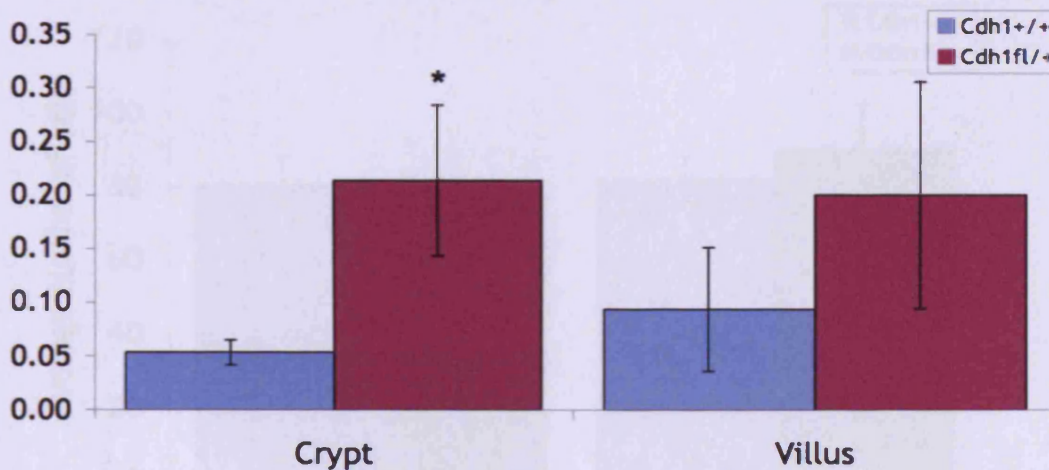


**Figure 7.9 IHC against cleaved caspase 3 confirms an increase in apoptotic cells in Cdh1$^{fl/+}$ mice**

Scoring of cleaved caspase 3 (Asp175) positive cells revealed an increase in apoptosis in the crypts of Cdh1$^{fl/+}$ mice compared to WT at both day 3 and day 15 post induction (*, p values 0.0404 and 0.0383 respectively, n≥3, Mann Whitney U test). There was an overall decrease in the number of apoptosis in the crypt in both Cdh1$^{fl/+}$ and WT tissue at day 15 compared to day 3. There was no difference in the presence of cleaved caspase 3 positive cells in the villi (p values 0.1914 and 0.092 respectively, n≥3, Mann Whitney U test). Error bars indicate standard deviation.

**Average number of cells per half crypt**

**Average number of cells per half villus**
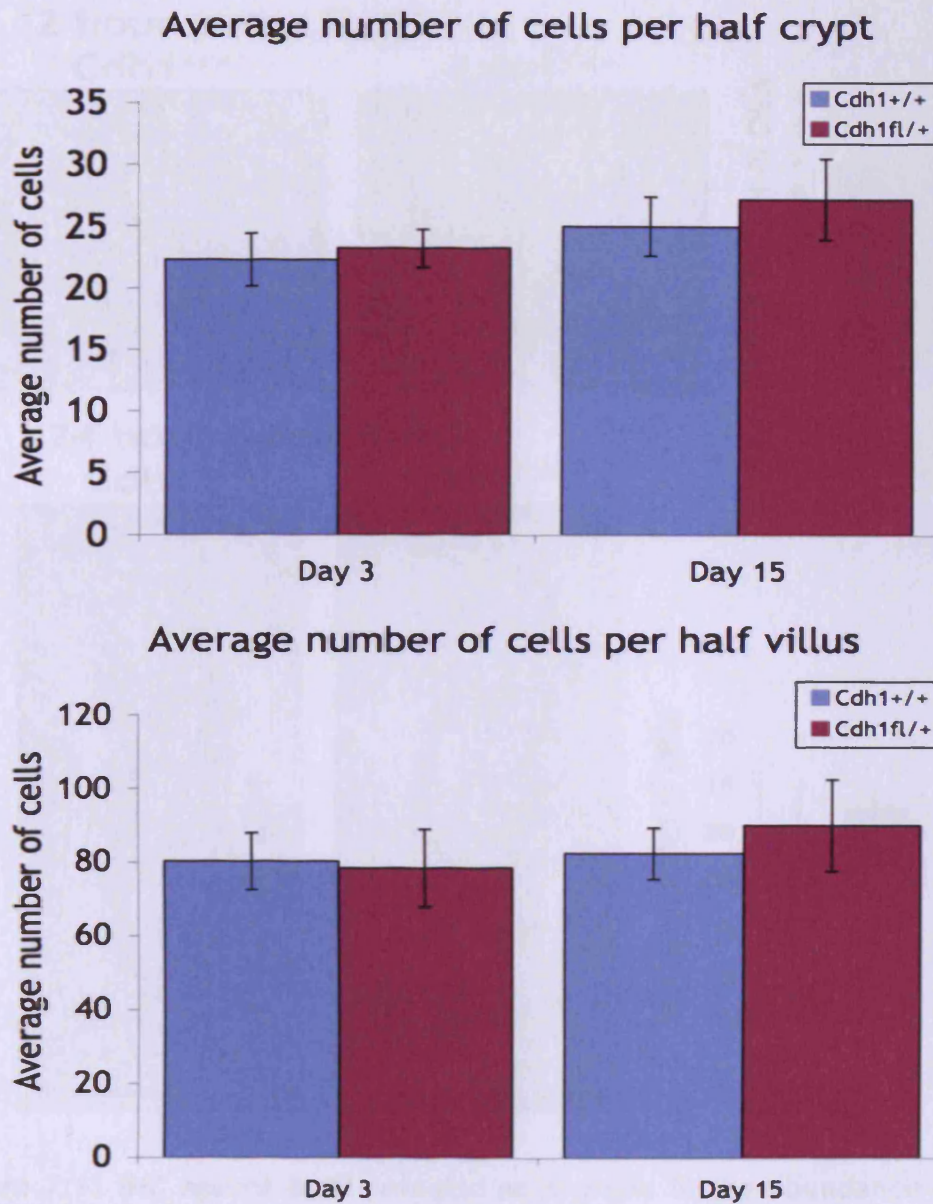
**Figure 7.10 Heterozygous E-cadherin loss had no effect on the number of cells per half crypt-villus**

Despite a significant increase in apoptosis in Cdh1$^{fl/+}$ mice, the number of cells present per half crypt and half villus in Cdh1$^{fl/+}$ tissue was not significantly altered from WT tissue at day 3 and day 15 post induction (p values >0.05, n≥3, Mann Whitney U test). Error bars indicate standard deviation.

**A   2 hour pulse BrdU**
Cdh1$^{+/+}$          Cdh1$^{fl/+}$

**B   24 hour pulse BrdU**
Cdh1$^{+/+}$          Cdh1$^{fl/+}$

**Figure 7.11 IHC against BrdU revealed no changes in the abundance of cells going through S phase in Cdh1$^{fl/+}$ mice**

(A, Left panel) IHC against BrdU was carried out on small intestinal tissue samples from mice that had been administered with a pulse of BrdU at 2 hours prior to sacrifice, IHC revealed the position of cells that had incorporated BrdU. Scale bars represent 50μm. (A, Right panel) BrdU positive cells were scored per half crypt of mice that had been administered with a 2 hour pulse of BrdU. Scoring revealed no changes in the abundance of BrdU positive cells in Cdh1$^{fl/+}$ compared to WT tissues (p value >0.05, n≥3, Mann Whitney U test). Error bars indicate standard deviation. (B, Left panel) IHC against BrdU in mice that had been administered with BrdU 24 hours prior to sacrifice. Staining reveals the position BrdU labeled cells have migrated to after 24 hours. Scale bars represent 100μm. (B, Right panel) BrdU positive cells were also scored per half crypt-villus of mice after 24 hours. Scoring revealed no changes in the abundance of BrdU positive cells in Cdh1$^{fl/+}$ compared to WT tissues (p value >0.05, n≥3, Mann Whitney U test). Error bars indicate standard deviation.

## 2 hour pulse of BrdU

## 2-24 hour pulse of BrdU
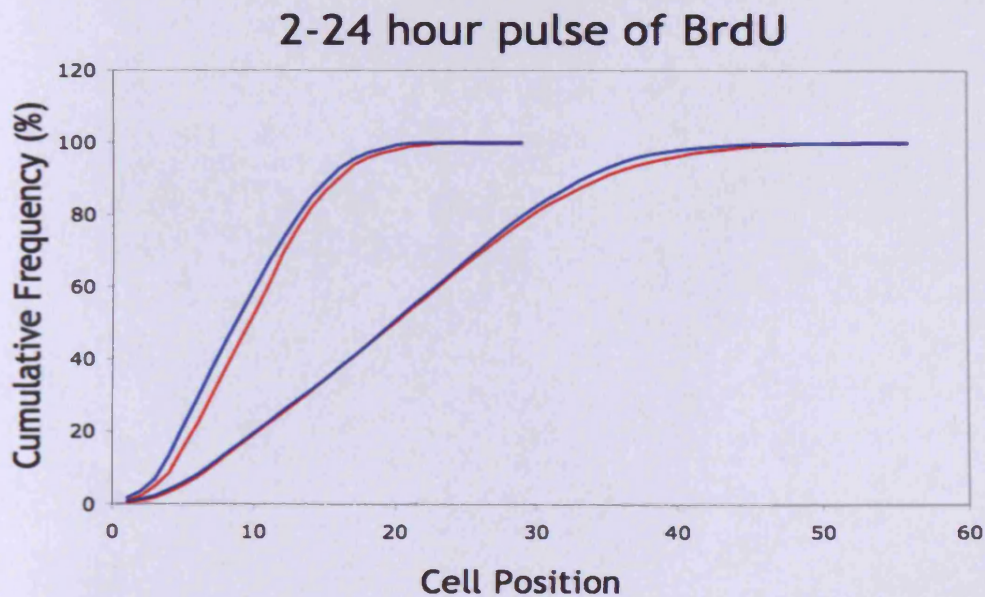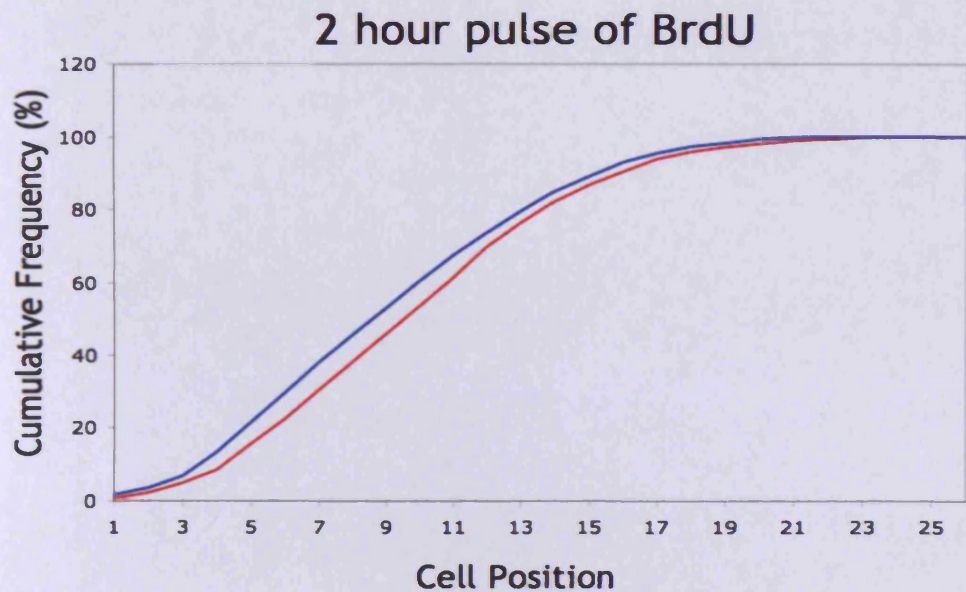
Figure 7.12 Cycling cells occupy lower positions in the crypt in Cdh1$^{fl/+}$ mice compared to WT

Key: blue line - Cdh1$^{fl/+}$, red line - WT.
(Upper panel) Cumulative frequency plot of the average position of BrdU labeled cells after a 2 hour pulse of BrdU. The cumulative frequency curve of Cdh1$^{fl/+}$ mice is significantly shifted from the WT curve (p value <0.001, n≥4, Kolmologrov-Smirnov test).
(Lower panel) Cumulative frequency plots of the average position of BrdU labeled cells after a 2 hour (left) and 24 hour (right) pulse of BrdU. There is no significant difference in the curves after 24 hours.

**Average number and position of BrdU and Caspase 3 positive cells along the crypt length**
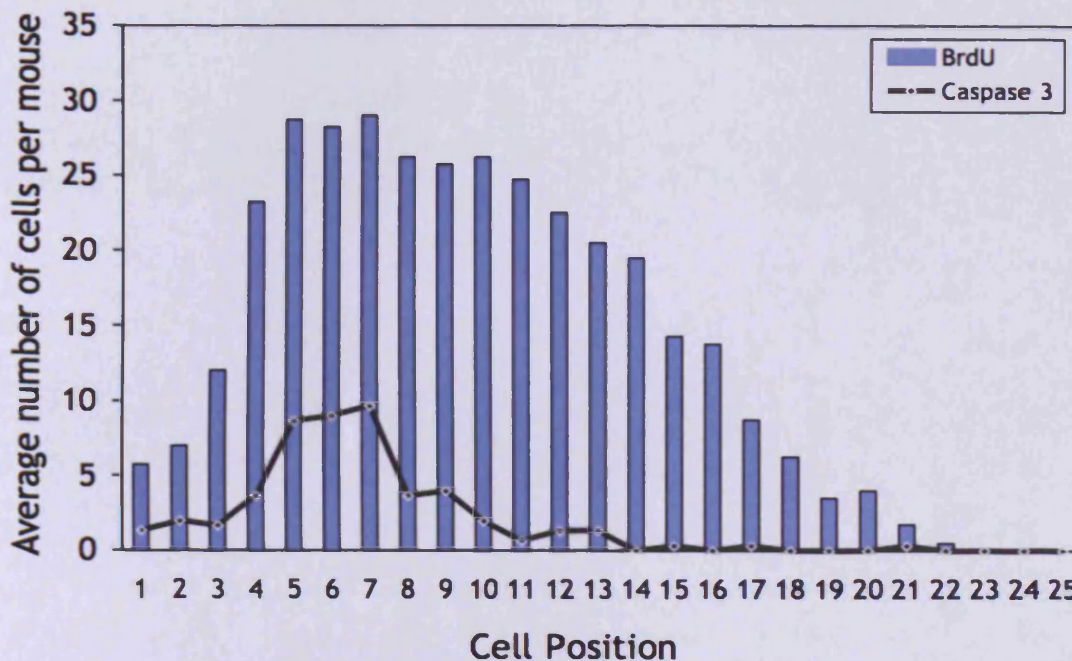
Figure 7.13 Quantification of BrdU and caspase 3 positive cell positions in Cdh1$^{fl/+}$ tissue revealed that the most frequent positions of apoptosis coincide with the most frequent positions of BrdU incorporation

*Key:*
Blue histogram bars – average number of BrdU positive cells at each position along the crypt length
Black line graph– average number of caspase 3 positive cells in each position along the crypt length
Quantification of the position of caspase 3 positive apoptotic cells and BrdU positive cells revealed that the positions in which caspase 3 positive apoptotic cells are frequently found coincides with the positions in which BrdU positive cells are frequently found.

## 7.2.10 E-cadherin loss alters the frequency of differentiated cell types in the small intestine

The effect of E-cadherin loss on the various differentiated cell types present in the small intestine was investigated by scoring quantity and localisation of each cell type in Cdh1$^{fl/fl}$ tissue and controls at day 3 post induction and Cdh1$^{fl/+}$ tissue at day 15 post induction. Methods used to visualise the various cell types were: alcian blue staining to mark mucins present in goblet cells, grimelius staining to mark argyrophilic granules in enteroendocrine cells, IHC against lysozyme present in the granules of paneth cells, and alkaline phosphastase staining to mark the apical/luminal membrane of absorptive enterocytes.

Homozygous E-cadherin loss (Cdh1$^{fl/fl}$) results in an overt loss of goblet and enteroendocrine cells (both predominantly found in the villus). In the few discernable 'crypt-villus' structures still present in Cdh1$^{fl/fl}$ tissue very few goblet cells were observed (Figure 7.14), similarly in grimelius stained small intestinal sections very few enteroendocrine cells were observed (Figure 7.15). However, due to the disordered nature of the crypt-villus like structures the abundance of differentiated cell types was not quantified. Despite obvious goblet and enteroendocrine cell loss in the remaining 'crypt-villus-like' structures the number of lysozyme positive paneth cells appeared to not differ greatly from WT tissue. However these cells were distributed throughout the 'crypt-like' structure rather than confined to the base (Figure 7.16). Alkaline phosphatase staining, which is normally expressed on the apical surface of absorptive enterocytes, appears to be very weak compared to WT tissue but the staining present is still localised to the luminal surface of the villus (Figure 7.17). This reduction in staining is likely to be caused by changes in cell morphology induced by E-cadherin loss, and loss of apical-basal polarity of the cells.

Alteration or loss of differentiated cell types in Cdh1$^{fl/fl}$ tissue is not a surprising finding, due to the severe disruption of intestinal epithelium integrity. More interestingly, changes in the abundance of some differentiated cell types occurs in tissues heterozygous for E-cadherin (Cdh1$^{fl/+}$). At day 3 post induction there were no alterations in the abundance of goblet, enteroendocrine and paneth cells (Figure 7.14, Figure 7.15, Figure 7.16). In Cdh1$^{fl/+}$ small intestinal tissue at both day 3 and day 15 post induction (images not shown for tissue taken at day 15 post induction) alkaline phosphatase remained localised to the luminal surface of enterocytes (Figure 7.17). However, at day 15 post induction there was a significant reduction in both goblet cells (5 ± 0.22 cells in Cdh1$^{fl/+}$ tissue compared to 6 ± 0.66 cells in WT tissue) and enteroendocrine cells (0.38 ± 0.05 cells in Cdh1$^{fl/+}$ tissue compared to 0.53 ± 0.05 cells

in WT tissue), (p values <0.05, n≥3, Mann Whitney U test) (Figure 7.14, Figure 7.15). However, there were no alterations in the number of paneth cells per crypt (p value = 0.5, n≥3, Mann Whitney U test) (Figure 7.16).

## Average number of goblet cells
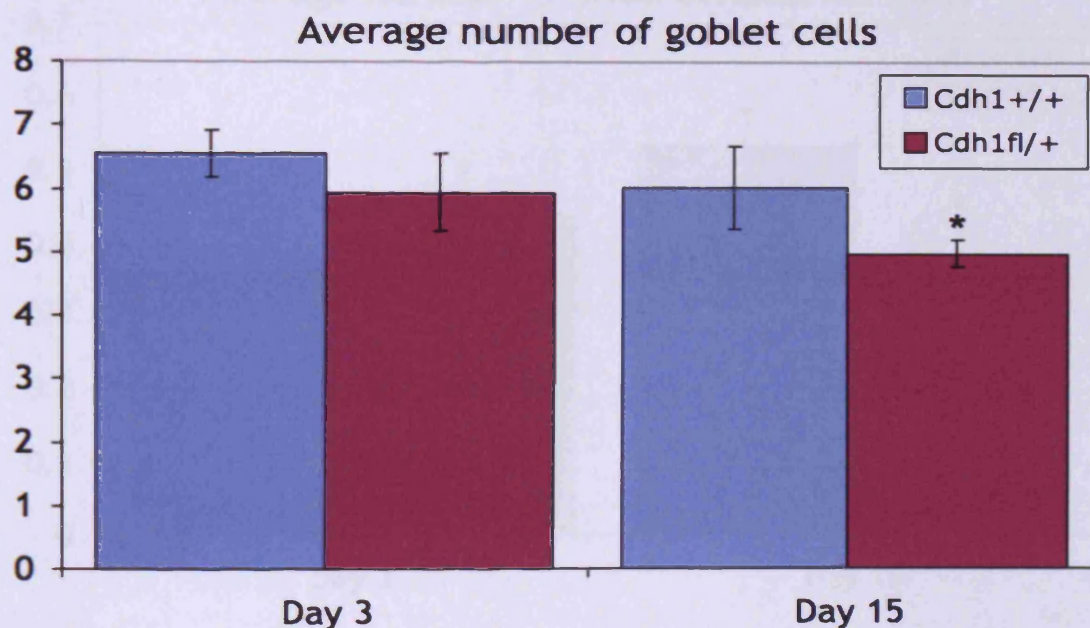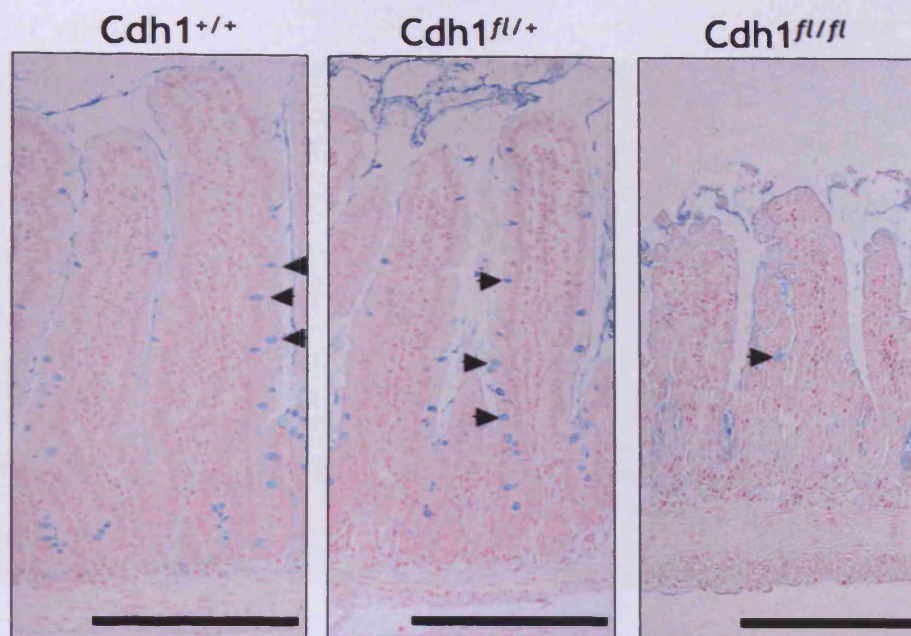
**Figure 7.14 Loss of goblet cells is evident in Cdh1$^{fl/fl}$ and Cdh1$^{fl/+}$ mice**

Small intestinal tissue sections from animals sacrificed at day 3 post induction were stained with alcian blue in order to visualise mucins present in goblet cells (images are of tissue from day 3 post induction). Scale bars represent 200µm. There was little evidence of goblet cells in Cdh1$^{fl/fl}$ tissue compared to control and WT tissue. There appeared to be no overt changes in goblet cell number between Cdh1$^{fl/+}$ and WT tissue, which was confirmed by goblet cell scoring per half crypt-villus at day 3 post induction. However, there was a significant decrease in the number of goblet cells per half crypt-villus in Cdh1$^{fl/+}$ tissue compared to WT tissue at day 15 post induction (*, p value 0.0404, n≥3, Mann Whitney U test). Error bars indicate standard deviation.
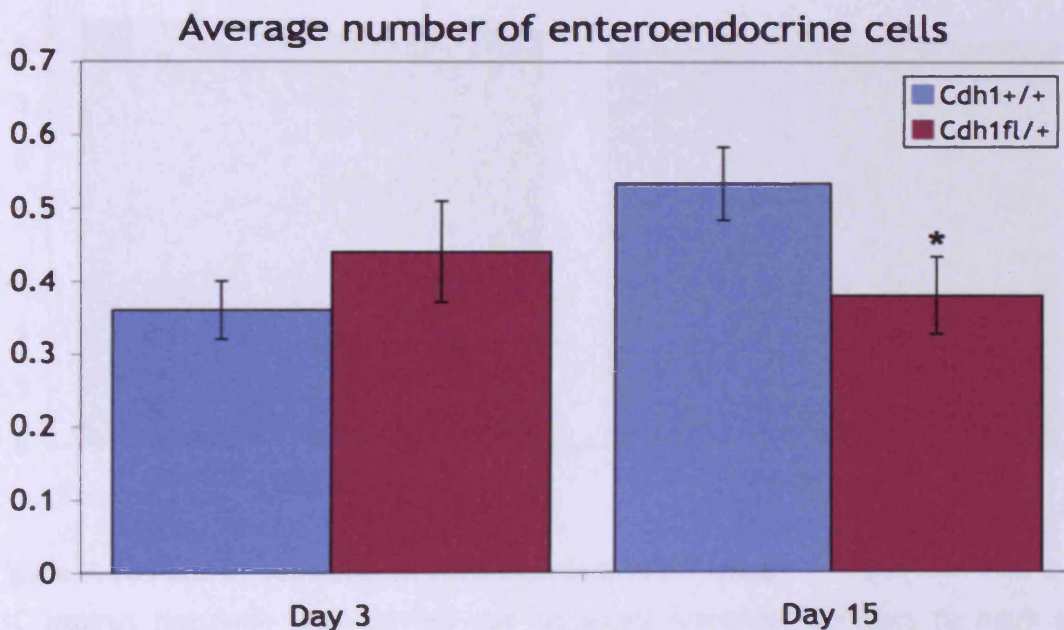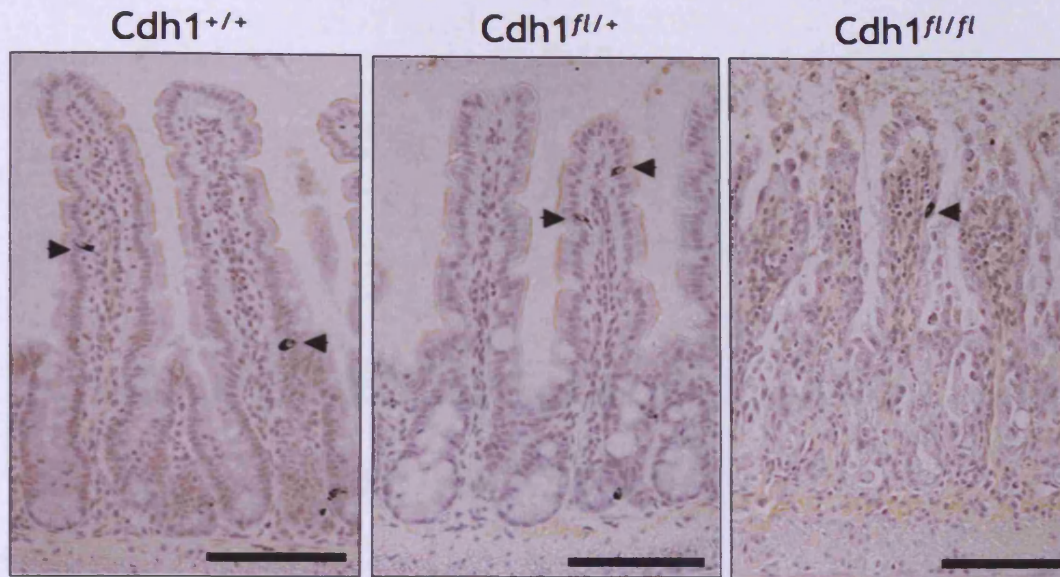
Figure 7.15 Loss of enteroendocrine cell is evident in Cdh1$^{fl/fl}$ and Cdh1$^{fl/+}$ mice

Grimelius staining was carried out on small intestinal sections to mark argyrophilic granules present in enteroendocrine cells (images are of tissue from day 3 post induction). Staining on tissue from mice sacrificed at day 3 post induction revealed no overt changes between Cdh1$^{fl/+}$ and WT tissue, but in the 'crypt-villus like' structures remaining in Cdh1$^{fl/fl}$ tissue there appeared to be a reduction of this cell type. Scale bars represent 100μm. Scoring of enteroendocrine cells at day 3 post induction in Cdh1$^{fl/+}$ and WT tissue revealed no changes, but a significant decrease in the abundance of enteroendocrine cells in Cdh1$^{fl/+}$ tissue compared to WT was observed at day 15 post induction (*, p value 0.0404, n≥3, Mann Whitney U test). Error bars indicate standard deviation.

Cdh1<sup>+/+</sup>     Cdh1<sup>fl/+</sup>     Cdh1<sup>fl/fl</sup>

## Average number of paneth cells
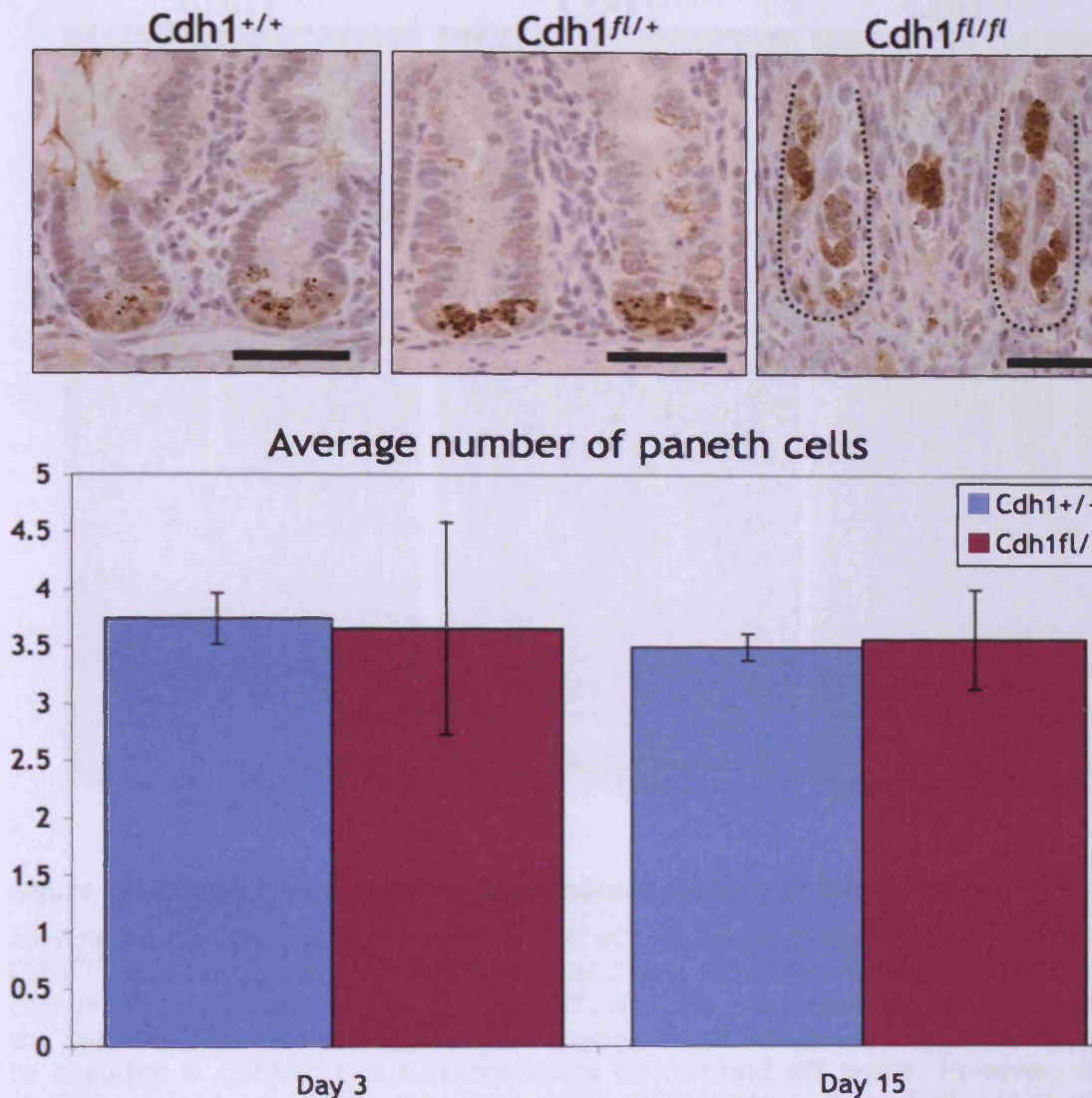
**Figure 7.16 Paneth cells are mislocalised in Cdh1$^{fl/fl}$ mice**

IHC against lysozyme was carried out on small intestinal sections to mark granules present in paneth cells from mice sacrificed at day 3 and day 15 post induction (images are of tissue from day 3 post induction). Staining revealed that paneth cells were confined to the base of the crypt in Cdh1$^{fl/+}$ mice at day 3 and day 15 post induction, but homozygous loss of E-cadherin (Cdh1$^{fl/fl}$) causes mislocalisation of the paneth cells. Dashed line indicates the remaining 'crypt-like' structures present in Cdh1$^{fl/fl}$ tissue. Scale bars represent 50μm. Scoring of paneth cells revealed no alterations in the number of paneth cells per crypt in Cdh1$^{fl/+}$ mice at day 3 and day 15 post induction (p values >0.05, n≥3, Mann Whitney U test). Error bars indicate standard deviation.

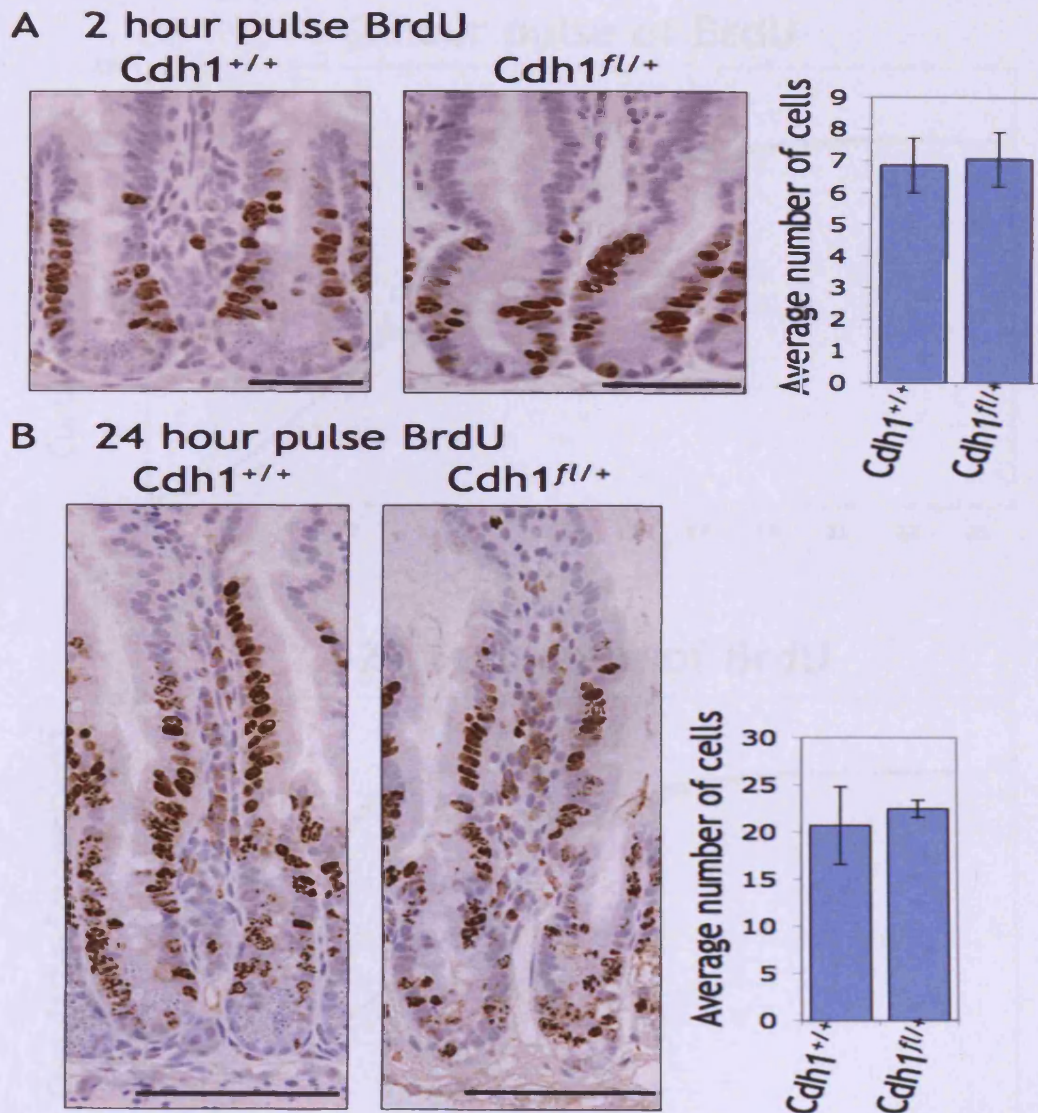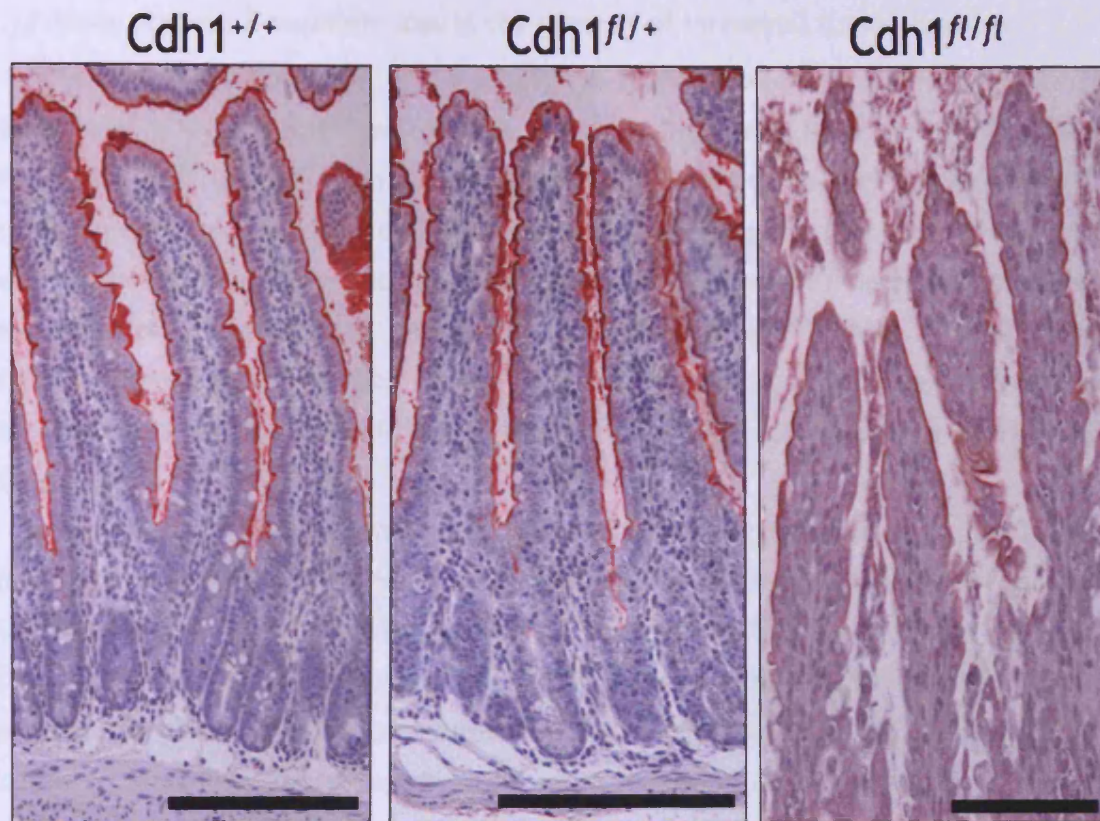**Figure 7.17 Reduction in alkaline phosphatase staining in Cdh1$^{fl/fl}$ mice**

Alkaline phosphatase staining was carried out on small intestinal tissue sections from Cdh1$^{fl/fl}$ mice and controls sacrificed at day 3 post induction. Staining revealed no overt changes in Cdh1$^{fl/+}$ tissue compared to WT, alkaline phosphatase remained localised to the apical surface of enterocytes. The abundance of alkaline phosphatase appeared to be depleted in Cdh1$^{fl/fl}$ tissue compared to control and WT tissue. However, the little staining present remained localised to the luminal surface of the 'villus-like' structure. Scale bars represent 200µm for Cdh1$^{fl/+}$ and WT images and 100µm for the Cdh1$^{fl/fl}$ image.

### 7.2.11 Heterozygous E-cadherin loss in the context of intestinal tumourigenesis

To investigate the role of E-cadherin in the development of invasive intestinal tumours, *Villin*CreER$^T$ Cdh1$^{fl/+}$ mice were crossed with Apc$^{fl/+}$ Pten$^{fl/fl}$ mice to generate *Villin*CreER$^T$ Apc$^{fl/+}$ Pten$^{fl/fl}$ Cdh1$^{fl/+}$ mice (herein referred to as Apc$^{fl/+}$ Pten$^{fl/fl}$ Cdh1$^{fl/+}$). Cdh1$^{fl/fl}$ mice were not used to investigate E-cadherin loss in this context due to the severe intestinal phenotype and rapid morbidity at 3-4 days after induction observed in these mice. As described in chapter 4, *Villin*CreER$^T$ Apc$^{fl/+}$ Pten$^{fl/fl}$ mice develop intestinal adenocarcinomas that invade into the intestinal submucosa, so these mice were used as a model in which to investigate the role of E-cadherin deficiency in tumourigenesis.

Apc$^{fl/+}$ Pten$^{fl/fl}$ Cdh1$^{fl/+}$ mice had a median survival time of 51 days post induction compared to Apc$^{fl/+}$ Pten$^{fl/fl}$ mice that had a median survival time of 81 days post induction. Analysis of the survival data revealed no significant difference between to the two cohorts. However, visual inspection of the survival curves does raise the possibility that there may be two subsets of mice within this cohort, one subset which succumb to morbidity more rapidly than controls (prior to 100 days), and one which show extended survival (Figure 7.18). The total number of tumours in the small intestine was determined by examination of methacarn fixed tissue. Overall, there was no significant difference in the number of tumours present in Apc$^{fl/+}$ Pten$^{fl/fl}$ Cdh1$^{fl/+}$ mice compared to the control cohort (Figure 7.18, B). However, when this data was plotted against mouse survival time there appeared to be a negative correlation between the number of tumours present along the length of the small intestine and survival time (Figure 7.18, C). Thus, suggesting that the Apc$^{fl/+}$ Pten$^{fl/fl}$ Cdh1$^{fl/+}$ mice that survived longer had less small intestinal tumours.

The grade of the tumours in each of the Apc$^{fl/+}$ Pten$^{fl/fl}$ Cdh1$^{fl/+}$ mice was determined using the criteria outlined in the methods section 2.6.5. Tumour grading revealed that Apc$^{fl/+}$ Pten$^{fl/fl}$ Cdh1$^{fl/+}$ mice bore significantly more microadenomas than Apc$^{fl/+}$ Pten$^{fl/fl}$ mice (p value = 0.0155, n$\geq$6, Mann Whitney U test). However, despite E-cadherin loss being associated with tumour invasiveness, there was only a marginal increase in the number of invasive tumours (grade 3 and 4) compared to the control cohort, which was not significantly altered from the control cohort (Figure 7.19, A). The grading data obtained was then separated according to the two groups that were suggested from the survival curve in Figure 7.18, A (i.e. the group of mice that succumbed to morbidity earlier than controls, and group that survived longer then controls), and compared to the grade distribution of tumours observed in Apc$^{fl/+}$ Pten$^{fl/fl}$ mice. These data revealed that the subset of Apc$^{fl/+}$ Pten$^{fl/fl}$ Cdh1$^{fl/+}$ mice that

succumbed to rapid morbidity had significantly higher numbers of non invasive benign lesions compared to Apc$^{fl/+}$ Pten$^{fl/fl}$ control mice (p value = 0.0096, n≥6, Mann Whitney U test, Figure 7.19, B). Interestingly, the subset of mice in Apc$^{fl/+}$ Pten$^{fl/fl}$ Cdh1$^{fl/+}$ that lived longer then the control cohort had a similar tumour grade distribution to the Apc$^{fl/+}$ Pten$^{fl/fl}$ controls (Figure 7.19, B). In conclusion, there are no significant changes in the survival time of Apc$^{fl/+}$ Pten$^{fl/fl}$ Cdh1$^{fl/+}$ mice after induction, or in the number and invasiveness of tumours these mice possess compared to the control cohort. However, evidence from the survival curve and the scatterplot of tumour number vs survival time suggests that there may be two subsets of mice within the Apc$^{fl/+}$ Pten$^{fl/fl}$ Cdh1$^{fl/+}$ cohort that have differing phenotype severities

IHC against E-cadherin was carried out on tumour tissue from Apc$^{fl/+}$ Pten$^{fl/fl}$ Cdh1$^{fl/+}$ mice to determine if the remaining allele of Cdh1 was still present in the tumours. E-cadherin staining revealed no obvious changes in E-cadherin expression in Apc$^{fl/+}$ Pten$^{fl/fl}$ Cdh1$^{fl/+}$ mice compared to controls. E-cadherin also remained localised to the basolateral membrane of the epithelial component of the tumours as observed in the control tumours (Figure 7.20).
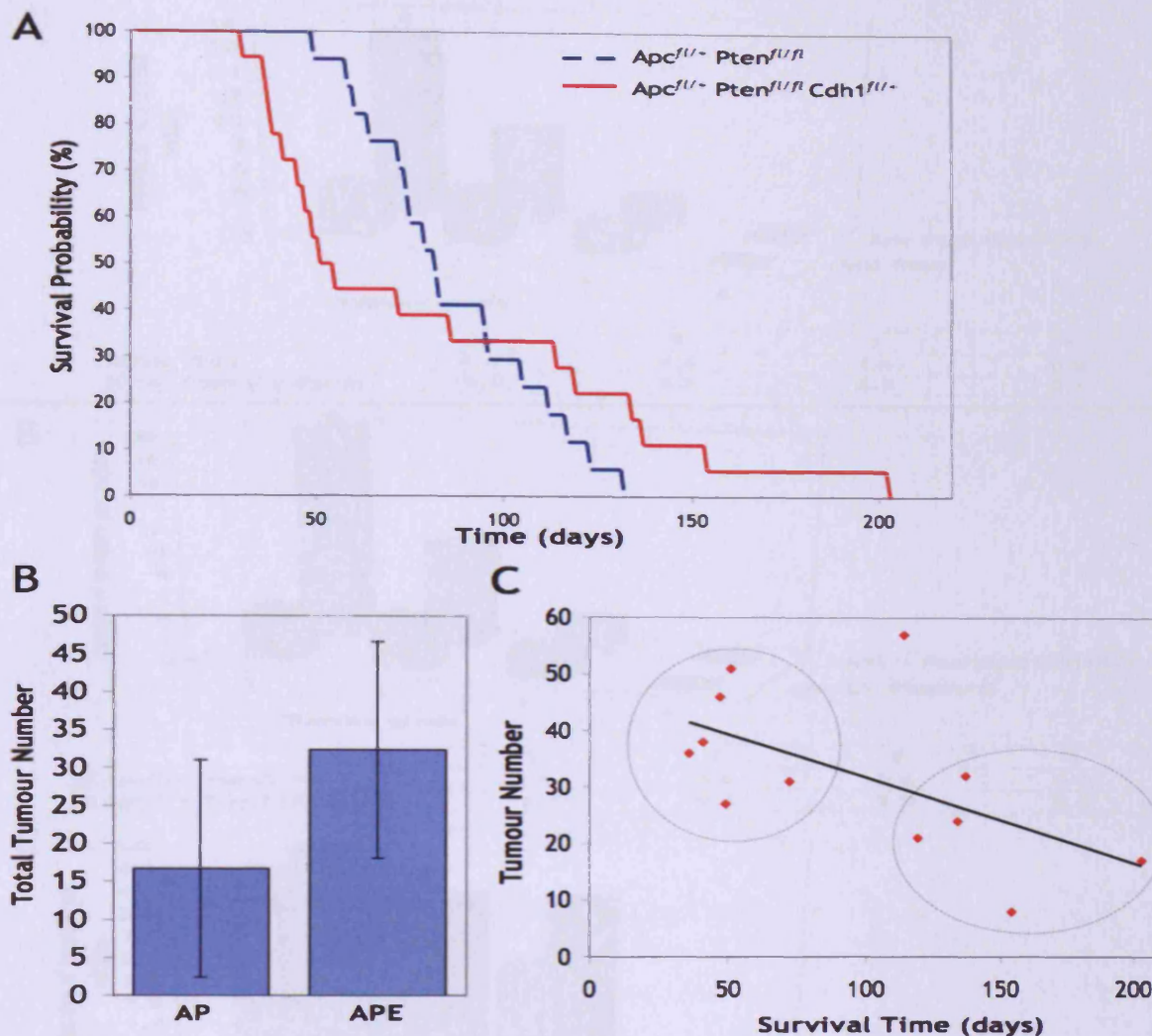
**Figure 7.18 The survival plot of Apc$^{fl/+}$ Pten$^{fl/fl}$ Cdh1$^{fl/+}$ mice appeared to be biphasic**

(A) Key: blue dashed line - Apc$^{fl/+}$ Pten$^{fl/fl}$ cohort, red solid line - Apc$^{fl/+}$ Pten$^{fl/fl}$ Cdh1$^{fl/+}$ cohort. Apc$^{fl/+}$ Pten$^{fl/fl}$ Cdh1$^{fl/+}$ mice appeared to have a biphasic survival profile, more than 50% of the cohort had a shorter lifespan than the Apc$^{fl/+}$ Pten$^{fl/fl}$ control cohort. However, a subset of the Apc$^{fl/+}$ Pten$^{fl/fl}$ Cdh1$^{fl/+}$ cohort had a longer lifespan than the control cohort. Statistical analysis revealed P values of 0.770 (Log-Rank test) and 0.205 (Wilcoxon test).

(B) Key: AP – Apc$^{fl/+}$ Pten$^{fl/fl}$ cohort, APE – Apc$^{fl/+}$ Pten$^{fl/fl}$ Cdh1$^{fl/+}$ cohort. There was no statistical difference between the total number of small intestinal tumours in the Apc$^{fl/+}$ Pten$^{fl/fl}$ Cdh1$^{fl/+}$ cohort compared to the control cohort, (p value = 0.0646, n≥3, Mann Whitney U test).

(C) A scatterplot of the total number of small intestinal tumours in Apc$^{fl/+}$ Pten$^{fl/fl}$ Cdh1$^{fl/+}$ mice against mouse survival time post induction revealed a trend towards less tumours as mouse survival increases (as indicated by black solid regression line [$R^2$ = 0.3356]). There also appeared to be two distinct groups (as indicated by dashed line circles). These data suggest that the distinct group of longer lived Apc$^{fl/+}$ Pten$^{fl/fl}$ Cdh1$^{fl/+}$ mice possess less small intestinal tumours than the shorter surviving group.

**A**

| | 1 | 2 | 3 | 4 |
|---|---|---|---|---|
| ■ Apc Pten | 4.4 | 4.6 | 2.6 | 0.0 |
| ■ Apc Pten Ecadherin | 16.3 | 8.2 | 2.8 | 0.1 |

**B**

| | 1 | 2 | 3 | 4 |
|---|---|---|---|---|
| ■ Apcfl/+ Ptenfl/fl | 4.4 | 4.6 | 2.6 | 0.0 |
| ■ Apcfl/+ Ptenfl/fl Cdh1fl/+ | 19.7 | 9.4 | 2.9 | 0.2 |

**C**

| | 1 | 2 | 3 | 4 |
|---|---|---|---|---|
| ■ Apcfl/+ Ptenfl/fl | 4.4 | 4.6 | 2.6 | 0.0 |
| ■ Apcfl/+ Ptenfl/fl Cdh1fl/+ | 4.7 | 3.7 | 3.7 | 0.0 |
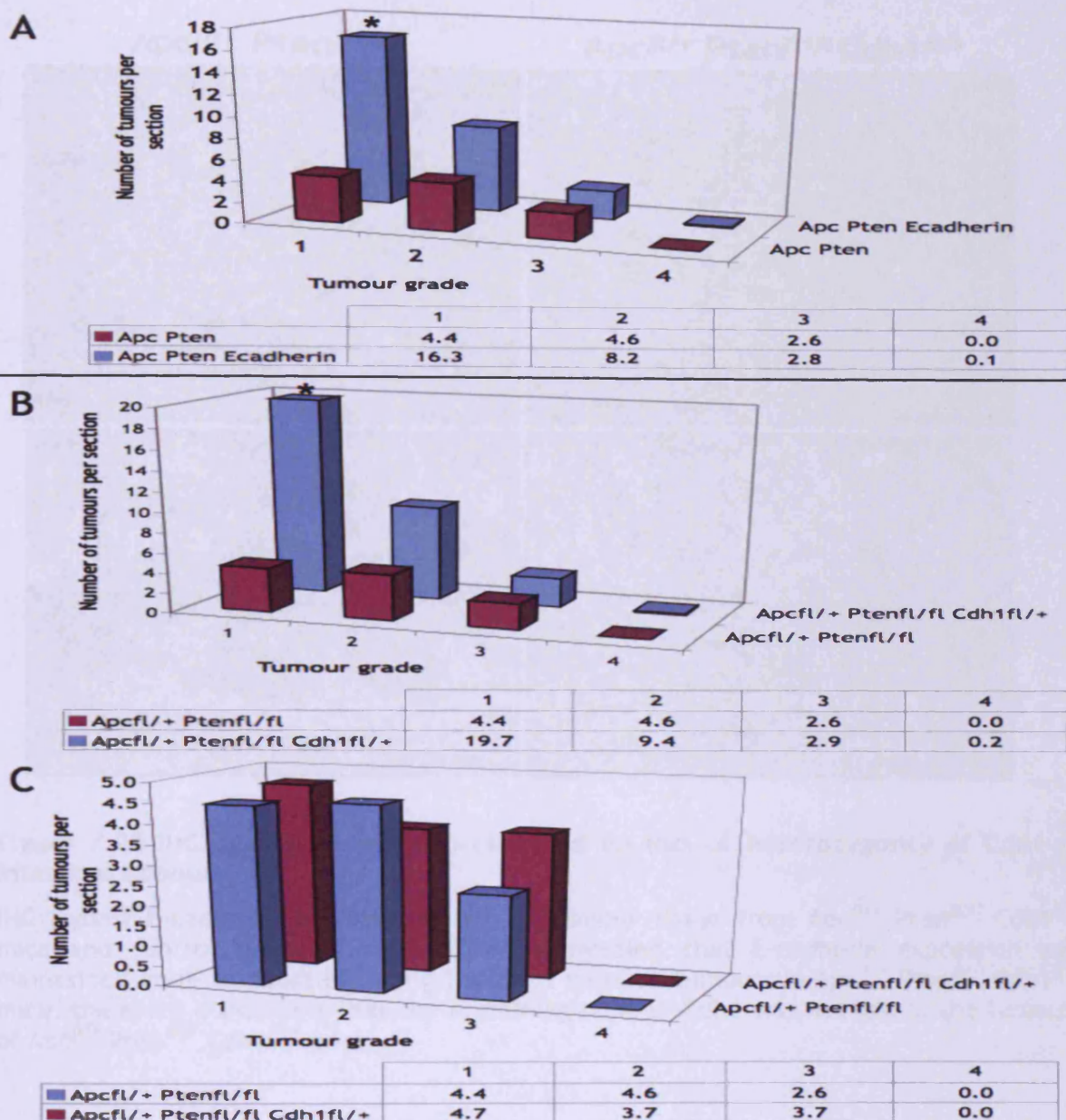
**Figure 7.19 Tumour grading revealed a substantial increase in the average number of smaller non invasive lesions in the majority of $Apc^{fl/+}$ $Pten^{fl/fl}$ $Cdh1^{fl/+}$ mice**

Key: grade 1 – microadenoma, grade 2 – adenoma, grade 3 – adenocarcinoma with submucosal invasion, grade 4 – adenocarcinoma with invasion through smooth muscle wall and underlying serosa (A) Tumour grading for the total in $Apc^{fl/+}$ $Pten^{fl/fl}$ $Cdh1^{fl/+}$ cohort. There were significantly more microadenomas present in $Apc^{fl/+}$ $Pten^{fl/fl}$ $Cdh1^{fl/+}$ mice compared to controls (*, p value = 0.0155, n≥6, Mann Whitney U test)
(B) Short lived $Apc^{fl/+}$ $Pten^{fl/fl}$ $Cdh1^{fl/+}$ mice possessed significantly higher numbers of microadenomas (*, p value = 0.0096, n≥6, Mann Whitney U test) in the small intestine compared to $Apc^{fl/+}$ $Pten^{fl/fl}$ control mice. A higher abundance of adenomas were observed in $Apc^{fl/+}$ $Pten^{fl/fl}$ $Cdh1^{fl/+}$ mice, however this was not significant (p value = 0.1425, n≥6, Mann Whitney U test). Heterozygous loss of E-cadherin causes a marginal increase in the number of invasive adenocarcinomas observed. (n = 12).
(C) Long lived $Apc^{fl/+}$ $Pten^{fl/fl}$ $Cdh1^{fl/+}$ mice had a similar average number of tumours per section to the $Apc^{fl/+}$ $Pten^{fl/fl}$ controls. (n = 6).

Apc$^{fl/+}$ Pten$^{fl/fl}$      Apc$^{fl/+}$ Pten$^{fl/fl}$ Cdh1$^{fl/+}$
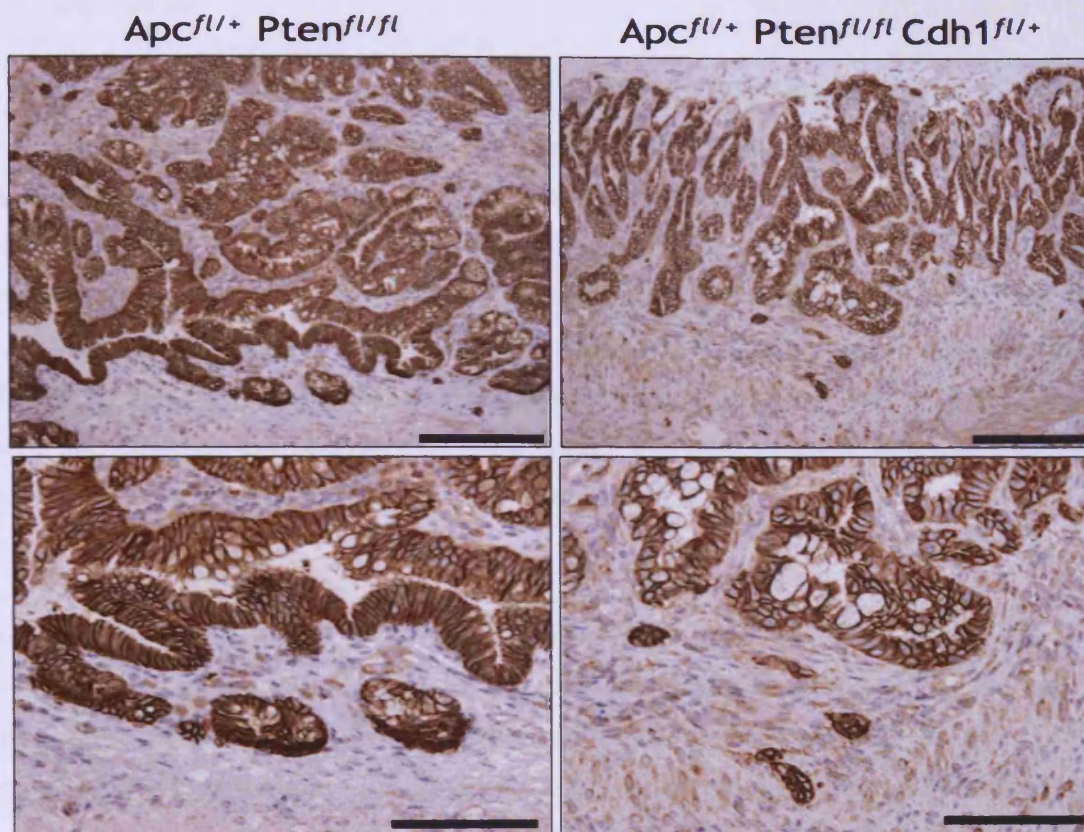
**Figure 7.20 IHC against E-cadherin revealed no loss of heterozygosity of Cdh1 in intestinal tumours**

IHC against E-cadherin was carried out on tumour tissue from Apc$^{fl/+}$ Pten$^{fl/fl}$ Cdh1$^{fl/+}$ mice and control tumour tissue. Staining revealed that E-cadherin expression was maintained in all tumours including the most invasive tumours in Apc$^{fl/+}$ Pten$^{fl/fl}$ Cdh1$^{fl/+}$ mice, therefore concluding that the remaining copy of Cdh1 was not lost in the tumours of Apc$^{fl/+}$ Pten$^{fl/fl}$ Cdh1$^{fl/+}$ mice.

## 7.3 Discussion

### 7.3.1 Conditional homozygous E-cadherin loss in the intestine is inviable in adult mice

Intestinal specific conditional recombination of the Cdh1 gene was induced in adult mice around 6-12 weeks of age. Recombination of loxP sites removed exons 4-15, which results in a null allele. No differences in health status between $Cdh1^{fl/fl}$, $Cdh1^{fl/+}$ and WT were evident before and immediately after induction. However, by days 3-4 post induction $Cdh1^{fl/fl}$ mice had become dehydrated and hunched so were sacrificed (Figure 7.1), whilst $Cdh1^{fl/+}$ and WT mice remained healthy. When dissected $Cdh1^{fl/fl}$ mice had little to no contents in their small intestines, suggesting that morbidity in these mice was due to dehydration and malnutrition.

### 7.3.2 Homozygous loss of E-cadherin causes loss of epithelial sheet integrity

When examined histologically, the small intestines of $Cdh1^{fl/fl}$ mice had lost all discernible mucosal structure with the remainder of shortened crypt-villus structures being engulfed by stromal cells (Figure 7.2). The catastrophic loss of mucosal structure is likely to render the organ useless, as the lack of any normal crypt-villus structures means that successful absorption of nutrients and water is highly unlikely. As intestinal crypt-villus structure was difficult to distinguish, quantification of cell number, apoptosis, mitosis and cell types was not possible. It was possible to see from the H&E images that there was a loss of crypt and villus cell number, an increase in caspase 3 positive cells and loss of goblet and enteroendocrine cells.

Interestingly the remaining crypt and villus-like structures remaining in $Cdh1^{fl/fl}$ small intestine appeared to maintain expression of E-cadherin (Figure 7.3). Despite maintaining membrane localisation of E-cadherin the epithelial cells appeared to have lost uniformity compared to $Cdh1^{fl/+}$ and WT tissue, so it is likely that these cells are no longer forming sufficient cell-to-cell contacts to maintain cellular structure. It is possible at this short timepoint after knockout of Cdh1 that some intact E-cadherin protein present prior to knockout has not yet turned over, and therefore is maintaining some of the epithelial sheet integrity. E-cadherin loss is evident in cells that were being shed from the epithelial sheet, so the protein must be completely lost before the cells are shed. Some, but not all of these shedding and shed cells stained positive for cleaved caspase 3, which is only found in cells undergoing apoptosis. This suggests that loss of E-cadherin and loss of cell-to-cell contacts may induce apoptosis via anoikis. As was observed in E-cadherin stained sections, high power H&E images of the remaining epithelial structures in the small intestines of $Cdh1^{fl/fl}$ mice revealed changes in

epithelial cell morphology and loss of epithelial polarity compared to WT and Cdh1$^{fl/+}$ control tissue (Figure 7.4).


### 7.3.3 Homozygous E-cadherin loss phenotype in the colon

There appeared to be a similar but more subtle phenotype observed in the colons of Cdh1$^{fl/fl}$ mice compared to the small intestinal phenotype. There appeared to be changes in luminal epithelial cell morphology (Figure 7.6), which is accompanied by a reduction (but not loss) of E-cadherin staining (Figure 7.7). There appeared to be an overt reduction in goblet cells and an increase in the presence of stromal cells. The subtle effect nullizygosity of E-cadherin has on the colon could be due to differential effects of the knockout on different tissues. However, Cdh1$^{fl/fl}$ mice only survive 3-4 days after induction so therefore the effects of E-cadherin loss may not be evident in the colon at these early timepoints due to its slower epithelial cell turnover compared to the small intestine. The latter explanation is more likely as even at day 3 there is some evidence of epithelial cell morphology changes, and subtle colonic architecture changes. The structural differences between small intestinal and colonic tissue may also affect the outcome of the knockout, i.e. the small intestine is made up of villus projections which may be more susceptible to mechanical stress and loss of epithelial cells than the colon, where the epithelial cells are compacted and form a more smooth lining.

The findings in this chapter both confirm and contrast recently published data by Schneider et al, where they also used the VillinCreER$^T$ transgene to conditionally delete E-cadherin in the intestine using a different loxP flanked Cdh1 construct (loxP sites flanking exons 6-10). They reported that homozygous mice survived until 6 days post induction and morbidity was a result of loss of the colonic mucosa, whereas in this study morbidity was likely to be caused by disruption of the small intestinal mucosa with much lesser effects on the colonic mucosa (Schneider et al., 2010). However Schneider et al also observed loss of the small intestinal mucosa, a reduction in goblet cell number and mislocalisation of paneth cells in Cdh1$^{fl/fl}$ mice, which was also shown in this study (Schneider et al., 2010). The differences in findings could be attributed to differing Cdh1 construct as the mouse used in this study had a smaller region of the Cdh1 gene deleted compared to the Cdh1 floxed mouse used in this study. Genetic background and housing conditions could also be contributory factors to the difference in findings. The mice used in the Schneider et al study were on the C57BL/6 background and housed in specific pathogen free conditions in a closed barrier system, whereas the mice used in

this study were on a mixed background and kept in conventional conditions so are likely to harbour more pathogens.

### 7.3.4 Heterozygous loss of E-cadherin has no effect on the integrity of crypt-villus structure

Unlike Cdh1$^{fl/fl}$ mice, Cdh1$^{fl/+}$ mice were healthy until the end of the experiment (~340 days post induction). The Cdh1$^{fl/+}$ mice that were aged did not develop tumours in the small intestine or colon, which is consistent with previous observations in Cdh1$^{+/-}$ mice (Smits et al., 2000). The Cdh1$^{fl/+}$ intestines examined at day 3 and day 15 post induction revealed normal intestinal architecture (Figure 7.2, Figure 7.6) and maintenance of basolateral E-cadherin staining in both small intestine and colon (Figure 7.3, Figure 7.7). Crypt and villus cell scoring established that there were no alterations in cell number in Cdh1$^{fl/+}$ mice. Importantly this confirmed that heterozygous loss of E-cadherin does not cause an overall loss of cells from the crypt or villus.

### 7.3.5 Heterozygous loss of E-cadherin enhances levels of apoptosis

Despite there being no overall changes in crypt and villus cell number in Cdh1$^{fl/+}$ mice, there was a significant increase in the number of apoptotic bodies and caspase 3 positive cells in the small intestinal crypts of Cdh1$^{fl/+}$ mice (Figure 7.8, Figure 7.9). To compensate for an increase in apoptosis one would expect this to be accompanied by an increase in proliferation to maintain intestinal homeostasis, yet mitosis and BrdU scoring revealed no differences between Cdh1$^{fl/+}$ and WT tissue at both day 3 and day 15 post induction (Figure 7.8, Figure 7.11). Although there was not an increase in BrdU positive cells in the crypt there was a significant alteration to the cumulative positioning of BrdU positive cells along the crypt axis in Cdh1$^{fl/+}$ mice that had received a 2 hour pulse of BrdU (Figure 7.12), indicating that BrdU positive cells are found in lower positions in the crypt in Cdh1$^{fl/+}$ mice compared to WT mice. When the positions of caspase 3 apoptotic cells along the crypt axis were plotted and overlayed with BrdU labeled cell position data it was clear that the most common positions in which apoptotic cells were found were also the most common positions in which BrdU labeled cycling cells were found (Figure 7.13). These data, taken together with the finding that there is no increase in BrdU positive cells in the crypt, leads to two hypotheses:

1. BrdU positive cells are found lower in the crypt due to migration of cycling cells to occupy the crypt positions vacated by apoptotic cells. This hypothesis therefore should

lead to overall smaller crypts, which is not observed, but perhaps the difference of 1-2 cells per crypt is not sufficient to result in statistical significance.

2. The finding that apoptotic cells are consistently found in the same lower crypt positions, may result in a locally higher incidence of proliferation in these positions to compensate for the cell loss, therefore, overall resulting in more BrdU positive cells observed in these lower crypt positions, which skews the cumulative frequency curve.

The significance of high levels of apoptosis at crypt cell positions 5-7 is unclear. One possible hypothesis is when a $Cdh1^{fl/+}$ cell migrates from the stem cell compartment, commonly regarded to be at the base of the crypt (Barker et al., 2007), into the transit amplifying (TA) zone it may need to break existing cell-to-cell contacts with surrounding paneth cells (that remain in the base of the crypt) and establish new cell-to-cell adhesions with neighbouring TA cells. Heterozygosity of Cdh1 may hinder the successful formation of new cell-to-cell adhesions and therefore the anoikis apoptotic program may be initiated. A study by Hofmann et al showed anoikis of human colonic epithelial cells is prevented by the maintenance of cell-to-cell contacts. They showed that human colonic epithelial cells that maintain cell-to-cell contacts show continual activation of the PI3K and Src pathways. However, when these contacts are broken, the pathways are downregulated and the cells undergo anoikis (Hofmann et al., 2007). Therefore, these pathways may be governing apoptosis in $Cdh1^{fl/+}$ mice.

Despite alteration of BrdU labeled cell positions after a 2 hour pulse of BrdU, after 24 hours the cumulative distribution of BrdU positive cells in $Cdh1^{fl/+}$ mice was not significantly altered from the WT cumulative distribution (Figure 7.12). This finding suggests that as BrdU positive cells are found at lower cell positions in $Cdh1^{fl/+}$ mice when they are initially labeled with BrdU (after 2 hours), the intestinal epithelial cells must migrate faster up the crypt-villus axis as after 24 hours they occupy the same positions as WT cells. E-cadherin has previously been shown to impact on intestinal cell migration; Schneider et al noted that homozygous E-cadherin loss caused expansion of BrdU positive cells along the crypt-villus length after a 24 hour pulse of BrdU compared to WT control (Schneider et al., 2010) which is consistent with the finding that heterozygous E-cadherin loss promotes migration. However the phenotype of heterozygous E-cadherin loss in the Schneider et al study was not addressed. Consistent with the finding that E-cadherin loss promotes migration, Hermiston et al showed that forced expression of E-cadherin in the mouse intestine resulted in retardation of cellular migration (Hermiston et al., 1996).

### 7.3.6 Heterozygous loss of E-cadherin causes loss of differentiated cell types

Heterozygous loss of E-cadherin had no effect on the abundance and localisation of paneth, enteroendocrine and goblet cells at day 3 post induction. However, at day 3 post induction alterations in cell lineage may not be evident, as the cells in the crypt-villus have not yet fully turned over (small intestine turns over every 4-5 days). At day 15 post induction there was a significant decrease in the abundance of both goblet and enteroendocrine cells in Cdh1$^{fl/+}$ small intestinal tissue compared to WT tissue (Figure 7.14, Figure 7.15). At day 15 post induction there was no alteration in paneth cell number or localisation in Cdh1$^{fl/+}$ tissue compared to WT tissue (Figure 7.16). The effect on paneth cells may not be evident at day 15 post induction as these cells are reported to turn over every 3-8 weeks (Bjerknes and Cheng, 1981b, Ireland et al., 2005). These findings could be explained by three hypotheses:

1 – Heterozygosity of Cdh1 affects terminal differentiation of goblet and enteroendocrine cells resulting in decreased abundance of the cell lineages. This possibly occurs through alteration of the Notch pathway that controls secretory cell lineages (Stanger et al., 2005, Fre et al., 2005).

2 – Early goblet and enteroendocrine cell precursors heterozygous for Cdh1 have increased propensity to undergo apoptosis, as higher levels of apoptosis are observed in Cdh1$^{fl/+}$ mice.

3. The high level of cell death in these mice may cause stochastic loss of all cell types and this is evidenced by loss of these differentiated cell types.

The conditional E-cadherin knockout study by Schneider et al showed that by using a low recombination induction regime *Villin*CreER$^T$ Cdh1$^{fl/fl}$ mice can survive whilst maintaining some areas of E-cadherin deficient intestine, thus allowing them to study the effect of homozygous E-cadherin loss on cell lineage. They found that homozygous E-cadherin loss caused abrogation of secretory cell fate, resulting in the reduction of goblet and paneth cells and the presence of secretory precursor cells that express both goblet and paneth cell markers (Schneider et al., 2010). It is possible that the alterations in secretory cell lineages observed both in the Schneider et al study and the findings in this study could be attributed to alterations in the Notch pathway. It has been shown that constitutive activation of the Notch pathway in mice leads to alterations in secretory cell fate decisions leading to loss of secretory cell types such as

goblet and enteroendocrine cells (Fre et al., 2005, Stanger et al., 2005). As Notch signalling relies on juxtacrine signalling abrogation of cell-to-cell adhesions by loss of E-cadherin expression may present a mechanism in which Notch signalling is altered.

The reduction of goblet cells and enteroendocrine cells may also be linked to the high incidence of apoptosis in $Cdh1^{fl/+}$ mice. Increased apoptosis may cause a stochastic loss of all cell types resulting in lower numbers of differentiated cell types compared to WT tissue. It may also be possible that apoptosis may be more selective and goblet and enteroendocrine precursor cells may be more susceptible to apoptosis in $Cdh1^{fl/+}$ mice.

### 7.3.7 Heterozygous E-cadherin does not promote tumour progression

$Cdh1^{fl/+}$ mice were crossed with an invasive intestinal tumour model, $VillinCreER^{T}$ $Apc^{fl/+}$ $Pten^{fl/fl}$ described in chapter 4. $Apc^{fl/+}$ $Pten^{fl/fl}$ $Cdh1^{fl/+}$ mice were induced and culled when symptomatic of disease. Interestingly, despite no significant difference in survival time of $Apc^{fl/+}$ $Pten^{fl/fl}$ $Cdh1^{fl/+}$ mice compared to controls, inspection of the survival plot suggests that the $Apc^{fl/+}$ $Pten^{fl/fl}$ $Cdh1^{fl/+}$ cohort could be separated into two subgroups. One group that has a shorter lifespan than controls, and another that has a longer lifespan than controls. When the survival data was plotted against tumour number for the $Apc^{fl/+}$ $Pten^{fl/fl}$ $Cdh1^{fl/+}$ cohort it suggested that there was a negative correlation between tumour number and survival, i.e. mice with a short survival time had a higher abundance of tumours, and mice with a longer survival time had a lower abundance of tumours (Figure 7.18, C). It is unclear why one group of $Apc^{fl/+}$ $Pten^{fl/fl}$ $Cdh1^{fl/+}$ mice live longer than the controls, but one possible explanation is that as heterozygous loss of E-cadherin induces higher levels of apoptosis in the small intestine as observed in section 7.2.6, there may be a stochastic loss of cells including cells that are the precursors of intestinal lesions. The longer lived $Apc^{fl/+}$ $Pten^{fl/fl}$ $Cdh1^{fl/+}$ mice may randomly have lost more cells that would form lesions and therefore have a lower tumour burden and have a longer survival time.

Grading of the tumours in $Apc^{fl/+}$ $Pten^{fl/fl}$ $Cdh1^{fl/+}$ mice revealed that heterozygous E-cadherin loss does not enhance tumour progression (Figure 7.19, A). No evidence of metastasis was observed locally or in the mesentery and pancreas, or in more distant organs such as the liver and lungs. Immunohistochemistry against E-cadherin revealed that E-cadherin was still expressed in even the most advanced tumours so therefore loss of heterozygosity of the Cdh1 gene did not occur (Figure 7.20). E-cadherin loss in human colorectal cancers is associated with tumour progression. As the second allele of Cdh1 was not lost in the tumours of $Apc^{fl/+}$ $Pten^{fl/fl}$ $Cdh1^{fl/+}$ mice the tumour cells were still

able to establish contacts with each other and therefore were not able to detach and metastasise. In this model haploinsufficiency of Cdh1 does not promote tumour progression however it does appear to promote tumour initiation as evidenced by the increased incidence of early lesions i.e. microadenomas and adenomas in $Apc^{fl/+}$ $Pten^{fl/fl}$ $Cdh1^{fl/+}$ mice (Figure 7.19, A,B). This confirms the finding by Smits et al that haploinsufficiency of Cdh1 in the context of an $Apc^{1638N}$ intestinal tumour model synergises with Apc loss to promote the initiation of tumours. Smits et al argued that this occurred through increased cytosolic β-catenin made available by decreased sequestering of the protein by E-cadherin at the cell membrane (Smits et al., 2000). Therefore in a situation in which the cell had lost the β-catenin destruction complex via loss of heterozygosity of Apc, there would be more β-catenin available and therefore enhance Wnt signalling. Further supporting this proposed mechanism of tumour initiation is the finding that E-cadherin only sequesters transcriptionally competent β-catenin at the cell membrane (Gottardi et al., 2001). Therefore depletion in the abundance of E-cadherin via heterozygosity may result in reduced sequestering of transcriptionally active β-catenin, which in turn leads to upregulation of Wnt signalling.

## 7.4 Summary

In summary, homozygous E-cadherin loss in the intestine in adult mice caused extensive destruction of the mucosal surface of the small intestine leading to rapid death after induction. Heterozygous E-cadherin loss however had no detrimental effect on mouse health, and no tumour phenotype long term. However, heterozygous loss of E-cadherin had a negative effect on goblet and enteroendocrine cell lineages as evidenced by a decreased abundance of these cell types, possibly through abrogation of differentiation of the cell types or as a result of the increased levels of apoptosis observed in $Cdh1^{fl/+}$ mice.

When $Cdh1^{fl/+}$ mice were crossed to an $Apc^{fl/+}$ $Pten^{fl/fl}$ invasive intestinal tumour model, loss of heterozygosity of Cdh1 was not observed in tumours. Haploinsufficiency of Cdh1 did not significantly alter survival of $Apc^{fl/+}$ $Pten^{fl/fl}$ $Cdh1^{fl/+}$ mice compared to controls. However, inspection of the survival curve suggested that the cohort could be split into two subgroups: one that had a shorter survival than control groups, and another than had survived longer than the control groups. There were no overall changes in the abundance of tumours in $Apc^{fl/+}$ $Pten^{fl/fl}$ $Cdh1^{fl/+}$ mice compared to controls, and tumour grading revealed that the tumours present in these mice were not more invasive than those observed in the control cohort. However, there was a

significant increase in the number of early lesions observed in $Apc^{fl/+}$ $Pten^{fl/fl}$ $Cdh1^{fl/+}$ mice compared to controls, suggesting that haploinsufficiency of Cdh1 promotes tumour initiation in these mice.

## 7.5 Further work

### 7.5.1 Further investigation of the $Cdh1^{fl/+}$ phenotype

$Cdh1^{fl/+}$ mice have increased levels of apoptosis, increased migratory rate and decreased abundance of goblet and enteroendocrine cells in the small intestinal epithelium. It would first be insightful to determine the localisation of the proteins involved in the adherens junction complex and whether the adherens junctions remain normal in appearance. Any abrogation or mislocalisation of these proteins and junctions would implicate a mechanism by which all these phenotypes may be occurring. For example insufficient adherens junctions may: cause apoptosis by a reduction in PI3K and Src signalling through induction of integrin/FAK signalling, destabilise cell-to-cell adhesions to enhance migration, and may lead to altered juxtacrine signalling i.e. notch signalling. It would also be useful to evaluate the activation status of the PI3K, Src and notch pathways.

### 7.5.2 Investigate the mechanism by which E-cadherin loss promotes tumour initiation

To confirm that it is indeed enhancement of the cytosolic β-catenin pool that promotes tumour initiation in $Apc^{fl/+}$ $Pten^{fl/fl}$ $Cdh1^{fl/+}$ mice, it would be useful to quantify the level of Wnt target activation in the tumours arising in these mice compared to tumours arising in the control mice. It would also be interesting to compare the localisation of β-catenin in normal intestinal tissue in $Apc^{fl/+}$ $Pten^{fl/fl}$ $Cdh1^{fl/+}$ mice with control tissue by IHC, and to quantify the abundance of transcriptionally active β-catenin in the cytoplasm of $Apc^{fl/+}$ $Pten^{fl/fl}$ $Cdh1^{fl/+}$ mice.

### 7.5.3 Study the effect of the homozygous E-cadherin loss within tumours

Homozygous loss of E-cadherin in the context of tumours could not be studied in this model as $VillinCreER^T$ $Cdh1^{fl/fl}$ mice succumb to rapid death after induction. It would be useful to be able to homozygously delete the Cdh1 gene specifically within a tumour to investigate how it would affect tumour progression. Unfortunately a tumour specific cre recombinase is not available, however knockout may be able to be achieved by

injection of adenoviral cre recombinase directly into a tumour but this would be a highly invasive and difficult procedure.

# Chapter 8: Investigating the role of Pten in the stromal fibroblasts and smooth muscle of the intestine

## 8.1 Introduction

As PTEN is implicated in an array of disorders, the effect of its loss has been extensively studied in mouse models. There have been a number of constitutive and conditional knockouts of the Pten gene in mice. Di Cristofano et al discovered that the Pten gene is essential for embryonic development, with Pten deficiency resulting in embryonic death at day E7.5. However, one intact copy of the gene was sufficient for normal embryonic development, as heterozygous Pten knockouts survived into adult hood. Some of these Pten$^{+/-}$ mice subsequently developed colon tumours with evidence of tumour invasiveness at about 3.5 months (Di Cristofano et al., 1998). Podsypanina et al found that the intestinal tumours found in Pten$^{+/-}$ mice only formed over lymphoid tissue, and some but not all displayed epithelial hyperplasia as well as abnormal lymphoid tissue (Podsypanina et al., 1999). These findings led to the investigation of homozygous deletion of Pten specifically within the intestine. A number of studies in which Pten had been conditionally deleted specifically in the intestinal epithelium have now been published. The first, a study by He et al, showed that deletion of Pten from the epithelium results in rapid intestinal tumourigenesis one month after Pten loss (He et al., 2007). However, findings from Langlois et al and Marsh et al showed that intestinal epithelial Pten loss is dispensable for normal intestinal function and does not cause rapid tumourigenesis (Langlois et al., 2009, Marsh et al., 2008).

The disparity between the phenotypes of the Pten loss models leads to the question as to why the former models resulted in rapid formation of tumours and the other epithelial models did not. One experimental difference between the He et al study and the other conditional knockouts of Pten was the Cre recombinase used to achieve deletion. He et al used the inducible *Mx1*Cre recombinase driven by the interferon inducible Mx1 promoter, whereas the other studies used *Ah* and *Villin*Cre recombinase driven by Cyp1a1 and Villin promoters respectively. *Mx1*Cre recombinase is expressed not only in the intestinal epithelium, but also in the underlying supporting stroma and immune cells (Kuhn et al., 1995, Schneider et al., 2003), so similarly to the constitutive Pten$^{+/-}$ animals, *Mx1*Cre Pten$^{fl/fl}$ animals have lost Pten from both the epithelium and underlying stroma of the intestine. Both *Ah*Cre and *Villin*Cre recombinases are expressed only in epithelia and not in stromal cells (Ireland et al., 2004, El Marjou et al., 2004). Taken together, the findings from the various Pten

deletion models suggest that loss of Pten from the supporting stroma is necessary for intestinal tumour formation in the mouse. The concept of alterations in the supporting stromal component of a tissue leading to an epithelial phenotype is not new. For example, the tumour suppressors Lkb1 and BMPRII have both been implicated in stromal-epithelial interactions, as when they are ablated from the stroma in the mouse intestine tumours develop (Beppu et al., 2008, Katajisto et al., 2008)

To investigate the role of Pten in the intestinal stroma, mice bearing a fibroblast specific *Col1A2*CreER$^T$ recombinase transgene (Zheng et al., 2002) were crossed with Pten$^{fl/fl}$ mice to generate *Col1A2*CreER$^T$-Pten$^{fl/fl}$ mice. *Col1A2*CreER$^T$ is expressed in the intestine in the stromal fibroblasts surrounding the crypts and in the smooth muscle. It is an inducible Cre recombinase activated by administration of tamoxifen via i.p. injection. *Col1A2*CreER$^T$-Pten$^{fl/fl}$ mice (hereafter referred to as *Col1A2*Cre$^+$-Pten$^{fl/fl}$) and control *Col1A2*CreER$^T$-Pten$^{+/+}$ mice (hereafter referred to as *Col1A2*Cre$^+$-Pten$^{+/+}$) were generated, induced and sacrificed when they became symptomatic of disease.

## 8.2 Results

### 8.2.1 *Col1A2*CreER$^T$ recombinase is specifically expressed in the stroma and smooth muscle of the small intestine

A number of strategies were used to ascertain the location of recombination of the Pten allele. IHC against Pten was carried out on small intestinal tissue sections from aged *Col1A2*Cre$^+$-Pten$^{fl/fl}$ mice, and also on small intestinal tissue sections from *Villin*Cre$^+$-Pten$^{fl/fl}$ mice and *Villin*Cre$^+$-Pten$^{+/+}$ mice as negative and positive controls respectively (Figure 8.1, B). IHC revealed that Pten protein was still present in the epithelium of *Col1A2*Cre$^+$-Pten$^{fl/fl}$ tissue comparable to the Pten immunostaining of *Villin*Cre$^+$-Pten$^{+/+}$ (WT) tissue. The *Villin*Cre$^+$-Pten$^{fl/fl}$ negative control tissue clearly shows loss of Pten protein specifically in the epithelium. Despite the positive epithelial immunostaining of Pten in *Col1A2*Cre$^+$-Pten$^{fl/fl}$ tissue, the location of Pten loss could not be definitely established by IHC, as no strong and coherent immunostaining for Pten could be visualised in unrecombined samples.

As it was not possible to determine loss of Pten in the stroma of the small intestinal tissue by examination of IHC stained sections for Pten, DNA recombination was confirmed by PCR carried out on gDNA from cell enriched samples from both the epithelial cell layer, and underlying stromal and smooth muscle cell layer of the small intestine (Figure 8.1, C). gDNA was extracted from an epithelial enriched sample obtained by scraping the mucosal surface of a section of the small intestine with a

scalpel. gDNA was also extracted from the remaining underlying smooth muscle and stromal layer left after mucosal scraping. Separate PCR reactions for the targeted and recombined allele of Pten were then carried out, confirming that a recombined band was only present in the samples enriched for stromal and smooth muscle cells but not in the epithelial cell enriched samples.

## 8.2.2 Stromal Pten loss does not affect stem cell marker expression or the proliferative cell compartment

Modulation of the stem cell niche via Pten loss may impact on the epithelial stem cell compartment through stromal-epithelial interactions. He et al, observed an increase in the abundance of stem cells in $Mx1$Cre-Pten$^{fl/fl}$ mice (He et al., 2007), so to investigate whether Pten loss from the stroma affects stem cell abundance the level of expression of stem cell markers, Lgr5 and Ascl2, were quantified by qRT-PCR. $Col1A2$Cre$^{+}$-Pten$^{fl/fl}$ mice were induced (via i.p. injection of tamoxifen) along with cre negative controls, sacrificed after 22 days and RNA was then extracted from epithelial enriched cell samples. There was no increase in the relative expression of stem cell markers Lgr5 and Ascl2 in $Col1A2$Cre$^{+}$-Pten$^{fl/fl}$ mice compared to $Col1A2$Cre$^{-}$-Pten$^{fl/fl}$ control mice (p values >0.05, n=4, Mann Whitney U test) (Figure 8.2, A). Expression of stem cell markers can be used as a surrogate indicator of the abundance of stem cells, but it is not informative of the proliferative activity of the stem cell and TA cell compartment. To address whether stromal loss of Pten impacted on the proliferative activity of epithelial cells, IHC was carried out against the Ki67 antigen on small intestinal tissue sections from $Col1A2$Cre$^{+}$-Pten$^{fl/fl}$ mice and control mice that were induced and sacrificed at 22 days post induction. The Ki67 antigen is expressed at all stages of the cell cycle and therefore is a marker of cell proliferation. The number of Ki67 positive cells were scored per half crypt (50 crypts were scored). $Col1A2$Cre$^{+}$Pten$^{fl/fl}$ tissue appeared to have a lower abundance of Ki67 positive cells compared to cre negative control tissue. However this was not statistically significant (p value = 0.0582, n=4, Mann Whitney U test) (Figure 8.2, B). There was however a marked increase in the presence of Ki67 positive nuclei of stromal fibroblasts, both at the pericryptal and smooth muscle region and the intravillus stroma (Figure 8.2, C, arrows).

**Figure 8.1 Recombination of the Pten allele occurs in the stroma and smooth muscle cells of *Col1A2*Cre<sup>+</sup>-Pten<sup>fl/fl</sup> mice**

(A) IHC against Pten shows epithelial Pten expression is maintained in *Col1A2*Cre<sup>+</sup>-Pten<sup>fl/fl</sup> mice compared to *Villin*Cre<sup>+</sup>-Pten<sup>fl/fl</sup> mice, which have epithelial specific loss of Pten. However, it is not possible to deduce the site of recombination in *Col1A2*Cre<sup>+</sup>-Pten<sup>fl/fl</sup> mice from IHC staining. IHC was carried out on intestinal tissue from aged *Col1A2*Cre<sup>+</sup>-Pten<sup>fl/fl</sup> mice (image in figure from mouse at day 603 post induction). Scale bars represent 200μm. (B) Key: L – 100bp DNA ladder, E – gDNA sample from epithelial cells, M – gDNA sample from smooth muscle and stroma. PCR for the recombined allele of Pten only yields a band in samples in which gDNA was extracted from intestinal samples enriched for smooth muscle and stromal cells taken from mice at 22 days post induction.
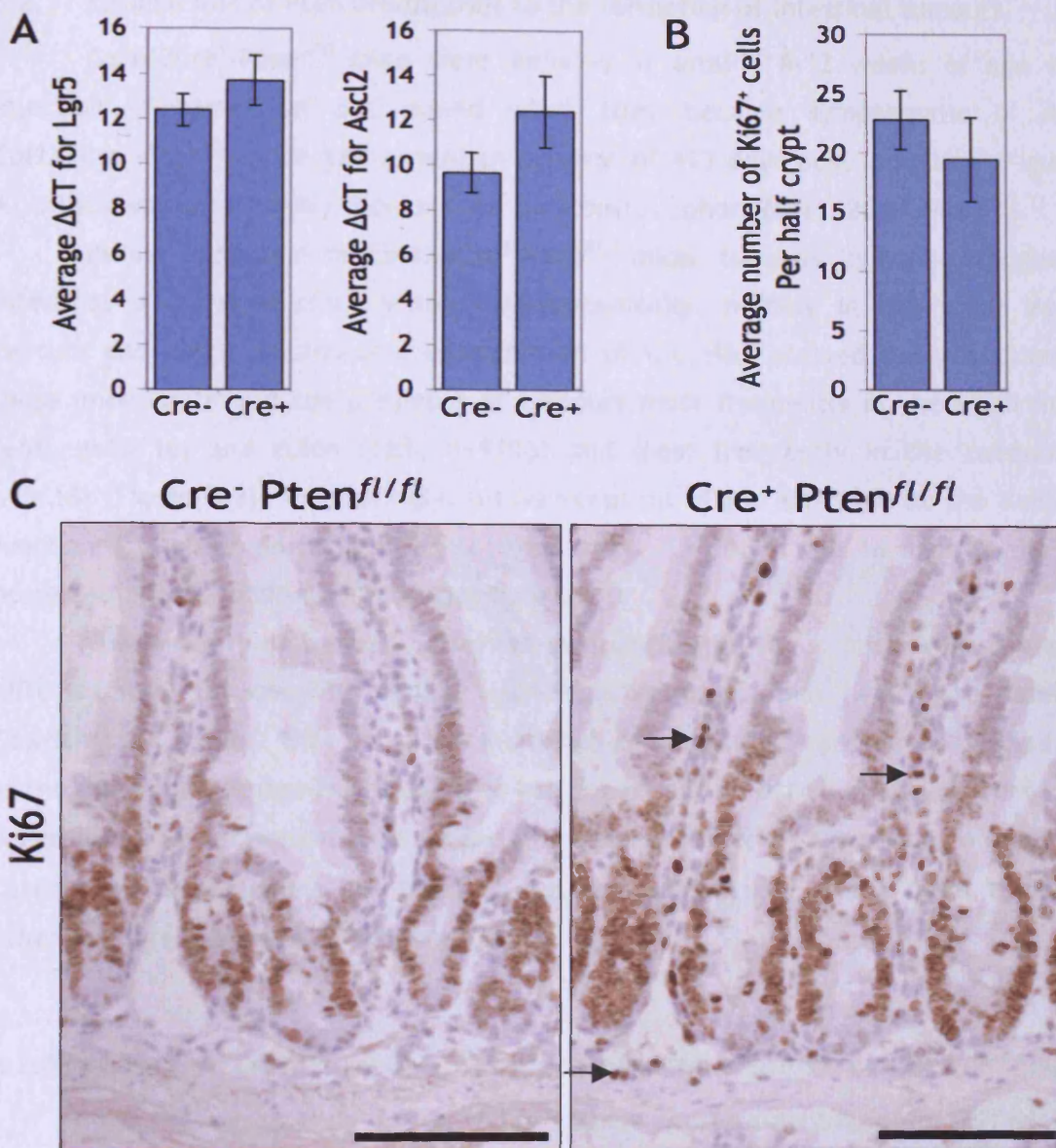
Figure 8.2 Loss of Pten from the stromal and smooth muscle fibroblasts of the small intestine does not affect the proliferative compartment of the epithelium

(A) Expression of the stem cell markers Lgr5 and Ascl2 was determined by qRT-PCR (carried out on small intestinal epithelial cDNA), as a surrogate marker of stem cell abundance. Expression analysis concluded that there was no overall change in Lgr5 or Ascl2 expression in experimental epithelium (*Col1A2*Cre$^+$Pten$^{fl/fl}$) compared to control epithelium. (B-C) IHC was also carried out against proliferation marker Ki67 on small intestinal tissue sections and positive cells were scored. Scoring revealed a trend towards lower average numbers of Ki67 positive cells per crypt, but it was not statistically significant (p value = 0.0582, n=4, Mann Whitney U test). Ki67 IHC revealed a marked increase in the presence of Ki67 positive nuclei in the stromal compartment of Cre$^+$ Pten$^{fl/fl}$ small intestine (indicated by arrows).

### 8.2.3 Stromal loss of Pten predisposes to the formation of intestinal tumours

*Col1A2*Cre$^+$-Pten$^{fl/fl}$ mice were induced at around 6-12 weeks of age via i.p. injection of tamoxifen and culled when they became symptomatic of disease. *Col1A2*Cre$^+$-Pten$^{fl/fl}$ mice had a median survival of 493 days post induction (Figure 8.1, A), which was significantly shorter than the control cohort (*Col1A2*Cre$^+$-Pten$^{+/+}$).

During dissection of *Col1A2*Cre$^+$-Pten$^{fl/fl}$ mice, tumours in sites throughout the intestinal tract were often visible macroscopically, namely in the small intestine, caecum and colon. Microscopic examination of the H&E stained tissue sections from these mice confirmed the presence of tumours most frequently in the small intestine (66%, n=10/16) and colon (56%, n=9/16) and least frequently in the caecum (31%, n=5/16) (Figure 8.3). Interestingly, intussusception of the intestine at the ileal-caecal junction was observed in (13%, n=2/10) of mice. 15 out of the 16 mice in the cohort possessed at least one intestinal tract tumour.

The majority of tumours observed in *Col1A2*Cre$^+$-Pten$^{fl/fl}$ mice were benign, well differentiated tumours with similar pathology to hamartomas (which are observed in Cowden's syndrome). There was one incidence of metastatic carcinoma that had spread to the diaphragm (image not shown), in the cohort of 16 *Col1A2*Cre$^+$-Pten$^{fl/fl}$ mice. There was evidence of activation of Wnt signalling as ascertained by the presence of nuclear β-catenin in the carcinoma but this was not observed in any of the other tumours (all other tumours were benign) (Figure 8.4).

### 8.2.4 Tumours in *Col1A2*Cre$^+$-Pten$^{fl/fl}$ mice retain Pten expression in the epithelium

Pten IHC was carried out on tumour tissue sections arising in *Col1A2*Cre$^+$-Pten$^{fl/fl}$ mice to confirm the presence of Pten in the epithelial component of the tumours. Pten immunostaining was present throughout the epithelial component of the tumours, however the stromal component of the tumours appeared to have reduced staining for Pten compared to the epithelium of the tumour (Figure 8.5). When the Pten stained sections of *Col1A2*Cre$^+$-Pten$^{fl/fl}$ tumours were compared to tumours stained for Pten that arose in other mouse models with intact stromal Pten, a striking difference in Pten expression was noted (Figure 8.5). Figure 8.5 shows a tumour from a *Villin*Cre$^+$-Pten$^{fl/fl}$ Kras$^{LSL/+}$ mouse stained for Pten. The epithelial component of this tumour is devoid of Pten immunostaining as *Villin*Cre recombinase is expressed in the intestinal epithelium, however there is strong Pten immunostaining in the stroma of these tumours compared to tumours in *Col1A2*Cre$^+$-Pten$^{fl/fl}$ mice.

Loss of Pten results in loss of negative regulation of the PI3K pathway, so IHC against phospho-Akt (Ser473) was carried out on tumour tissue sections. As predicted, phospho-Akt was upregulated in the stroma of the tumours; stromal upregulation of phospho-Akt is not observed in tumours from *Villin*Cre$^+$-Pten$^{fl/fl}$ Kras$^{LSL/+}$ mice (Figure 8.5). This indicated that the PI3K pathway was being specifically activated in the stroma of *Col1A2*Cre$^+$-Pten$^{fl/fl}$ tumours. However, stromal phospho-Akt staining was not found ubiquitously throughout the tumour stroma, but in patches.

### 8.2.5 Stromal Pten loss possibly mediates tumourigenesis through stromal-epithelial interactions via the PI3K-MAPK/ERK pathways

Immunostaining of phospho-Akt revealed that the PI3K pathway was active in patches of the stroma in intestinal tumours from *Col1A2*Cre$^+$-Pten$^{fl/fl}$ mice. To begin to address how this stromal upregulation might lead to the formation of an epithelial tumour, IHC against phospho-Erk a marker of Ras-Raf-Mek-Erk/MAPK pathway activation (another commonly implicated pathway in CRC) was carried out.

IHC revealed that in areas of the tumours in which the stroma stained strongly for phospho-Akt, the adjacent epithelial cells frequently stained strongly for phospho-Erk (Figure 8.6). This suggests that stromal activation of the PI3K pathway in the tumour somehow stimulates MAPK/Erk activation in the tumour epithelium. IHC against Ki67 was also carried out to visualise the level of proliferation in the tumours. Ki67 immunostaining revealed that paradoxically the areas of tumour epithelium that stained strongly for phospho-Erk, and were hence surrounded by phopsho-Akt positive stroma, had very few positive nuclei for Ki67 (Figure 8.6). This indicates that the areas of tumour that appeared to have active PI3K and MAPK/Erk signalling were not actively proliferating.
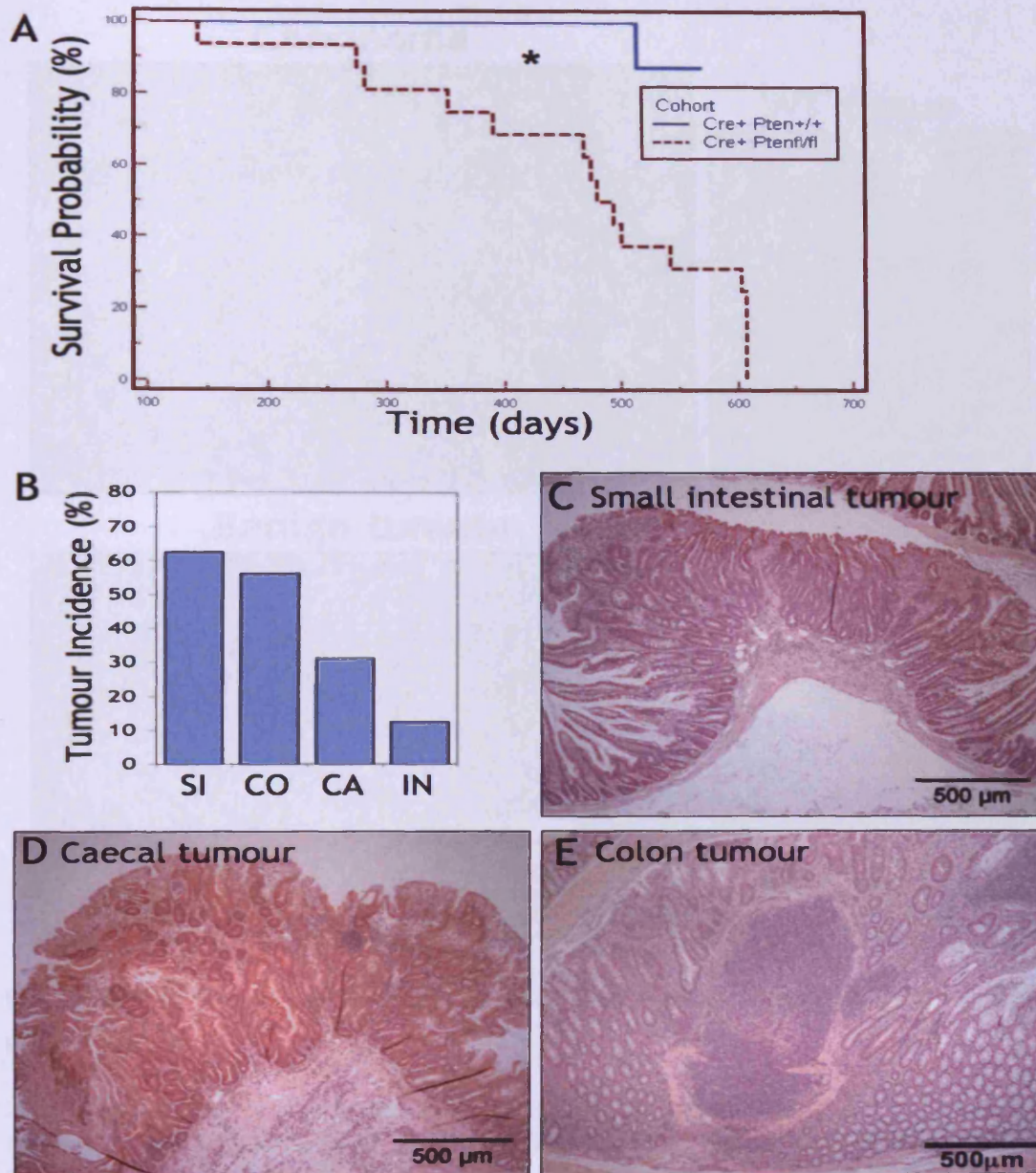
**Figure 8.3 Stromal loss of Pten decreases mouse lifespan and predisposes to benign intestinal tumours**

(A) Survival curve of *Col1A2*Cre$^+$-Pten$^{fl/fl}$ mice revealed a significant decrease in lifespan compared to the WT control cohort (*, p value < 0.001, Logrank test). (B) Distribution of tumour types found in *Col1A2*Cre$^+$-Pten$^{fl/fl}$ mice (n=16). Key: SI = Small Intestinal tumour, CO = Colon tumour, CA = Caecal tumour, IN = intussusception. 15/16 of the tissue samples examined possessed at least one tumour in the intestinal tract. (C-E) H&E stained sections of the intestinal tumour types observed in *Col1A2*Cre$^+$-Pten$^{fl/fl}$ mice.
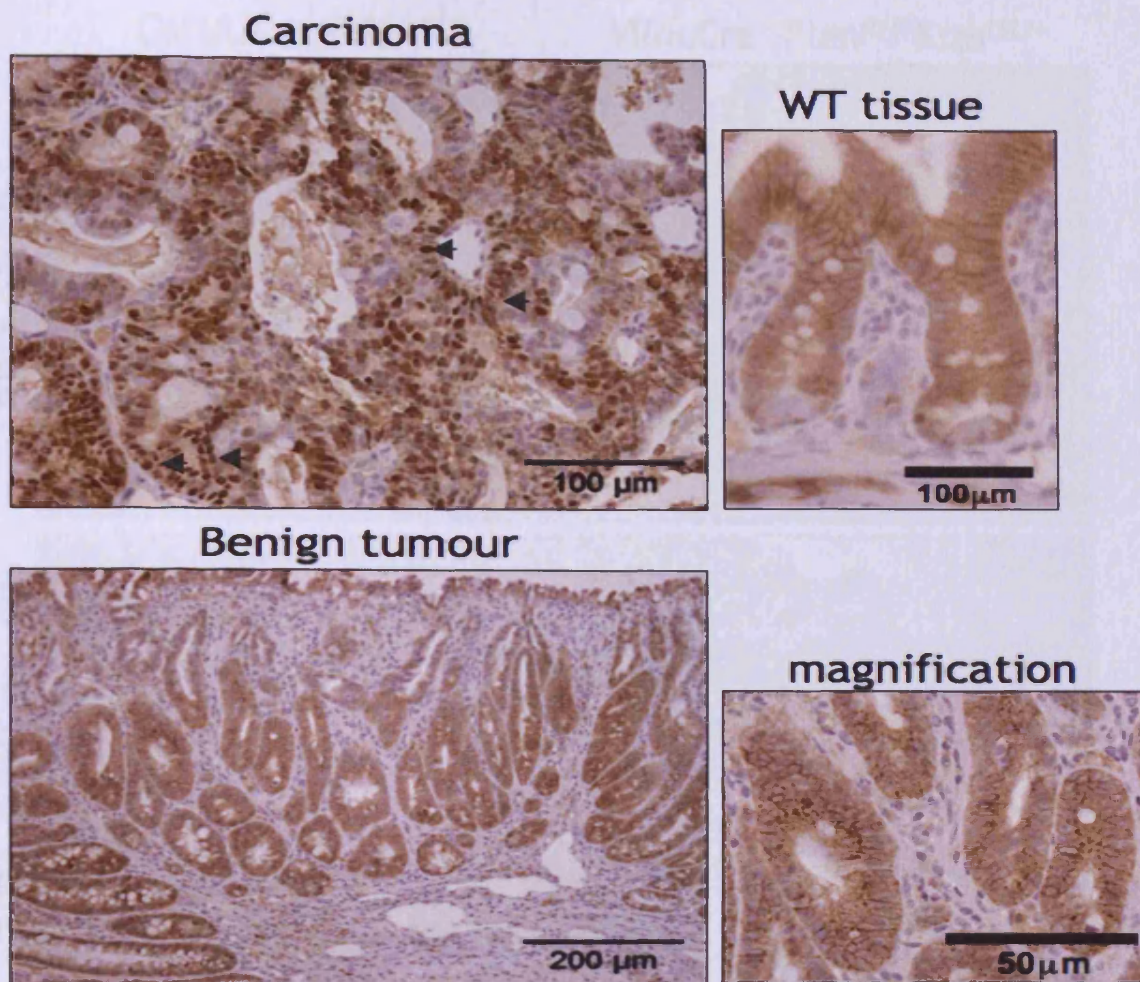
**Figure 8.4 The Wnt pathway is not active in benign tumours found in *Col1A2*Cre⁺-Pten^{fl/fl} mice**

IHC for β-catenin (a surrogate marker of Wnt pathway activation) was carried out on tumour tissue sections from in *Col1A2*Cre⁺-Pten^{fl/fl} mice. IHC indicated that the Wnt signalling pathway is not activated in the majority of intestinal tumours found in *Col1A2*Cre⁺-Pten^{fl/fl} mice – all of which were benign tumours. Only one case of Wnt activation in a tumour was observed, in a metastatic carcinoma. Arrow heads indicate cells with nuclear β-catenin staining.
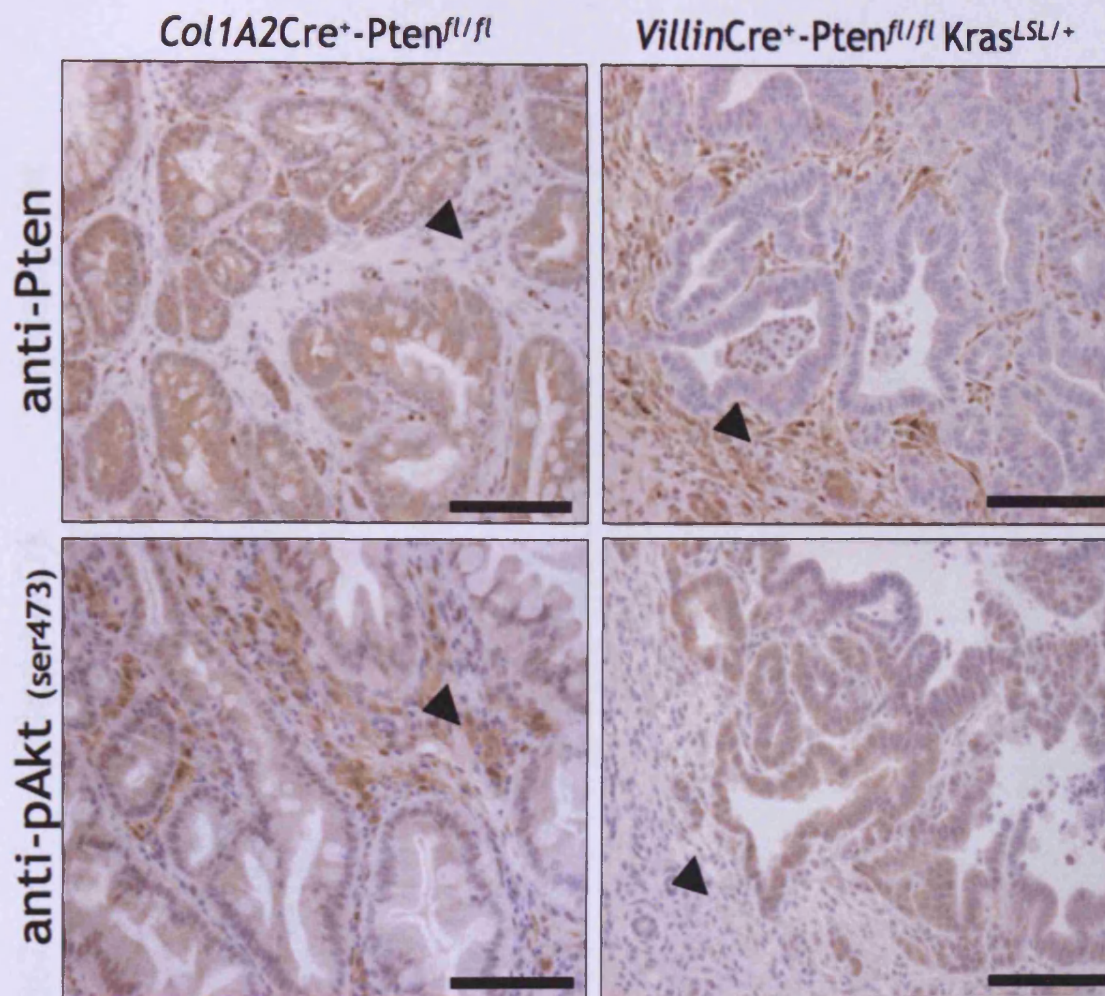
**Figure 8.5** *Col1A2*Cre⁺-Pten*ᶠˡ/ᶠˡ* tumours lack stromal Pten immunostaining but have upregulated stromal phospho-Akt immunostaining

IHC for Pten and phospho-Akt (ser473) (pAkt) was carried out on tumour tissue sections from *Col1A2*Cre⁺-Pten*ᶠˡ/ᶠˡ* mice in which Pten had been deleted from the stroma and tumour tissue from *Villin*Cre⁺-Pten*ᶠˡ/ᶠˡ* Kras*ᴸˢᴸ/⁺* mice, which had intact Pten in the stroma. Pten immunostaining confirmed the presence of Pten protein in the epithelial component of *Col1A2*Cre⁺-Pten*ᶠˡ/ᶠˡ* tumours. However the stromal component of the tumours appeared to be devoid of Pten immunostaining compared to *Villin*Cre⁺-Pten*ᶠˡ/ᶠˡ* Kras*ᴸˢᴸ/⁺* tumours, which had Pten deleted from the epithelia but not the stroma. Phospho-Akt immunostaining revealed upregulation of the activated form of the Akt protein, predominantly in the stroma of *Col1A2*Cre⁺-Pten*ᶠˡ/ᶠˡ* tumours. The opposite was observed in *Villin*Cre⁺-Pten*ᶠˡ/ᶠˡ* Kras*ᴸˢᴸ/⁺* tumours. Scale bars represent 100μm.
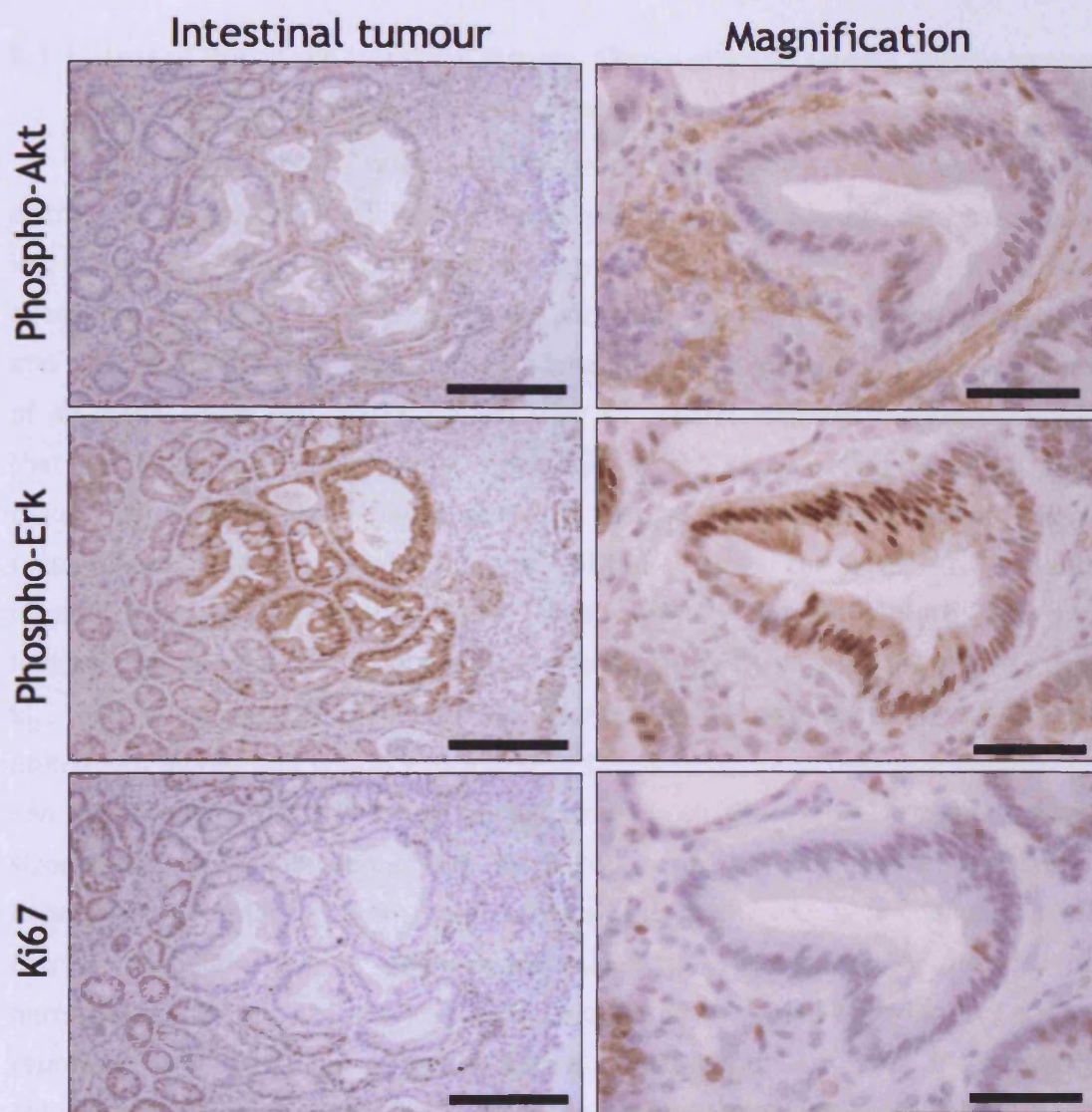
**Figure 8.6 Stromal phospho-Akt staining coincides with strong phospho-Erk staining but not Ki67 staining**

IHC was carried out on serial sections of tumour tissue for the active forms of Akt and Erk, which are involved in the PI3K and Ras-Raf-Mek-Erk/MAPK pathways respectively. Immunostaining for phospho-Akt was located in the stromal compartment of the tumours; it was not present ubiquitously throughout the tumour but present in patches. Phospho-Erk immunostaining was present in the epithelium adjacent to the areas of the stroma that stained strongly for phospho-Akt. Ki67 staining revealed that the epithelial areas that stained strongly for phospho-Erk were not actively cycling. Scale bars represent 200µm low power, 50µm magnification.

## 8.3 Discussion

### 8.3.1 Loss of Pten from intestinal stromal fibroblasts and smooth muscle has no impact on the proliferative component of the epithelium

*Col1A2*Cre$^+$-Pten$^{fl/fl}$ mice were induced around 6-12 weeks of age, recombination of the loxP flanked Pten alleles was confirmed by PCR at day 22 post induction and Pten IHC further confirmed the presence of Pten in the epithelial cell layer of the intestine in aged mice (Figure 8.1). At day 22 post induction loss of Pten from stromal fibroblasts and smooth muscle (i.e. the stem cell niche) does not impact on the relative expression of epithelial stem cell markers compared to control samples (Figure 8.2). Suggesting that the abundance of epithelial stem cells is the same in experimental and control tissue. He et al showed that conditional loss of Pten in the intestine using *Mx1*Cre recombinase causes expansion of the epithelial stem cell compartment and causes musashi positive stem cells to leave their normally quiescent state, and divide - as indicated by an increase in double labeled musashi positive and Ki67 positive cells (He et al., 2007). As *Mx1*Cre recombinase expression is not confined to the intestinal epithelium alone, but is also expressed in the underlying stroma and immune cells, one can hypothesise that Pten must be lost from both the epithelium and the underlying stroma to cause expansion of the stem cell pool. The observation in chapter 5 that expression of epithelial stem cell markers Lgr5 and Ascl2 is unchanged in *Villin*Cre$^+$-Pten$^{fl/fl}$ epithelium further supports this suggestion. One caveat of the data presented here is that the stem cell markers used to quantify stem cell abundance, Lgr5 and Ascl2, represent what is thought to be the actively cycling stem cell pool and musashi positive cells are thought to encompass quiescent stem cells and their progenitors (Li and Clevers, 2010). Thus, as in the He et al study it would be useful to quantify the numbers of musashi and Ki67 double positive cells and the expression of Bmi1, another proposed quiescent stem cell marker, in *Col1A2*Cre$^+$-Pten$^{fl/fl}$ tissue to see if stromal loss of Pten affects the quiescent stem cell population. He et al also showed that *Mx1*Cre$^+$-Pten$^{fl/fl}$ mice have an expansion in proliferative cells as indicated by an increase in abundance of BrdU positive cells. Scoring of cycling cells indicated that there was no expansion of the proliferative compartment in *Col1A2*Cre$^+$-Pten$^{fl/fl}$ mice. Despite there being no expansion of the proliferative component of the epithelium, IHC for Ki67 revealed an apparent expansion of proliferative fibroblasts in the stromal component of the small intestine. Normally very few stromal fibroblasts are actively cycling, which is observed in the cre negative control in Figure 8.2, C.

## 8.3.2 Loss of Pten from the supporting stromal/smooth muscle component of the intestine alone causes the formation of tumours

Despite loss of Pten from the stromal fibroblasts and smooth muscle having no effect on epithelial cell proliferation at short time points, *Col1A2*Cre$^+$-Pten$^{fl/fl}$ mice that were induced and aged were predisposed to the formation of intestinal tumours. Aged *Col1A2*Cre$^+$-Pten$^{fl/fl}$ mice became symptomatic of intestinal tumours from approximately 270 days post induction, as indicated by swelling of the abdomen, prolapse and blood in faeces. Benign tumours were observed along the length of the small intestine, caecum and colon (Figure 8.3), and all of these tumours still possessed epithelial immunostaining for Pten (as visualised by IHC) (Figure 8.5).

In the study by He et al, intestinal tumours were observed rapidly, after one month post induction of *Mx1*Cre (He et al., 2007). In contrast, tumours were observed in *Col1A2*Cre$^+$-Pten$^{fl/fl}$ mice at much later time points post induction. The study described in this chapter differed from the He et al study, as *Col1A2*Cre$^+$-Pten$^{fl/fl}$ mice were only sacrificed when they became symptomatic of disease not at one month after induction (as was carried out in the He et al study). However, *Col1A2*Cre$^+$-Pten$^{fl/fl}$ mice sacrificed at day 22 post induction showed no evidence of intestinal tumours. The differences in outcome of my experiment and the He et al experiment, are likely to be attributed to the exact cellular compartments in which Pten is lost in *Mx1*Cre mice. Data from Schneider et al show that *Mx1*Cre recombinase acts in the underlying stroma and smooth muscle cells of the intestine (Schneider et al., 2003) and a different study by He et al confirmed that Mx1Cre was expressed in the intestinal epithelium (He et al., 2004). He et al used a lacZ/EGFP reporter mouse to assess the sites of recombination in *Mx1*Cre mice; they confirmed expression of the reporter gene in intestinal epithelium but the image in Figure 2,a of the report (shown in Figure 8.7) also appears to show expression in the underlying stroma and smooth muscle of the intestine (He et al., 2004). Taken together these two studies confirm that *Mx1*Cre acts in both the epithelial and stromal components of the intestine. Indeed, He et al acknowledge that the expansion of stromal cells in the tumours found in *Mx1*Cre$^+$-Pten$^{fl/fl}$ mice and therefore the rapid onset of tumourigenesis in *Mx1*Cre mice could be due to the deletion of Pten in both stromal and epithelial compartments of the intestine. It should also be noted that induction of *Mx1*Cre evokes an immune response and as *Mx1*Cre is also expressed in immune cells, so this clearly has ramifications for the interpretation of this model.

**Figure 8.7 EGFP reporter expression in the small intestine of *Mx1Cre* mice (taken from He et al, 2004)**

He et al showed using a conditional EGFP reporter mouse that Mx1Cre is expressed and acts within the small intestinal epithelium. However, expression was also noted in the underlying stroma/smooth muscle of the small intestine, as indicated by the white arrow heads.

### 8.3.3   Stromal-epithelial interactions in *Col1A2*Cre[+]-Pten^{fl/fl} tumours

IHC carried out on intestinal tumour sections in Figure 8.6 revealed that strong immunostaining for phospho-Erk in epithelial parts of the tumour coincided with the presence of stromal phospho-Akt immunostaining, suggesting that the stromal-epithelial interactions that are governing tumourigenesis involve cross talk between the PI3K and MAPK/Erk pathways. A study published by Trimboli et al has implicated the PI3K, JNK and MAPK pathways in the stromal contribution of Pten loss to mammary tumourigenesis (Trimboli et al., 2009). Similar to the model described in this chapter, they investigated loss of Pten from the stromal fibroblasts but in the context of a model predisposed to epithelial mammary tumour formation, and found Pten loss to promote tumourigenesis through elevated expression and activation of Ets2, a downstream target of the MAPK/Erk pathway. They show that stromal specific deletion of Pten results in epithelial upregulation of phospho-Erk and phospho-Ets2 in the mammary gland. It is however, unclear whether activation of Ets2 would play the same role in the promotion of intestinal tumourigenesis as Múnera et al have shown that intestinal specific deletion of Ets2 actually enhances azoxymethane induced colon tumour formation (Munera et al., 2011).

How stromal upregulation of phospho-Akt activates the MAPK/Erk pathway in the epithelium is unclear. The MAPK/Erk pathway is activated in a number of ways, through receptor tyrosine kinases (RTK), integrins and calcium signalling. The downstream

actions of phospho-Akt in the stromal fibroblasts must some how activate these receptors expressed on the epithelial cell surface in order to activate the MAPK/Erk pathway. Activation of the PI3K pathway in stromal fibroblasts of the tumour may send paracrine signals to the adjacent epithelium to activate the MAPK/Erk pathway through the production and secretion of ligands for RTKs or the release of calcium ions, or through activation of outside-in signalling via integrins by juxtacrine signaling to epithelial cells in contact with stromal fibroblasts. Intestinal stromal fibroblasts are known to secrete insulin-like growth factor-1 (IGF-1), which can activate the MAPK/Erk pathway. Recent findings have shown that the production of IGF-1 by intestinal stromal cells is stimulated by activation of the PI3K pathway (Leen et al., 2011). Therefore, this may present a possible mechanism by which stromal cells are signalling to the epithelium in these tumours.

IHC for the proliferation marker Ki67 revealed that areas of tumour epithelium that had strong phospho-Erk immunostaining were predominantly negative for Ki67 immunostaining (Figure 8.6). This finding suggests that these areas of the tumour were not actively cycling, and therefore may be senescent. The MAPK/Erk pathway has previously been shown to induce cellular senescence in intestinal cell lines (Boucher et al., 2004). One can postulate that this lack of proliferation maybe the reason why the tumours observed in $Col1A2Cre^+$-$Pten^{fl/fl}$ rarely progress to invasive adenocarcinoma and carcinoma.

### 8.3.4 Epithelial vs stromal deletion of Pten

Both Marsh et al and Langlois et al reported that there were no intestinal tumours present in mice that had Pten deficient epithelium in mice older than 200 days post induction and ~500 days after birth respectively (Marsh et al., 2008, Langlois et al., 2009). However, as described in chapter 6 a subset (40%) of $VillinCre$-$Pten^{fl/fl}$ mice aged over 500 days post induction that were culled when they were symptomatic of disease possessed some benign small intestinal tumours. $Col1A2Cre^+$-$Pten^{fl/fl}$ mice possessed intestinal tumours as early as 270 days post induction and these tumours are well differentiated tumours that resemble hamartomas, whereas in $VillinCre$-$Pten^{fl/fl}$ mice, the few tumours that did arise were sessile serrated adenomas. These findings suggest that cell specific loss of Pten gives rise to tumours of differing morphologies and Pten loss from the intestinal stroma causes earlier onset of tumourigenesis and increased tumourigenecity compared to epithelial cell loss of Pten.

## 8.4 Summary

CRC has long been regarded as a cancer of the epithelium and therefore the vast majority of CRC research has focused on genetic alterations in the intestinal epithelium. The findings in this chapter along with some other studies (Beppu et al., 2008, Katajisto et al., 2008) demonstrate the dependence of the intestinal epithelium on a genetically intact supporting stroma, and deletion of tumour suppressors can negatively impact on intestinal epithelial homeostasis. The findings in this chapter indicate that loss of Pten from the stromal and smooth muscle fibroblasts alone, is sufficient for tumour formation in the mouse intestine. This is also the first indication that activation of the PI3K signalling pathway in the intestinal stroma can give rise to epithelial aberrations and tumours through stromal-epithelial interactions. What downstream targets of phospho-Akt and how they relay growth signals to the epithelium is unclear, but this mechanism is likely to involve MAPK/Erk signalling. The stark contrast in tumourigenicity in mice that are deficient for Pten in the stromal/smooth muscle intestinal component and those that have Pten deficiency in the epithelial intestinal component, highlights the important role Pten plays in the intestinal stem cell niche. In light of these findings, and a recent link to PTEN loss in the tumour stroma, which reports an upregulation of the non-coding RNA microRNA-21 (which degrades PTEN mRNA) in the stroma of human CRCs and its association with poor survival (Nielsen et al., 2011), it would be insightful to investigate the stromal components of human CRCs for PTEN alterations.

## 8.5 Further Work

### 8.5.1 Elucidating a mechanism of tumourigenesis

The data presented in this chapter represent the early findings into the investigation of how stromal/smooth muscle loss of Pten predisposes to intestinal tumourigenesis. Much work needs to be carried out to ascertain the mechanism by which this occurs. As tumour formation in the mammary model of stromal Pten loss seems to be mediated by a Pten-Ets2 axis, it would be useful to carry out IHC against phospho-Ets2, however as previously mentioned the relationship between Pten and phospho-Ets2 may be mammary specific. As stromal inactivation of both the TGF-β and BMP pathways has been implicated in intestinal epithelial aberrations it would be useful to ascertain whether these pathways were downregulated in the stromal Pten model. It would also be insightful to carry out IHC against IGF-1 to ascertain if it is expressed in the tumour stroma. Further work on short time points should also be carried out to statistically prove that stromal cells are more actively cycling in $Col1A2Cre^+$-$Pten^{fl/fl}$ mice.

## 8.5.2 Tumour senescence and tumour progression?

As mentioned the tumours in $Col1A2Cre^{+}$-$Pten^{fl/fl}$ mice appear not to be cycling and may be senescent. Further confirmation of this, can be achieved by immunostaining for another cell cycle related protein, proliferating cell nuclear antigen (PCNA), and by carrying out senescence-associated β-galactosidase staining, along with IHC for upregulation of cell cycle inhibitors such as p16 and p21 to indicate whether the tumours are indeed senescent.

How stromal loss of Pten contributes to tumour progression would be the next step in elucidating the role of Pten in the intestinal stroma. This could be approached by crossing a $Col1A2Cre^{+}$-$Pten^{fl/fl}$ mouse with an $Apc^{Min}$ mouse, which is predisposed to spontaneous intestinal tumour formation.

# Chapter 9: General Discussion

## 9.1 Developing a metastatic mouse model of CRC

Colorectal cancer (CRC) is the second most common cause of death from cancer, predominantly owing to patients usually presenting at the clinic when the disease has reached the late stages (CancerResearchUK, 2010). Current treatment strategies rely on the use of a combination of cytotoxic drugs and the targeted therapeutic cetuximab – an epidermal growth factor receptor (EGFR) inhibitor. Despite these treatments, mortality rates are still high, therefore better therapies are needed to treat late stage disease. Currently, all preclinical drug testing is carried out on xenografted human tumours in immunocompromised mice. Most of the drugs that show efficacy in preclinical models often fail when they reach clinical trials (Garber, 2006). Therefore, preclinical therapeutic testing must become more predictive of how a drug will work on human tumours. One of the ways to achieve this, may be by testing new therapeutics on autochthonous mouse models of cancer, i.e. mouse models that develop cancers in the tissues of interest, for example through genotoxic insult or genetic knockout. This would therefore allow drugs to be tested in an *in vivo* immune proficient setting, on tumours arising from endogenous mouse tissues. This would more faithfully recapitulate the human situation, in comparison to drug testing on transplanted human tumours in an immune deficient setting.

There are very few mouse models of CRC that develop beyond the adenoma stage, which is a major caveat when endeavouring to test new therapeutics designed for the later stages of disease. The development of mouse models of metastatic CRC has been the subject of much research. A model described by Hung et al, has recently shown that Apc$^{fl/fl}$ Kras$^{LSL/+}$ develop metastatic colon cancer after induction via adenoviral insertion of the cre recombinase transgene (Hung et al., 2010). However, this model involves invasive surgical procedures that require anaesthesia of the mouse. Therefore, models of metastatic CRC that involve less invasive procedures are required. Previous studies by the Clarke lab have described a mouse model that develops invasive intestinal adenocarcinomas – the *Ah*Cre-Apc$^{fl/+}$ Pten$^{fl/fl}$ mouse (Marsh et al., 2008). One aspect of the work outlined in this thesis, was to develop this model by the addition of further mutations in an attempt to allow the tumours that arise in *Ah*Cre-Apc$^{fl/+}$ Pten$^{fl/fl}$ mice to become metastatic. Two strategies were taken to try and achieve metastatic intestinal tumours. First was the addition of an activating Kras mutation, and the second was additional loss of cell adhesion protein E-cadherin. *Villin*Cre recombinase was used to

223

achieve intestinal specific transgenesis, to prevent any confounding effects from non-intestinal phenotypes.

### 9.1.1 Pten loss and Kras activation promotes tumour initiation and progression in a Wnt-driven tumour model

The rationale behind the addition of a Kras mutation to the $Apc^{fl/+}$ $Pten^{fl/fl}$ tumour model was based on the potential for synergy between Pten and Kras mutations, owing to the role of Kras in activation of both the PI3K and MAPK/Erk pathways (Rodriguez-Viciana et al., 1996). The progression of tumours in $Apc^{fl/+}$ $Pten^{fl/fl}$ mice coincides with elevated levels of phospho-Akt, and therefore increased activation of the PI3K pathway. Thus, synergy between Pten and Kras may allow progression of the tumours through enhanced PI3K pathway activation, as Kras activates the PI3K pathway and Pten inhibits it.

As hypothesised, the tumours that arose in $VillinCre-Apc^{fl/+}$ $Pten^{fl/fl}$ $Kras^{LSL/+}$ mice were more invasive than those observed in $VillinCre-Apc^{fl/+}$ $Pten^{fl/fl}$ mice (described in chapter 4). However, $Apc^{fl/+}$ $Pten^{fl/fl}$ $Kras^{LSL/+}$ mice had an increased number of tumours overall compared to $Apc^{fl/+}$ $Pten^{fl/fl}$ mice. As a result of this increased abundance of tumours, combined with the presence of more advanced tumours, $Apc^{fl/+}$ $Pten^{fl/fl}$ $Kras^{LSL/+}$ mice had a shorter lifespan than $Apc^{fl/+}$ $Pten^{fl/fl}$ mice. Therefore, addition of a Kras mutation to $Apc^{fl/+}$ $Pten^{fl/fl}$ mice promoted tumour initiation and progression. However, these tumours did not progress to metastasis. Despite this, due to the well-defined survival profile, the level of tumour progression and the involvement of common mutations found in human CRC (i.e. KRAS, APC), this model may be useful for preclinical testing of novel therapeutics. For example, patients that bear KRAS mutations often do not respond to cetuximab treatment (Lievre et al., 2006). As a result of this, inhibitors of pathways downstream of KRAS such as PI3K and MEK inhibitors are being developed. Therefore, the $VillinCre-Apc^{fl/+}$ $Pten^{fl/fl}$ $Kras^{LSL/+}$ mouse model would be a useful preclinical model to test these therapeutics, as the mice bear mutations in genes involved in both pathways and later stage invasive adenocarcinomas.

### 9.1.2 Synergy between Pten and Kras mutations potentially acts through the PI3K pathway

Synergy between Pten and Kras mutations is evidenced by disrupted intestinal homeostasis (outlined in chapters 3 and 5), and accelerated tumourigenesis (outlined in chapters 4 and 6). However, whether this synergy occurs through a number of pathways

or through one pathway is uncertain. The presence of elevated levels of the active form of Akt, phospho-Akt, in small intestinal tissue of $Pten^{fl/fl}$ $Kras^{LSL/+}$ and $Apc^{fl/+}$ $Pten^{fl/fl}$ $Kras^{LSL/+}$ mice, in chapters 3 and 5 suggests that homeostasis is altered through hyperactivation of Akt, and therefore hyperactivation of the PI3K pathway. PI3K activation has previously been associated with increased proliferation and loss of apoptosis *in vitro* (Itoh et al., 2002) and has been associated with increased proliferation *in vivo* (He et al., 2007) as well as hyperplasia of the intestine *in vivo* (Ferrand et al., 2005). However, activation of the PI3K pathway in the *in vivo* model described in Ferrand et al was also associated concomitantly with activation of a number of other signalling pathways, which may have contributed to the phenotype. My findings also indicate that the effect of PI3K activation on intestinal homeostasis also appears to depend on the level of activation. Low levels of phospho-Akt, hence low levels of PI3K pathway activation, results in subtle phenotypes (such as enhanced cellular migration), high levels of phospho-Akt results in more severe phenotypes (such as villus bifurcations and hyperplasia, these findings are outlined in chapter 5). The role the PI3K pathway plays in intestinal homeostasis must however be more robustly tested, through administration of PI3K inhibitors to $Pten^{fl/fl}$ $Kras^{LSL/+}$ mice.

### 9.1.3 $Pten^{fl/fl}$ $Kras^{LSL/+}$ mice as a preclinical model of metastatic CRC

Interestingly, long-term control, $Pten^{fl/fl}$ $Kras^{LSL/+}$ mice, developed metastatic carcinoma of the intestine after a long latency period, and the acquisition of a spontaneous somatic canonical Wnt-activating mutation. However, $Pten^{fl/fl}$ $Kras^{LSL/+}$ mice are unsuitable for therapeutic treatment due to low frequencies of mice possessing metastases. The reason why not all mice developed metastases is likely to be due to the long period before the mouse is symptomatic of disease, so therefore some mice succumbed to other age-related illnesses. Another caveat of using these mice for therapeutic treatment is the lack of overt external evidence of the presence of tumours, and more importantly metastatic spread. This caveat may be overcome by the use of imaging technologies such as positron emission tomography (PET), or magnetic resonance imaging (MRI). These imaging techniques can be used to detect the presence of metastases at the earliest stages, and then used to monitor the tumours during treatment. $Pten^{fl/fl}$ $Kras^{LSL/+}$ mice may also be useful for the study of biomarkers of advanced CRC, discovery of a signature of blood biomarkers that correlate with disease progression would be a useful tool to screen the animals for disease stage.

### 9.1.4 Wnt-activating mutation: tumour initiator or promoter?

The observation that all invasive adenocarcinomas and metastatic carcinomas that develop in Pten$^{fl/fl}$ Kras$^{LSL/+}$ mice had evidence of canonical-Wnt activation, taken together with the observation that Apc$^{fl/+}$ Pten$^{fl/fl}$ Kras$^{LSL/+}$ mice that were induced by the low recombination induction regimen do not progress to metastasis, suggests that the point at which a Wnt-activating mutation is acquired may be pivotal to whether the tumour metastasises. In humans there is evidence of Wnt-activation being a secondary event in tumourigenesis, particularly in sessile serrated adenomas (Wu et al., 2008, Yachida et al., 2009). It may also be plausible that during the long latency period between induction and morbidity the tumours that arise in Pten$^{fl/fl}$ Kras$^{LSL/+}$ mice may also have acquired other genetic mutations, e.g. p53 or Smad4 mutations, which may also be key factors to explaining why the tumours in these mice metastasise. Accumulation of mutations may be driven by Pten loss, as Pten loss has been suggested to promote genomic instability, independently of its lipid phosphatase activity but through its role in the nucleus. Pten loss has been shown to cause genomic instability through its association with centromeres and regulation of Rad51 expression (Shen et al., 2007, Gupta et al., 2009), so causing instability through loss of DNA damage repair and alteration of cell cycle checkpoints. Thus, loss of Pten in the mouse intestine may confer a mutator phenotype allowing additional mutations to frequently accumulate in these mice.

### 9.1.5 Pten$^{fl/fl}$ Kras$^{LSL/+}$ mice may represent a model of serrated adenocarcinoma

The serrated adenocarcinoma pathway is thought to represent an alternative pathway of CRC formation to the Fearon-Vogelstein model (Makinen et al., 2001, Huang et al., 2004). The differences between the two pathways are not only histological but there are also molecular differences, i.e. the traditional Fearon-Vogelstein pathway of CRC progression is through LOH, and the Serrated Adenocarcinoma pathway of CRC progression is through methylation and microsatellite instability. Through histological examination of the array of tumours that arise Pten$^{fl/fl}$ Kras$^{LSL/+}$ mice, one can postulate that the adenocarcinomas and metastatic carcinomas that arise in these mice develop from benign serrated adenomas (which are often observed synchronously with advanced tumours). Benign sessile serrated adenomas are frequently observed in these mice but traditional 'Apc-initiated' adenomas are never observed. Evidence of serration in advanced adenocarcinomas, carcinomas and metastases along with evidence of invasion and progression in sessile serrated adenomas support the hypothesis that the metastatic

carcinomas indeed arise from benign sessile serrated adenomas. However, the caveat of being unable to follow an individual lesion longitudinally in this model prevents conclusive proof of this hypothesis. The $Pten^{fl/fl}$ $Kras^{LSL/+}$ mouse model represents a potential mouse model of the serrated adenocarcinoma CRC progression pathway, and challenges the notion that a Wnt-activating mutation is required for tumourigenesis. This study, along with a recent study by Bennecke et al, in which mice bearing an activating Kras mutation and loss of the cell cycle inhibitor Ink4A/Arf also develop serrated adenomas and metastatic carcinoma (Bennecke et al., 2010) supports the hypothesis that CRC can arise from serrated adenomas.

## 9.1.6 The role of E-cadherin in tumour progression

Another strategy used to try and promote metastasis in the $Apc^{fl/+}$ $Pten^{fl/fl}$ mice was the additional loss of the cell adhesion protein E-cadherin. Loss of E-cadherin is positively correlated with increased progression of CRCs (Dorudi et al., 1995, Dorudi et al., 1993), so to address whether E-cadherin loss promotes tumour progression $Apc^{fl/+}$ $Pten^{fl/fl}$ $Cdh1^{fl/+}$ mice were generated, and the findings described in chapter 7. I was only able to investigate the contribution of heterozygous loss of E-cadherin on tumour progression, as homozygous loss of E-cadherin in adult mouse intestine resulted in extensive disruption of the intestinal epithelium and rapid morbidity. Heterozygous loss of E-cadherin does not promote tumour progression and overall survival and tumour number was unaltered in $Apc^{fl/+}$ $Pten^{fl/fl}$ $Cdh1^{fl/+}$ mice compared to control mice. However, through careful examination of tumour stage and survival data it remains possible that a subgroup of $Apc^{fl/+}$ $Pten^{fl/fl}$ $Cdh1^{fl/+}$ mice have higher numbers of small lesions than the control group. The observation that heterozygous loss of E-cadherin promotes tumour initiation has been previously reported. Increased tumour initiation is thought to be driven by release of transcriptionally active β-catenin via E-cadherin loss, resulting in activation of the canonical-Wnt pathway (Smits et al., 2000). The tumours that arise in $Apc^{fl/+}$ $Pten^{fl/fl}$ $Cdh1^{fl/+}$ mice do not show loss or reduction of E-cadherin immunostaining. Therefore, loss of heterozygosity of the remaining allele of Cdh1 (E-cadherin) did not occur in the tumours. The rapid demise of mice in which E-cadherin had been completely ablated proved to be the major caveat of this study, as this prevented the investigation of complete loss of E-cadherin within in the context of tumour progression.

In humans, loss of E-cadherin expression in a tumour is thought to promote tumour progression (Dorudi et al., 1995, Dorudi et al., 1993). However, the tumours

227

observed in the various mouse models described in this thesis show no evidence of loss or downregulation of E-cadherin expression, and heterozygous loss of E-cadherin in an intestinal tumour model does not promote tumour progression. Taken together, these findings suggest that E-cadherin does not appear to play a pivotal role in intestinal tumour progression in the mouse.

## 9.2 Stromal-epithelial interactions of Pten

PTEN is a major tumour suppressor that is commonly found to be mutated in many cancers including breast (Li et al., 1997, Saal et al., 2008), prostate (Li et al., 1997, Wang et al., 1998, Feilotter et al., 1998) and endometrial cancer (Risinger et al., 1997, Tashiro et al., 1997). Germline mutation of the gene in humans gives rise to PTEN Hamartoma Tumour Syndromes (PHTS), individuals with these syndromes are predisposed to benign tumours of the GI tract that have the capacity to progress to malignant disease (Carlson et al., 1984). Mouse models of constitutive deletion of Pten showed that homozygotes were inviable, but heterozygotes, like PHTS patients, were predisposed to GI tract tumours (Di Cristofano et al., 1998, Podsypanina et al., 1999). Studies in which conditional deletion of Pten was achieved specifically in the intestinal epithelium yielded contrasting results. He et al found using Mx1Cre mediated recombination, that loss of Pten from the adult mouse intestinal epithelium resulted in rapid tumour formation (He et al., 2007). In contrast, studies from Marsh et al and Langlois et al found that intestinal epithelial loss of Pten mediated by AhCre and VillinCre recombination did not predispose to intestinal tumour formation (Marsh et al., 2008, Langlois et al., 2009). Both constitutive, and Mx1Cre induced Pten loss, allows mutation of the gene from the underlying supporting stroma of the intestine as well as the epithelium. The aim of the study outlined in the final chapter of this thesis was to investigate how stromal fibroblast specific loss of Pten impacts on the intestinal epithelium.

### 9.2.1 Stromal loss of Pten promotes tumourigenesis

To investigate the disparity between the outcomes of the conditional Pten loss mouse models, Col1A2Cre$^+$ Pten$^{fl/fl}$ mice were generated. Col1A2Cre is expressed constitutively in intestinal stromal fibroblasts and smooth muscle, and is activated upon administration of tamoxifen. Short-term deletion of Pten from the small intestinal stromal compartment did not impact upon the epithelial stem cell compartment or enhance epithelial cell proliferation, as was reported in Mx1Cre$^+$ Pten$^{fl/fl}$ mice, which

lack Pten in both the stromal and epithelial compartments (He et al., 2007). However, there was an overt increase in the abundance of Ki67 positive cells in the small intestinal stroma. Long-term stromal loss of Pten predisposes to the formation of benign tumours throughout the intestine; these tumours are similar in morphology to hamartomas. The tumours in *Col1A2*Cre$^+$ Pten$^{fl/fl}$ mice have a large stromal component, and often, elevated levels of phospho-Akt are observed in the stromal component that directly correlate with elevated phospho-Erk and lower Ki67 immunostaining in the adjacent epithelium. It appears that loss of Pten from the intestinal stroma promotes tumourigenesis by stromal-epithelial interactions that involve paracrine activation of MAPK/Erk signalling. It also appears that elevated MAPK/Erk activation may result in cellular senescence, suggested by areas of strong phospho-Erk immunostaining coinciding with low Ki67 immunostaining. However, if the tumours are indeed senescent, it could also be driven by non-oncogenic mechanisms but by Pten loss. Pten loss has previously been associated with induction of cellular senescence in the prostate, through p53 dependent mechanisms (Chen et al., 2005). However, it is not known whether Pten loss induced senescence is prostate specific and if the same is observed in the intestine.

This is the first study that indicates that stromal loss of Pten is sufficient to promote intestinal tumourigenesis. The idea that manipulation of gene expression in the stromal component of a tissue can impact on epithelial homeostasis has previously been investigated. In particular, intestinal stromal specific ablation of Lkb1 gives rise to hamartomas (Katajisto et al., 2008). Interestingly, hamartomas are also observed in *Col1A2*Cre$^+$ Pten$^{fl/fl}$ mice; these similar phenotypes may be owing to both loss of Lkb1 and loss of Pten causing activation of the mTOR pathway. Taken together, these findings oppose the traditional view that tumours that are derived from epithelial tissues are caused by mutations in the epithelial cells, and genetic alterations in the stromal cells surrounding the epithelium may play a pivotal role in tumourigenesis.

## 9.2.2 The role of Pten in tumourigenesis

The deletion of Pten in the mouse has resulted in inconsistent phenotypes between models, in the case of the intestine. Constitutive heterozygous loss of Pten predisposes to intestinal tumours (Di Cristofano et al., 1998, Podsypanina et al., 1999), as does conditional homozygous loss of Pten from the epithelial and stromal small intestinal layers (He et al., 2007). However, epithelial specific homozygous loss of Pten, has been reported to not give rise to intestinal tumours (Langlois et al., 2009, Marsh et

al., 2008). Despite this, my findings indicate that after a long latency period (>500 days post induction), intestinal epithelial specific loss of Pten gives rise to benign tumours, but not with complete penetrance (chapter 6). I have also found that homozygous loss of Pten, specifically in the stromal fibroblasts and smooth muscle gives rise to benign intestinal tumours, similar to hamartomas, at shorter timepoints after induction (chapter 8). Taken together, this disparity of phenotypes observed between these models leads me to propose two possibilities about the function of Pten.

The first is that Pten may play a role in senescence in the mouse intestine, which may be more pronounced depending on the level of Pten loss and the compartment in which Pten is deleted. Pten loss induced senescence is also thought to be dose-dependent, in mouse embryonic fibroblasts and *in vivo*, in the prostate, homozygous loss of Pten promotes senescence, whereas cells heterozygous for Pten do not undergo senescence (Chen et al., 2005). If Pten has the same effect on cellular senescence in the intestine, it may provide some explanation as to why mice that have a constitutive heterozygous deletion of Pten develop intestinal tumours. Therefore it would be insightful to ascertain whether senescence is induced in the intestine when Pten is homozygously deleted in the epithelium, and in addition to this, investigate if epithelial specific, heterozygous loss of Pten promotes tumourigenesis. The second possibility is that PTEN may play a more intricate role in human CRC, and loss of expression in particular compartments of the intestine may promote tumourigenesis. Upregulation of microRNA-21, a microRNA that is targeted toward PTEN (among other mRNAs) has been noted in human tumours (Nielsen et al., 2011). Therefore, investigation into the expression levels of PTEN in human CRCs via IHC would be insightful.

# Reference List

ADLER, V., SCHAFFER, A., KIM, J., DOLAN, L. & RONAI, Z. (1995) UV irradiation and heat shock mediate JNK activation via alternate pathways. *The Journal of biological chemistry*, 270, 26071-7.

ALMOGUERA, C., SHIBATA, D., FORRESTER, K., MARTIN, J., ARNHEIM, N. & PERUCHO, M. (1988) Most human carcinomas of the exocrine pancreas contain mutant c-K-ras genes. *Cell*, 53, 549-54.

ANDREU, P., COLNOT, S., GODARD, C., GAD, S., CHAFEY, P., NIWA-KAWAKITA, M., LAURENT-PUIG, P., KAHN, A., ROBINE, S., PERRET, C. & ROMAGNOLO, B. (2005) Crypt-restricted proliferation and commitment to the Paneth cell lineage following Apc loss in the mouse intestine. *Development (Cambridge, England)*, 132, 1443-51.

AUCLAIR, B. A., BENOIT, Y. D., RIVARD, N., MISHINA, Y. & PERREAULT, N. (2007) Bone morphogenetic protein signaling is essential for terminal differentiation of the intestinal secretory cell lineage. *Gastroenterology*, 133, 887-96.

BARKER, N., RIDGWAY, R. A., VAN ES, J. H., VAN DE WETERING, M., BEGTHEL, H., VAN DEN BORN, M., DANENBERG, E., CLARKE, A. R., SANSOM, O. J. & CLEVERS, H. (2009) Crypt stem cells as the cells-of-origin of intestinal cancer. *Nature*, 457, 608-11.

BARKER, N., VAN ES, J. H., KUIPERS, J., KUJALA, P., VAN DEN BORN, M., COZIJNSEN, M., HAEGEBARTH, A., KORVING, J., BEGTHEL, H., PETERS, P. J. & CLEVERS, H. (2007) Identification of stem cells in small intestine and colon by marker gene Lgr5. *Nature*, 449, 1003-7.

BARNARD, J. A., WARWICK, G. J. & GOLD, L. I. (1993) Localization of transforming growth factor beta isoforms in the normal murine small intestine and colon. *Gastroenterology*, 105, 67-73.

BATLLE, E., HENDERSON, J. T., BEGHTEL, H., VAN DEN BORN, M. M., SANCHO, E., HULS, G., MEELDIJK, J., ROBERTSON, J., VAN DE WETERING, M., PAWSON, T. & CLEVERS, H. (2002) Beta-catenin and TCF mediate cell positioning in the intestinal epithelium by controlling the expression of EphB/ephrinB. *Cell*, 111, 251-63.

BENNECKE, M., KRIEGL, L., BAJBOUJ, M., RETZLAFF, K., ROBINE, S., JUNG, A., ARKAN, M. C., KIRCHNER, T. & GRETEN, F. R. (2010) Ink4a/Arf and oncogene-induced senescence prevent tumor progression during alternative colorectal tumorigenesis. *Cancer cell*, 18, 135-46.

BEPPU, H., MWIZERWA, O. N., BEPPU, Y., DATTWYLER, M. P., LAUWERS, G. Y., BLOCH, K. D. & GOLDSTEIN, A. M. (2008) Stromal inactivation of BMPRII leads to colorectal epithelial overgrowth and polyp formation. *Oncogene*, 27, 1063-70.

BHOWMICK, N. A., CHYTIL, A., PLIETH, D., GORSKA, A. E., DUMONT, N., SHAPPELL, S., WASHINGTON, M. K., NEILSON, E. G. & MOSES, H. L. (2004) TGF-beta signaling in fibroblasts modulates the oncogenic potential of adjacent epithelia. *Science (New York, N.Y*, 303, 848-51.

BJERKNES, M. & CHENG, H. (1981a) Methods for the isolation of intact epithelium from the mouse intestine. *The Anatomical record*, 199, 565-74.

BJERKNES, M. & CHENG, H. (1981b) The stem-cell zone of the small intestinal epithelium. I. Evidence from Paneth cells in the adult mouse. *The American journal of anatomy*, 160, 51-63.

BLUMENTHAL, G. M. & DENNIS, P. A. (2008) PTEN hamartoma tumor syndromes. *European journal of human genetics*, 16, 1289-300.

BOS, J. L., FEARON, E. R. & HAMILTON, S. R. (1987) Prevalence of ras gene mutations in human colorectal cancers. *Nature*, 327, 293-297.

BOUCHER, M. J., JEAN, D., VEZINA, A. & RIVARD, N. (2004) Dual role of MEK/ERK signaling in senescence and transformation of intestinal epithelial cells. *American journal of physiology*, 286, G736-46.

BOUTROS, M., PARICIO, N., STRUTT, D. I. & MLODZIK, M. (1998) Dishevelled activates JNK and discriminates between JNK pathways in planar polarity and wingless signaling. *Cell*, 94, 109-18.

BRONNER, C. E., BAKER, S. M., MORRISON, P. T., WARREN, G., SMITH, L. G., LESCOE, M. K., KANE, M., EARABINO, C., LIPFORD, J., LINDBLOM, A. & ET AL. (1994) Mutation in the DNA mismatch repair gene homologue hMLH1 is associated with hereditary non-polyposis colon cancer. *Nature*, 368, 258-61.

BURKERT, J., OTTO, W. R. & WRIGHT, N. A. (2008) Side populations of gastrointestinal cancers are not enriched in stem cells. *The Journal of pathology*, 214, 564-73.

CALCAGNO, S. R., LI, S., COLON, M., KREINEST, P. A., THOMPSON, E. A., FIELDS, A. P. & MURRAY, N. R. (2008) Oncogenic K-ras promotes early carcinogenesis in the mouse proximal colon. *International journal of cancer*, 122, 2462-70.

CANCERRESEARCHUK (2009) Bowel cancer - symptoms and treatment. *Cancer Stats*.

CANCERRESEARCHUK (2010) UK Cancer Mortality Statistics in 2008.

CANCERRESEARCHUK (2011) Cancer incidence for common cancers - UK statistics 2007.

CARLSON, G. J., NIVATVONGS, S. & SNOVER, D. C. (1984) Colorectal polyps in Cowden's disease (multiple hamartoma syndrome). *American Journal of Surgical Pathology*, 8, 763-770.

CARRAGHER, L. A., SNELL, K. R., GIBLETT, S. M., ALDRIDGE, V. S., PATEL, B., COOK, S. J., WINTON, D. J., MARAIS, R. & PRITCHARD, C. A. (2010) V600EBraf induces gastrointestinal crypt senescence and promotes tumour progression through enhanced CpG methylation of p16INK4a. *EMBO molecular medicine*, 2, 458-71.

CHAN, T. L., YUEN, S. T., KONG, C. K., CHAN, Y. W., CHAN, A. S., NG, W. F., TSUI, W. Y., LO, M. W., TAM, W. Y., LI, V. S. & LEUNG, S. Y. (2006) Heritable germline epimutation of MSH2 in a family with hereditary nonpolyposis colorectal cancer. *Nature genetics*, 38, 1178-83.

CHAN, T. L., ZHAO, W., LEUNG, S. Y. & YUEN, S. T. (2003) BRAF and KRAS mutations in colorectal hyperplastic polyps and serrated adenomas. *Cancer research*, 63, 4878-81.

CHEN, S. D., CHEN, Y. B., PENG, Y., XU, J., CHEN, S. S., ZHANG, J. L., LI, Z. Z. & TAN, Z. (2010) Role of PI3K/Akt signaling in the protective effect of magnesium sulfate against ischemia-perfusion injury of small intestine in rats. *Chinese medical journal*, 123, 1447-52.

CHEN, Z., TROTMAN, L. C., SHAFFER, D., LIN, H. K., DOTAN, Z. A., NIKI, M., KOUTCHER, J. A., SCHER, H. I., LUDWIG, T., GERALD, W., CORDON-CARDO, C. & PANDOLFI, P. P. (2005) Crucial role of p53-dependent cellular senescence in suppression of Pten-deficient tumorigenesis. *Nature*, 436, 725-730.

CHENG, H. & LEBLOND, C. P. (1974) Origin, differentiation and renewal of the four main epithelial cell types in the mouse small intestine. V. Unitarian Theory of the origin of the four epithelial cell types. *The American journal of anatomy*, 141, 537-61.

CLARKE, A. R., CUMMINGS, M. C. & HARRISON, D. J. (1995) Interaction between murine germline mutations in p53 and APC predisposes to pancreatic neoplasia but not to increased intestinal malignancy. *Oncogene*, 11, 1913-20.

CLARKE, M. F., DICK, J. E., DIRKS, P. B., EAVES, C. J., JAMIESON, C. H., JONES, D. L., VISVADER, J., WEISSMAN, I. L. & WAHL, G. M. (2006) Cancer stem cells--perspectives on current status and future directions: AACR Workshop on cancer stem cells. *Cancer research,* 66, 9339-44.

CLEVERS, H. (2006) Wnt/beta-catenin signaling in development and disease. *Cell,* 127, 469-80.

COOMBES, J. L. & MALOY, K. J. (2007) Control of intestinal homeostasis by regulatory T cells and dendritic cells. *Seminars in immunology,* 19, 116-26.

COSENTINO, L., SHAVER-WALKER, P. & HEDDLE, J. A. (1996) The relationships among stem cells, crypts, and villi in the small intestine of mice as determined by mutation tagging. *Developmental dynamics,* 207, 420-8.

COSO, O. A., CHIARIELLO, M., YU, J. C., TERAMOTO, H., CRESPO, P., XU, N., MIKI, T. & GUTKIND, J. S. (1995) The small GTP-binding proteins Rac1 and Cdc42 regulate the activity of the JNK/SAPK signaling pathway. *Cell,* 81, 1137-46.

CREAMER, B. (1967) The turnover of the epithelium of the small intestine. *British medical bulletin,* 23, 226-30.

DALERBA, P., DYLLA, S. J., PARK, I. K., LIU, R., WANG, X., CHO, R. W., HOEY, T., GURNEY, A., HUANG, E. H., SIMEONE, D. M., SHELTON, A. A., PARMIANI, G., CASTELLI, C. & CLARKE, M. F. (2007) Phenotypic characterization of human colorectal cancer stem cells. *Proceedings of the National Academy of Sciences of the United States of America,* 104, 10158-63.

DERKSEN, P. W., LIU, X., SARIDIN, F., VAN DER GULDEN, H., ZEVENHOVEN, J., EVERS, B., VAN BEIJNUM, J. R., GRIFFIOEN, A. W., VINK, J., KRIMPENFORT, P., PETERSE, J. L., CARDIFF, R. D., BERNS, A. & JONKERS, J. (2006) Somatic inactivation of E-cadherin and p53 in mice leads to metastatic lobular mammary carcinoma through induction of anoikis resistance and angiogenesis. *Cancer cell,* 10, 437-49.

DI CRISTOFANO, A., PESCE, B., CORDON-CARDO, C. & PANDOLFI, P. P. (1998) Pten is essential for embryonic development and tumour suppression. *Nature Genetics,* 19, 348-355.

DIEHL, J. A., CHENG, M., ROUSSEL, M. F. & SHERR, C. J. (1998) Glycogen synthase kinase-3beta regulates cyclin D1 proteolysis and subcellular localization. *Genes & development,* 12, 3499-511.

DINULESCU, D. M., INCE, T. A., QUADE, B. J., SHAFER, S. A., CROWLEY, D. & JACKS, T. (2005) Role of K-ras and Pten in the development of mouse models of endometriosis and endometrioid ovarian cancer. *Nature medicine,* 11, 63-70.

DISE, R. S., FREY, M. R., WHITEHEAD, R. H. & POLK, D. B. (2008) Epidermal growth factor stimulates Rac activation through Src and phosphatidylinositol 3-kinase to promote colonic epithelial cell migration. *American journal of physiology,* 294, G276-85.

DOETSCHMAN, T., GREGG, R. G., MAEDA, N., HOOPER, M. L., MELTON, D. W., THOMPSON, S. & SMITHIES, O. (1987) Targetted correction of a mutant HPRT gene in mouse embryonic stem cells. *Nature,* 330, 576-8.

DORUDI, S., HANBY, A. M., POULSOM, R., NORTHOVER, J. & HART, I. R. (1995) Level of expression of E-cadherin mRNA in colorectal cancer correlates with clinical outcome. *British journal of cancer,* 71, 614-6.

DORUDI, S., SHEFFIELD, J. P., POULSOM, R., NORTHOVER, J. M. & HART, I. R. (1993) E-cadherin expression in colorectal cancer. An immunocytochemical and in situ hybridization study. *The American journal of pathology,* 142, 981-6.

DOUARD, R., MOUTEREAU, S., PERNET, P., CHIMINGQI, M., ALLORY, Y., MANIVET, P., CONTI, M., VAUBOURDOLLE, M., CUGNENC, P. H. & LORIC, S. (2006)

Sonic Hedgehog-dependent proliferation in a series of patients with colorectal cancer. *Surgery,* 139, 665-70.

DUKES, C. (1980) The classification of cancer of the rectum. *Diseases of the Colon &amp; Rectum,* 23, 605-611.

DYMECKI, S. M. (1996) Flp recombinase promotes site-specific DNA recombination in embryonic stem cells and transgenic mice. *Proceedings of the National Academy of Sciences of the United States of America,* 93, 6191-6.

EL MARJOU, F., JANSSEN, K. P., CHANG, B. H. J., LI, M., HINDIE, V., CHAN, L., LOUVARD, D., CHAMBON, P., METZGER, D. & ROBINE, S. (2004) Tissue-specific and inducible Cre-mediated recombination in the gut epithelium. *Genesis,* 39, 186-193.

EPPERT, K., SCHERER, S. W., OZCELIK, H., PIRONE, R., HOODLESS, P., KIM, H., TSUI, L. C., BAPAT, B., GALLINGER, S., ANDRULIS, I. L., THOMSEN, G. H., WRANA, J. L. & ATTISANO, L. (1996) MADR2 maps to 18q21 and encodes a TGFbeta-regulated MAD-related protein that is functionally mutated in colorectal carcinoma. *Cell,* 86, 543-52.

EVANS, M. J. & KAUFMAN, M. H. (1981) Establishment in culture of pluripotential cells from mouse embryos. *Nature,* 292, 154-6.

FAZELI, A., DICKINSON, S. L., HERMISTON, M. L., TIGHE, R. V., STEEN, R. G., SMALL, C. G., STOECKLI, E. T., KEINO-MASU, K., MASU, M., RAYBURN, H., SIMONS, J., BRONSON, R. T., GORDON, J. I., TESSIER-LAVIGNE, M. & WEINBERG, R. A. (1997) Phenotype of mice lacking functional Deleted in colorectal cancer (Dcc) gene. *Nature,* 386, 796-804.

FEARON, E. R., CHO, K. R., NIGRO, J. M., KERN, S. E., SIMONS, J. W., RUPPERT, J. M., HAMILTON, S. R., PREISINGER, A. C., THOMAS, G., KINZLER, K. W. & ET AL. (1990) Identification of a chromosome 18q gene that is altered in colorectal cancers. *Science (New York, N.Y,* 247, 49-56.

FEARON, E. R. & VOGELSTEIN, B. (1990) A genetic model for colorectal tumorigenesis. *Cell,* 61, 759-67.

FEIL, R., BROCARD, J., MASCREZ, B., LEMEUR, M., METZGER, D. & CHAMBON, P. (1996) Ligand-activated site-specific recombination in mice. *Proceedings of the National Academy of Sciences of the United States of America,* 93, 10887-90.

FEILOTTER, H. E., NAGAI, M. A., BOAG, A. H., ENG, C. & MULLIGAN, L. M. (1998) Analysis of PTEN and the 10q23 region in primary prostate carcinomas. *Oncogene,* 16, 1743-1748.

FERRAND, A., BERTRAND, C., PORTOLAN, G., CUI, G., CARLSON, J., PRADAYROL, L., FOURMY, D., DUFRESNE, M., WANG, T. C. & SEVA, C. (2005) Signaling pathways associated with colonic mucosa hyperproliferation in mice overexpressing gastrin precursors. *Cancer research,* 65, 2770-7.

FISHEL, R., LESCOE, M. K., RAO, M. R., COPELAND, N. G., JENKINS, N. A., GARBER, J., KANE, M. & KOLODNER, R. (1993) The human mutator gene homolog MSH2 and its association with hereditary nonpolyposis colon cancer. *Cell,* 75, 1027-38.

FRE, S., HUYGHE, M., MOURIKIS, P., ROBINE, S., LOUVARD, D. & ARTAVANIS-TSAKONAS, S. (2005) Notch signals control the fate of immature progenitor cells in the intestine. *Nature,* 435, 964-8.

GARBER, K. (2006) Realistic rodents? Debate grows over new mouse models of cancer. *Journal of the National Cancer Institute,* 98, 1176-8.

GEBHARD, A. & GEBERT, A. (1999) Brush cells of the mouse intestine possess a specialized glycocalyx as revealed by quantitative lectin histochemistry. Further evidence for a sensory function. *The journal of histochemistry and cytochemistry,* 47, 799-808.

GERBE, F., BRULIN, B., MAKRINI, L., LEGRAVEREND, C. & JAY, P. (2009) DCAMKL-1 expression identifies Tuft cells rather than stem cells in the adult mouse intestinal epithelium. *Gastroenterology*, 137, 2179-80; author reply 2180-1.

GOSSEN, M. & BUJARD, H. (1992) Tight control of gene expression in mammalian cells by tetracycline-responsive promoters. *Proceedings of the National Academy of Sciences of the United States of America*, 89, 5547-51.

GOTTARDI, C. J., WONG, E. & GUMBINER, B. M. (2001) E-cadherin suppresses cellular transformation by inhibiting beta-catenin signaling in an adhesion-independent manner. *The Journal of cell biology*, 153, 1049-60.

GREGORIEFF, A., PINTO, D., BEGTHEL, H., DESTREE, O., KIELMAN, M. & CLEVERS, H. (2005) Expression pattern of Wnt signaling components in the adult intestine. *Gastroenterology*, 129, 626-38.

GROSSMANN, J., WALTHER, K., ARTINGER, M., RUMMELE, P., WOENCKHAUS, M. & SCHOLMERICH, J. (2002) Induction of apoptosis before shedding of human intestinal epithelial cells. *The American journal of gastroenterology*, 97, 1421-8.

GUERRA, C., MIJIMOLLE, N., DHAWAHIR, A., DUBUS, P., BARRADAS, M., SERRANO, M., CAMPUZANO, V. & BARBACID, M. (2003) Tumor induction by an endogenous K-ras oncogene is highly dependent on cellular context. *Cancer Cell*, 4, 111-120.

GUPTA, A., YANG, Q., PANDITA, R. K., HUNT, C. R., XIANG, T., MISRI, S., ZENG, S., PAGAN, J., JEFFERY, J., PUC, J., KUMAR, R., FENG, Z., POWELL, S. N., BHAT, A., YAGUCHI, T., WADHWA, R., KAUL, S. C., PARSONS, R., KHANNA, K. K. & PANDITA, T. K. (2009) Cell cycle checkpoint defects contribute to genomic instability in PTEN deficient cells independent of DNA DSB repair. *Cell cycle (Georgetown, Tex*, 8, 2198-210.

HAIGIS, K. M., KENDALL, K. R., WANG, Y., CHEUNG, A., HAIGIS, M. C., GLICKMAN, J. N., NIWA-KAWAKITA, M., SWEET-CORDERO, A., SEBOLT-LEOPOLD, J., SHANNON, K. M., SETTLEMAN, J., GIOVANNINI, M. & JACKS, T. (2008) Differential effects of oncogenic K-Ras and N-Ras on proliferation, differentiation and tumor progression in the colon. *Nature genetics*, 40, 600-8.

HALL, P. A., COATES, P. J., ANSARI, B. & HOPWOOD, D. (1994) Regulation of cell number in the mammalian gastrointestinal tract: the importance of apoptosis. *Journal of cell science*, 107 ( Pt 12), 3569-77.

HARAMIS, A. P., BEGTHEL, H., VAN DEN BORN, M., VAN ES, J., JONKHEER, S., OFFERHAUS, G. J. & CLEVERS, H. (2004) De novo crypt formation and juvenile polyposis on BMP inhibition in mouse intestine. *Science (New York, N.Y*, 303, 1684-6.

HARDWICK, J. C., VAN DEN BRINK, G. R., BLEUMING, S. A., BALLESTER, I., VAN DEN BRANDE, J. M., KELLER, J. J., OFFERHAUS, G. J., VAN DEVENTER, S. J. & PEPPELENBOSCH, M. P. (2004) Bone morphogenetic protein 2 is expressed by, and acts upon, mature epithelial cells in the colon. *Gastroenterology*, 126, 111-21.

HAY, E. D. (1995) An overview of epithelio-mesenchymal transformation. *Acta anatomica*, 154, 8-20.

HE, X. C., YIN, T., GRINDLEY, J. C., TIAN, Q., SATO, T., TAO, W. A., DIRISINA, R., PORTER-WESTPFAHL, K. S., HEMBREE, M., JOHNSON, T., WIEDEMANN, L. M., BARRETT, T. A., HOOD, L., WU, H. & LI, L. (2007) PTEN-deficient intestinal stem cells initiate intestinal polyposis. *Nature Genetics*, 39, 189-198.

HE, X. C., ZHANG, J., TONG, W. G., TAWFIK, O., ROSS, J., SCOVILLE, D. H., TIAN, Q., ZENG, X., HE, X., WIEDEMANN, L. M., MISHINA, Y. & LI, L. (2004) BMP signaling inhibits intestinal stem cell self-renewal through suppression of Wnt-beta-catenin signaling. *Nature genetics*, 36, 1117-21.

HERMISTON, M. L., WONG, M. H. & GORDON, J. I. (1996) Forced expression of E-cadherin in the mouse intestinal epithelium slows cell migration and provides evidence for nonautonomous regulation of cell fate in a self-renewing system. *Genes & development*, 10, 985-96.

HEWITSON, P., GLASZIOU, P., IRWIG, L., TOWLER, B. & WATSON, E. (2007) Screening for colorectal cancer using the faecal occult blood test, Hemoccult. *Cochrane database of systematic reviews (Online)*, CD001216.

HIGASHIDANI, Y., TAMURA, S., MORITA, T., TADOKORO, T., YOKOYAMA, Y., MIYAZAKI, J., YANG, Y., TAKEUCHI, S., TAGUCHI, H. & ONISHI, S. (2003) Analysis of K-ras codon 12 mutation in flat and nodular variants of serrated adenoma in the colon. *Diseases of the colon and rectum*, 46, 327-32.

HILL, R., CALVOPINA, J. H., KIM, C., WANG, Y., DAWSON, D. W., DONAHUE, T. R., DRY, S. & WU, H. (2010) PTEN loss accelerates KrasG12D-induced pancreatic cancer development. *Cancer research*, 70, 7114-24.

HILL, R. P. (2006) Identifying cancer stem cells in solid tumors: case not proven. *Cancer research*, 66, 1891-5; discussion 1890.

HIRSCHMANN-JAX, C., FOSTER, A. E., WULF, G. G., NUCHTERN, J. G., JAX, T. W., GOBEL, U., GOODELL, M. A. & BRENNER, M. K. (2004) A distinct "side population" of cells with high drug efflux capacity in human tumor cells. *Proceedings of the National Academy of Sciences of the United States of America*, 101, 14228-33.

HOFMANN, C., OBERMEIER, F., ARTINGER, M., HAUSMANN, M., FALK, W., SCHOELMERICH, J., ROGLER, G. & GROSSMANN, J. (2007) Cell-cell contacts prevent anoikis in primary human colonic epithelial cells. *Gastroenterology*, 132, 587-600.

HOHENSTEIN, P., MOLENAAR, L., ELSINGA, J., MORREAU, H., VAN DER KLIFT, H., STRUIJK, A., JAGMOHAN-CHANGUR, S., SMITS, R., VAN KRANEN, H., VAN OMMEN, G. J., CORNELISSE, C., DEVILEE, P. & FODDE, R. (2003) Serrated adenomas and mixed polyposis caused by a splice acceptor deletion in the mouse Smad4 gene. *Genes, chromosomes & cancer*, 36, 273-82.

HOWE, J. R., BAIR, J. L., SAYED, M. G., ANDERSON, M. E., MITROS, F. A., PETERSEN, G. M., VELCULESCU, V. E., TRAVERSO, G. & VOGELSTEIN, B. (2001) Germline mutations of the gene encoding bone morphogenetic protein receptor 1A in juvenile polyposis. *Nature genetics*, 28, 184-7.

HOWE, J. R., ROTH, S., RINGOLD, J. C., SUMMERS, R. W., JARVINEN, H. J., SISTONEN, P., TOMLINSON, I. P., HOULSTON, R. S., BEVAN, S., MITROS, F. A., STONE, E. M. & AALTONEN, L. A. (1998) Mutations in the SMAD4/DPC4 gene in juvenile polyposis. *Science (New York, N.Y*, 280, 1086-8.

HUANG, C. S., O'BRIEN M, J., YANG, S. & FARRAYE, F. A. (2004) Hyperplastic polyps, serrated adenomas, and the serrated polyp neoplasia pathway. *The American journal of gastroenterology*, 99, 2242-55.

HUANG, C. Y., HSIAO, J. K., LU, Y. Z., LEE, T. C. & YU, L. C. (2011) Anti-apoptotic PI3K/Akt signaling by sodium/glucose transporter 1 reduces epithelial barrier damage and bacterial translocation in intestinal ischemia. *Laboratory investigation; a journal of technical methods and pathology*, 91, 294-309.

HUBER, M. A., KRAUT, N. & BEUG, H. (2005) Molecular requirements for epithelial-mesenchymal transition during tumor progression. *Current opinion in cell biology*, 17, 548-58.

HUNG, K. E., MARICEVICH, M. A., RICHARD, L. G., CHEN, W. Y., RICHARDSON, M. P., KUNIN, A., BRONSON, R. T., MAHMOOD, U. & KUCHERLAPATI, R. (2010) Development of a mouse model for sporadic and metastatic colon tumors and its use in assessing drug treatment. *Proceedings of the National Academy of Sciences of the United States of America*, 107, 1565-70.

HUNT MORGAN, T. (1919) The Physical Basis of Heredity. *Monographs on Experimental Biology.*

HUNTER, N. L., AWATRAMANI, R. B., FARLEY, F. W. & DYMECKI, S. M. (2005) Ligand-activated Flpe for temporally regulated gene modifications. *Genesis (New York, N.Y.,* 41, 99-109.

IACOPETTA, B., RUSSO, A., BAZAN, V., DARDANONI, G., GEBBIA, N., SOUSSI, T., KERR, D., ELSALEH, H., SOONG, R., KANDIOLER, D., JANSCHEK, E., KAPPEL, S., LUNG, M., LEUNG, C. S. S., KO, J. M., YUEN, S., HO, J., LEUNG, S. Y., CRAPEZ, E., DUFFOUR, J., YCHOU, M., LEAHY, D. T., O'DONOGHUE, D. P., AGNESE, V., CASCIO, S., DI FEDE, G., CHIECO-BIANCHI, L., BERTORELLE, R., BELLUCO, C., GIARETTI, W., CASTAGNOLA, P., RICEVUTO, E., FICORELLA, C., BOSARI, S., ARIZZI, C. D., MIYAKI, M., ONDA, M., KAMPMAN, E., DIERGAARDE, B., ROYDS, J., LOTHE, R. A., DIEP, C. B., MELING, G. I., OSTROWSKI, J., TRZECIAK, L., GUZIN?SKA-USTYMOWICZ, K., ZALEWSKI, B., CAPELLA, G. M., MORENO, V., PEINADO, M. A., LO?NNROTH, C., LUNDHOLM, K., SUN, X. F., JANSSON, A., BOUZOURENE, H., HSIEH, L. L., TANG, R., SMITH, D. R., ALLEN-MERSH, T. G., KHAN, Z. A. J., SHORTHOUSE, A. J., SILVERMAN, M. L., KATO, S. & ISHIOKA, C. (2006) Functional categories of TP53 mutation in colorectal cancer: Results of an International Collaborative Study. *Annals of Oncology,* 17, 842-847.

IRELAND, H., HOUGHTON, C., HOWARD, L. & WINTON, D. J. (2005) Cellular inheritance of a Cre-activated reporter gene to determine Paneth cell longevity in the murine small intestine. *Developmental dynamics,* 233, 1332-6.

IRELAND, H., KEMP, R., HOUGHTON, C., HOWARD, L., CLARKE, A. R., SANSOM, O. J. & WINTON, D. J. (2004) Inducible Cre-mediated control of gene expression in the murine gastrointestinal tract: effect of loss of beta-catenin. *Gastroenterology,* 126, 1236-46.

ITOH, N., SEMBA, S., ITO, M., TAKEDA, H., KAWATA, S. & YAMAKAWA, M. (2002) Phosphorylation of Akt/PKB is required for suppression of cancer cell apoptosis and tumor progression in human colorectal carcinoma. *Cancer,* 94, 3127-34.

IWANAGA, K., YANG, Y., RASO, M. G., MA, L., HANNA, A. E., THILAGANATHAN, N., MOGHADDAM, S., EVANS, C. M., LI, H., CAI, W. W., SATO, M., MINNA, J. D., WU, H., CREIGHTON, C. J., DEMAYO, F. J., WISTUBA, II & KURIE, J. M. (2008) Pten inactivation accelerates oncogenic K-ras-initiated tumorigenesis in a mouse model of lung cancer. *Cancer research,* 68, 1119-27.

JANG, K. S., SONG, Y. S., JANG, S. H., MIN, K. W., NA, W., JANG, S. M., JUN, Y. J., LEE, K. H., CHOI, D. & PAIK, S. S. (2010) Clinicopathological significance of nuclear PTEN expression in colorectal adenocarcinoma. *Histopathology,* 56, 229-39.

JANSSEN, K. P., ALBERICI, P., FSIHI, H., GASPAR, C., BREUKEL, C., FRANKEN, P., ROSTY, C., ABAL, M., EL MARJOU, F., SMITS, R., LOUVARD, D., FODDE, R. & ROBINE, S. (2006) APC and oncogenic KRAS are synergistic in enhancing Wnt signaling in intestinal tumor formation and progression. *Gastroenterology,* 131, 1096-109.

JANSSEN, K. P., EL-MARJOU, F., PINTO, D., SASTRE, X., ROUILLARD, D., FOUQUET, C., SOUSSI, T., LOUVARD, D. & ROBINE, S. (2002) Targeted expression of oncogenic K-ras in intestinal epithelium causes spontaneous tumorigenesis in mice. *Gastroenterology,* 123, 492-504.

JASS, J. R. (2005) Serrated adenoma of the colorectum and the DNA-methylator phenotype. *Nature clinical practice,* 2, 398-405.

JASS, J. R., BIDEN, K. G., CUMMINGS, M. C., SIMMS, L. A., WALSH, M., SCHOCH, E., MELTZER, S. J., WRIGHT, C., SEARLE, J., YOUNG, J. & LEGGETT, B. A.

(1999) Characterisation of a subtype of colorectal cancer combining features of the suppressor and mild mutator pathways. *Journal of clinical pathology*, 52, 455-60.

JASS, J. R., WHITEHALL, V. L., YOUNG, J. & LEGGETT, B. A. (2002) Emerging concepts in colorectal neoplasia. *Gastroenterology*, 123, 862-76.

JENNE, D. E., REIMANN, H., NEZU, J., FRIEDEL, W., LOFF, S., JESCHKE, R., MULLER, O., BACK, W. & ZIMMER, M. (1998) Peutz-Jeghers syndrome is caused by mutations in a novel serine threonine kinase. *Nature genetics*, 18, 38-43.

KAESTNER, K. H., SILBERG, D. G., TRABER, P. G. & SCHUTZ, G. (1997) The mesenchymal winged helix transcription factor Fkh6 is required for the control of gastrointestinal proliferation and differentiation. *Genes & development*, 11, 1583-95.

KAMBARA, T., SIMMS, L. A., WHITEHALL, V. L., SPRING, K. J., WYNTER, C. V., WALSH, M. D., BARKER, M. A., ARNOLD, S., MCGIVERN, A., MATSUBARA, N., TANAKA, N., HIGUCHI, T., YOUNG, J., JASS, J. R. & LEGGETT, B. A. (2004) BRAF mutation is associated with DNA methylation in serrated polyps and cancers of the colorectum. *Gut*, 53, 1137-44.

KARAMITOPOULOU, E., ZLOBEC, I., PATSOURIS, E., PEROS, G. & LUGLI, A. (2011) Loss of E-cadherin independently predicts the lymph node status in colorectal cancer. *Pathology*, 43, 133-7.

KATAJISTO, P., VAAHTOMERI, K., EKMAN, N., VENTELA, E., RISTIMAKI, A., BARDEESY, N., FEIL, R., DEPINHO, R. A. & MAKELA, T. P. (2008) LKB1 signaling in mesenchymal cells required for suppression of gastrointestinal polyposis. *Nature genetics*, 40, 455-9.

KATSO, R., OKKENHAUG, K., AHMADI, K., WHITE, S., TIMMS, J. & WATERFIELD, M. D. (2001) Cellular function of phosphoinositide 3-kinases: implications for development, homeostasis, and cancer. *Annual review of cell and developmental biology*, 17, 615-75.

KEINO-MASU, K., MASU, M., HINCK, L., LEONARDO, E. D., CHAN, S. S., CULOTTI, J. G. & TESSIER-LAVIGNE, M. (1996) Deleted in Colorectal Cancer (DCC) encodes a netrin receptor. *Cell*, 87, 175-85.

KELLY, P. N., DAKIC, A., ADAMS, J. M., NUTT, S. L. & STRASSER, A. (2007) Tumor growth need not be driven by rare cancer stem cells. *Science (New York, N.Y*, 317, 337.

KHALEGHPOUR, K., LI, Y., BANVILLE, D., YU, Z. & SHEN, S. H. (2004) Involvement of the PI 3-kinase signaling pathway in progression of colon adenocarcinoma. *Carcinogenesis*, 25, 241-8.

KIM, B. G., LI, C., QIAO, W., MAMURA, M., KASPRZAK, B., ANVER, M., WOLFRAIM, L., HONG, S., MUSHINSKI, E., POTTER, M., KIM, S. J., FU, X. Y., DENG, C. & LETTERIO, J. J. (2006) Smad4 signalling in T cells is required for suppression of gastrointestinal cancer. *Nature*, 441, 1015-9.

KINZLER, K. W., NILBERT, M. C., SU, L. K., VOGELSTEIN, B., BRYAN, T. M., LEVY, D. B., SMITH, K. J., PREISINGER, A. C., HEDGE, P., MCKECHNIE, D. & ET AL. (1991) Identification of FAP locus genes from chromosome 5q21. *Science (New York, N.Y*, 253, 661-5.

KINZLER, K. W. & VOGELSTEIN, B. (1998) Landscaping the cancer terrain. *Science (New York, N.Y*, 280, 1036-7.

KISTNER, A., GOSSEN, M., ZIMMERMANN, F., JERECIC, J., ULLMER, C., LUBBERT, H. & BUJARD, H. (1996) Doxycycline-mediated quantitative and tissue-specific control of gene expression in transgenic mice. *Proceedings of the National Academy of Sciences of the United States of America*, 93, 10933-8.

KOLTERUD, A., GROSSE, A. S., ZACHARIAS, W. J., WALTON, K. D., KRETOVICH, K. E., MADISON, B. B., WAGHRAY, M., FERRIS, J. E., HU, C., MERCHANT, J. L.,

DLUGOSZ, A. A., KOTTMANN, A. H. & GUMUCIO, D. L. (2009) Paracrine Hedgehog signaling in stomach and intestine: new roles for hedgehog in gastrointestinal patterning. *Gastroenterology*, 137, 618-28.

KORINEK, V., BARKER, N., MOERER, P., VAN DONSELAAR, E., HULS, G., PETERS, P. J. & CLEVERS, H. (1998) Depletion of epithelial stem-cell compartments in the small intestine of mice lacking Tcf-4. *Nature genetics*, 19, 379-83.

KOSINSKI, C., STANGE, D. E., XU, C., CHAN, A. S., HO, C., YUEN, S. T., MIFFLIN, R. C., POWELL, D. W., CLEVERS, H., LEUNG, S. Y. & CHEN, X. (2010) Indian hedgehog regulates intestinal stem cell fate through epithelial-mesenchymal interactions during development. *Gastroenterology*, 139, 893-903.

KRAEHENBUHL, J. P. & NEUTRA, M. R. (2000) Epithelial M cells: differentiation and function. *Annual review of cell and developmental biology*, 16, 301-32.

KRANENBURG, O. (2005) The KRAS oncogene: past, present, and future. *Biochimica et biophysica acta*, 1756, 81-2.

KUHN, R., SCHWENK, F., AGUET, M. & RAJEWSKY, K. (1995) Inducible gene targeting in mice. *Science (New York, N.Y*, 269, 1427-9.

LANGLOIS, M. J., ROY, S. A., AUCLAIR, B. A., JONES, C., BOUDREAU, F., CARRIER, J. C., RIVARD, N. & PERREAULT, N. (2009) Epithelial phosphatase and tensin homolog regulates intestinal architecture and secretory cell commitment and acts as a modifier gene in neoplasia. *The FASEB journal*, 23, 1835-44.

LEACH, F. S., NICOLAIDES, N. C., PAPADOPOULOS, N., LIU, B., JEN, J., PARSONS, R., PELTOMAKI, P., SISTONEN, P., AALTONEN, L. A., NYSTROM-LAHTI, M. & ET AL. (1993) Mutations of a mutS homolog in hereditary nonpolyposis colorectal cancer. *Cell*, 75, 1215-25.

LEEN, J. L., IZZO, A., UPADHYAY, C., ROWLAND, K. J., DUBE, P. E., GU, S., HEXIMER, S. P., RHODES, C. J., STORM, D. R., LUND, P. K. & BRUBAKER, P. L. (2011) Mechanism of action of glucagon-like peptide-2 to increase IGF-I mRNA in intestinal subepithelial fibroblasts. *Endocrinology*, 152, 436-46.

LI, J., YEN, C., LIAW, D., PODSYPANINA, K., BOSE, S., WANG, S. I., PUC, J., MILIARESIS, C., RODGERS, L., MCCOMBIE, R., BIGNER, S. H., GIOVANELLA, B. C., ITTMANN, M., TYCKO, B., HIBSHOOSH, H., WIGLER, M. H. & PARSONS, R. (1997) PTEN, a putative protein tyrosine phosphatase gene mutated in human brain, breast, and prostate cancer. *Science (New York, N.Y*, 275, 1943-7.

LI, L. & CLEVERS, H. (2010) Coexistence of quiescent and active adult stem cells in mammals. *Science (New York, N.Y*, 327, 542-5.

LI, X. H., ZHENG, H. C., TAKAHASHI, H., MASUDA, S., YANG, X. H. & TAKANO, Y. (2009) PTEN expression and mutation in colorectal carcinomas. *Oncology reports*, 22, 757-64.

LI, Y., DOWBENKO, D. & LASKY, L. A. (2002) AKT/PKB phosphorylation of p21Cip/WAF1 enhances protein stability of p21Cip/WAF1 and promotes cell survival. *The Journal of biological chemistry*, 277, 11352-61.

LIEVRE, A., BACHET, J. B., LE CORRE, D., BOIGE, V., LANDI, B., EMILE, J. F., COTE, J. F., TOMASIC, G., PENNA, C., DUCREUX, M., ROUGIER, P., PENAULT-LLORCA, F. & LAURENT-PUIG, P. (2006) KRAS mutation status is predictive of response to cetuximab therapy in colorectal cancer. *Cancer research*, 66, 3992-5.

LIN, Z., COHEN, P., NISSAN, A., ALLWEIS, T. M., FREUND, H. R. & HANANI, M. (1998) Bacterial wall lipopolysaccharide as a cause of intussusception in mice. *Journal of pediatric gastroenterology and nutrition*, 27, 301-5.

LIU, W., DONG, X., MAI, M., SEELAN, R. S., TANIGUCHI, K., KRISHNADATH, K. K., HALLING, K. C., CUNNINGHAM, J. M., BOARDMAN, L. A., QIAN, C., CHRISTENSEN, E., SCHMIDT, S. S., ROCHE, P. C., SMITH, D. I. & THIBODEAU,

S. N. (2000) Mutations in AXIN2 cause colorectal cancer with defective mismatch repair by activating beta-catenin/TCF signalling. *Nature genetics*, 26, 146-7.

LIVET, J., WEISSMAN, T. A., KANG, H., DRAFT, R. W., LU, J., BENNIS, R. A., SANES, J. R. & LICHTMAN, J. W. (2007) Transgenic strategies for combinatorial expression of fluorescent proteins in the nervous system. *Nature*, 450, 56-62.

LONGACRE, T. A. & FENOGLIO-PREISER, C. M. (1990) Mixed hyperplastic adenomatous polyps/serrated adenomas. A distinct form of colorectal neoplasia. *The American journal of surgical pathology*, 14, 524-37.

LOPEZ-GARCIA, C., KLEIN, A. M., SIMONS, B. D. & WINTON, D. J. (2010) Intestinal stem cell replacement follows a pattern of neutral drift. *Science (New York, N.Y*, 330, 822-5.

LUO, F., BROOKS, D. G., YE, H., HAMOUDI, R., POULOGIANNIS, G., PATEK, C. E., WINTON, D. J. & ARENDS, M. J. (2009) Mutated K-ras(Asp12) promotes tumourigenesis in Apc(Min) mice more in the large than the small intestines, with synergistic effects between K-ras and Wnt pathways. *International journal of experimental pathology*, 90, 558-74.

LYNCH, H. T., LANSPA, S., SMYRK, T., BOMAN, B., WATSON, P. & LYNCH, J. (1991) Hereditary nonpolyposis colorectal cancer (Lynch syndromes I & II). Genetics, pathology, natural history, and cancer control, Part I. *Cancer genetics and cytogenetics*, 53, 143-60.

MA, J., MENG, Y., KWIATKOWSKI, D. J., CHEN, X., PENG, H., SUN, Q., ZHA, X., WANG, F., WANG, Y., JING, Y., ZHANG, S., CHEN, R., WANG, L., WU, E., CAI, G., MALINOWSKA-KOLODZIEJ, I., LIAO, Q., LIU, Y., ZHAO, Y., SUN, Q., XU, K., DAI, J., HAN, J., WU, L., ZHAO, R. C., SHEN, H. & ZHANG, H. (2010) Mammalian target of rapamycin regulates murine and human cell differentiation through STAT3/p63/Jagged/Notch cascade. *The Journal of clinical investigation*, 120, 103-14.

MADISON, B. B., BRAUNSTEIN, K., KUIZON, E., PORTMAN, K., QIAO, X. T. & GUMUCIO, D. L. (2005) Epithelial hedgehog signals pattern the intestinal crypt-villus axis. *Development (Cambridge, England)*, 132, 279-89.

MADISON, B. B., MCKENNA, L. B., DOLSON, D., EPSTEIN, D. J. & KAESTNER, K. H. (2009) FoxF1 and FoxL1 link hedgehog signaling and the control of epithelial proliferation in the developing stomach and intestine. *The Journal of biological chemistry*, 284, 5936-44.

MAKINEN, M. J. (2007) Colorectal serrated adenocarcinoma. *Histopathology*, 50, 131-50.

MAKINEN, M. J., GEORGE, S. M., JERNVALL, P., MAKELA, J., VIHKO, P. & KARTTUNEN, T. J. (2001) Colorectal carcinoma associated with serrated adenoma--prevalence, histological features, and prognosis. *The Journal of pathology*, 193, 286-94.

MALKIN, D., LI, F. P., STRONG, L. C., FRAUMENI, J. F., JR., NELSON, C. E., KIM, D. H., KASSEL, J., GRYKA, M. A., BISCHOFF, F. Z., TAINSKY, M. A. & ET AL. (1990) Germ line p53 mutations in a familial syndrome of breast cancer, sarcomas, and other neoplasms. *Science (New York, N.Y*, 250, 1233-8.

MARSH, V., WINTON, D. J., WILLIAMS, G. T., DUBOIS, N., TRUMPP, A., SANSOM, O. J. & CLARKE, A. R. (2008) Epithelial Pten is dispensable for intestinal homeostasis but suppresses adenoma development and progression after Apc mutation. *Nature genetics*, 40, 1436-44.

MASHIMO, H., WU, D. C., PODOLSKY, D. K. & FISHMAN, M. C. (1996) Impaired defense of intestinal mucosa in mice lacking intestinal trefoil factor. *Science (New York, N.Y*, 274, 262-5.

MASSAGUE, J., BLAIN, S. W. & LO, R. S. (2000) TGFbeta signaling in growth control, cancer, and heritable disorders. *Cell,* 103, 295-309.

MAY, R., RIEHL, T. E., HUNT, C., SUREBAN, S. M., ANANT, S. & HOUCHEN, C. W. (2008) Identification of a novel putative gastrointestinal stem cell and adenoma stem cell marker, doublecortin and CaM kinase-like-1, following radiation injury and in adenomatous polyposis coli/multiple intestinal neoplasia mice. *Stem cells (Dayton, Ohio),* 26, 630-7.

MENDE, I., MALSTROM, S., TSICHLIS, P. N., VOGT, P. K. & AOKI, M. (2001) Oncogenic transformation induced by membrane-targeted Akt2 and Akt3. *Oncogene,* 20, 4419-23.

MERG, A. & HOWE, J. R. (2004) Genetic conditions associated with intestinal juvenile polyps. *American Journal of Medical Genetics - Seminars in Medical Genetics,* 129 C, 44-55.

MILLER, K. A., YEAGER, N., BAKER, K., LIAO, X. H., REFETOFF, S. & DI CRISTOFANO, A. (2009) Oncogenic Kras requires simultaneous PI3K signaling to induce ERK activation and transform thyroid epithelial cells in vivo. *Cancer research,* 69, 3689-94.

MILLS, N. E., FISHMAN, C. L., ROM, W. N., DUBIN, N. & JACOBSON, D. R. (1995) Increased prevalence of K-ras oncogene mutations in lung adenocarcinoma. *Cancer research,* 55, 1444-7.

MINDEN, A., LIN, A., MCMAHON, M., LANGE-CARTER, C., DERIJARD, B., DAVIS, R. J., JOHNSON, G. L. & KARIN, M. (1994) Differential activation of ERK and JNK mitogen-activated protein kinases by Raf-1 and MEKK. *Science (New York, N.Y,* 266, 1719-23.

MOGHADDAM, A. A., WOODWARD, M. & HUXLEY, R. (2007) Obesity and risk of colorectal cancer: a meta-analysis of 31 studies with 70,000 events. *Cancer epidemiology, biomarkers & prevention,* 16, 2533-47.

MONTGOMERY, R. K., CARLONE, D. L., RICHMOND, C. A., FARILLA, L., KRANENDONK, M. E., HENDERSON, D. E., BAFFOUR-AWUAH, N. Y., AMBRUZS, D. M., FOGLI, L. K., ALGRA, S. & BREAULT, D. T. (2011) Mouse telomerase reverse transcriptase (mTert) expression marks slowly cycling intestinal stem cells. *Proceedings of the National Academy of Sciences of the United States of America,* 108, 179-84.

MORIN, P. J., SPARKS, A. B., KORINEK, V., BARKER, N., CLEVERS, H., VOGELSTEIN, B. & KINZLER, K. W. (1997) Activation of beta-catenin-Tcf signaling in colon cancer by mutations in beta-catenin or APC. *Science (New York, N.Y,* 275, 1787-90.

MOSER, A. R., DOVE, W. F., ROTH, K. A. & GORDON, J. I. (1992) The Min (multiple intestinal neoplasia) mutation: its effect on gut epithelial cell differentiation and interaction with a modifier system. *The Journal of cell biology,* 116, 1517-26.

MOSER, A. R., PITOT, H. C. & DOVE, W. F. (1990) A dominant mutation that predisposes to multiple intestinal neoplasia in the mouse. *Science (New York, N.Y,* 247, 322-4.

MULLER, P. A., CASWELL, P. T., DOYLE, B., IWANICKI, M. P., TAN, E. H., KARIM, S., LUKASHCHUK, N., GILLESPIE, D. A., LUDWIG, R. L., GOSSELIN, P., CROMER, A., BRUGGE, J. S., SANSOM, O. J., NORMAN, J. C. & VOUSDEN, K. H. (2009) Mutant p53 drives invasion by promoting integrin recycling. *Cell,* 139, 1327-41.

MUMM, J. S. & KOPAN, R. (2000) Notch signaling: from the outside in. *Developmental biology,* 228, 151-65.

MUNCAN, V., SANSOM, O. J., TERTOOLEN, L., PHESSE, T. J., BEGTHEL, H., SANCHO, E., COLE, A. M., GREGORIEFF, A., DE ALBORAN, I. M., CLEVERS, H. & CLARKE, A. R. (2006) Rapid loss of intestinal crypts upon conditional

deletion of the Wnt/Tcf-4 target gene c-Myc. *Molecular and cellular biology*, 26, 8418-26.

MUNERA, J., CECENA, G., JEDLICKA, P., WANKELL, M. & OSHIMA, R. G. (2011) Ets2 Regulates Colonic Stem Cells and Sensitivity to Tumorigenesis. *Stem cells (Dayton, Ohio)*.

MUNOZ, N. M., UPTON, M., ROJAS, A., WASHINGTON, M. K., LIN, L., CHYTIL, A., SOZMEN, E. G., MADISON, B. B., POZZI, A., MOON, R. T., MOSES, H. L. & GRADY, W. M. (2006) Transforming growth factor beta receptor type II inactivation induces the malignant transformation of intestinal neoplasms initiated by Apc mutation. *Cancer research*, 66, 9837-44.

NICE (2011) National Institute for Health and Clinical Excellence guidelines for the treatment of colorectal cancer.

NIELSEN, B. S., JORGENSEN, S., FOG, J. U., SOKILDE, R., CHRISTENSEN, I. J., HANSEN, U., BRUNNER, N., BAKER, A., MOLLER, S. & NIELSEN, H. J. (2011) High levels of microRNA-21 in the stroma of colorectal cancers predict short disease-free survival in stage II colon cancer patients. *Clinical & experimental metastasis*, 28, 27-38.

NIGRO, J. M., BAKER, S. J., PREISINGER, A. C., JESSUP, J. M., HOSTETTER, R., CLEARY, K., BIGNER, S. H., DAVIDSON, N., BAYLIN, S., DEVILEE, P. & ET AL. (1989) Mutations in the p53 gene occur in diverse human tumour types. *Nature*, 342, 705-8.

NORAT, T., BINGHAM, S., FERRARI, P., SLIMANI, N., JENAB, M., MAZUIR, M., OVERVAD, K., OLSEN, A., TJONNELAND, A., CLAVEL, F., BOUTRON-RUAULT, M. C., KESSE, E., BOEING, H., BERGMANN, M. M., NIETERS, A., LINSEISEN, J., TRICHOPOULOU, A., TRICHOPOULOS, D., TOUNTAS, Y., BERRINO, F., PALLI, D., PANICO, S., TUMINO, R., VINEIS, P., BUENO-DE-MESQUITA, H. B., PEETERS, P. H., ENGESET, D., LUND, E., SKEIE, G., ARDANAZ, E., GONZALEZ, C., NAVARRO, C., QUIROS, J. R., SANCHEZ, M. J., BERGLUND, G., MATTISSON, I., HALLMANS, G., PALMQVIST, R., DAY, N. E., KHAW, K. T., KEY, T. J., SAN JOAQUIN, M., HEMON, B., SARACCI, R., KAAKS, R. & RIBOLI, E. (2005) Meat, fish, and colorectal cancer risk: the European Prospective Investigation into cancer and nutrition. *Journal of the National Cancer Institute*, 97, 906-16.

O'BRIEN, C. A., POLLETT, A., GALLINGER, S. & DICK, J. E. (2007) A human colon cancer cell capable of initiating tumour growth in immunodeficient mice. *Nature*, 445, 106-10.

O'GORMAN, S., FOX, D. T. & WAHL, G. M. (1991) Recombinase-mediated gene activation and site-specific integration in mammalian cells. *Science (New York, N.Y*, 251, 1351-5.

OOTANI, A., LI, X., SANGIORGI, E., HO, Q. T., UENO, H., TODA, S., SUGIHARA, H., FUJIMOTO, K., WEISSMAN, I. L., CAPECCHI, M. R. & KUO, C. J. (2009) Sustained in vitro intestinal epithelial culture within a Wnt-dependent stem cell niche. *Nature medicine*, 15, 701-6.

ORBAN, P. C., CHUI, D. & MARTH, J. D. (1992) Tissue- and site-specific DNA recombination in transgenic mice. *Proceedings of the National Academy of Sciences of the United States of America*, 89, 6861-5.

OUELLETTE, A. J. & SELSTED, M. E. (1996) Paneth cell defensins: endogenous peptide components of intestinal host defense. *The FASEB journal*, 10, 1280-9.

OWEN, R. L. & JONES, A. L. (1974) Epithelial cell specialization within human Peyer's patches: an ultrastructural study of intestinal lymphoid follicles. *Gastroenterology*, 66, 189-203.

PADBERG, G. W., SCHOT, J. D., VIELVOYE, G. J., BOTS, G. T. & DE BEER, F. C. (1991) Lhermitte-Duclos disease and Cowden disease: a single phakomatosis. *Annals of neurology*, 29, 517-23.

PARK, Y., HUNTER, D. J., SPIEGELMAN, D., BERGKVIST, L., BERRINO, F., VAN DEN BRANDT, P. A., BURING, J. E., COLDITZ, G. A., FREUDENHEIM, J. L., FUCHS, C. S., GIOVANNUCCI, E., GOLDBOHM, R. A., GRAHAM, S., HARNACK, L., HARTMAN, A. M., JACOBS, D. R., JR., KATO, I., KROGH, V., LEITZMANN, M. F., MCCULLOUGH, M. L., MILLER, A. B., PIETINEN, P., ROHAN, T. E., SCHATZKIN, A., WILLETT, W. C., WOLK, A., ZELENIUCH-JACQUOTTE, A., ZHANG, S. M. & SMITH-WARNER, S. A. (2005) Dietary fiber intake and risk of colorectal cancer: a pooled analysis of prospective cohort studies. *Jama*, 294, 2849-57.

PARSONS, D. W., WANG, T. L., SAMUELS, Y., BARDELLI, A., CUMMINS, J. M., DELONG, L., SILLIMAN, N., PTAK, J., SZABO, S., WILLSON, J. K. V., MARKOWITZ, S., KINZLER, K. W., VOGELSTEIN, B., LENGAUER, C. & VELCULESCU, V. E. (2005) Colorectal cancer: Mutations in a signalling pathway. *Nature*, 436, 792.

PEETERS, T. & VANTRAPPEN, G. (1975) The Paneth cell: a source of intestinal lysozyme. *Gut*, 16, 553-8.

PELLEGRINET, L., RODILLA, V., LIU, Z., CHEN, S., KOCH, U., ESPINOSA, L., KAESTNER, K. H., KOPAN, R., LEWIS, J. & RADTKE, F. (2011) Dll1- and Dll4-mediated Notch signaling is required for homeostasis of intestinal stem cells. *Gastroenterology*.

PERL, A. K., WILGENBUS, P., DAHL, U., SEMB, H. & CHRISTOFORI, G. (1998) A causal role for E-cadherin in the transition from adenoma to carcinoma. *Nature*, 392, 190-3.

PERSAD, S., TROUSSARD, A. A., MCPHEE, T. R., MULHOLLAND, D. J. & DEDHAR, S. (2001) Tumor suppressor PTEN inhibits nuclear accumulation of beta-catenin and T cell/lymphoid enhancer factor 1-mediated transcriptional activation. *The Journal of cell biology*, 153, 1161-74.

PETITJEAN, A., ACHATZ, M. I., BORRESEN-DALE, A. L., HAINAUT, P. & OLIVIER, M. (2007) TP53 mutations in human cancers: functional selection and impact on cancer prognosis and outcomes. *Oncogene*, 26, 2157-65.

PINTO, D., GREGORIEFF, A., BEGTHEL, H. & CLEVERS, H. (2003) Canonical Wnt signals are essential for homeostasis of the intestinal epithelium. *Genes & development*, 17, 1709-13.

PODSYPANINA, K., ELLENSON, L. H., NEMES, A., GU, J., TAMURA, M., YAMADA, K. M., CORDON-CARDO, C., CATORETTI, G., FISHER, P. E. & PARSONS, R. (1999) Mutation of Pten/Mmac1 in mice causes neoplasia in multiple organ systems. *Proceedings of the National Academy of Sciences of the United States of America*, 96, 1563-1568.

POTTEN, C. S., BOOTH, C. & PRITCHARD, D. M. (1997) The intestinal epithelial stem cell: the mucosal governor. *International journal of experimental pathology*, 78, 219-43.

POTTEN, C. S., BOOTH, C., TUDOR, G. L., BOOTH, D., BRADY, G., HURLEY, P., ASHTON, G., CLARKE, R., SAKAKIBARA, S. & OKANO, H. (2003) Identification of a putative intestinal stem cell and early lineage marker; musashi-1. *Differentiation; research in biological diversity*, 71, 28-41.

POTTEN, C. S. & GRANT, H. K. (1998) The relationship between ionizing radiation-induced apoptosis and stem cells in the small and large intestine. *British journal of cancer*, 78, 993-1003.

POTTEN, C. S., HUME, W. J., REID, P. & CAIRNS, J. (1978) The segregation of DNA in epithelial stem cells. *Cell*, 15, 899-906.

243

POTTEN, C. S., OWEN, G. & BOOTH, D. (2002) Intestinal stem cells protect their genome by selective segregation of template DNA strands. *Journal of cell science*, 115, 2381-8.

POWELL, S. M., ZILZ, N., BEAZER-BARCLAY, Y., BRYAN, T. M., HAMILTON, S. R., THIBODEAU, S. N., VOGELSTEIN, B. & KINZLER, K. W. (1992) APC mutations occur early during colorectal tumorigenesis. *Nature*, 359, 235-7.

PROLLA, T. A., BAKER, S. M., HARRIS, A. C., TSAO, J. L., YAO, X., BRONNER, C. E., ZHENG, B., GORDON, M., RENEKER, J., ARNHEIM, N., SHIBATA, D., BRADLEY, A. & LISKAY, R. M. (1998) Tumour susceptibility and spontaneous mutation in mice deficient in Mlh1, Pms1 and Pms2 DNA mismatch repair. *Nature genetics*, 18, 276-9.

QIU, W., LEIBOWITZ, B., ZHANG, L. & YU, J. (2010) Growth factors protect intestinal stem cells from radiation-induced apoptosis by suppressing PUMA through the PI3K/AKT/p53 axis. *Oncogene*, 29, 1622-32.

RAJAGOPALAN, H., BARDELLI, A., LENGAUER, C., KINZLER, K. W., VOGELSTEIN, B. & VELCULESCU, V. E. (2002) Tumorigenesis: RAF/RAS oncogenes and mismatch-repair status. *Nature*, 418, 934.

REED, K. R., MENIEL, V. S., MARSH, V., COLE, A., SANSOM, O. J. & CLARKE, A. R. (2008) A limited role for p53 in modulating the immediate phenotype of Apc loss in the intestine. *BMC cancer*, 8, 162.

REITMAIR, A. H., REDSTON, M., CAI, J. C., CHUANG, T. C., BJERKNES, M., CHENG, H., HAY, K., GALLINGER, S., BAPAT, B. & MAK, T. W. (1996) Spontaneous intestinal carcinomas and skin neoplasms in Msh2-deficient mice. *Cancer research*, 56, 3842-9.

RENEHAN, A. G., TYSON, M., EGGER, M., HELLER, R. F. & ZWAHLEN, M. (2008) Body-mass index and incidence of cancer: a systematic review and meta-analysis of prospective observational studies. *Lancet*, 371, 569-78.

RICCI-VITIANI, L., LOMBARDI, D. G., PILOZZI, E., BIFFONI, M., TODARO, M., PESCHLE, C. & DE MARIA, R. (2007) Identification and expansion of human colon-cancer-initiating cells. *Nature*, 445, 111-5.

RIETHMACHER, D., BRINKMANN, V. & BIRCHMEIER, C. (1995) A targeted mutation in the mouse E-cadherin gene results in defective preimplantation development. *Proceedings of the National Academy of Sciences of the United States of America*, 92, 855-9.

RIJSEWIJK, F., SCHUERMANN, M., WAGENAAR, E., PARREN, P., WEIGEL, D. & NUSSE, R. (1987) The Drosophila homolog of the mouse mammary oncogene int-1 is identical to the segment polarity gene wingless. *Cell*, 50, 649-57.

RISINGER, J. I., HAYES, A. K., BERCHUCK, A. & BARRETT, J. C. (1997) PTEN/MMAC1 mutations in endometrial cancers. *Cancer Research*, 57, 4736-4738.

RODRIGUEZ-VICIANA, P., WARNE, P. H., VANHAESEBROECK, B., WATERFIELD, M. D. & DOWNWARD, J. (1996) Activation of phosphoinositide 3-kinase by interaction with Ras and by point mutation. *The EMBO journal*, 15, 2442-51.

RYCHAHOU, P. G., JACKSON, L. N., SILVA, S. R., RAJARAMAN, S. & EVERS, B. M. (2006) Targeted molecular therapy of the PI3K pathway: therapeutic significance of PI3K subunit targeting in colorectal carcinoma. *Annals of surgery*, 243, 833-42; discussion 843-4.

SAAL, L. H., GRUVBERGER-SAAL, S. K., PERSSON, C., LOVGREN, K., JUMPPANEN, M., STAAF, J., JONSSON, G., PIRES, M. M., MAURER, M., HOLM, K., KOUJAK, S., SUBRAMANIYAM, S., VALLON-CHRISTERSSON, J., OLSSON, H., SU, T., MEMEO, L., LUDWIG, T., ETHIER, S. P., KROGH, M., SZABOLCS, M., MURTY, V. V., ISOLA, J., HIBSHOOSH, H., PARSONS, R. & BORG, A. (2008) Recurrent gross mutations of the PTEN tumor suppressor gene in breast cancers with deficient DSB repair. *Nature genetics*, 40, 102-7.

SAMUELS, Y., DIAZ, L. A., JR., SCHMIDT-KITTLER, O., CUMMINS, J. M., DELONG, L., CHEONG, I., RAGO, C., HUSO, D. L., LENGAUER, C., KINZLER, K. W., VOGELSTEIN, B. & VELCULESCU, V. E. (2005) Mutant PIK3CA promotes cell growth and invasion of human cancer cells. *Cancer cell*, 7, 561-73.

SAMUELS, Y., WANG, Z., BARDELLI, A., SILLIMAN, N., PTAK, J., SZABO, S., YAN, H., GAZDAR, A., POWELL, S. M., RIGGINS, G. J., WILLSON, J. K., MARKOWITZ, S., KINZLER, K. W., VOGELSTEIN, B. & VELCULESCU, V. E. (2004) High frequency of mutations of the PIK3CA gene in human cancers. *Science (New York, N.Y,* 304, 554.

SANCHO, R., NATERI, A. S., DE VINUESA, A. G., AGUILERA, C., NYE, E., SPENCER-DENE, B. & BEHRENS, A. (2009) JNK signalling modulates intestinal homeostasis and tumourigenesis in mice. *The EMBO journal*, 28, 1843-54.

SANGIORGI, E. & CAPECCHI, M. R. (2008) Bmi1 is expressed in vivo in intestinal stem cells. *Nature genetics*, 40, 915-20.

SANSOM, O. J., MENIEL, V., WILKINS, J. A., COLE, A. M., OIEN, K. A., MARSH, V., JAMIESON, T. J., GUERRA, C., ASHTON, G. H., BARBACID, M. & CLARKE, A. R. (2006) Loss of Apc allows phenotypic manifestation of the transforming properties of an endogenous K-ras oncogene in vivo. *Proceedings of the National Academy of Sciences of the United States of America*, 103, 14122-7.

SANSOM, O. J., MENIEL, V. S., MUNCAN, V., PHESSE, T. J., WILKINS, J. A., REED, K. R., VASS, J. K., ATHINEOS, D., CLEVERS, H. & CLARKE, A. R. (2007) Myc deletion rescues Apc deficiency in the small intestine. *Nature*, 446, 676-9.

SANSOM, O. J., REED, K. R., HAYES, A. J., IRELAND, H., BRINKMANN, H., NEWTON, I. P., BATLLE, E., SIMON-ASSMANN, P., CLEVERS, H., NATHKE, I. S., CLARKE, A. R. & WINTON, D. J. (2004) Loss of Apc in vivo immediately perturbs Wnt signaling, differentiation, and migration. *Genes & development*, 18, 1385-90.

SATO, T., VAN ES, J. H., SNIPPERT, H. J., STANGE, D. E., VRIES, R. G., VAN DEN BORN, M., BARKER, N., SHROYER, N. F., VAN DE WETERING, M. & CLEVERS, H. (2011) Paneth cells constitute the niche for Lgr5 stem cells in intestinal crypts. *Nature*, 469, 415-418.

SATO, T., VRIES, R. G., SNIPPERT, H. J., VAN DE WETERING, M., BARKER, N., STANGE, D. E., VAN ES, J. H., ABO, A., KUJALA, P., PETERS, P. J. & CLEVERS, H. (2009) Single Lgr5 stem cells build crypt-villus structures in vitro without a mesenchymal niche. *Nature*, 459, 262-5.

SAUER, B. & HENDERSON, N. (1988) Site-specific DNA recombination in mammalian cells by the Cre recombinase of bacteriophage P1. *Proceedings of the National Academy of Sciences of the United States of America*, 85, 5166-70.

SCHNEIDER, A., ZHANG, Y., GUAN, Y., DAVIS, L. S. & BREYER, M. D. (2003) Differential, inducible gene targeting in renal epithelia, vascular endothelium, and viscera of Mx1Cre mice. *American journal of physiology*, 284, F411-7.

SCHNEIDER, M. R., DAHLHOFF, M., HORST, D., HIRSCHI, B., TRULZSCH, K., MULLER-HOCKER, J., VOGELMANN, R., ALLGAUER, M., GERHARD, M., STEININGER, S., WOLF, E. & KOLLIGS, F. T. (2010) A key role for E-cadherin in intestinal homeostasis and Paneth cell maturation. *PloS one*, 5, e14325.

SCHWENK, F., BARON, U. & RAJEWSKY, K. (1995) A cre-transgenic mouse strain for the ubiquitous deletion of loxP-flanked gene segments including deletion in germ cells. *Nucleic acids research*, 23, 5080-1.

SHAKER, A. & RUBIN, D. C. (2010) Intestinal stem cells and epithelial-mesenchymal interactions in the crypt and stem cell niche. *Translational research*, 156, 180-7.

SHAO, J., WASHINGTON, M. K., SAXENA, R. & SHENG, H. (2007) Heterozygous disruption of the PTEN promotes intestinal neoplasia in APCmin/+ mouse: roles of osteopontin. *Carcinogenesis,* 28, 2476-83.

SHEN, W. H., BALAJEE, A. S., WANG, J., WU, H., ENG, C., PANDOLFI, P. P. & YIN, Y. (2007) Essential role for nuclear PTEN in maintaining chromosomal integrity. *Cell,* 128, 157-70.

SHENG, H., SHAO, J., TOWNSEND, C. M., JR. & EVERS, B. M. (2003) Phosphatidylinositol 3-kinase mediates proliferative signals in intestinal epithelial cells. *Gut,* 52, 1472-8.

SHI, Y. & MASSAGUE, J. (2003) Mechanisms of TGF-beta signaling from cell membrane to the nucleus. *Cell,* 113, 685-700.

SHIBATA, H., TOYAMA, K., SHIOYA, H., ITO, M., HIROTA, M., HASEGAWA, S., MATSUMOTO, H., TAKANO, H., AKIYAMA, T., TOYOSHIMA, K., KANAMARU, R., KANEGAE, Y., SAITO, I., NAKAMURA, Y., SHIBA, K. & NODA, T. (1997) Rapid colorectal adenoma formation initiated by conditional targeting of the Apc gene. *Science (New York, N.Y,* 278, 120-3.

SLUSS, H. K., BARRETT, T., DERIJARD, B. & DAVIS, R. J. (1994) Signal transduction by tumor necrosis factor mediated by JNK protein kinases. *Molecular and cellular biology,* 14, 8376-84.

SMIT, V. T., BOOT, A. J., SMITS, A. M., FLEUREN, G. J., CORNELISSE, C. J. & BOS, J. L. (1988) KRAS codon 12 mutations occur very frequently in pancreatic adenocarcinomas. *Nucleic acids research,* 16, 7773-82.

SMITH, G., CAREY, F. A., BEATTIE, J., WILKIE, M. J., LIGHTFOOT, T. J., COXHEAD, J., GARNER, R. C., STEELE, R. J. & WOLF, C. R. (2002) Mutations in APC, Kirsten-ras, and p53--alternative genetic pathways to colorectal cancer. *Proceedings of the National Academy of Sciences of the United States of America,* 99, 9433-8.

SMITS, R., RUIZ, P., DIAZ-CANO, S., LUZ, A., JAGMOHAN-CHANGUR, S., BREUKEL, C., BIRCHMEIER, C., BIRCHMEIER, W. & FODDE, R. (2000) E-cadherin and adenomatous polyposis coli mutations are synergistic in intestinal tumor initiation in mice. *Gastroenterology,* 119, 1045-53.

SNIPPERT, H. J., VAN DER FLIER, L. G., SATO, T., VAN ES, J. H., VAN DEN BORN, M., KROON-VEENBOER, C., BARKER, N., KLEIN, A. M., VAN RHEENEN, J., SIMONS, B. D. & CLEVERS, H. (2010) Intestinal crypt homeostasis results from neutral competition between symmetrically dividing Lgr5 stem cells. *Cell,* 143, 134-44.

SOBIN, L. & WITTEKIND, C. (1997) TNM Classification of Malignant Tumours. *Wiley and Sons.*

STANGER, B. Z., DATAR, R., MURTAUGH, L. C. & MELTON, D. A. (2005) Direct regulation of intestinal fate by Notch. *Proceedings of the National Academy of Sciences of the United States of America,* 102, 12443-8.

SU, L. K., KINZLER, K. W., VOGELSTEIN, B., PREISINGER, A. C., MOSER, A. R., LUONGO, C., GOULD, K. A. & DOVE, W. F. (1992) Multiple intestinal neoplasia caused by a mutation in the murine homolog of the APC gene. *Science (New York, N.Y,* 256, 668-70.

SUZUKI, A., YAMAGUCHI, M. T., OHTEKI, T., SASAKI, T., KAISHO, T., KIMURA, Y., YOSHIDA, R., WAKEHAM, A., HIGUCHI, T., FUKUMOTO, M., TSUBATA, T., OHASHI, P. S., KOYASU, S., PENNINGER, J. M., NAKANO, T. & MAK, T. W. (2001) T cell-specific loss of Pten leads to defects in central and peripheral tolerance. *Immunity,* 14, 523-534.

TAKAHASHI, H., ISHII, H., NISHIDA, N., TAKEMASA, I., MIZUSHIMA, T., IKEDA, M., YOKOBORI, T., MIMORI, K., YAMAMOTO, H., SEKIMOTO, M., DOKI, Y. & MORI, M. (2010) Significance of Lgr5(+ve) Cancer Stem Cells in the Colon and Rectum. *Annals of surgical oncology,* published online ahead of print.

TAKAKU, K., MIYOSHI, H., MATSUNAGA, A., OSHIMA, M., SASAKI, N. & TAKETO, M. M. (1999) Gastric and duodenal polyps in Smad4 (Dpc4) knockout mice. *Cancer research*, 59, 6113-7.

TAKAKU, K., OSHIMA, M., MIYOSHI, H., MATSUI, M., SELDIN, M. F. & TAKETO, M. M. (1998) Intestinal tumorigenesis in compound mutant mice of both Dpc4 (Smad4) and Apc genes. *Cell*, 92, 645-56.

TAKEICHI, M. (1993) Cadherins in cancer: implications for invasion and metastasis. *Current opinion in cell biology*, 5, 806-11.

TASHIRO, H., BLAZES, M. S., WU, R., CHO, K. R., BOSE, S., WANG, S. I., LI, J., PARSONS, R. & ELLENSON, L. H. (1997) Mutations in PTEN are frequent in endometrial carcinoma but rare in other common gynecological malignancies. *Cancer Research*, 57, 3935-3940.

THIAGALINGAM, S., LENGAUER, C., LEACH, F. S., SCHUTTE, M., HAHN, S. A., OVERHAUSER, J., WILLSON, J. K., MARKOWITZ, S., HAMILTON, S. R., KERN, S. E., KINZLER, K. W. & VOGELSTEIN, B. (1996) Evaluation of candidate tumour suppressor genes on chromosome 18 in colorectal cancers. *Nature genetics*, 13, 343-6.

THOMAS, K. R. & CAPECCHI, M. R. (1987) Site-directed mutagenesis by gene targeting in mouse embryo-derived stem cells. *Cell*, 51, 503-12.

TORLAKOVIC, E., SKOVLUND, E., SNOVER, D. C., TORLAKOVIC, G. & NESLAND, J. M. (2003) Morphologic reappraisal of serrated colorectal polyps. *The American journal of surgical pathology*, 27, 65-81.

TRIMBOLI, A. J., CANTEMIR-STONE, C. Z., LI, F., WALLACE, J. A., MERCHANT, A., CREASAP, N., THOMPSON, J. C., CASERTA, E., WANG, H., CHONG, J. L., NAIDU, S., WEI, G., SHARMA, S. M., STEPHENS, J. A., FERNANDEZ, S. A., GURCAN, M. N., WEINSTEIN, M. B., BARSKY, S. H., YEE, L., ROSOL, T. J., STROMBERG, P. C., ROBINSON, M. L., PEPIN, F., HALLETT, M., PARK, M., OSTROWSKI, M. C. & LEONE, G. (2009) Pten in stromal fibroblasts suppresses mammary epithelial tumours. *Nature*, 461, 1084-91.

TROBRIDGE, P., KNOBLAUGH, S., WASHINGTON, M. K., MUNOZ, N. M., TSUCHIYA, K. D., ROJAS, A., SONG, X., ULRICH, C. M., SASAZUKI, T., SHIRASAWA, S. & GRADY, W. M. (2009) TGF-beta receptor inactivation and mutant Kras induce intestinal neoplasms in mice via a beta-catenin-independent pathway. *Gastroenterology*, 136, 1680-8 e7.

VAN DEN BRINK, G. R. (2007) Hedgehog signaling in development and homeostasis of the gastrointestinal tract. *Physiological reviews*, 87, 1343-75.

VAN DEN BRINK, G. R., BLEUMING, S. A., HARDWICK, J. C., SCHEPMAN, B. L., OFFERHAUS, G. J., KELLER, J. J., NIELSEN, C., GAFFIELD, W., VAN DEVENTER, S. J., ROBERTS, D. J. & PEPPELENBOSCH, M. P. (2004) Indian Hedgehog is an antagonist of Wnt signaling in colonic epithelial cell differentiation. *Nature genetics*, 36, 277-82.

VAN DER FLIER, L. G., HAEGEBARTH, A., STANGE, D. E., VAN DE WETERING, M. & CLEVERS, H. (2009a) OLFM4 is a robust marker for stem cells in human intestine and marks a subset of colorectal cancer cells. *Gastroenterology*, 137, 15-7.

VAN DER FLIER, L. G., VAN GIJN, M. E., HATZIS, P., KUJALA, P., HAEGEBARTH, A., STANGE, D. E., BEGTHEL, H., VAN DEN BORN, M., GURYEV, V., OVING, I., VAN ES, J. H., BARKER, N., PETERS, P. J., VAN DE WETERING, M. & CLEVERS, H. (2009b) Transcription factor achaete scute-like 2 controls intestinal stem cell fate. *Cell*, 136, 903-12.

VAN DOP, W. A., HEIJMANS, J., BULLER, N. V., SNOEK, S. A., ROSEKRANS, S. L., WASSENBERG, E. A., VAN DEN BERGH WEERMAN, M. A., LANSKE, B., CLARKE, A. R., WINTON, D. J., WIJGERDE, M., OFFERHAUS, G. J., HOMMES, D. W., HARDWICK, J. C., DE JONGE, W. J., BIEMOND, I. & VAN DEN BRINK, G. R.

(2010) Loss of Indian Hedgehog activates multiple aspects of a wound healing response in the mouse intestine. *Gastroenterology*, 139, 1665-76, 1676 e1-10.

VAN DOP, W. A., UHMANN, A., WIJGERDE, M., SLEDDENS-LINKELS, E., HEIJMANS, J., OFFERHAUS, G. J., VAN DEN BERGH WEERMAN, M. A., BOECKXSTAENS, G. E., HOMMES, D. W., HARDWICK, J. C., HAHN, H. & VAN DEN BRINK, G. R. (2009) Depletion of the colonic epithelial precursor cell compartment upon conditional activation of the hedgehog pathway. *Gastroenterology*, 136, 2195-2203 e1-7.

VAN ES, J. H., DE GEEST, N., VAN DE BORN, M., CLEVERS, H. & HASSAN, B. A. (2010) Intestinal stem cells lacking the Math1 tumour suppressor are refractory to Notch inhibitors. *Nature communications*, 1, 1-5.

VAN ES, J. H., VAN GIJN, M. E., RICCIO, O., VAN DEN BORN, M., VOOIJS, M., BEGTHEL, H., COZIJNSEN, M., ROBINE, S., WINTON, D. J., RADTKE, F. & CLEVERS, H. (2005) Notch/gamma-secretase inhibition turns proliferative cells in intestinal crypts and adenomas into goblet cells. *Nature*, 435, 959-63.

VANDUSSEN, K. L. & SAMUELSON, L. C. (2010) Mouse atonal homolog 1 directs intestinal progenitors to secretory cell rather than absorptive cell fate. *Developmental biology*, 346, 215-23.

VARNAT, F., DUQUET, A., MALERBA, M., ZBINDEN, M., MAS, C., GERVAZ, P. & RUIZ I ALTABA, A. (2009) Human colon cancer epithelial cells harbour active HEDGEHOG-GLI signalling that is essential for tumour growth, recurrence, metastasis and stem cell survival and expansion. *EMBO molecular medicine*, 1, 338-51.

VARNAT, F., ZACCHETTI, G. & RUIZ I ALTABA, A. (2010) Hedgehog pathway activity is required for the lethality and intestinal phenotypes of mice with hyperactive Wnt signaling. *Mechanisms of development*, 127, 73-81.

VERMEULEN, L., DE SOUSA, E. M. F., VAN DER HEIJDEN, M., CAMERON, K., DE JONG, J. H., BOROVSKI, T., TUYNMAN, J. B., TODARO, M., MERZ, C., RODERMOND, H., SPRICK, M. R., KEMPER, K., RICHEL, D. J., STASSI, G. & MEDEMA, J. P. (2010) Wnt activity defines colon cancer stem cells and is regulated by the microenvironment. *Nature cell biology*, 12, 468-76.

VERMEULEN, L., TODARO, M., DE SOUSA MELLO, F., SPRICK, M. R., KEMPER, K., PEREZ ALEA, M., RICHEL, D. J., STASSI, G. & MEDEMA, J. P. (2008) Single-cell cloning of colon cancer stem cells reveals a multi-lineage differentiation capacity. *Proceedings of the National Academy of Sciences of the United States of America*, 105, 13427-32.

VLEMINCKX, K., VAKAET, L., JR., MAREEL, M., FIERS, W. & VAN ROY, F. (1991) Genetic manipulation of E-cadherin expression by epithelial tumor cells reveals an invasion suppressor role. *Cell*, 66, 107-19.

VOGELSTEIN, B., LANE, D. & LEVINE, A. J. (2000) Surfing the p53 network. *Nature*, 408, 307-10.

WALDRIP, W. R., BIKOFF, E. K., HOODLESS, P. A., WRANA, J. L. & ROBERTSON, E. J. (1998) Smad2 signaling in extraembryonic tissues determines anterior-posterior polarity of the early mouse embryo. *Cell*, 92, 797-808.

WANG, S. I., PARSONS, R. & ITTMANN, M. (1998) Homozygous deletion of the PTEN tumor suppressor gene in a subset of prostate adenocarcinomas. *Clinical Cancer Research*, 4, 811-815.

WANG, Y., WANG, L., IORDANOV, H., SWIETLICKI, E. A., ZHENG, Q., JIANG, S., TANG, Y., LEVIN, M. S. & RUBIN, D. C. (2006) Epimorphin(-/-) mice have increased intestinal growth, decreased susceptibility to dextran sodium sulfate colitis, and impaired spermatogenesis. *The Journal of clinical investigation*, 116, 1535-46.

WICHA, M. S., LIU, S. & DONTU, G. (2006) Cancer stem cells: an old idea--a paradigm shift. *Cancer research,* 66, 1883-90; discussion 1895-6.

WIJNHOVEN, B. P., DINJENS, W. N. & PIGNATELLI, M. (2000) E-cadherin-catenin cell-cell adhesion complex and human cancer. *The British journal of surgery,* 87, 992-1005.

WILLIAMS, P. L., WARWICK, R., DYSON, M. & BANNISTER, L. H. (1989) Gray's Anatomy. *Churchill Livingstone,* 37th Edition.

WINESETT, M. P., RAMSEY, G. W. & BARNARD, J. A. (1996) Type II TGF(beta) receptor expression in intestinal cell lines and in the intestinal tract. *Carcinogenesis,* 17, 989-95.

WOLIN, K. Y., YAN, Y., COLDITZ, G. A. & LEE, I. M. (2009) Physical activity and colon cancer prevention: a meta-analysis. *British journal of cancer,* 100, 611-6.

WRIGHT, N. A. & ALISON, M. (1984) The Biology of Epithelial Cell Populations. *Oxford University Press,* 2.

WU, J. M., MONTGOMERY, E. A. & IACOBUZIO-DONAHUE, C. A. (2008) Frequent beta-catenin nuclear labeling in sessile serrated polyps of the colorectum with neoplastic potential. *American journal of clinical pathology,* 129, 416-23.

YACHIDA, S., MUDALI, S., MARTIN, S. A., MONTGOMERY, E. A. & IACOBUZIO-DONAHUE, C. A. (2009) Beta-catenin nuclear labeling is a common feature of sessile serrated adenomas and correlates with early neoplastic progression after BRAF activation. *The American journal of surgical pathology,* 33, 1823-32.

YANG, Q., BERMINGHAM, N. A., FINEGOLD, M. J. & ZOGHBI, H. Y. (2001) Requirement of Math1 for secretory cell lineage commitment in the mouse intestine. *Science (New York, N.Y,* 294, 2155-8.

YANG, W., BANCROFT, L., LIANG, J., ZHUANG, M. & AUGENLICHT, L. H. (2005) p27kip1 in intestinal tumorigenesis and chemoprevention in the mouse. *Cancer research,* 65, 9363-8.

YAUCH, R. L., GOULD, S. E., SCALES, S. J., TANG, T., TIAN, H., AHN, C. P., MARSHALL, D., FU, L., JANUARIO, T., KALLOP, D., NANNINI-PEPE, M., KOTKOW, K., MARSTERS, J. C., RUBIN, L. L. & DE SAUVAGE, F. J. (2008) A paracrine requirement for hedgehog signalling in cancer. *Nature,* 455, 406-10.

YOU, S., OHMORI, M., PENA, M. M., NASSRI, B., QUITON, J., AL-ASSAD, Z. A., LIU, L., WOOD, P. A., BERGER, S. H., LIU, Z., WYATT, M. D., PRICE, R. L., BERGER, F. G. & HRUSHESKY, W. J. (2006) Developmental abnormalities in multiple proliferative tissues of Apc(Min/+) mice. *International journal of experimental pathology,* 87, 227-36.

ZHENG, B., ZHANG, Z., BLACK, C. M., DE CROMBRUGGHE, B. & DENTON, C. P. (2002) Ligand-dependent genetic recombination in fibroblasts : a potentially powerful technique for investigating gene function in fibrosis. *The American journal of pathology,* 160, 1609-17.

ZHU, L., GIBSON, P., CURRLE, D. S., TONG, Y., RICHARDSON, R. J., BAYAZITOV, I. T., POPPLETON, H., ZAKHARENKO, S., ELLISON, D. W. & GILBERTSON, R. J. (2009) Prominin 1 marks intestinal stem cells that are susceptible to neoplastic transformation. *Nature,* 457, 603-7.

## Appendix 1: Publication List

Davies EJ, Marsh V, Clarke AR.; Origin and maintenance of the intestinal cancer stem cell; 2011; Molecular Carcinogenesis; 50(4); 254-63. (Review)

Marsh V, Davies EJ, Williams GT, Clarke AR.; Pten loss and k-Ras activation synergise to drive carcinoma of the biliary tract; 2011; Cancer Research; Submitted.